Giommi, Alessandro (2021) *Does the small conductance Ca2+-activated K+ current (ISK) flow under physiological conditions in rabbit and human atrial isolated cardiomyocytes?* PhD thesis.

Does the small conductance Ca^{2+}-activated K$^+$ current (I$_{SK}$) flow under physiological conditions in rabbit and human atrial isolated cardiomyocytes?

Alessandro Giommi

B.Sc., M.Sc.

Submitted in fulfilment of the requirements for the degree of

Doctor of Philosophy

Date 05/01/2021

Institute of Cardiovascular and Medical Sciences College of Medical, Veterinary and Life Sciences University of Glasgow

Abstract

Background: Small conductance Ca^{2+}-activated K^+ current (I_{SK}) may change cardiac atrial action potentials (AP) in response to altered $[Ca^{2+}]_i$; a potential therapeutic target for treating atrial fibrillation (AF). However, the contribution of I_{SK} to atrial APs under physiological conditions is unclear. Furthermore, I_{SK} may be enhanced in ventricles by heart failure, but whether by $[Ca^{2+}]_i$ elevation in the non-failing ventricle is unknown. Aims: To test whether I_{SK} flows under normal or increased global $[Ca^{2+}]_i$, or with sub-sarcolemmal $[Ca^{2+}]_i$ increase from APs in human and rabbit atrial cells. Also, to test an I_{SK} blocker, ICAGEN (ICA), on rabbit left ventricular (LV) ion currents under $[Ca^{2+}]_i$ elevation from Na^+/Ca^{2+}-exchanger ($I_{Na/Ca}$) stimulation. Methods: Myocytes were isolated enzymatically from hearts removed from anaesthetised rabbits, and from atrial tissues from consenting patients undergoing cardiac surgery. Whole-cell patch clamp (37°C) was used to record ion currents and APs (at 1, 2 or 3Hz), with $[Ca^{2+}]_i$ measured using Fura-2. Results: A positive control tested stability/timing of K^+ current (I_{K1}) block: Ba^{2+} (0.5 mM) significantly and reversibly decreased inward I_{K1} (at -115 mV) in 94% of LV cells, from -38.9±5.9 to -12.9±4.5 pA/pF (by 67%), and in 92% of atrial cells, by 43% ($P<0.05$, mean±SE, t-test, n=16-25 cells, 11-16 rabbits). Atrial I_{SK} was investigated, under increasing $[Ca^{2+}]_i$ (100-500 nM; with 5 mM BAPTA), with apamin (100 nM) and ICA (1 µM). Neither drug affected inward or outward current ($P>0.05$) at any $[Ca^{2+}]_i$, in rabbit or human (5-26 cells, 7-11 rabbits, 3-4 patients). APs recorded at 1 Hz (rabbit) were prolonged by 4-AP (I_{TO} blocker; positive control): action potential depolarization at 30% repolarization (APD_{30}) by 72%, at 70% repolarization (APD_{70}) by 31%. By contrast, ICA (1 µM) had no effect on APD_{30-90}, maximum diastolic potential (MDP), or V_{max}, in human or rabbit. ICA at 10 µM (non-specific) increased APD_{70-90} vs time-matched controls. At 2 or 3 Hz, 1 µM ICA again had no effect on APs. In rabbit LV cells, stimulating $I_{Na/Ca}$ increased $[Ca^{2+}]_i$ (up to 2.8 µM) and inward /outward currents. ICA (1 µM) had no effect on $[Ca^{2+}]_i$ or currents, whereas subsequent $NiCl_2$ (10 mM; $I_{Na/Ca}$ blocker) decreased them. By contrast, ICA 10 µM decreased outward (by 35%) and inward (49%) current, and $[Ca^{2+}]_i$ (77%), with no effect of subsequent $NiCl_2$. Conclusions: In rabbit and human atrial isolated myocytes, I_{SK} may not flow under physiological conditions, nor during short bursts of supra-physiological stimulation, so atrial I_{SK} activation (and thus its potential pharmacological inhibition during AF) may require changes to cellular electrophysiology or cell signalling systems to develop a sensitivity to I_{SK}

block. Furthermore, in non-failing LV myocytes, 1 μM ICA-sensitive I_{SK} may not be activated by $[Ca^{2+}]_i$-elevation, and high ICA conc. may inhibit $I_{Na/Ca}$.

Table of contents

List of Tables

List of Figures

Acknowledgements

I would like to express infinite gratitude toward Dr Antony Workman (1st supervisor) for the continuous support over my entire project, and beyond. Not to mention the help received from Professor Godfrey Smith (2nd supervisor) during the multiple meetings, from which I would come out filled with papers and covered of his advices and brainstormed information. A huge thanks to Dr Priyanka Saxena, as my third supervisor, and Dr Aline Gurgel for the proven patience and the great knowledge about electrophysiology, calcium imaging and much more, that they shared with me. My endless gratitude to Aileen Rankin and Michael Dunne, without whom I would have been lost, and without a spare cell to use. Also, thanks to Caron Hawksby for every impeccable human cell isolation and for the Scottish slang lessons. Lastly, thanks to Linda for keeping the lab always in order and ready for the experiments.

Thanks to Thomas Jespersen and Malene Roost Lytsen for organising the European network AFib-TrainNet, which allowed me to meet many brilliant students and people, with whom I have shared innumerable experiences.

Also, I would like to thank the Golden Jubilee Foundation cardiothoracic surgical teams; the research nurses and fellows; the administrative staff; and the patients who provided human atrial tissues. Also, my gratitude goes to Acesion for the kind gift of ICAGEN.

My gratitude goes also to Bo Hjorth Bentzen and to Acesion Pharma (ApS) for hosting me at the 9th floor of the Maersk Tower during my secondment and for helping me learning new techniques. Also, thanks to Rafel Simó Vicens for introducing me to all the staff and students and for the amazing parties on the balcony.

Finally, I must spend this last paragraph to thank my family, which supported me morally and food-wise (Italian food still the best of course), with packages filled with delicious "salumi e formaggi" which stands for salami and

cheese, but doesn't cover, not even slightly, the true intrinsic meaning behind those words. I also must thank my girlfriend, Erica, who endured my silliness and frustration and for her encouragement and patience before and during the (long) period of writing of this thesis.

Publications and abstracts

Giommi A., Gurgel A.R., Saxena P., Smith G.L., Workman A.J. 'An investigation of small conductance Ca^{2+}-activated K^+ current (I_{SK}) in rabbit and human atrial cardiomyocytes. Proc Physiol Soc 2019; 43: PC041.".

Conference posters

Giommi A., Gurgel A.R., Saxena P, Smith G.L., Workman A.J. 'An investigation of small conductance Ca^{2+}-activated K^+ current (ISK) in rabbit and human atrial cardiomyocytes.' 43rd EWGCCE (March 2019, Lisbon, PT)

Giommi A., Gurgel A.R., Saxena P, Smith G.L., Workman A.J. 'An investigation of small conductance Ca^{2+}-activated K^+ current (ISK) in rabbit and human atrial cardiomyocytes.' The Physiological Society conference (July 2019, Aberdeen, UK)

Abstracts prepared and ready for submission

Giommi A, Smith GL, Workman AJ. 'Does the small conductance Ca^{2+}-activated K^+ current (I_{SK}) flow during atrial action potential repolarisation under physiological conditions?' Ready for submission to Phys Soc, July 2021

Giommi A., Smith G.L., Workman A.J. 'Small conductance Ca^{2+}-activated K^+ current (I_{SK}) may not be activated by $[Ca^{2+}]_i$ elevation in non-failing ventricular myocytes.' Ready for submission to Phys Soc, July 2021

Author's declarations

All surgical procedures on rabbits, as well as enzymatic cell isolation were performed by technical staff (Mrs Aileen Rankin, Mr Michael Dunne and Caron Hawksby). I declare that all experimental work is my own and has not, in whole or in part, been submitted for any other degree.

Abbreviations

AA	Atrial appendage
ACE	Angiotensin converting enzyme
AF	Atrial fibrillation
AHP	Afterhyperpolarization
AP	Action Potential
APD	Action potential duration
APD_{30}	Action Potential Duration at 30% Repolarisation
APD_{70}	Action Potential Duration at 70% Repolarisation
APD_{90}	Action Potential Duration at 90% Repolarisation
AVN	Atrio-ventricular node
AVR	Aortic valve replacement
AW	Atrial wall
BAPTA	(1,2-bis (o-aminophenoxy) ethane-N,N,N′,N′-tetraacetic acid)
BDM	2,3-butanedione monoxime
BK	Big conductance
BSA	Bovine serum albumin
C	Capacitance
CABG	Coronary artery bypass graft
CCB	Calcium channel blocker
CHF	Chronic heart failure
CICR	Calcium induced calcium release
cSEVC	Continuous single electrode voltage clamp
DAD	Delayed afterdepolarisation
DMSO	Dimethyl sulphoxide
EAD	Early afterdepolarisation
E-C	Excitation-contraction
EC_{50}	Half maximal effective concentration
ECG	Electrocardiogram
Em	Membrane potential
ERP	Effective repolarisation period
G	Giga
hERG	Human Ether-à-go-go-Related Gene
HR	Heart rate
HT	Hypertension
I	Current
I:V	Current: voltage relationship
ICA	ICAGEN
I_{CaCl}	Calcium activated chloride current
Ica-L	L-type Ca^{2+} current
IK	Intermediate conductance
I_{KAS}	Apamin-sensitive potassium current
$I_{K,ACh}$	Acetylcholine-activated inward-rectifying K^+ current
IKr	Inward rectifier K^+ current (rapid)

IKs	Slow delayed rectifier K+ current
I_{Na}	Sodium current
I_{SK},/$I_{K,Ca}$	Small conductance calcium-activated potassium current
Ito	Transient-outward K+ channel
KB	Kraftbrüe
LA	Left atria
LTCC	L-type Ca^{2+} channel
LV	Left ventricle
LV	Left ventricle
LVEF	Left ventricular ejection fraction
MDP	Maximum diastolic potential
MI	Myocardial infarction
MVR	Mitral valve replacement
NCX	Na+/Ca^{2+} exchanger
PFA	Paraformaldehyde.
PMT	Photomultiplier tube
RA	Right atria
RT	Room temperature
RyRs	Ryanodine receptors
SA	Sino-Atrial
SERCA	Sarco-Endoplasmic Reticulum Ca^{2+}-ATPase
SK	Small conductance
SR	Sarcoplasmic reticulum
TdP	Torsade de pointes
TMC	Time-matched control
VF	Ventricular fibrillation
Vm	Resting potential
Vmax	Maximal upstroke velocity
WinWCP	Windows whole cell patch clamp software

Chapter 1 General Introduction

1.1 Electrophysiological properties of cardiac tissue

1.1.1 The excitation-contraction coupling in normal hearts

Cardiac excitation-contraction coupling is a finely balanced physiological mechanism that begins with electrical signals in individual cardiomyocytes, action potentials (AP), and concludes with contraction of the whole heart (5). The depolarization stimulus that generates the AP initiates in a specific cardiac region called the sinoatrial node (SAN), which represents the primary pacemaker structure in healthy hearts. The cardiac impulse propagates through the atria causing depolarization and then contraction of the atrial musculature. Subsequently, the stimulus reaches the atrioventricular node (AVN) located at the base of the atrial septum which, together with SAN, represent the fastest route of AP propagation in normal heart. The AVN works as an access to the His-Purkinje system and provokes a conduction delay between the atria and the ventricles. In fact, the fast pathway input to the AVN presents relatively short conduction delay and long refractory period, which play a crucial role in preventing the transmission of high frequency atrial APs to the ventricles, for example, during atrial fibrillation (AF) (13, 14). Finally, from the AVN, the AP waveform propagates into the ventricular tissue via the conductive cells of the bundle of His and Purkinje fibers and spreads throughout areas of ventricular cardiomyocytes, triggering coordinated cardiac pumping action (See Fig. 1.1).
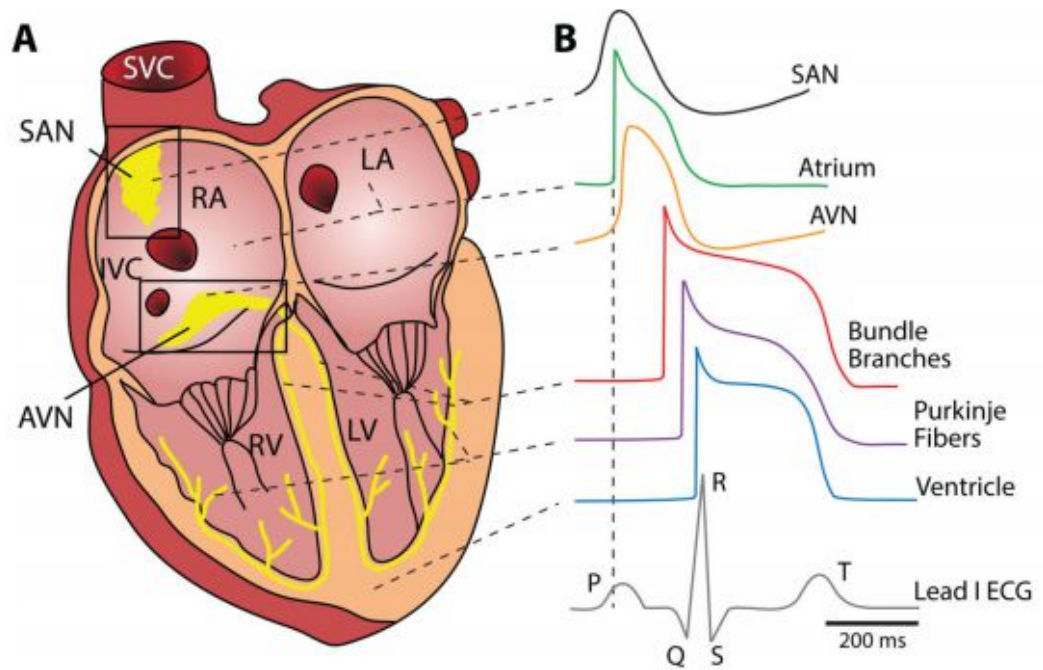
Figure 1.1 Representation of the heart and the cardiac conducting system . A) Representation of different regions of the human heart and the corresponding B) AP waveforms (below is a representative lead I ECG). Illustration taken from (5).

1.1.2 Ion channel currents and the cardiac action potential in atrial and ventricular myocytes

Different ion currents define the 5 distinct phases (phase 0-4) that characterize the cardiac action potential (Fig. 1.2). The expression of these channels along with the shape and duration of the action potential varies among different species, and within the same species in diverse subregions of the heart (10) (Fig. 1.1 B). In particular, the differences in Na^+, Ca^{2+}, and K^+ channel expression define the amplitude, shape and duration of the action potential, which are crucial physiological variables. These factors play a pivotal role in the modulation of the strength of the contraction, the length of the refractory period and the unidirectional propagation of activity that leads to the generation of cardiac sinus rhythms (SR).

The cardiac action potential is the product of the sequential activation and inactivation of inward and outward currents, which in turn are influenced by the changing membrane potential (voltage). Upon AP initiation, the sudden shift in membrane voltage to positive values represent the start of the systolic period known as phase 0 (depolarization) of the AP and is driven by influx of Na^+ ions, I_{Na}, through the $Na_V1.5$ channel. The first phase of depolarization is followed by the phase 1 (early repolarization) caused by the inactivation of $Na_v1.5$ and the activation of the transient outward K^+ currents, divided into $I_{to,fast}$ and $I_{to,slow}$ (15). In figure 1.2 it is possible to appreciate the differences in repolarization time course, driven by the K^+ currents, between atria and ventricle. In particular, this early repolarization phase of the atrial AP is also shaped by the ultra-rapid delayed rectifier K^+ current (I_{Kur}), which is absent, or negligible, in ventricle (16). In addition, I_{Kur} will play a role from phase 1 to phase 3 due to its slow and partial inactivation (17). Following the early repolarization, the phase 2 (plateau) occurs, which requires the balance between repolarizing outward K^+ currents and depolarizing inward Ca^{2+} currents. The depolarization is caused by a net Ca^{2+} influx mainly through $Ca_v1.2$ (L-Type) channels, which activate at voltage positive to -30mV and inactivate slowly (18).
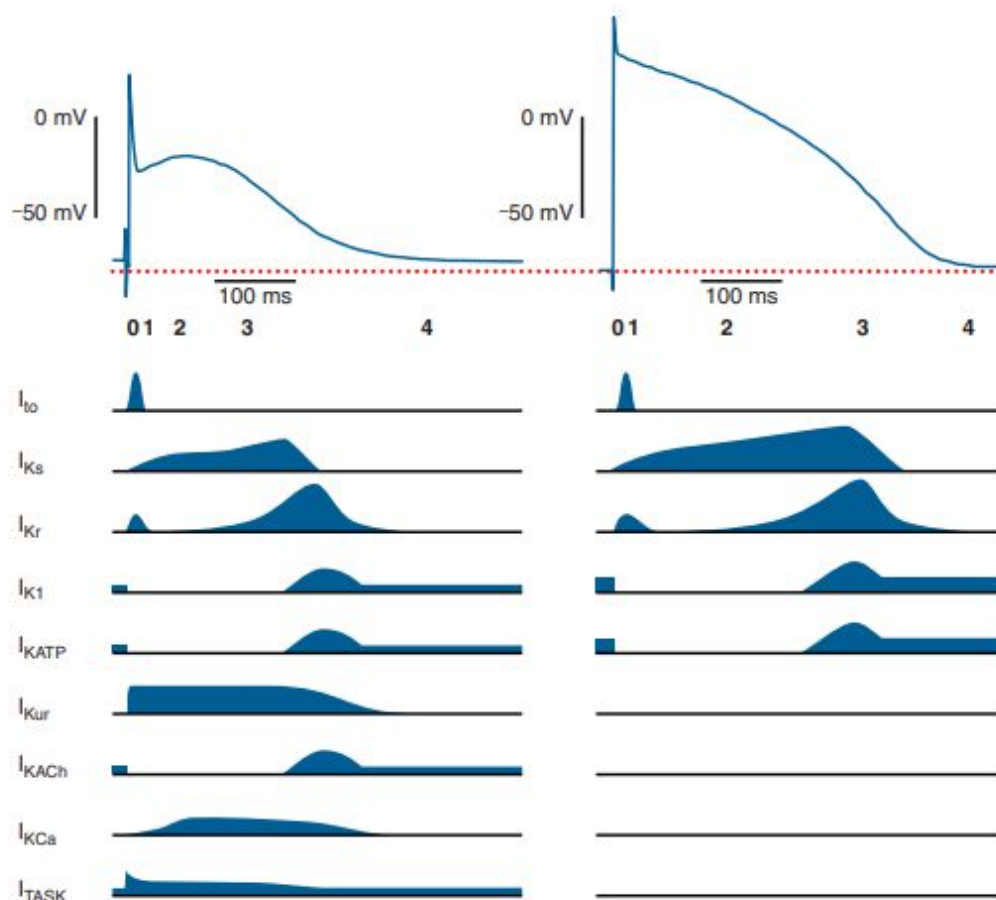
Figure 1.2 Cardiac action potentials and repolarizing currents that determine the AP shape in atrium and ventricle.

Original traces from an action potential recording in human atrial trabecula (left) and ventricular septum (right). Note that the atrial resting membrane potential (RMP) is less negative than the ventricular RMP (indicated by the red dotted line). K^+ current contributions to the different phases (0 –4) of the action potential are shown below with an approximate physiological time course. The current amplitudes are arbitrary and do not reflect their relative size. Taken from (10).

The inactivation of the L-type Ca^{2+} channels is both voltage- and Ca^{2+}- dependent and together with the activation of K^+ channels determines the end of phase 2 of the action potential (19). The K^+ currents that take part in this phase are the slow delayed rectifier (I_{Ks}) and the rapid delayed rectifier (I_{Kr}). I_{Ks} shows a linear current-voltage (I-V) relation, is activated slowly and at more

positive potentials, whereas I_{Kr}, characterized by a strong inward rectification, activates more rapidly and at more negative potentials (20, 21). While these two K$^+$ currents participate in both atrial and ventricular repolarization, I_{Kur} is predominantly expressed in mammalian atria. The activation of these K$^+$ currents along with the inward rectifying K$^+$ current (I_{K1}) initiates the final phase of cardiac repolarization, also called phase 3. During this phase, the capability of I_{Ks}, I_{Kr} and I_{K1} to compensate for each other in the eventuality that one should fail, play a crucial role in securing the stability of the cardiac electrical activity, constituting the so called "cardiac repolarization reserve" (22). When full repolarization is achieved the phase 4 of the AP begins and it ends with the firing of a second AP. During this interval, the cardiac myocytes membrane is at resting potential, which is stabilised mainly by I_{K1} conducted via $K_{ir}2.x$ channels (23). In addition to the main repolarizing currents (I_{Ks}, I_{Kr}, I_{K1}) there are other K$^+$ currents which have been shown to play a role in cardiac repolarization (Fig. 1.2). Most importantly, the majority of the K$^+$ channels that conduct these currents are predominantly expressed in atria. Among these currents there are the acetylcholine-activated inward-rectifying K$^+$ current ($I_{K,ACh}$) and I_{Kur}, which given their major importance in atria rather than ventricle, have been widely studied as possible atrial-selective targets in the treatment of diseases such as atrial fibrillation (24-26). However, in addition to these well-known currents, in recent years, another atrial-predominant channel family, the small-conductance Ca^{2+}-activated K$^+$ channels ($K_{Ca}2.x$), the main subject of this thesis, has been shown to be involved in atrial repolarization in both animals and humans (27-30). The $K_{Ca}2.x$ channels family, the currents they pass ($I_{K,Ca}$, also known as I_{SK}) and the possible role in AF, will be described more deeply later in this introduction.

1.2 Calcium involvement in electrical signalling and contraction

Ca^{2+} ions represent the most common second-messenger molecules and are involved in numerous cell functions including cardiac electrical activity and contraction. However, the intracellular Ca^{2+} levels must be tightly regulated through numerous binding and specialized extrusion proteins to prevent a prolonged intracellular Ca^{2+} ([Ca^{2+}]$_i$) overload and the consequent cell death. Normal [Ca^{2+}]$_i$ during rest is around 100nM, which is 20,000-fold lower compared to the concentration outside the cell (~2mM). The difference between the intracellular and the extracellular concentration creates a high electrochemical

$[Ca^{2+}]$ gradient that allows Ca^{2+} inside the cell through voltage-gated calcium channels (L- and T-type), which activate subsequent to depolarization of the sarcolemma due to propagation of the AP. The current generated by the opening of the L-type calcium channels (ICaL), during the plateau phase of the AP, permits the small Ca^{2+} influx to trigger a much greater release of Ca^{2+} from the sarcoplasmic reticulum (SR) through the cardiac ryanodine receptors (RyRs). This positive-feedback process, known as calcium-induced calcium-release (CICR), provokes a significant increase in $[Ca^{2+}]_i$ (to 0.6-2 μM) that allows Ca^{2+} to bind to the protein troponin-C (TnC), which then stimulates the actin-myosin interaction and promotes myocyte contraction (Fig. 1.3) (31). As the contraction step is completed the Ca^{2+} must dissociate from the myofilament and be extruded from the cytosol to allow myocyte relaxation, and this is achieved through several routes. A negative-feedback mechanism occurs and the transient rise in $[Ca^{2+}]_i$ determines the Ca^{2+}-dependent inactivation of the L-type channels by the formation of the Ca^{2+}-calmodulin complex (Ca-CaM), which bind to the carboxyl tail of the Ca^{2+} channel and deactivates it (32). The main contribution to the Ca^{2+} sequestration from the cytosol comes from the SR Ca^{2+}-ATPase (SERCA) pump, which promotes the reuptake of the activator-Ca^{2+} into the SR. Whereas, the extrusion of Ca^{2+} to the extracellular space is mainly carried out by the electrogenic transporter sodium-calcium exchanger (NCX), which couples the extrusion of 1 Ca^{2+} with a the influx of 3 Na^+, producing a net inward current, $I_{Na/Ca}$ (Fig. 1.3) (2).
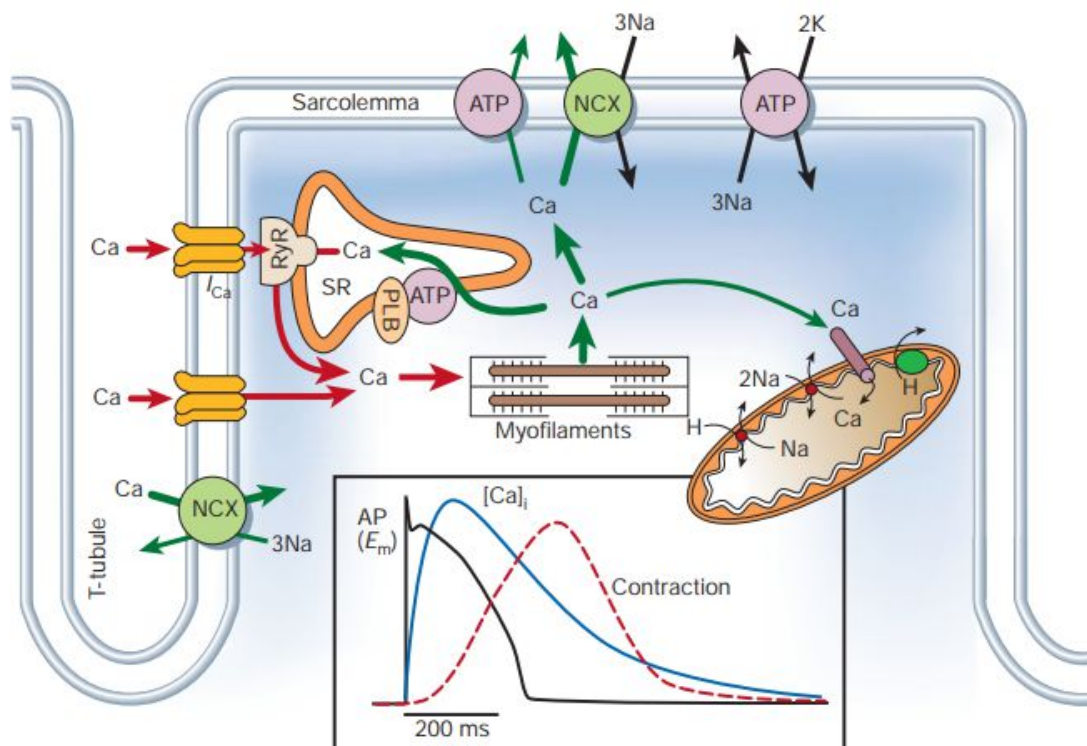
Figure 1.3 Diagram representing the Ca^{2+} transport system in cardiac myocytes.

Inset shows the time course of Ca^{2+} transient and contraction relative to the firing of an action potential (ATP, ATPase; NCX, Na+/Ca2+ exchanger; PLB, phospholamban; SR, sarcoplasmic reticulum; RyR, Ryanodine receptor) measured in a rabbit ventricular myocytes at 37°C. Taken from (2).

1.3 Atrial fibrillation

Atrial fibrillation (AF) was first documented on 12 leads electrocardiograms (ECG) more than 100 years ago (33, 34), it is nowadays considered as a major global health problem. AF is the most common sustained cardiac arrhythmia observed in the clinic with a prevalence of approximately 1% in the general population that increase with aging (35). The median age of patients with AF is 75 years, so that 50% of AF occurs in the 6% of the population 75 years of age or older. However, given the possibility of AF being asymptomatic (silent AF) and, therefore, undiagnosed, the "true" percentage can probably rise to 2% of the population (36). The normal rhythm of the heart is characterized by coordinated electrical activity starting from the SAN, propagating to the atria and reaching the ventricle (Fig. 1.4 A). Whereas, AF presents completely irregular and disorganized electrical activity due to the spontaneous firing from sources different than SAN (Fig. 1.4 B). It is well accepted that the major source of these abnormal premature beats, intimately related to the onset and perpetuation of AF, resides in the pulmonary veins (PVs) (37, 38). The AVN plays a crucial role in filtering the impulses from the atria, which during AF are fired at rates of 400-600 times per minute. Nevertheless, the ventricular rate during AF become affected as well (increased to ~150 beats/min), and elevated heart rate results from the interaction between atrial rate and the effectiveness of AVN filtering (14). The improper and fast activation of the atria is reproduced in the ECG, where P waves (depolarization of the atria) are replaced by an undulating baseline and the QRS complexes (depolarization of the ventricles) are irregular (Fig. 1.4 A-B). AF is associated with increased cardiac morbidity and mortality, the risk of which almost double when compared with aged-matched controls (14, 39, 40). The compromised atria contraction, if prolonged, leads to stasis of blood in the atria and promotes formation of thromboemboli which can propagate to different organs and potentially lead to infarction; mainly stroke. Stroke rates have been shown to be comparable between sustained and paroxysmal AF (41), and overall, ~16% of all ischemic brain infarcts have been associated with AF (42). Although, controversy exists among studies regarding the increased risk of death carried by AF-associated stroke (43-49). Also, it is well documented that sustained AF in patients with fast ventricular response may result in functional and structural changes of the ventricle leading to

tachycardia-induced cardiomyopathy. (50-52). Furthermore, the sustained high atrial rates of AF also cause electrical and structural remodelling of the atria (6, 53).
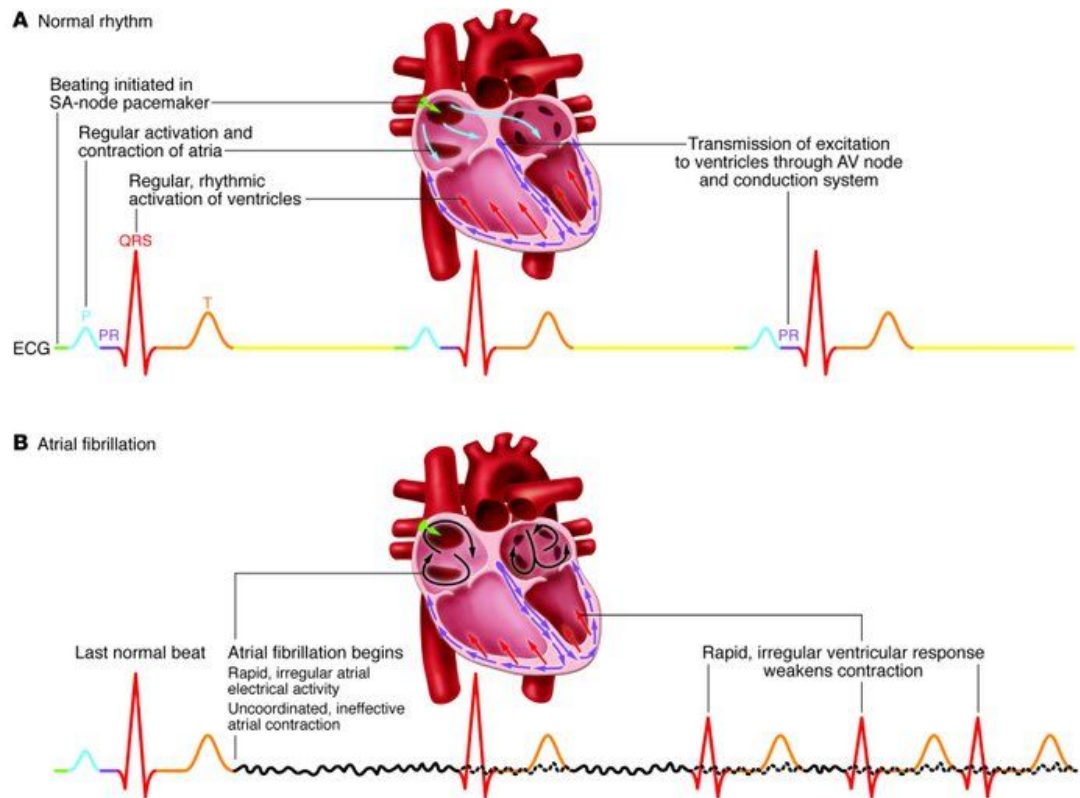
Figure 1.4 Electrical propagation and ECG recordings in sinus rhythm and during AF.

(A) Top: normal ECG recording showing sinus rhythm. Schematics of major events in one cardiac activation cycle: rhythm is initiated by the SA node pacemaker, resulting in atrial depolarization (P waves), followed by atrioventricular conduction via the AV node and His-Purkinje conducting system, leading to ventricular depolarization (QRS complex). (B) Bottom: ECG showing onset of AF after one regular normal beat. Atrial activation is now rapid and irregular, producing an undulating baseline that is visible when not obscured by larger QRS and T waves (ventricle repolarization) (continuous atrial activity during this phase is represented by dotted lines). During atrial fibrillation the uncoordinated atrial conduction makes the atria quiver and the ventricular contraction irregular. Ventricular activation, now driven by the fibrillating atria, occurs rapidly and irregularly, weakening cardiac contraction efficiency and causing clinical symptoms. Taken from (1, 2).

1.4 Atrial fibrillation: fundamental mechanisms and electrical remodelling

The understanding of AF pathophysiology, over the past decades, has drastically improved as a result of a better understanding of the role of the remodelling of the atria within this disease (8, 54). The adaptation and remodelling of the atrial myocardial electrical and mechanical activity can occur in response to a variety of stimuli or diseases; including AF itself. Hypertension, mitral valve disease, and congestive heart failure (CHF) are only a few of the diverse cardiac disorders that can predispose to AF (14, 55). The remodelling processes that occur, consequently to these pathological conditions, generate the substrate for the fundamental mechanisms of arrhythmogenesis: abnormal automaticity, triggered activity and reentry (Fig. 1.5).
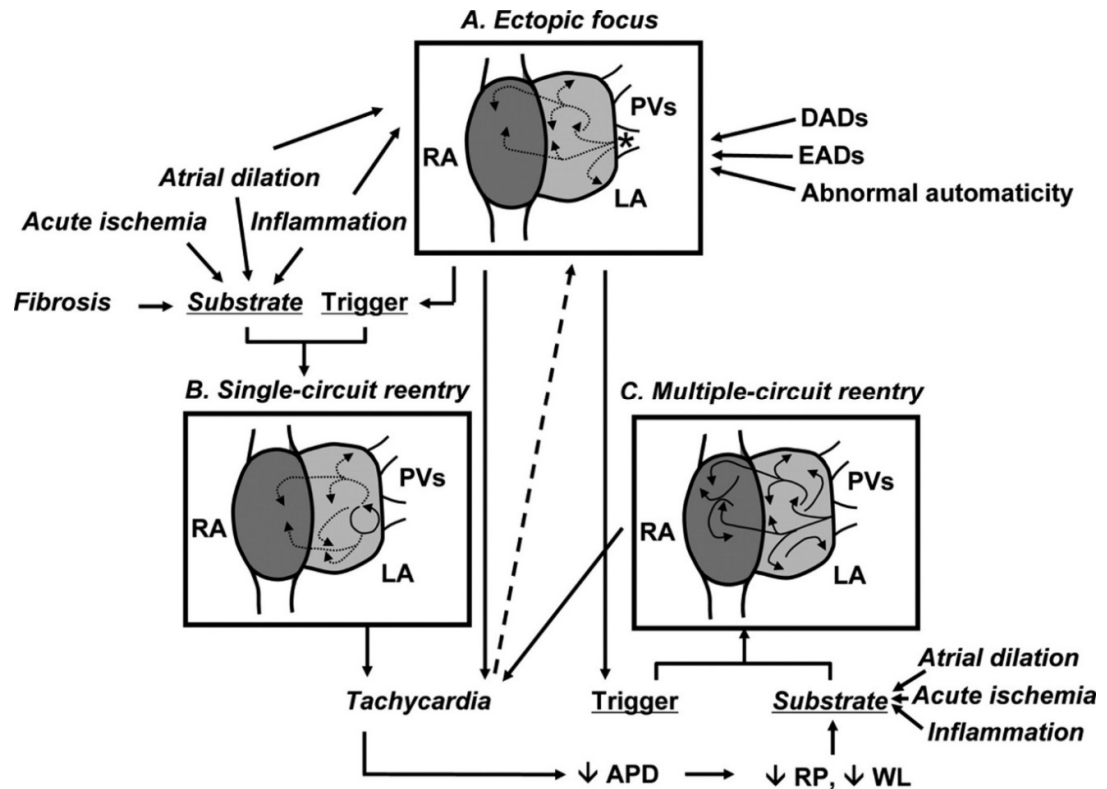
Figure 1.5 Schema indicating the complex inter-relationships between the fundamental mechanisms of arrhythmogenesis, human atrial electrophysiological remodelling and atrial pathophysiologies known to be associated with AF in humans.

Taken from (8).

Earlier in this introduction, the time-course of a normal action potential and the currents that contribute to shape the atrial AP were described. If the balance between inward currents (depolarization of the membrane through flux of positive ions) and outward currents (repolarization of the cell interior making it more negative by efflux of positive ions) changes in favour of the former, the cell membrane is able to reach the "threshold potential" and to fire an action potential. This mechanism in the SAN, differently from other region of the heart, generates spontaneous diastolic depolarization (automaticity) that is the basis of the pacemaker activity. However, if automaticity occurs in a region different from the SAN, the cell in that region will reach the threshold potential earlier and lead to the event defined as abnormal focal activity (or abnormal automaticity, AA) (56) (Fig. 1.6).
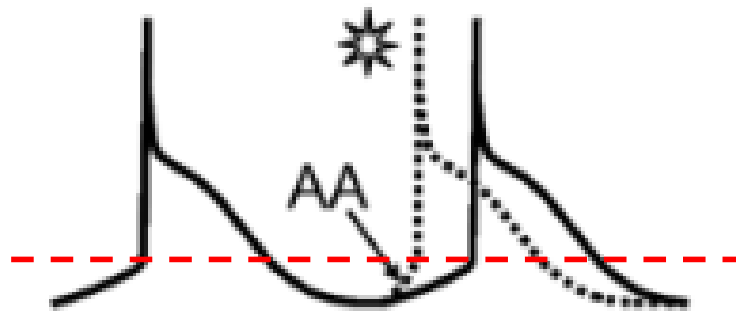
Figure 1.6 Representation of abnormal 'automaticity'.
Typical human atrial action potentials in bold, with hypothetical dashed lines indicating abnormal rapid firing event due to increased depolarization rate. Red dashed line designates threshold potential. Adapted from (6).

The premature firing of an action potential can also depend on afterdepolarizations and, in this instance, the ensuing arrhythmogenic mechanism is known as triggered activity. Afterdepolarizations are defined as oscillations in membrane potential which, if reaching threshold, generates a successive action potential that follows the upstroke of the earlier one (57). If a premature impulse, propagating between different zone of tissue, encounters a region of unidirectional block, this can cause reentry. The reentry is rapid circuitous activation, which can occur when the depolarising wave front comes

across areas that are capable of being re-excited, and therefore, are no longer in refractory period (5, 6). These fundamental mechanisms and their implications in AF will be detailed in the following sections.

1.4.1 Abnormal automaticity

Although different areas of the heart have the intrinsic capability for automaticity, the SAN remains the fastest pacemaker under normal conditions. However, abnormal automaticity risk can increase during acute myocardial ischemia, ß-adrenergic stimulation or decreased vagal activity (58). The region which has been found to be more prone to accommodate focal (nonreentrant) arrhythmias is around pulmonary veins. In fact, specialized cells with pacemaker activity are located in this region, the resting membrane potential of PV myocytes is less negative as a consequence of reduced I_{K1} and the action potential duration (APD) is shorter, also due to smaller I_{Ca}, compared to LA-free wall cells (59, 60). Considering these characteristics, if the rate at which these cells reach threshold exceeds that of the sinoatrial node (SAN), then an ectopic rhythm will supersede. Generally, this form of rapid and regular tachycardia, called paroxysmal (episodic) tachycardia or atrial flutter may come and go, while progression into more persistent and eventually permanent AF can arise from stabilization of the altered rhythm (8).

1.4.2 Triggered activity

Pacemaker activity can initiate at an ectopic focus either in the atria or in the ventricle, as a consequence of ischemia-induced depolarization or increased sympathetic activity, and lead to afterdepolarizations. As briefly described earlier, this form of abnormal impulses can generate a new action potential if critical threshold for activation is reached. Depending on the phase of the preceding action potential during which they occur, two types of afterdepolarization have been classified: early (EADs) and delayed (DADs) afterdepolarizations.

The EAD is a depolarising afterpotential that begins before the complete repolarization of an action potential (Fig. 1.7 A). Therefore, EADs are expected to disrupt the plateau level of the action potential or occur during phase 3 (late

EADs) of repolarization. EADs have been most closely related to arrhythmias that are bradycardia-related and are associated with slow pacing or a long pause (61). On the other hand, DADs are defined as oscillation in the membrane potential that occur when repolarization of the action potential is completed (phase 4) and are frequently associated with tachycardia. Hence, EADs are more prominent at slow stimulation rates and low levels of extracellular potassium, while DADs appear more frequently at fast rates and is usually induced by increased intracellular levels of calcium (62).

EADs are more frequently induced in conducting tissues (Purkinje fibers) rather than in isolated myocardial tissues (63), albeit their presence has been documented in atrial preparations (64). Several cellular mechanisms are involved in the generation of EADs, including elevated intracellular Ca^{2+} and a reduction in rapid and slow delayed rectifier currents (I_{Kr} and I_{Ks}). However, the combination of a markedly prolonged time-dependent I_{Na} activation and a reduction of the repolarization reserve, both accounting for the prolongation of the action potential, can involve reactivation of a Ca^{2+} current ($I_{Ca,L}$) in its 'window region' voltage range (65) allowing the time- and voltage- dependent recovery from inactivation of it and to self-amplify sufficiently to reverse repolarization, generating the EAD upstroke. In the scenario which sees $I_{Ca,L}$ predominate on the repolarization, the current can facilitate the AP upstroke that can result in a triggered beat or a run of triggered beats (66).

DADs are generated during conditions of calcium overload, which induce spontaneous calcium release from the SR. This SR calcium release during the phase 4 of the AP (Fig. 1.7 B) activates the transient inward current (I_{TI}) responsible for membrane depolarization. I_{TI} comprises the nonselective cationic current (I_{NS}) the sodium–calcium exchange current ($I_{Na/Ca}$), and the calcium-activated chloride current, ($I_{Cl,Ca}$) (67, 68). If the voltage oscillation produced by the DAD is sufficient to reach the critical threshold it will lead to triggered activity.
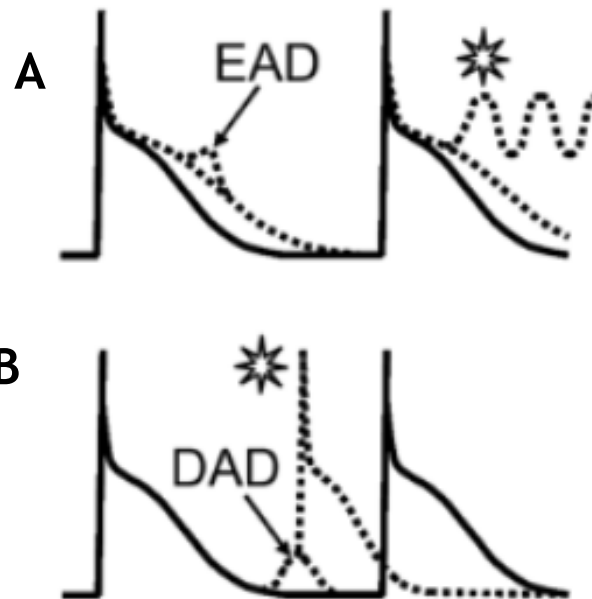
Figure 1.7 Representations of A) EADs and B) DAD in human atrial myocytes.

Typical human atrial action potentials in bold and afterdepolarizations represented by dashed lines. Star symbol indicate triggered activity generated by EADs and DADs. Adapted from (6).

It is worth mentioning that the mechanism underlying the development of both late-phase 3 EADs, more clinically relevant, is similar to the one that generates DADs and conventional Ca_i-dependent EAD (69). In fact, during shortening of the atrial APD $I_{Na/Ca}$ and $I_{Cl,Ca}$, normally weakly inward, are strongly recruited consequently to the spontaneous release of calcium from the SR and contribute to the generation of Ca_i-dependent EADs as well as DADs (61, 67). The apparent difference resides in the type of SR release, which can occur

spontaneously (i.e. non-$I_{Ca,L}$-gated) before repolarization is complete for conventional EADs/DADs, and normally $I_{Ca,L}$-gated for late EADs. In conclusion, although there is a strong implication for EADs and/or DADs as primary triggers for promoting arrhythmias such as AF, the complete mechanism remains not fully understood (58, 70).

1.4.3 Reentry

The mechanism of reentry involves the presence of a functional (electrical) or anatomical (obstacle) block around which the wave front can travel and return to the refractory tissue when it is newly excitable, this creates a circuit (2 dimensional circus-type, Fig. 1.8). However, for the perpetuation of the reentry, all points within the circuit must recover from refractoriness before the re-entrant impulse arrival (excitable gap), which has to travel sufficiently slowly to allow such recovery. In contrast, if the excitation wave has a long duration and propagates at a high rate, the whole circuit would be excited at the same time, causing the excitation to die out. The distance travelled by the impulse (wavelength, λ) is the product of the effective refractory period (ERP) and the conduction velocity (θ). Thus, the rate of propagation of an impulse is defined as the distance covered by that impulse in one refractory period. Therefore, any variable that could reduce the conduction velocity or ERP, thus reducing wavelength, or prolong conduction time or increase path length will promote reentry and consequently AF. Decreased AP maximal upstroke velocity (V_{max}) consequent to a reduced I_{Na} or decreased I_{Cal} or increase potassium currents, will reduce AP duration (APD) and ERP, hence, reentry will be more likely and more re-entrant circuits can fit in the same area.
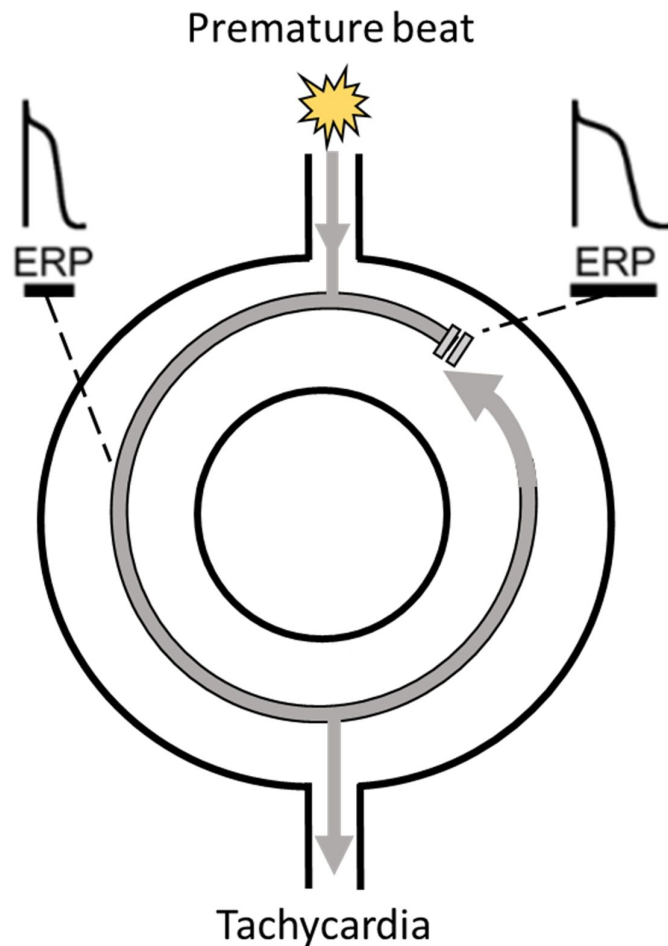
Figure 1.8 Schematic display of the formation of a 2 dimensional re-entrant circuit.

The premature impulse divides at a functional or anatomical obstacle and blocks conduction at tissue with normal (right side) but conducts with short (left) ERP and re-enters previously refractory zone, biting at its own tail of refractoriness. Inspired by (6).

The first detailed model of functional reentry, named the "leading-circle model" (Fig. 1.8-1.9) was firstly described by Allessie et al. (71, 72). Since then a different but related concept has been suggested from advances in biophysics and theoretical analysis, named "spiral wave" reentry (Fig. 1.9) (11, 73). Technically, a spiral wave is a two-dimensional wave of excitation which keeps its shape and rotates around a core of constant size with unvarying angular velocity. In cardiac tissue, the generation of a spiral wave can depend on self-organizing source of functional reentry activity, termed rotor. A rotor is the neighbourhood of the wavetip of a wavefront in an excitable medium. Basically,

it is the core centre around which the wave rotates, and it does not propagate forward like the rest of the wavefront. In the scenario represented in figure 1.8, a wavefront is initiated by an ectopic beat which traverses the recovery front following a previous sinus beat. The tissue in different states of refractoriness
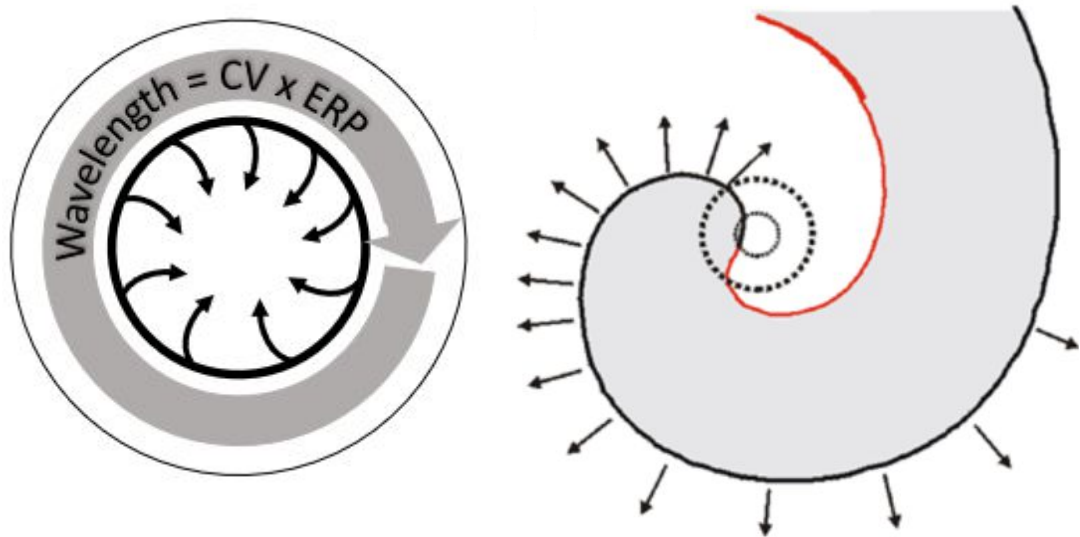
Figure 1.9 (Left) *The leading circle concept*:

Activity establishes itself in the smallest pathway that can support reentry, shown as the tight fit between the wavelength (big grey arrow) and the circuit path. Inside the leading circle, centripetal wavelets (small arrows) emanating from it constantly maintain the central core in a refractory state. **(Right)** *Spiral wave model*: Schematic diagram of a spiral wave with the activation front shown in black and the repolarization front in red, with the grey area being the refractory tissue. The outer arrows depict the direction of the depolarization front. The point at which the red and black curves meet has an undefined voltage state and is usually referred to as the phase singularity point. Modified from (11).

will define the direction of propagation of the wavefront, which will curve, tangentially in 3-dimensions, in the direction of the newly excitable myocytes. This wavefront can continue as long as tissue recovers from refractoriness, until it completes a full revolution. The point where the repolarization and the activation fronts meet (dashed circled line, figure 1.8 right) represents the phase singularity (11). In conclusion, "spiral wave" and "leading-circle" concepts

differs for level of complexity, but more importantly the first predicts an antiarrhythmic effect of Na$^+$ current inhibition, in contrast to the leading circle, due to increased core size and decreased maximum curvature, possibly leading to termination of reentry, consistent with experimental observation (74, 75)

1.5 "AF begets AF": through atrial remodelling

The occurrence of AF has been shown to cause structural and electrical remodelling through acceleration of atrial rate, which promotes AF, thus leading to advancement and auto perpetuation of AF (8). It is nowadays well established that the presence and sustainability of AF, the longer it persists, lower the probability of successful cardioversion, and increases the difficulty to manage AF (76) a process named "AF begets AF". In a goat model of induced AF, atrial tachypacing led to remodelling of the atrium, progressive shortening of ERP and AF interval over 24 hours with an increase in λ which favoured AF vulnerability and duration (77). The mechanism of the shortening of atrial refractoriness by AF are not completely understood. However, the electrical remodelling, during AF, is characterized by a maladaptation of the atrial effective refractory period (aERP) to changes in APD (77). By this means, the physiological rate adaptation, which results in proportional shortening of APD and ERP with increased heart rate, is poor or absent and it could be one of the causes of AF sustainability (77, 78).

These results have been also documented in humans, where chronic AF was shown to be associated with an attenuation in adaptation of the ADP and ERP parameters to fast rates (79). Rate-dependent reduction in I_{CaL} and I_{TO} has been shown in both humans and animals, which could account, albeit partially, for the APD rate response (79-81).

1.6 AF- induced cellular electrophysiological remodelling and $[Ca^{2+}]_i$ changes

AF is sustained by re-entrant circuits propagating in a re-modelled atria, which generates rapid electrical activity (up to 600 beats per minute) (82, 83). The almost tenfold increase in atrial rate, provoked by recent-onset AF, produces substantially increased influx of Ca^{2+} through I_{Ca} at each action potential (84). The consequent calcium overload leads to a rapid cell response, aimed to mitigate the effect of an intracellular Ca^{2+} load, inactivating I_{Ca} (85). However, this mechanism of defence might result in a shortening of the aERP as described by Yue et al. in dogs after rapid atrial pacing for 42 days (80). These findings are also in agreement with the study made by Lai et al. in 1999, in humans with persistent AF for more than 3 months, who found a downregulation in mRNA levels of L-Type calcium channels and sarcoplasmic reticular Ca^{2+}-ATPase. Furthermore, a long-term change during AF involves the decrease of SR Ca^{2+}-ATPase, which is responsible for calcium reuptake into the SR, which will produce an accumulation of intracellular Ca^{2+} (86). This may result from rapid atrial depolarization which cause the cells to spend more time in the systolic phase, allowing additional Ca^{2+} influx into the cytosol and further CICR. Studies in goats or dogs demonstrate, mitochondria swelling and disruption of sarcoplasmic reticulum with rapid atrial pacing (87-89), all characteristic consequences of intracellular calcium overload. Additionally, changes in atrial diameter and pressure during contractility, during several days of AF, appear to occur in parallel with electrical remodelling (90), implying a possible correlation between these two processes. However, after long periods of AF (weeks to months) contractile dysfunction may require several weeks to months for recovery (91-94), while ERP and atrial activation may recover within days or a few weeks, respectively, supporting the crucial role of duration of AF for successful therapeutic intervention (77, 95-98).

Overall, it appears clear that calcium overload plays a pivotal role in atria electrical remodelling. In particular, the protective effect, against electrical remodelling and atrial contractile dysfunction, of the calcium antagonist verapamil has been shown by several authors (89, 99, 100), which however seems to lose effectiveness after long lasting AF (101). In support to this finding, the L-Type Ca^{2+} channel agonist Bay K8644 promoted atrial hypocontractility after the

cessation of short periods of AF (100). However, electrical remodelling has been shown to be caused also by a reduction of I_{CaL} during sustained atrial tachycardia (80) and the use of a different L-type Ca^{2+} channel agonist, Bay Y5959, increased atrial contractility and prolonged the refractory period (90).

1.7 Classification, management and treatment of atrial fibrillation

AF can be defined as a "sustained" asymptomatic episode lasting at least 30 seconds (102). From there, it can be categorized as *paroxysmal* AF when recurrent AF (≥two episodes) terminates spontaneously within 7 days or in less than 48 hours with electrical or pharmacologic cardioversion; *persistent* when continuous AF is sustained beyond 7 days or if it is cardioverted ≥48 hours, but prior to 7 days; *longstanding persistent* AF is defined as continuous AF of greater than 12 months duration; *permanent* AF refers to a group of patients for which a decision has been made to not pursue further with treatment to restore or maintain sinus rhythm (103).

During AF the ventricular rate become affected as well, due to the limited impulse-carrying capacity of the AVN, causing the majority of the symptoms and increasing the mortality rate associated with increased risk of stroke and congestive heart failure (104-106). The most important therapeutic goal in management of AF is stroke prevention, the risk of which is reduced by oral anticoagulant (OACs), like warfarin (vitamin K antagonists) (107), albeit this drug is frequently not administered (108). Since 2011 novel oral anticoagulants (NOACs, non-vitamin K antagonists) have been introduced in substitution of warfarin for patients with non-valvular AF (109). However, prevention of stroke does not prevent the unpleasant, sometimes debilitating, symptoms of AF, nor mitigate the deleterious consequences of reduced and irregular atrial contraction. Furthermore, blood thinning drugs are not without risk of bleeding. Therefore, it is desirable to try to prevent the abnormal atrial rhythm during AF. When it comes to the treatment of the abnormal rhythm, two principal strategies are adopted: *rate control* or *rhythm control*. The latter one aims to restore and maintain the sinus rhythm, while rate control, used as an alternative strategy, simply regulates the ventricular response rate of AF. Although the optimal rate is currently not clear, the recommendation is to maintain a ventricular rate of <80 beats per minute (bpm) at rest and <115 bpm at moderate exercise (110).

Rate control is usually accomplished with the use of drugs that can prolong the AVN conduction, such as digoxin, beta blockers or calcium channel blockers (e.g. verapamil, diltiazem), which slow conduction in the AVN by blocking the major depolarizing current in nodal cells ($I_{Ca,L}$). However, rate control by AV-nodal ablation and permanent ventricular pacing is recommended in patients with AF when rate control with medications or rhythm control therapies failed (109). On the other hand, rhythm control is performed by availing of antiarrhythmic drugs (e.g. amiodarone, disopyramide, flecainide), electrical cardioversion, catheter ablation, surgical procedures (both surgical ablation and cut-and-sew technique) or a combination of these methods. Regarding rhythm control therapy, although catheter ablation results are more effective than antiarrhythmic drugs in maintaining sinus rhythm (111), it remains unclear if catheter ablation improves the long-time survival and reduces cardiovascular events but, currently, rhythm control is indicated for symptom improvement in AF patients (111-113). Nonetheless, many studies comparing rhythm control versus rate control have not been able to show clear advantage of the first over the strategy of controlling the ventricular rate and allowing atrial fibrillation to persist, in reducing the risk of stroke and mortality (114-118). Overall, freedom from AF after catheter ablation (CA) remains a powerful predictor of stroke-free survival while the use of antiarrhythmic drugs (AADs) after CA, except in some cases (119, 120), has been documented to increase mortality (119, 121, 122). Generically, AADs have four modes of action (123), targeting either Na^+, K^+ or Ca^{2+} channels or interfering with intracellular mechanism regulated by adrenergic activity. Specifically, Class I drugs produce moderate (Ia), weak (Ib), or marked (Ic) Na^+ channel block and provoke reduction of excitability and enhance post-excitatory refractoriness. They reduce AP phase 0 slope and overshoot while increasing (Ia), reducing (Ib), or conserving (Ic) AP duration (APD) and effective refractory period (ERP), respectively (75, 124). Class II drugs targets β-adrenergic receptors reducing sinoatrial node (SAN) pacing rates and slow atrioventricular node (AVN) AP conduction (125). Class III drugs, comprising K^+ channel blockers, delay AP phase 3 repolarization and lengthen the ERP. Finally, Class IV blocks Ca^{2+} channel reducing heart rate and conduction (123). The possible cause behind the adverse association of AADs and all-cause mortality in patients can be attributed to the proarrhythmic effect of these drugs in situation like myocardial ischemia (MI) or sympathetic stimulation (121, 126). Additionally, Amiodarone, the most

frequently prescribed AAD, has important side effects, including Cushingoid appearance, proximal myopathy, adrenal suppression, and reactivation of retinal toxoplasmosis as well as alterations in thyroid gland function test and thyroid hormones (127).

1.8 Atrial regional heterogeneity: atrial-selective targets

CA techniques and device based therapies for cardiac arrhythmias have improved over the years, but there is still a necessity of AADs for any comprehensive therapeutic strategy. However, as briefly discussed, AADs are also not without risk, e.g. cardiac and extracardiac toxicity or partial efficacy. This paragraph will focus on atrial selective antifibrillatory agents targeting atrial specific channels.

As mentioned, triggers and reentry propagation of electrical signals are fundamental mechanisms of AF. Therefore, any approach aimed to prolong ERP and to terminate reentry-based arrhythmias constitute a valid strategy. Typical Class III AADs, targeting K^+ channel subspecies, includes I_{Kr} blockers dofetilide, ibutilide or d,l-sotalol, and nonselective blockers like amiodarone and dronedarone, which are defined as multichannel inhibitors (128-131). In fact, these last two antiarrhythmic agents have been shown to block a variety of ion channels among atria and ventricle (e.g. I_{Kr} in ventricle, $I_{K,ACh}$ in atria), including transmembrane Na^+, K^+, Ca^{2+}, and slow L- type calcium currents (e.g. IC_{50}: I_{Ca-L} 0.2 µM and 10 µM respectively for Dronedarone and Amiodarone) (132). Given that the K^+ channels inhibited by these drugs are expressed across the heart, both atrial and ventricular signalling will be influenced, and it is obvious that many of their undesired and deleterious effects on the ventricle would be reduced if they target solely, or at least predominantly, atrial ion channels.

Regional differences in ion channels distribution between atria and ventricular cells, generate imbalance of inward and outward ion currents between these two regions of the heart, creating the perfect opportunity for pharmacological atrial-selective strategies, and to try to prevent pro-arrhythmic effects in the ventricle (133, 134). Some of these currents have already been mentioned, like I_{Kur} (135) and $I_{K,Ach}$ (136), however, atrial selectivity could also be achieved by targeting atrial Na^+ channels exploiting rate-dependent blocking

properties, which allow a strong suppression in the atria compared to the ventricle of Na^+ current during high activation rate, typical of AF (137). The more depolarized resting membrane potential in atria cells and the more negative steady-state inactivation is sufficient to reduce Na^+ channel availability in comparison with ventricle during diastole (138). Therefore, the fraction of resting channels is smaller in atrial versus ventricular cells at RMPs. As a consequence of this, high frequencies during AF favour drug binding during the APs and restrict drug dissociation during the short diastolic intervals. Thus, atrial cells show a greater accumulation of use-dependent Na^+ channel block (139).

The ultra-rapid rectifier K^+ channel (Kv1.5) encoded by KCNA5, which conducts I_{Kur}, were first cloned from the human heart in 1991 and found to be present in atria but not in ventricles (140, 141). Although targeting this current seems to represent an optimal atrial-selective approach, it remains a great challenge because agents directed to block I_{Kur} often also inhibit other currents (e.g. I_{Na} by vernakalant and $I_{TO}/I_{K,ACh}/CA\text{-}I_{K,ACh}$ by AVE011) (142, 143). In addition, data from both humans and animals for I_{Kur} are equivocal regarding a possible reduction of this current during AF (80, 144, 145). Despite these evidences, recent studies describe that selective I_{Kur} inhibition causes shortening of APD_{90} in SR, while producing APD_{90} and ERP prolongation in human permanent AF tissue, probably due to an overall reduction in atrial repolarization reserve due to AF-induced remodelling (146). Different compounds targeting I_{Kur} with more attractive selectivity profile have been investigated (147). Nevertheless, the potential clinical benefit of this atrial-selective target in antiarrhythmic therapy is still not confirmed.

The acetylcholine (ACh)-regulated potassium current, $I_{K,ACh}$, is conducted through G-protein coupled inwardly rectifying K^+ channels (GIRK1 and GIRK4) whose α-subunits are encoded by Kir3.1/Kir3.4. These form heteromeric assembly Kir3.1/GIRK1 and Kir3.4/GIRK4, encoded by KCNJ3 and KCNJ5 respectively (148, 149). These channels have been found to be more abundant in atrial than in ventricular muscle (150, 151), constituting another interesting atrial selective antiarrhythmic target in AF. GIRK channels have been shown to mediate AF induced by vagal stimulation via activation of muscarinic M_2 receptors in mice (152). $I_{K,ACh}$ hyperpolarizes the membrane and shortens atrial

action potentials duration, thereby contributing to maintenance of AF by promoting reentry (reduced wavelength) and/or stabilizing rotors. Despite parasympathetic-regulated $I_{K,ACh}$ is becoming reduced in long-term AF (153), a constitutively active (CA) $I_{K,ACh}$, which does not require its endogenous agonist, contribute to basal inward rectification in AF (25). These are the reasons which make $I_{K,ACh}$ an interesting target for AF therapy. Selective block of $I_{K,ACh}$ has revealed clear antiarrhythmic effects, by prolongation of the ERP, in different in vivo models of experimental AF and in vitro (136). A more recent study described decreased incidence of AF, reduced duration of AF and prolonged aERP in conscious dogs by selective inhibition of $I_{K,ACh}$ (with tertiapin-Q, a derivative of the honeybee toxin tertiapin) (154). However, species differences regarding the relative roles of different atrial ionic currents, continue to raise difficulties in translating antiarrhythmic results obtained in animals to those in humans. Therefore, results obtained in experimental animal models of AF should be translated to human clinical settings with caution, with further studies required to assess the role of $I_{K,ACh}$ block in patient with AF (154).

1.9 Small conductance Ca^{2+}-activated K^+ channels

The presence of Ca^{2+}-activated K^+ current (KCa) has been observed firstly in red blood cells, where their activation caused membrane afterhyperpolarization (AHP) and cell shrinking (155). From there, based on their physiological role and pharmacology, multiple subtypes of these channels have been identified. Then cloning has revealed three subfamilies of channel subunits: big conductance KCa1.1 (encoded by KCNMA1), intermediate conductance KCa3.1(encoded by KCNN4) and small conductance KCa2.1, KCa2.2, KCa2.3 (encoded by KCNN1, KCNN2 and KCNN3, respectively) channels. From now on the trivial name (SK1-3) of small conductance Ca^{2+}-activated K^+ channels, the focus of this thesis, will be used for simplicity, although the correct IUPAC nomenclature is KCa2.x. SK channels are tetrameric with each subunit displaying a *Shaker-like* membrane topology of six-transmembrane segments, with intracellular N- and C-termini and S5 and S6 in line with the pore (Fig. 1.10). Finally, in contrast with the other channel subfamilies, SK channels have not been reported to present regulatory ß-subunits (156). The expression of SK channels has been documented in different tissues, from nervous system, skeletal muscle, vasculature, smooth muscle and cardiac tissue (157-162).
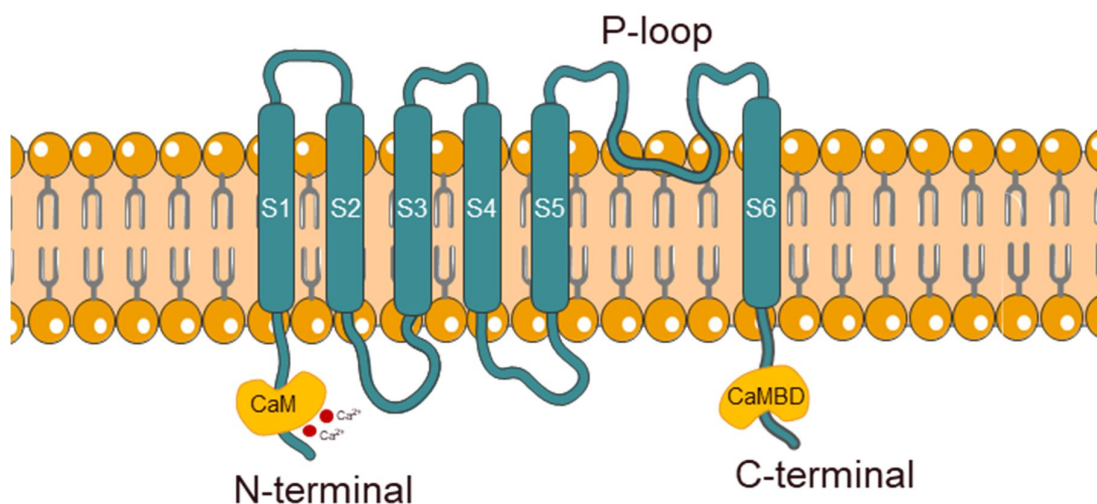
Figure 1.10 Representation of a single SK channel subunit.

Each subunit has six transmembrane segments, S1-S6, and both intracellular N and C-termini. The pore of the channel is formed between S5 and S6, and within it lies the P-loop. The calcium-sensing protein CaM is bound to SK subunits through the CaMBD region, located at the C-terminal. Image created using elements from SMART, Servier Medical Art by Servier, licensed under a Creative Commons Attribution 3.0 Unported License. Adapted from Zhang X. et al (11).

The latter (cardiac tissue) is the region of interest of this thesis, where the investigation of SK channel has been addressed. Moreover, the main part of this work has been focused on atrium, where SK channels have been documented to be predominantly expressed, compared to ventricle, where they seem to play a negligible role (27-29). Evidence for homo- and heteromultimerization of cardiac SK subunits has been provided from studies in both human and mice myocytes where mutation in SK1 and SK3 channel subunits suppressed wild-type SK2 currents (163, 164). As shown in both human and animal cells, SK channels are rapidly activated by a rise in $[Ca^{2+}]_i$ (27, 30), at a rate similar for the rapid activation of ligand-gated ion channels, with all three subtypes exhibiting a similar Ca^{2+} dose-response relationship, yielding half maximal activation at approximately 300 nM $[Ca^{2+}]_i$ with a Hill coefficient of ~4 (165-167). This gives rise to a fast activating inwardly rectifying K^+ current (168-170). The activation

of SK channels is achieved solely by submicromolar $[Ca^{2+}]_i$ and is voltage-independent, making SK a unique class among KCa channels (161). These characteristics allow SK channels to directly translate changes in intracellular Ca^{2+} with changes in K^+ conductance (171). However, Ca^{2+} does not bind directly to SK channels but to calmodulin (CaM) which is constitutively bound to the channel subunit via a CaM-binding domain (CaMBD) in the C-terminus of each α-subunit (Fig. 1.10).

In hippocampal neurons LTCCs and SK channels have been shown to be functionally coupled, exploiting the proximity and submembrane calcium microdomains, with the latter contributing to the regulation of neuronal excitability and function in different brain regions (161, 172). This regulation is controlled by the level of $[Ca^{2+}]_i$, which rises along with neuronal firing activity and leads to a remarkable increase in SK current amplitude providing a negative-feedback mechanism reducing neuronal excitability by prolongation of the AHP (173). In addition, the coupling between L-type Ca^{2+} channels (LTCCs) and SK channels has been described in cardiac tissue, which is achieved by colocalization of the 2 channels via their interaction with the cytoskeletal protein α-actinin 2 (174).

1.9.1 Pharmacological inhibition and identification of SK channels

SK channels were first characterised pharmacologically in cultured rat skeletal muscles using the toxin apamin (175). This octadecapeptide, found in the venom of the honey bee (Apis mellifera), was one of the first peptides shown to block selectively the SK channels and was used in their identification and characterization (176, 177). SK channels have been shown to be selectively blocked by apamin, in human and mouse atrial cells, and in Xenopus oocytes expression vector, in concentrations ranging from 50 pM to 100 nM (27, 178), which distinguish them from all other KCa channels. Dose-response curves revealed specific affinity for the apamin-induced inhibition of the three SK channel-subtypes, which could allow the determination of the expression pattern of the different subtypes in native tissue (179). Besides apamin, SK channel inhibition can be achieved by using other blockers, including scorpion toxins such as scyllatoxin and tamapin (161). For example, by delineating the channel-binding surfaces of two toxins (Leiurotoxin I and PO5) Lei-Dab[7] was generated,

which represents a highly selective inhibitor of SK2 channels (180). Later, different non-peptidic selective blockers of SK channels, like dequalinium, were identified (181) and the development of this chemotype led to other derivate agents such as UCL1684, which display similar potency to apamin (182). During an initial structure-activity relationship (SAR) study, Gentles. et al. described the level of activity of a small neutral molecule, N-(pyridin-2-yl)-4- (pyridin-2-yl)thiazol-2-amine (ICA), which showed excellent potency as an SK blocker. The compound, which display the [^{125}I] apamin binding site, appears to compete off the peptide for the apamin binding site and they hypothesized that it could act by blocking the channels through its chelation to a cation (183). A different type of compounds like isoquinoline analogues related to bicuculline and N-methyl laudanosine have been reported, as well as the non-apamin displacing 2-aminobenzimidazoles, such as NS8593 (184, 185). The latter represent an example of a novel class of synthetic SK channel inhibitors that do not block the channel pore, rather acting as negative gating modulators (186, 187). A compound from this class, (R)-N-(benzimidazol-2-yl)-1,2,3,4- tetrahydro-1-naphthylamine (NS8593), has been shown, in human, mice and rat neurons, to decrease the Ca^{2+}-sensitivity of SK channels, and inhibited all the SK1-3 subtypes indiscriminately (at 500 nM [Ca^{2+}]$_i$), however, this only slightly affected the maximal Ca^{2+} activated SK current (186). Although these compounds appear promising, the classical SK channels pharmacology has largely focused on the peptide apamin, which acts as an allosteric inhibitor occluding the pore of SK channels (188). As stated earlier, SK-subtypes have differential sensitivity toward apamin, with SK2 channels being highly sensitive (IC$_{50}$ 0.03–0.14 nM) whereas SK1 channels are the least sensitive (IC$_{50}$ in the 0.1–12 nM) and SK3 channels are intermediate (IC$_{50}$ 0.6–4 nM) (179, 189). The binding site for apamin is located in both the pore region, between S5 and S6, and at a serine residue located in the extracellular region between S3 and S4 (178, 190). The lower sensitivity of SK1 channels to apamin compared to SK2 channels is due to replacement of this serine residue with a threonine on the SK1 subunit (190, 191). Apamin, targeting SK channels, has been studied as a possible therapeutic treatment for learning deficit, in preservation of red blood cells and also for Parkinson disorders (192, 193). However, if on one hand the specific distribution of apamin in the central nervous system (CNS) and its capacity to cross the brain blood barrier (BBB) make a drug delivery system based on apamin feasible, the

toxicity of this peptide does not permit the use of it (194). In fact, the administration of apamin caused neuronal over-excitability with epileptic activity and tremors with a relatively low LD_{50} (2.5 μM/Kg) (194, 195).

Therefore, attention has been switched to another compound, briefly introduced earlier, N-(pyridin-2-yl)-4- (pyridin-2-yl)thiazol-2-amine, also known as ICA, which is considered as a pore blocker of SK channels acting at the apamin binding site (183, 196). This compound represents a 2-aminothiazol derivate which showed high potency and selectivity for the inhibition of cardiac SK channels (29, 183). Moreover, the antiarrhythmic effects of this small neutral molecule has been shown in rat, guinea pig, and rabbit ex vivo and in vivo models of AF (196) as well as in isolated rat right atrium (197). Finally, ICA has also been shown to significantly prolong APD_{90} in isolated myocytes from sinus rhythm patients (29).

1.9.2 SK channels in the heart

Changes of $[Ca^{2+}]_i$ in cardiac muscle significantly influence various transmembrane currents and at least some of the resultant effects may be accounted for by assuming the existence of Ca^{2+}-activated K^+ channels in the heart. Nevertheless, a review published by Eisner in 1983 concluded that there were not convincing results to support the existence of a K^+-specific current activated solely by an increase in $[Ca^{2+}]_i$ (i.e. SK current) (198). However, a few years later, the presence of a Ca^{2+}-activated K^+ current, larger in atria than ventricles was reported (199). Until a decade ago, after no further significant publications about the functional role of cardiac SK channels were reported, Xu et al. described the molecular identity and functional significance of SK channels in human and mouse hearts. With this study they confirmed the observation made by Giles et.al in 1988, showing the presence of SK2 channels functionally expressed predominantly in the atria compared to the ventricle, in accordance with the apamin-sensitive current recorded in both chambers (27). These results were confirmed two years later by Tuteja et al., who also showed atrial selective distribution of both SK1 and SK2 channel subtypes in mouse hearts, through quantification of SK channels transcripts using real-time quantitative PCR (RT-PCR) from single, isolated cardiomyocytes (28). SK channels have since been

reported, by many studies, to be expressed in atrial cardiomyocytes of various species, including rats, mice, rabbits, dogs and humans (27-29, 196, 200-202).

However, the function played by these channels is still disputed. While SK channels have been shown to contribute to the AHP modulating the firing properties of neurons, in cardiomyocytes the SK current, recorded as apamin-sensitive current activated by increased $[Ca^{2+}]_i$, has been shown to contribute to the late phase of the cardiac repolarization (27, 28). In contrast, Nagy et al. questioned the significance of previous observations concluding that SK channels play a negligible role in cardiac repolarization under physiological conditions. Although the study was conducted using different conditions of either high $[Ca^{2+}]_i$ (900nM) or under attenuated repolarisation reserve with 100nM apamin (203), it represents a solid and elegant study, which strongly opposes the previous findings. However, as they speculate, SK channels role in disease needs further investigation. During AF, the tenfold increase in atrial rate substantially raises $[Ca^{2+}]_i$ (14, 84), which could trigger SK channels and promote APD shortening favouring the perpetuation of AF. Hence, SK channels may represent an attractive target to modulate atrial conduction during atrial arrhythmias.

1.9.3 SK channels in chronic AF-remodelled atria

As described earlier in this chapter, chronic AF is characterized by a shortening of the AP due to electrical remodelling (204). The first indication that SK might play a role in atrial electrical remodelling was demonstrated by Ozgen, et al. (2007), who showed that intermitting burst focus in PVs leads to APD shortening mediated by SK2 channel trafficking to the membrane and consequent upregulation of the apamin-sensitive outward current, which facilitates propagation of triggered activity (201). However, the duration of AF in this study was only of few hours (3 hours intermittent burst pacing), and so shouldn't be expected to cause any remodelling. Subsequently, Zhang et al. availing themselves of a mouse model with overexpression of SK2 channel, provided evidence of a possible role of these channels in producing profound changes in AVN conduction under pathological conditions characterized by increased $[Ca^{2+}]_i$, like AF (162). Additional support to these results was provided by Li, et al. in 2009, who reported prolongation of the atrial APD, especially during late repolarization, in SK2 null mutant mice compared to WT littermates. Moreover, APD were further prolonged in homozygous mutant mice compared to

heterozygous animals, consistent with a significant role of SK2 channel in the repolarization of the atrial myocytes. These results were solidified by the evidence of absence of apamin-sensitive current in atrial myocytes isolated from SK2 homozygous mutant animals On the other hand, no changes in ventricular APD was observed in the mutant mice compared to the WT counterpart. In addition, during *in vivo* electrophysiological recordings in SK2 knockout mice, the occurrence of atrial arrhythmias associated with prolongation of the AVN conduction was observed. Importantly, null mutation of the SK2 and relative APs prolongation promoted atrial arrhythmias, possibly correlated with increased frequency of EADs (200). These important findings highlight the possibility for a pro-arrhythmic effect consequent to pharmacological inhibition of SK channels, with relevant clinical implications. A year later, in a meta-analysis of genome-wide association studies Ellinor et al. identified a new locus for lone AF (atrial fibrillation in the absence of overt cardiovascular disease or precipitating illness) (205) at the calcium activated potassium channel gene, KCNN3, which, however, does not necessarily indicate involvement in the pathogenesis of AF (206). However, more recent studies corroborated the association of synonymous single-nucleotide polymorphisms (SNP) in KCNN3 with lone AF (207, 208). Additional ex vivo and in vivo studies with small animal models of experimental AF, demonstrated the antiarrhythmic effects of SK channel inhibition (196, 209, 210). Relevantly, quantitative real-time PCR analyses showed significantly higher transcript for SK2 and SK3 subtypes compared to SK1 in human atria, with the first two being ~50% lower in AF compared to sinus rhythm indicating a profound change of gene expression consequent to atria remodelling (29). In addition, the study revealed no effect of the putative selective blocker ICA (1 µM) or the negative allosteric modulator NS8593 on chronic AF patients, while both SK channels blockers reduced, albeit moderately, inwardly rectifying K^+ current in sinus rhythm patients (29). Other studies reported similar results (211, 212), while others have reported a significantly increase in atrial SK2 current density in patients with persistent AF (213). Skibsbye et al. hypothesized a possible up-regulation of SK channels followed by down-regulation during long-lasting AF consequent to electrical remodelling (29). A more recent study reported comparable findings, with significant reduction of mRNA and protein levels for all SK1-3 subtypes in chronic AF, however, the resultant increase in current is explained by an improved SK

channel $[Ca^{2+}]_i$ - sensitivity in AF patients mainly due to Ca^{2+}/Calmodulin-dependent protein kinase II (CaMKII) phosphorylation and $[Ca^{2+}]_i$ elevation (30). CaMKII can increase Ca^{2+} entry through L-type Ca^{2+} channels and affect Ca^{2+} uptake and release through the SR by phosphorylation of cardiac regulatory proteins like phospholamban (PLB) (214, 215). On the other hand, long-term defence mechanisms against the progressive Ca^{2+} loading due to the fast atrial rate in AF, include decreased I_{Ca} and reduced Ca^{2+} entry aimed to prevent Ca^{2+} overload (80, 81, 216), which might explain a reduced/absent I_{SK} in chronic AF (cAF).

1.9.4 I_{SK} in new-onset or paroxysmal AF

Based on the discrepancies between the mentioned studies, currently the role of SK channels and whether I_{SK} is up-or down-regulated in remodelled atria is still far from being clear. However, it is true that some studies on animal models of acutely induced AF (i.e. non-remodelled atria) showed an antiarrhythmic effect of SK channels inhibition in both ex vivo and in vivo (196, 197, 209, 210). Diness et al. showed for the first time the possibility of prevention and reversion of AF consequent to inhibition of SK channels. Specifically, two pore blockers (UCL1684 and ICA) and a negative modulator (NS8593) were tested in 3 different species (rat, guinea pig and rabbit) both in isolated hearts and in an vivo model of paroxysmal AF (196). Relevant to the study presented in this thesis, ICA (1μM) terminated and prevented the reinduction of induced-AF in all hearts (196). These results suggests that SK channels may participate in initiation and perpetuation of AF. However, studies on single atrial cells from SK2 null mutant mice showed APD_{90} prolongation compared to control, which was associated with increased propensity to EADs and AF inducibility (200). This proposes a possible protective role played by SK channels against the insurgence of AF. Clearly in contrast with previous findings made by Diness et al., this has important clinical implications concerning the current use of pharmacological inhibitors of K^+ channels, and on the future possibility of developing a pharmacological treatment targeting specifically SK channels in the atria. Especially, given the contrasting findings, further investigation of SK channels role in new-onset or paroxysmal AF are needed; circumstances under which I_{SK} has not been studied yet in human atrial myocytes. In fact, considering that remodelling has not yet occurred during these

conditions, SK channels contribution to cardiac repolarization may still be relevant to physiological conditions. Moreover, it has been shown that cellular Ca^{2+}-overload, consequent to the increased atrial rate (84), may play a role in the pathogenesis of short-term electrical and mechanical dysfunction, which can occur even after brief periods of atrial tachycardia, producing a shortening of the aERP (92, 99, 100, 217-219). Therefore, taken all together, these studies leave space for speculation of a possible role of I_{SK} during paroxysmal AF, where channels expression is not compromised and the increased $[Ca^{2+}]_i$ can increase the current to an extent that it may substantially contribute to the shortening of aERP, thus promoting the perpetuation of AF.

1.10 General Aims

The previously described discrepancies between studies raise doubts regarding the possible role of SK channels in cardiac repolarization during both short and long-term AF. The majority of the single-cell studies cited above have investigated I_{SK} activity either with non-physiological solutions or calculated $[Ca^{2+}]_i$, which can lead to misleading results. Moreover, most of the patch-clamp experiments were performed in myocytes from cAF patients, where SK channels have been found to be down-regulated. On the other hand, only one study (203) focused the attention on the role of I_{SK} under physiological conditions, although mostly in the ventricle. Hence, there is a demand for further investigation of I_{SK} under physiological conditions in atria. In particular, as mentioned above, this could be especially relevant to new-onset AF where $[Ca^{2+}]_i$ is elevated by the increased atrial rate. Therefore, the overall aim of this thesis is to partially elucidate these focal points by addressing the role of SK channel under physiological conditions, using a well-established (apamin) and a putative selective (ICA) blocker, using the ruptured whole-cell patch clamp technique in human and rabbit atrial cells. Along with electrophysiological recordings, the role of Ca^{2+} in the activation of SK channels will be investigated by using precisely measured buffered $[Ca^{2+}]_i$ exceeding global average systolic levels. Also, high pacing frequency will be used, intended to elevate $[Ca^{2+}]_i$ physiologically in atrial cells.

1.10.1 Specific aims

• Learn whole cell patch-clamp technique availing of a well-studied pharmacological intervention. By this means, I have tested the block provided by $BaCl_2$ on I_{K1} to verify my patch-clamping configuration, reversal of intervention and software precision in order to create a positive control. (Chapter 2)

• Use calcium imaging techniques to generate precise $[Ca^{2+}]_i$ (typical of global diastolic-to-systolic values) solutions by titration of Ca^{2+} with a fast buffer (BAPTA). Verify the $[Ca^{2+}]_i$ in cells and generate calibration curves to compare the measurements in vitro with those in single rabbit left atrial myocytes (Chapter 3)

• Test I_{SK} $[Ca^{2+}]_i$ -sensitivity by generating a Ca^{2+} dose-response curve for I_{SK} at both room and physiological temperature using inside-out patch clamp technique for electrical recordings. (Chapter 4)

• Utilize the buffered $[Ca^{2+}]_i$ solutions to study I_{SK} in voltage-clamped single rabbit and human atrial myocytes using the two SK pore blockers mentioned above. (Chapter 5)

• Investigate the possible I_{SK} contribution to AP repolarization, in human and rabbit atrial myocytes, under physiological conditions and at high pacing frequency meant to increase $[Ca^{2+}]_i$ physiologically, using ICA at both selective and unselective concentrations. (Chapter 6)

• Reproduce a protocol to gradually raise $[Ca^{2+}]_i$ through activation of sodium-calcium exchanger current ($I_{Na/Ca}$). Then exploit this protocol to elicit I_{SK} and investigate the effect of the SK blocker ICA at physiological $[K^+]$ in both atrial and ventricle single rabbit myocytes. (Chapter 7)

Chapter 2 Measurements of inward rectifying potassium current (I_{K1}) in rabbit and human cardiomyocytes: validation of patch-clamp method using a predictable pharmacological response

2.1 Background

The small conductance calcium-activated K^+ (SK) channels, as the name suggests, are characterized by a current of small amplitude (I_{SK}), as previous studies among different species have demonstrated. For example, in the study from Yu et al., I_{SK} (recorded as apamin-sensitive current, I_{SK}) at – 120 mV was – 1.5 ± 0.2 pA/pF in patients from sinus rhythm, using 100nM apamin with 900nM $[Ca^{2+}]_i$ (211), while Xu et al. reported I_{SK} of -2.5 pA/pF at -120mV in mouse atrial myocytes with 50pM apamin and 500nM $[Ca^{2+}]_i$ (27). Interestingly, Nagy et al. reported a complete lack of effect of 100nM apamin on SK current in both action potential and voltage clamped (with 900nM $[Ca^{2+}]_i$) single canine and rat myocytes (203). Therefore, albeit the presence of high $[Ca^{2+}]_i$ and the use of reasonably elevated concentration of a specific SK channel blocker (apamin) the resulting current is small and potentially difficult to detect. For this reason, before starting the investigation of I_{SK} I sought for a positive control relying on a stimulation protocol similar to those observed in previous SK current studies (27, 29, 203). Thus, a ramp voltage-pulse protocol was chosen to test temporal stability, timing, and reversibility of a well-established pharmacological intervention: the inwardly rectifying K^+ current (I_{K1}) block by Ba^{2+}. In fact, this extracellular ion has been shown to be a potent selective blocker of both the inward and outward components of I_{K1} in a voltage-dependent manner (220-222). Although, at high concentration (i.e. >10mM) barium is known to have multiple off-target effects, such as L-type calcium channels and, consequently, it can be unspecific for I_{K1} (223, 224). However, at the concentration used in my experiments (0.5mM) Ba^{2+} provides a selective block of I_{K1} (225, 226). Importantly, barium has been widely adopted by previous publications to show the difference of rectification properties of I_{K1} between ventricle and atrium. From these studies I_{K1} current density results are higher in the ventricles than in the atria and the outward current-voltage (I/V) relationship, which is characterized by an "n shape" or ''negative slope conductance'' at depolarized potentials (from -60mV

and -20mV) is virtually absent in atrial cells but tends to be prominent in ventricular myocyte I_{K1} (199, 227-229). Also, the outward component of I_{K1} plays the most important physiological role, generating the resting membrane potential and modulating the final repolarization phase of the action potential in both atria and ventricle (23, 199). However, the inward rectifier currents like I_{K1}, preferentially conduct K^+ inwardly rather than in the outward direction. In fact, at voltages negative to the equilibrium potential for potassium (more negative than -95.9 mV based on [K^+] in solutions) the conductance of the I_{K1} ion channels is time- and voltage-independent, so the I/V relationship for I_{K1} is a straight line, also known as an ohmic relationship. Moreover, at these voltages, the current density of I_{K1} is relatively large and the block provided by Ba^{2+} is expected to be equally big, which drive the rationale for the design of the positive control protocol.

2.2 Section aims

• Learn whole cell patch-clamp technique availing of a predictable pharmacological experiment with barium chloride ($BaCl_2$ or Ba^{2+}).

• Seek for a solid response in order to test my patch-clamping configuration, reversal of intervention and software precision.

• Measure currents using voltage ramps to check and validate voltage control (theoretical E_K versus observed reversal potential), especially when using corrections like liquid-liquid junction potential (LLJP).

• Create a positive control by testing temporal stability, timing, and reversibility of K^+ current (I_{K1}) block by Ba^{2+}.

Ba^{2+} was chosen because is well known and produces a predictable effect at 0.5 mM providing a selective block of I_{K1} at this concentration (222, 225). Through measurements of I_{K1}, one of the aims was to check and validate the voltage control by comparing the measured E_K value to the calculated value. To do so, the bigger ventricle I_{K1} current density was exploited, which allowed to measure E_K directly from raw traces recorded using my setup, as shown later in this chapter. Secondly, this study also aimed to study the already observed substantial difference in I_{K1} densities between atria and ventricles in rabbits

(199). In particular, this study was performed in rabbit left atrial (LA) and ventricle (LV) and human right atrial (RA) myocytes. Furthermore, since I_{SK} will be studied on both single rabbit and human atrial cardiomyocytes, it was required to test inter-cellular as well as inter animal or patient variation in both control currents and drug response. The purpose was to optimise the protocol by accounting for any variation in currents under drug or simply control conditions. This includes biological variations as well as lack of drug effect. Finally, given the possible correlation of I_{K1} with arrythmias (230, 231) and its striking inward rectification properties, it appeared a perfect starter model for the study of potassium currents that share these characteristics, such as I_{SK}

2.3 Methods

2.3.1 Solutions for cell isolation of rabbit cardiomyocytes

- **Isolation medium:** 130 mM NaCl, 4.5 mM KCl, 3.5 mM $MgCl_2 \cdot 6H_2O$, 0.4 mM NaH_2PO_4, 5 mM HEPES, 10 mM glucose. Solution pH was adjusted to 7.25 at 37°C using 1 M KOH.

- **Krebs solution:** 120 mM NaCl, 20 mM HEPES, 5.4 mM KCl, 0.52 mM NaH2PO4, 3.5 mM $MgCl_2 \cdot 6H_2O$, 20 mM taurine, 10 mM creatine and 11.1.mM glucose hexahydrate. Solution pH was adjusted to 7.4 at 37°C using 1 M NaOH.

- **Kraft-Bruhe (KB) solution**: 70 mM KOH, 40 mM KCl, 50 mM L-glutamic acid, 20 mM taurine, 20 mM KH_2PO_4, 3 mM $MgCl_2 6H_2O$, 10 mM glucose, 10 mM HEPES, 0.5 mM EGTA, pH 7.4 at 37°C using 1 M KOH.
- **Enzyme**: Collagenase enzyme (Type II powder; Worthington Biochemical Corporation) was added to KB solution (217 IU/mL) and re-circulated through the perfusion system for ~5 minutes until the heart tissue began to moderately swell and lighten in colour.

2.3.2 Animals

Animals used in this work were male New Zealand White rabbits (2.5-3.5kg) sourced from Envigo (Huntingdon, UK). Procedures and experiments involving rabbit cells (UK Project Licences: 60/4206, 70/8835) were approved by Glasgow University Ethics Review Committee and conformed with the guidelines from Directive 2010/63/EU of the European Parliament on the protection of animals used for scientific purposes.

2.3.3 Cell isolation of rabbit cardiomyocytes

All animal handling and procedures including surgical interventions and Langendorff procedures were carried out by laboratory technicians Aileen Rankine and Michael Dunne. Ventricular and atrial myocytes were isolated from male New Zealand White rabbits. Rabbits were anaesthetized of 0.5mL/kg Euthatal (200 mg/mL, Sodium pentobarbitone, Rhone Merieux Inc, Athens, GA, USA) mixed with 500IU of heparin (CP Pharmaceutical Ltd, Wrexham, UK) via the

left marginal ear vein. Following absence of pain reflexes, hearts were quickly excised with ~0.5 cm of the ascending aorta and placed in ice-cold KB (Ca^{2+}-free) solution to inhibit muscle contraction, which has significant beneficial effects on the long-term viability of adult cardiac myocyte (232). Excess tissue was trimmed away and the heart was connected to Langendorff perfusion system (Fig. 2.1). The heart was retrogradely perfused with calcium-free oxygenated KB (37°C) using a peristaltic pump at a constant flow rate of 20ml/min for 5 minutes. The heart was then perfused with enzyme solution, which was collected and re-circulated. After 3 min, 100 mM $CaCl_2$ solution was added to achieve a final calcium concentration of 0.05 mM. The presence of calcium ions has been reported to enhance the binding of collagen-binding domain to collagen (233). Digestion was continued for 5-6 minutes, until the heart began to soften to the touch and lighten in colour. A this point the heart was perfused with KB solution containing a 10 g/L bovine serum albumin (BSA) containing 0.075 mM calcium. In infarcted hearts, the apex and a 3-5 mm rim around the infarct zone were removed. This procedure was adopted because the edge or border zone cells were subjected to ischaemia and then reperfused, which means that they present a varying extent of damage. So, eventual results obtained from these cells would be difficult to evaluate statistically, given the extensive electrophysiologic inhomogeneity within the ischemic subendocardium (234). The equivalent apical region was removed in Sham animals to keep consistency between sham and MI rabbits. Perfusion was stopped and the heart was dissected. The ventricles were cut into ~1 mm^2 segments in BSA solution. Tissue pieces were placed in a 15 mL culture flask and placed on a shaker for 20 min. Cells were gently triturated with a Pasteur pipette to further dissociate myocytes, and the supernatant was filtered through polyamide mesh (250 μm pore size) prior to resuspension in KB solution.

2.3.4 Rabbit cells preparation for experimentation

Ventricle cells were left to settle by gravity only (exploiting cell size) for 10min. Atrial cells were manually centrifuged for <1min at ~500rpm (31g). All cells experienced serial incubations using 15mL Falcon tubes containing Krebs and increasing calcium concentrations (using 1M stock $CaCl_2$ solution): 100 μM, 300 μM, 1 mM, and 1.8 mM $CaCl_2$, respectively. Experiments were only performed

on cells with clear striation and showing no signs of abnormal electrical behaviour, such as EADs, alternans, or irregular beats.
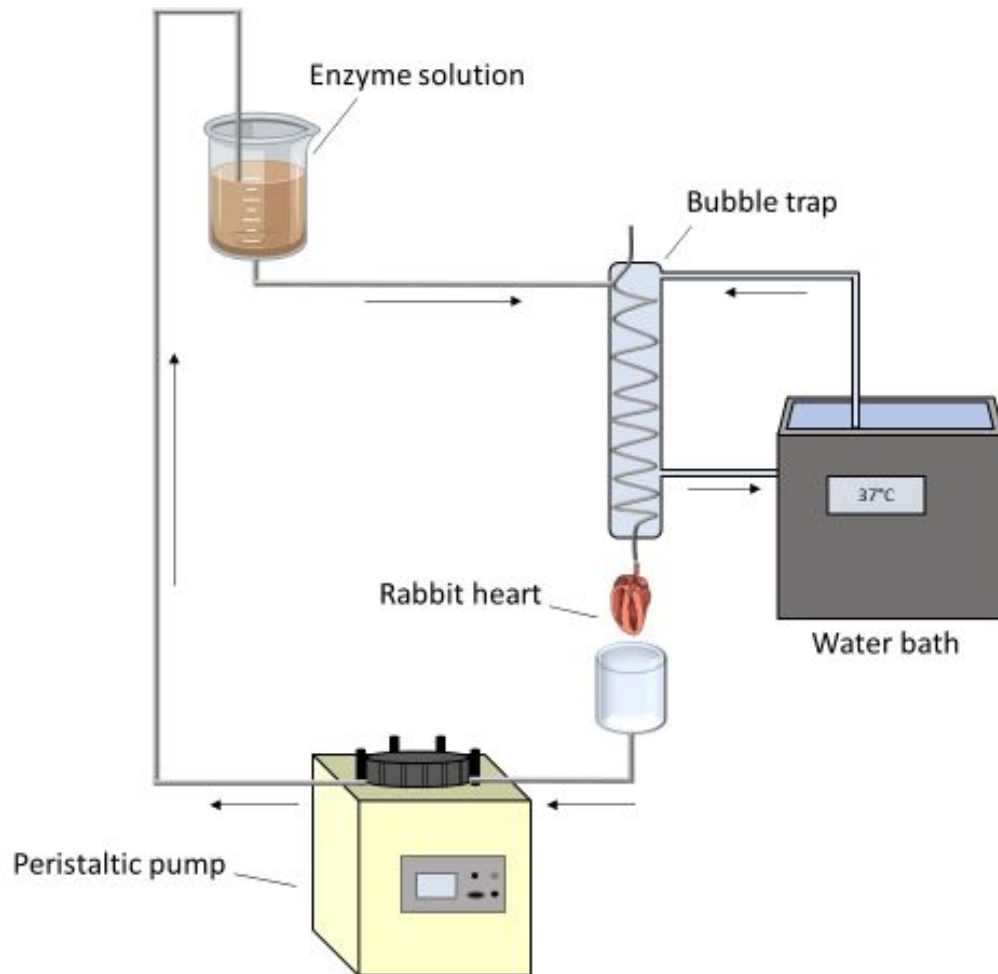
Figure 2.1 Schematic depiction of the Langendorff perfusion system.
Simplified diagram of Langendorff setup using peristaltic pump and water bath system for retro-perfusion of coronary arteries with enzyme solution at 37°C.

2.3.5 Specimen collection and cell isolation of human cardiomyocytes

2.3.5.1 Isolation solutions:

- **Ca-free solution 'B':** NaCl 120 mM, KCl 5.4 mM, MgSO$_4$ 5 mM, pyruvate 5 mM, glucose 20 mM, taurine 20 mM, NaHEPES 10 mM, nitrilotriacetic acid 5 mM and titrated to pH 7.0 with NaOH 1 M solution.
- **solution 'C':** (NaCl 120 mM, KCl 5.4 mM, MgSO$_4$ 5 mM, pyruvate 5 mM, glucose 20 mM, taurine 20 mM, NaHEPES 10 mM, nitrilotriacetic acid 5 mM, CaCl$_2$ 50 µM and titrated to pH 7.0 with NaOH 1M solution)
- **Enzymes:** Collagenase (CLS 1 Type 1, Worthington 330 IU/ml) and Protease enzyme (protease type XXIV powder, final protease concentration: 4U/ml; Worthington Biochemical Corporation) were added to KB solution (217 IU/mL).

2.3.5.2 Ethical approval

The tip of the right atrial appendage was obtained from patients undergoing cardiac surgery whose characteristics are shown in Table 1. Procedures and experiments involving human atrial cells were approved by the West of Scotland Research Ethics Service REC 99MC002 (up to 20th July 2017), then REC 17/WS/0134 (from 21st July 2017). Written, informed consent was obtained from all patients. The investigation conforms with the principles outlined in the Declaration of Helsinki(235).

2.3.5.3 Cell isolation

The tip of the right atrial appendage (weight: typically, 0.25 g) was removed at the time of cardiac cannulation for aortopulmonary bypass and collected in 50ml KB (Kraft-Bruhe solution) in a labelled plastic screw top bottle. Then the tissue was placed on a glass slide, cleaned of visible connective tissue and fat and chopped with scalpels into chunks of ~1mm^3 (in KB). Subsequently, these chunks were transported to the laboratory for processing within 30-35 minutes of excision. Atrial cells were isolated by enzymatic dissociation and mechanical disaggregation, using the chunk method described in detail

previously by Escande et al. (236) and subsequently modified by Harding (237) and Workman(79). These chunks were then transferred to a beaker which was placed into a water bath maintained at 37°C, shaken at 130 strokes per minute and continuously oxygenated in 40 ml nominally Ca-free solution 'B'. The 'chunks' were hand filtered through nylon gauze (200 μm mesh, Barr & Wray, Lanark, UK) and transferred to another beaker containing a fresh sample of 40 ml oxygenated solution 'B' at 3-minute intervals in order to prevent hypoxia and remove any toxic metabolites like methylglyoxal (a by-product of glycolysis). After a total of 12 minutes agitation the sample was transferred to another beaker containing 15 ml solution 'C' with protease (Type XXIV, Sigma, 4 IU/ml) added and were incubated under identical conditions for a further 45 minutes. This semi-digested sample was then placed in another 12 ml of modified solution 'C' with collagenase (CLS 1 Type 1, Worthington 330 IU/ml) added in the absence of protease and incubated for consecutive periods of 15, 15 and 20 minutes. Each of these three cell suspensions was filtered through nylon gauze, as before. These three "filtrates" formed three consecutive aliquots which were then centrifuged (Model $P_{K_1}10$, A.L.C. International) for two minutes at 40 g. The resulting supernatant was aspirated by hand and discarded and the remaining cells were re-suspended for a maximum of 10 minutes in 1 ml of Kraftbrühe (KB) solution214 (KOH 70 mM, KCl 40nM, L-glutamic acid 50 mM, taurine 20 mM, KH_2PO_4 20 mM, $MgCl_2$ 3 mM, glucose 10 mM, NaHEPES 10 mM, EGTA 0.5 mM and titrated to a pH of 7.2 with 1M KOH solution) in order to wash off any remaining enzymes.

Patients characteristics	No. of patients	n(%)	
Patient demographics			
male	18	82	
Age (years)	70.1±2.3		
Female	4	18	
Age (years)	70±3.5		
Mean heart rate (beats/min)	65.1±2.6		
Pre-op drugs			
Beta-Blocker	17	77	
CCB	3	14	
ACE- Inhibitor	14	64	
Digoxin	1	5	
Nicorandil	3	14	
Eplerenone	0	0	
Nitrate	14	64	
Statin	20	91	
Other(s)	6	27	
Operative Procedure			
CABG	20	91	
AVR	6	27	
CABG + AVR	6	27	
CABG+MVR	0	0	
LVEF			
None (Normal)	9	41	
Mild	0	0	
Moderate	3	14	
Severe	1	5	
Pre-op disease			
History of HT	12	55	
History of MI	10	46	
Angina	17	77	
Diabetes	5	23	
Tissue			
AA	18	82	
AW	4	18	

Table 1 Patient clinical characteristics.

CABG = coronary artery bypass graft, MVR = mitral valve replacement, AVR = aortic valve replacement, Pre-op = before surgery, ACE = angiotensin converting enzyme, CCB = calcium channel blocker, LVEF =left ventricular ejection fraction, MI= myocardial infarction, HT= hypertension, AA=atrial appendage, AW= atrial wall, PFA=Paraformaldehyde.

The centrifugation process was then repeated and after removing as much of the KB solution as possible the cells were re-suspended in 1 ml of a low calcium solution (NaCl 130 mM, KCl 4 mM, $CaCl_2$ 0.2 mM, $MgCl_2$ 1 mM, NaHEPES 10 mM, glucose 10 mM and titrated to a pH of 7.4 with 1M NaOH solution). Each of the three aliquots was transferred to a separate petri-dish for storage at room temperature prior to use in experiments. Cells were examined under high power (x40) light microscopy (Nikon TMS microscope) and cells which were isolated, striated, elongated, straight-edged and stable in the perfusion chamber were selected for electrophysiological recordings (Fig. 2.2).
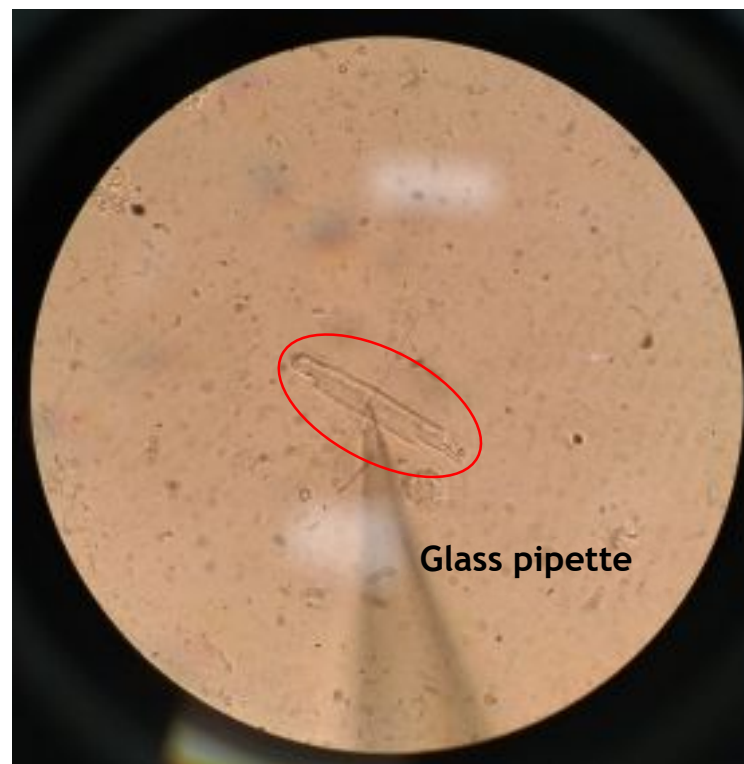
Figure 2.2 Photograph of human atrial myocyte (red circle) obtained by 40x resolution objective during whole-cell patch clamp configuration.

2.4 Solutions and experimental conditions

2.4.1 Solution used for functional characterization of both human and rabbit cardiomyocytes

In general, the perfusate, or external solution (EPSS2: extracellular physiological salt solution), was composed of: 140 mM NaCl, 4 mM KCl, 1.8 mM $CaCl_2 \cdot 2H_2O$), 1.0 mM $MgCl_2 \cdot 6H_2O$, 11 mM glucose, 10 mM HEPES. pH adjusted to 7.4 with 1M NaOH. The external perfusate could be collected to measure drug concentrations.

The internal (PIP35: pipette solution) solution, contained: 130mM K-aspartate, 15mM KCl, 10mM NaCl, 1mM $MgCl_2 \cdot 6H_2O$, 10mM HEPES, 0.1mM EGTA, pH adjusted to 7.25 with 1M KOH. The resulting liquid–liquid junction potential (+9 mV; bath relative to pipette) was compensated for *a priori* (79, 238). All experiments were performed at 37°C.

2.4.2 Electrical recordings and analysis

Electrophysiological signals were recorded from single cardiac myocytes in the whole-cell ruptured patch clamp configuration using AxoClamp 2B patch-clamp amplifier (Axon Instruments) and WinWCP 5.3.4 electrophysiology software (J. Dempster, University of Strathclyde, UK). Patch pipettes (2.5-5 MΩ filled with intracellular solution) were pulled from borosilicate glass capillaries 1.2 OD

+50 mV

0 mV

1000 ms

50 mV

-120 mV
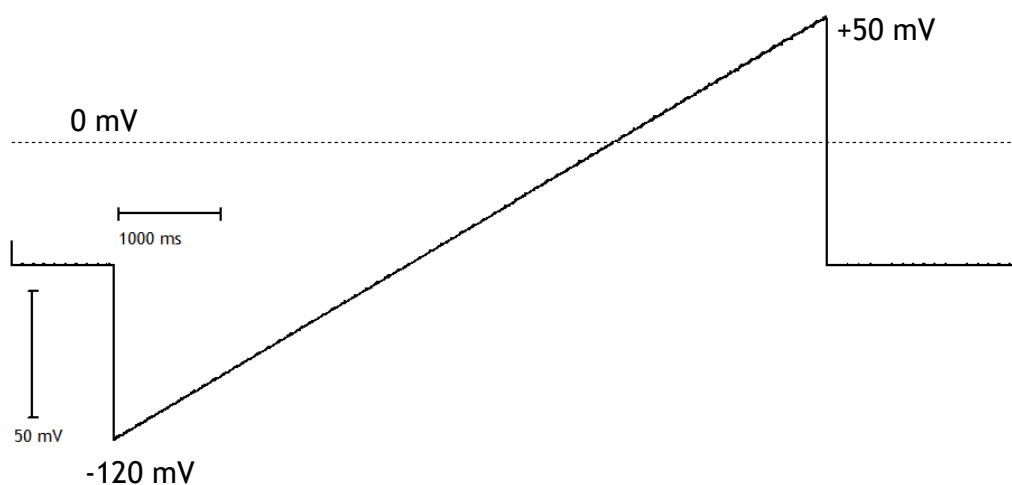
Figure 2.3 Voltage ramp protocol used during recordings of I_{K1}

(outer diameter) x 0.69 x 100 L (length) mm (Harvard Apparatus, USA) with a gravity puller (model PP-83, NARISHIGE, USA). Voltage-dependent activation of I_{K1} was measured by stimulating cells at 0.1 Hz from a holding potential of −50 mV, with voltage ramp (for quasi steady-state) of 7s duration increasing from −120 to +50 mV (Fig. 2.3) replicating from Marshall et al.(222). I_{K1} amplitude was calculated as the barium-sensitive current at -115mv. Data are presented as mean ± standard error of the mean (s.e.m) unless otherwise stated. Statistical analyses were performed using GraphPad Prism 8. Single comparison of means was conducted using standard 2-tailed t-test (paired where appropriate). For parametric data, one-way ANOVA followed by multiple comparison tests were used to compare three or more groups of data. For non-parametric, independent datasets, Mann-Whitney U test or Spearman correlation were used. All tests were set at a significance threshold of P<0.05.

2.5 Conversion of current amplitude to current density

The peak current (picoamperes, pA) at -115mV was normalized for each cell capacitance (picofarad, pF), which was calculated using the algorithm showed in the following equation (239):

$$C = \frac{Q}{V} = -\frac{1}{V} \iint\limits_{\Gamma} \varepsilon(x, y)\nabla\phi(x, y)\mathrm{d}\Gamma$$

Equation 1 The relationship between capacitance and the permittivity distribution can be formulated by this equation:
Where *Q* is the electric charge; *V* represents the potential difference between two electrodes forming the capacitance; *ε* *(x, y)* and *φ* *(x, y)* indicate the permittivity and electrical potential distributions, respectively; ∇ is the divergence: represents the volume density of the outward flux of a vector field from an infinitesimal volume around a given point; Γ stands for the electrode

Consequently to normalization I plotted the peak current density at -115mV, that is the electric current per unit of capacitance and has as units pA/pF for each cell at any conditions.

2.6 Principles of whole cell patch clamp

Neher and Sakmann originally described the whole cell configuration of the patch clamp technique as a variant used to measure ion currents within living cells (240). This technique requires the use of heat-polished micropipettes containing an electrolyte solution (similar to the intracellular milieu) and a silver chloride wire. The pipette is gently lowered onto the surface of an enzymatically isolated cardiac myocyte maintained in a perfusate solution which mimics the extracellular milieu. Using gentle suction, the pipette attaches to the cell and forms a tight, high resistance electrical seal with a patch of membrane in the order of approximately 100 GΩ. The advantage of a pipette-membrane seal of greater resistance, termed a giga-seal, is that background electrical noise or interference is reduced, less current 'leaks' around the pipette into the perfusion chamber reducing inaccuracy of measurements and the mechanical stability is improved. Once the seal is obtained the current flowing through the pipette is identical to the current flowing through the membrane covered by the pipette. At this point it is possible to rupture the patch of membrane by further application of gentle suction allowing low resistance access to the whole cell and enables the measurement of ion currents flowing across the whole cell membrane. This is known as the whole cell configuration and was used for the majority of experiments in this thesis. Measurements of these ion currents can be made using a single electrode voltage clamp technique. Using this technique, the cell membrane potential is controlled by use of an amplifier which both measures the membrane potential and can change it to a pre-set command potential by injection of the necessary amount of charge. The magnitude of this charge represents the size of the current that flows at the command potential and is measured using the same electrode. In order to limit vibration artefacts cells were permitted to sediment in the perfusion bath (RC-24E fast exchange perfusion chamber, Warner instruments) (Fig. 2.5) positioned on an air suspension table (Wentworth laboratories) (Fig. 2.4) coupled with an AxoClamp2B amplifier.

2.7 Measuring current or voltage using the whole cell patch clamp configuration

2.7.1 Patch clamp setup

The arrangement of the equipment for patch clamp is shown in Figure 2.5. The microscope, perfusion chamber, microelectrodes and micromanipulator (Narishige group) were mounted on an air table in order to minimise vibration and were all earthed to eliminate electrical noise. The reservoirs for external solution were mounted above the level of the perfusion chamber on the wire cage on the left. A suction bottle, located on the floor beneath the perfusion chamber, allowed the collection of external solution by the use of a pump. The amplifier, oscilloscope and computer, programmed to generate stimulus protocols and acquire data, were all placed in a tower on the right side (not in the picture). All the equipment was "isolated" inside a wire cage (Faraday cage) in order to minimize any electrical noise.
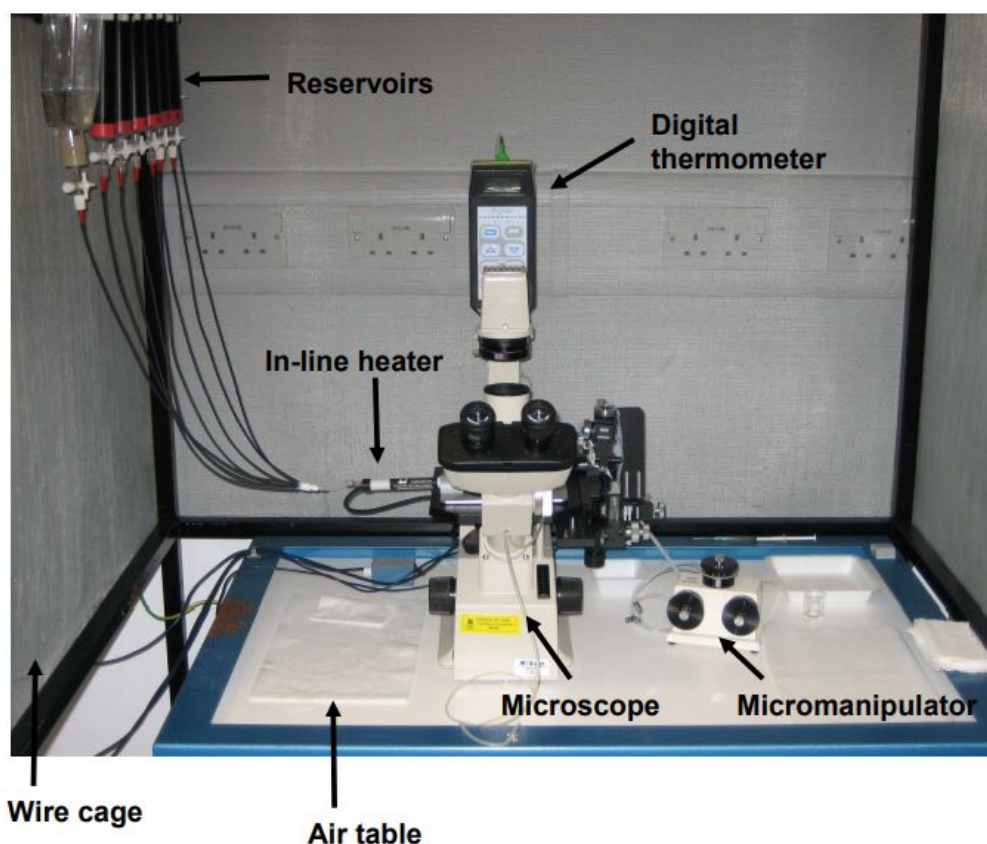
Figure 2.4 Picture of patch clamp equipment.
The perfusion chamber and microelectrodes were located on the microscope stage.

2.7.2 The perfusion chamber

After the isolation, a small aliquot (~200 μl) of cell suspension was dropped into the bath of the polycarbonate perfusion chamber (RC-24E fast exchange perfusion chamber, Warner) mounted on the stage of a microscope (Nikon TMS). The myocytes were allowed to settle and adhere to a glass coverslip that sealed the bottom of the well of the perfusion chamber illustrated in Figure 2.5. The External solution flowed into the perfusion port by gravity flow from a reservoir mounted at a higher level than the perfusion chamber at a rate of approximately 2 ml/minute. The diamond shape of the bath provides laminar solution flow and prevents cell from being washed away, while the very small

bath volume facilitates very fast solution exchange. Before the external solution entered the well it flowed through an in-line heater (Warner Instrument Corporation Model SH-27A Inline Heater) which heated the solution to 35-37°C. The temperature was monitored using a temperature probe placed inside the bath (see Fig. 2.6). Each reservoir is joined by a small channel which allowed equalisation of the volumes of solution among the wells. This means that from the perfusion port the solution could reach the suction tube in a continuous flow. The electrical circuit between the earth electrode and the recording electrode (in the bath) was completed using an agar bridge. The agar bridge well was filled with a 3 M KCl solution into which the earth electrode was placed. The role of the agar bridge was to keep the Cl^- concentration around the earth electrode constant, as fluctuations in the concentration of Cl^- would have resulted in an offset voltage between the earth and recording electrode. The agar bridges were made by heating short lengths of borosilicate glass capillaries without inner filaments (Clark electromedical instruments) into "U" shapes that were filled by immersion in agarose (3% Gibco BRL, Life Technologies inc. MD, USA) which was dissolved in 3 M KCl solution (salt bridges were stored in the 3 M KCl solution).

Suction
reservoir

Agar
bridge

Earth
electrode

Suction
tube slot

Agar
bridge
well

Perfusion
port

Top View

Bath

Glass pipette above the
bath chamber

Side view

3.8 mm
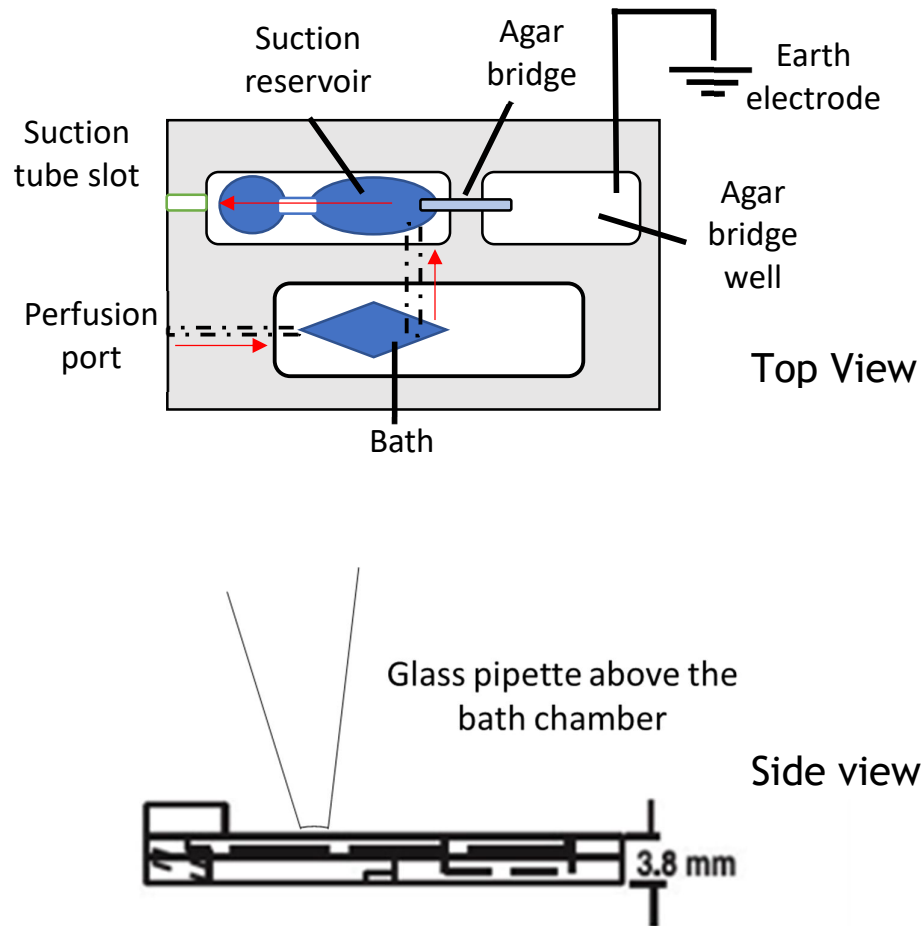
Figure 2.5 Schemata of the perfusion chamber apparatus.

Red arrows show the direction of the flow.
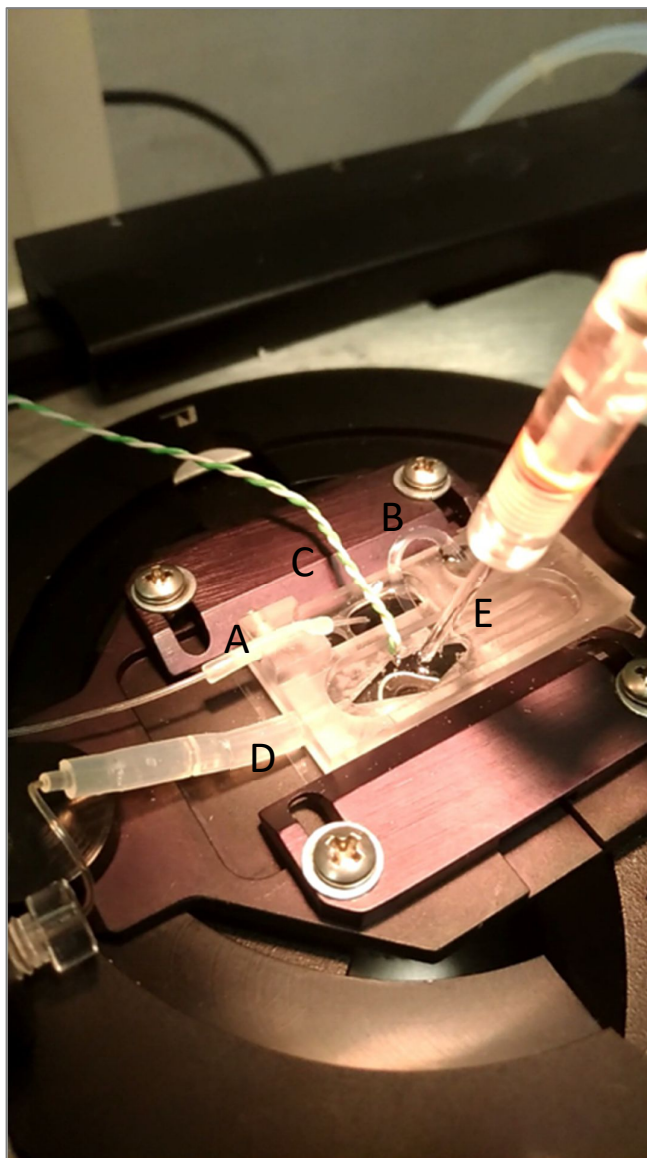
Figure 2.6 Picture of the microscope stage:
(A Suction tube slot; B) Agar bridge; C) Temperature
probe; D) Perfusion port; E) Glass patch pipette.

2.8 Micropipette electrodes

Pipette microelectrodes were constructed in advance by hand cutting a ~15cm long (1.5 mm outer diameter x 1.17 mm inner diameter), borosilicate thin wall with filament capillary (Clark Electromedical), with a diamond tip cutter in 2 segments of 7 cm each. Then each segment was pulled using a vertical, two stage, micropipette puller. Each microelectrode was pulled in two steps, the first at 12 A (current flowing through heating element) and the second at 9 A and then the tips of the resulting micropipettes were heat polished. From this process resulted an average resistance (Rp) of 2-5 MΩ at the tip. The polishing process removed any imperfections that might damage the cell membrane and prevent the formation of the high resistance seal. A silver-chloride wire was placed into the micropipette and connected to the amplifier. Before each day's experiment, both this wire and the wire used as the earth electrode, were cleaned and chlorinated using electrolysis and a chloride containing solution. The electrical resistance of a number of microelectrodes was measured to enable adjustments to be made in the pulling process. This enabled the microelectrode resistance to be kept low and thus minimising voltage errors relative to the cell seal resistance and, therefore, diminishing the leakage current when patching the cells. The resistance was measured before patching a cell by applying a 1 mV voltage pulse once the electrode was lowered into the external solution. The current generated across the electrode tip by the voltage step was measured and the resistance calculated using Ohms Law (R=V/I).

2.9 Continuous single-electrode voltage clamp (cSEVC) in whole-cell patch clamp: voltage offset compensation

An AxoClamp2B amplifier was used in cSEVC mode in conjunction with the software programme WinWCP (J Dempster, Strathclyde University) to record ion currents. The voltage at the top of the pipette is controlled by a voltage-clamp circuit and the cell membrane potential was measured at the same time. In cSEVC, the same electrode is used simultaneously for voltage recording and for current passing. The voltage recorded at the top of the pipette is the sum of the resting membrane potential (Vm), which the experimenter wishes to control, and the current-induced voltage drop across the pipette. The current through the series resistance of the pipette and the residual resistance of the ruptured

patch is often sufficiently large to introduce significant voltage errors which can affect the current recordings and can be compensated for either prior to, or during, recordings using the amplifier. Firstly, when the electrode is lowered into the external solutions offset potentials occur, which includes a current which flows between the internal and external solutions, that contain different concentrations of potassium ions, known as the liquid-liquid junction potential (LLJP). Adjusting the "junction null" control on the amplifier inserts a compensatory voltage in an attempt to correct for all voltage offsets, including that of the LLJP. However, when the electrode is in contact with the inside of the cell and the cytoplasm has dialysed with the pipette solution, the liquid junction potential no longer exists, as the internal solution of the electrode is the same as the interior of the cell, and so the LLJP compensatory voltage would then slightly re-assert itself (upon going in whole cell) as a voltage error (of the same magnitude of the LLJP) if not correctly adjusted for. Therefore, to make this adjustment, according to the method of Neher 1992, the electrode was nulled "a-priori" at a predetermined voltage that is the same size but opposite polarity to that of the LLJP (238). The value of the LLJP, when using the external solution and internal solution described in this chapter, has been measured as +9 mV (bath relative to pipette; according to the Barry Convention) (79), and so the "a-priori" nulling voltage was -9 mV. The validity of this LLJP compensation method was further confirmed by comparing the measured E_K with the theoretical E_K (data shown in results). Following adjustment of the "junction null" a square voltage pulse was applied from a holding potential of zero to -1 mV in order to measure the electrode resistance. The electrode was then lowered onto the cell membrane of a single myocyte using a micromanipulator and gentle suction applied in order to obtain a gigaseal. At this point, a second voltage pulse was applied, from a holding potential of -40 with a step to -50 mV, in order to visualise the capacity transients of the electrode which could then be nullified with the "fast magnitude" control on the amplifier. Further gentle suction was then applied in order to rupture the patch of cell membrane at the tip of the electrode and gain access to the interior of the cell. This generates further larger current transients as the voltage pulse charges the cell membrane capacitance. These current transients along with the pipette resistance are associated with voltage errors during peak I_{K1} recording, which were minimized by bridge-balancing prior to sealing and expected to be <5 mV. The final setting

on the whole cell capacitance control is a measure of the capacitance of the cell, which is proportional to its surface area and this was recorded for all cells patch clamped. The values of the cell membrane capacitance and the access resistance can be directly read from the Axopatch amplifier controls. The absolute value of the membrane capacitance was displayed on the whole-cell capacitance dial after the whole-cell current transient has been eliminated. This value may be used to estimate the surface area of the cell assuming that the membrane capacitance per unit area is 1 μF/cm^2. The final setting on the series resistance control is a measure of the combined resistance of the electrode tip and the open patch in the membrane. This resistance was kept to a minimum by ensuring only low resistance electrodes were used and only cells in which a high resistance seal was initially achieved. However, even with low series resistance, large currents can result in a significant voltage error whereby the voltage recorded by the amplifier is different from that actually occurring at the cell membrane. The voltage error was minimised by using series resistance compensation. Series resistance compensation was used to keep the average voltage error less than 5mV. Once the current transients were compensated for, various voltage pulse protocols, designed using the WinWCP software, were applied in order to measure currents.

2.10 Results

2.10.1 Comparison between measured E_k and theoretical E_k in rabbit left ventricle myocytes: a test of correct voltage measurements

The equilibrium potential for potassium (E_K) was calculated using the Nernst-Planck equation, which is a conservation of mass equation used to describe the motion of a charged chemical species in a fluid medium. Cell membrane potential is the results of ions, differently charged, moving through the phospholipidic layer and establishing an electrical gradient. The resulting electrical gradient grows in magnitude until it exactly balances the chemical gradient. When the chemical and electrical gradients are equal in magnitude, the ion is said to be in electrochemical equilibrium, and the membrane potential that is established at equilibrium is said to be the equilibrium potential ($V_{eq.}$) for that ion under the existing concentration gradient. For potassium ions the

chemical gradient ($\Delta G_{Chemical}$) and the electrical gradient ($\Delta G_{Electrical}$) can be defined as:

$$AG_{Chemical} = RTln\frac{[K^+]o}{[K^+]i} \qquad \text{eq(1)}$$

$$AG_{Electrical} = (+1)FV \qquad \text{eq(2)}$$

Where R is the gas constant, T is the absolute temperature, F is the Faraday constant, V is the voltage, and z is the valence of K^+ (+1). Since during electrochemical equilibrium $\Delta G_{Electrical}$ and $\Delta G_{Chemical}$ are equal, the next equation follows:

$$(+1)FV = RTln\frac{[K^+]o}{[K^+]i} \quad \text{eq(3)}$$

Solving for V:

$$V_{eq.} = \frac{RT}{(+1)F} ln\frac{[K^+]o}{[K^+]i} \qquad \text{eq(4)}$$

Substituting for the concentration of $[K^+]_o$ (4mM) and $[K^+]_i$ (145mM) to the equation (4) a value of -95.9mV was obtained, which represents the calculated value for E_K. Using the Nernst-Planck equation the potential that will be established across the membrane based on the valence and concentration gradient of K^+ was calculated, but provided that only K^+ channels are present. During cell stimulation using a voltage ramp protocol a classic striking inward rectification of I_{K1} was observed. As expected Kir2.x channels pass inward currents at potentials more negative than the reversal potential of K^+ (E_K) but allow significantly less current at more positive potentials compared to non-rectifying channels (241) (Fig. 2.7). As a consequence of this channel behaviour, and as described previously, the conductance through the inwardly rectifying K^+ channel present an ohmic portion (242), termed ohmic because it follow Ohm's law (221), for voltages more negative than -100mV, which was used to draw a slanted line that would eventually cross the 0 mV baseline. The voltage at the intersection point, in theory should be E_K as calculated from the Nernst equation. In the present experiment, the measured intersection voltage was -94.6 ± 0.5mV (measured E_K; n=6 cells; n=6 rabbits), which is less than 1mV different from the calculated E_K of 95.9mV. Thus, validating my voltage control for the subsequent voltage-clamp experiments.
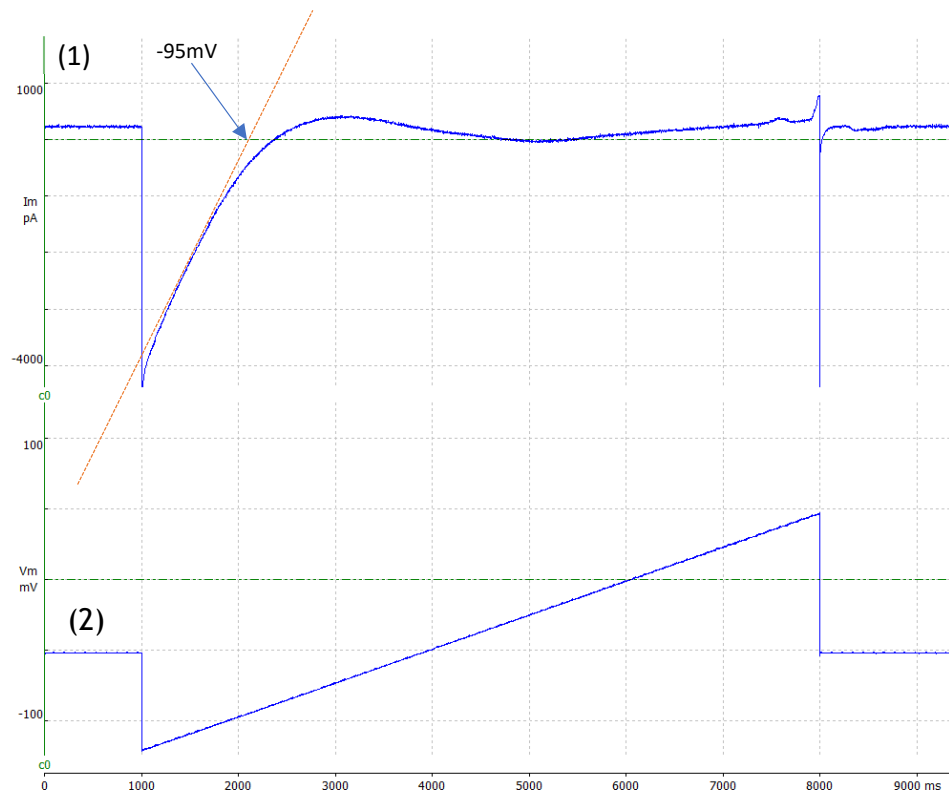
Figure 2.7 Representative raw current trace used for E_K measurement in rabbit left ventricle myocytes.

1) Slanted line representing the oblique asymptote which describe the ohmic Kir2.x channel behaviour on voltage more negative of E_K. The oblique asymptote was defined by the equation: y=mx + b, where m≠0. Oblique asymptotes occur when the degree of the denominator of a rational function is one less than the degree of the numerator. 2) The voltage ramp protocol shown below the current trace is described in the method section 3.4.8. The figure has been generated with the electrophysiology software WinWCP (version 5.3.4).

2.10.2 Investigation of effects of a pharmacological intervention (acute BaCl$_2$ superfusion), in terms of response timing, magnitude and inter-cellular variability: the positive control

Intracellular and extracellular biochemical differences can have profound effects on cell phenotype. These dissimilarities cause genetically identical cells to vary significantly in their responsiveness to stimuli and drugs even in a uniform environment (243, 244). Importantly, this could also be expected to be the case when applying SK blockers. Since SK blocker responses are also expected to be small in magnitude – e.g.: sensitive fraction of 15% of the total current (29)- it was decided to first investigate the variation in response to a drug anticipated to have a relatively large effect: BaCl$_2$ at 0.5 mM (222), as a suitable positive control for later measurements of I$_{SK}$.
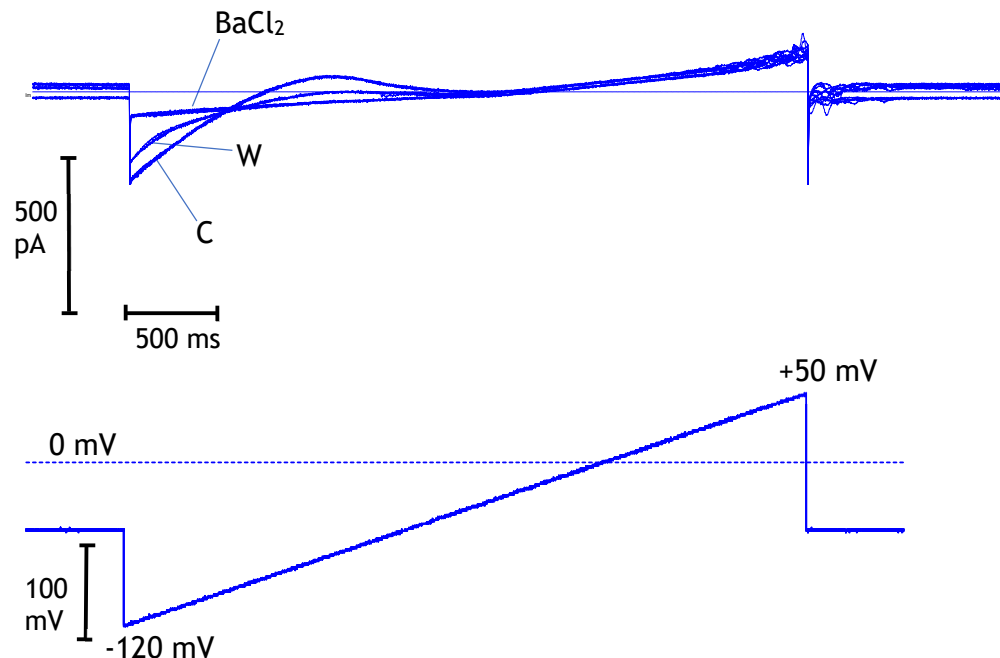
Figure 2.8 Effect of BaCl$_2$ on a single rabbit left atrium isolated myocyte. Representative traces showing the effect of BaCl$_2$ (0.5mM) during stimulation at 0.1Hz (10s). C (control), W (washout), Ba^{2+} (Barium Chloride). All the records are performed at physiological temperature (37°C). Traces were generated using WinWCP 5.3.4.

Several traces were recorded during my pharmacological experiments where Ba^{2+} was administrated at a concentration of 0.5 mM for at least 90s, at which time it was usually possible to observe full effect of the drug (time-course of effect and time of effect onset at ~30s, Fig. 2.9 and Fig.2.10, respectively). This concentration is expected to provide reasonable selectivity for Kir2.1 channel (245). The barium as a bivalent cation enters the inward rectifier channel binding site and blocks it, denying the potassium transient to repolarize the cell (246) (Fig. 2.8). The validation of the effect of barium on the current was tested, firstly, by following the time-course of the control traces and ensuring that the administration of the Ba^{2+} causes a shift of the trace that goes in the opposite direction compared to the voltage ramp driven current.
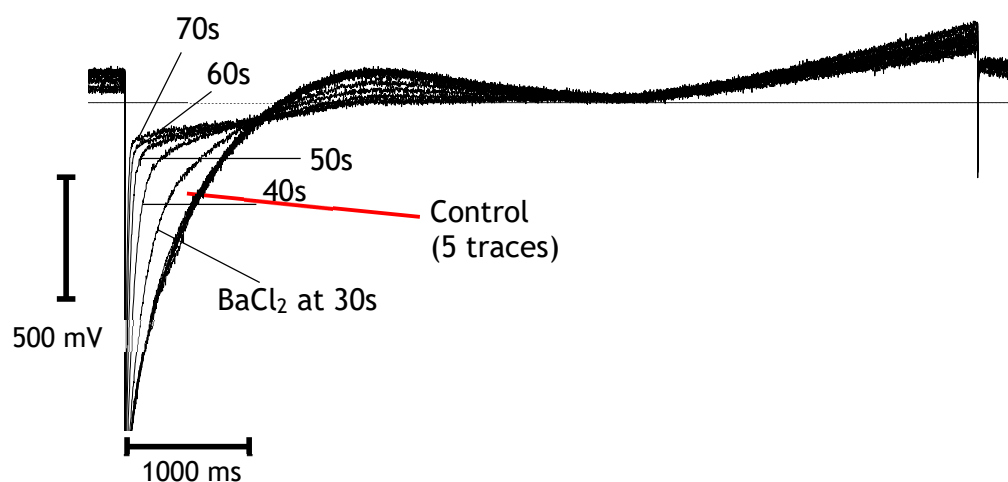
Figure 2.9 Representative traces showing typical time-course of the effect of BaCl$_2$ recorded in rabbit left ventricle.

The red line indicates the 5 superimposed traces for control (i.e. 50s of recording) showing the stability of the recordings prior to administration of BaCl$_2$. Each black line indicates the time course of the effect of BaCl$_2$ at each consecutive recording (i.e. every 10s)
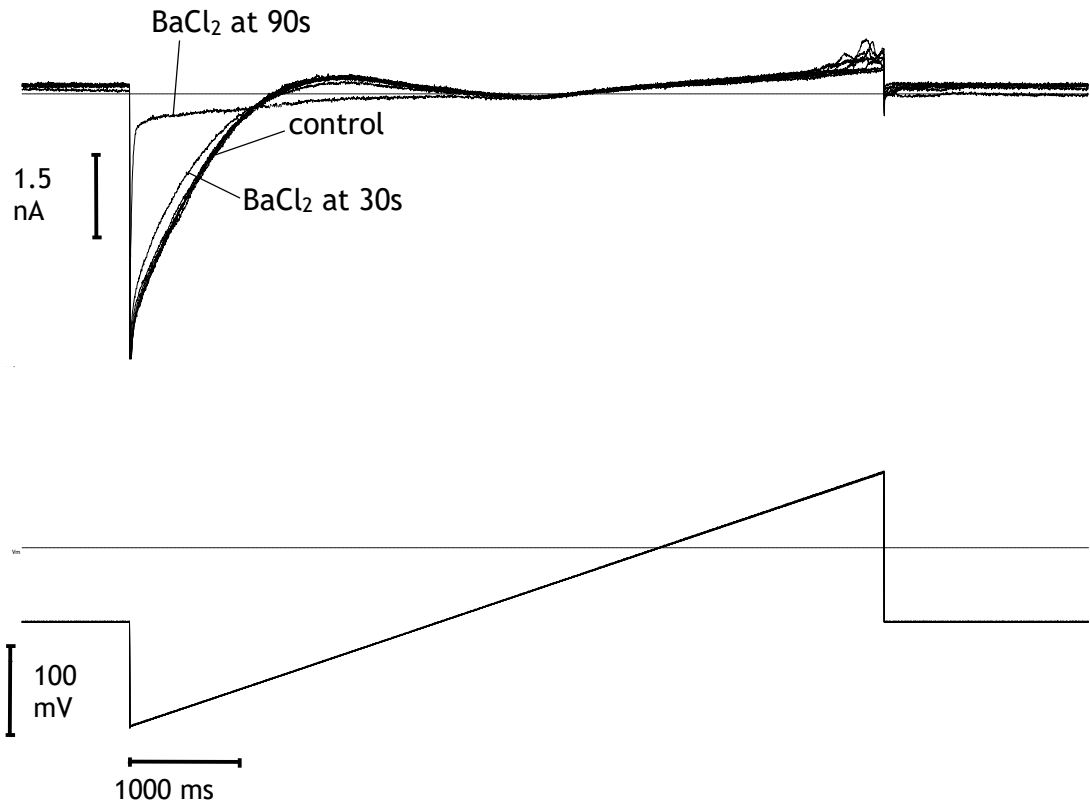
Figure 2.10 Representative traces showing typical time of effect onset and time to full effect of BaCl$_2$.

At 30s the typical start of barium effect is visible and the full block of I$_{K1}$ provide by BaCl$_2$ (0.5 mM) occurred at 90s.

Im

5000 pA

Vm

50 mV

1000 ms
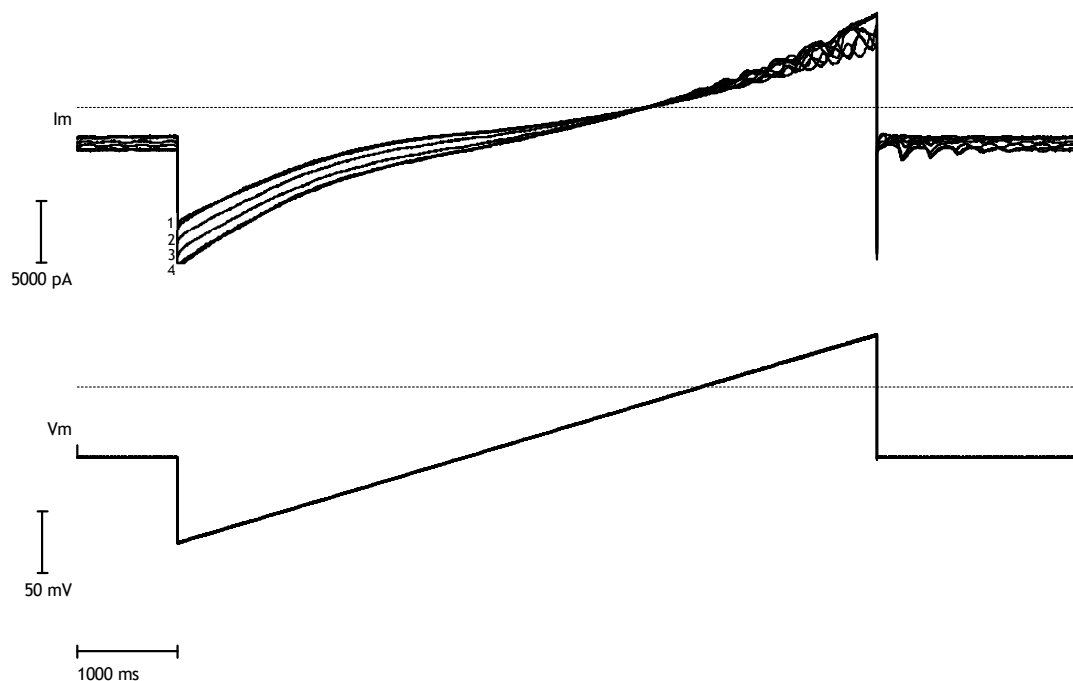
Figure 2.11 Representative control current trace showing the time-course of seal-loss.

Seal leakage provokes a drift of the current traces (after 60 s), which start following the voltage-ramp. Numbers 1-4 represent current traces every 60s of recording. Traces were generated using WinWCP 5.3.4.

To understand this concept, it is necessary to remember the Ohm's law (**V**(voltage)=**R**(resistance)•**I**(current)). The simplest resistor, which can be defined as a hypothetical channel which is independent of time and voltage, has a linear current-voltage (I/V) relationship. This behaviour can be experienced when the patch-pipette loses the seal, which immediately provokes a drop in the resistance given by the cell (Fig. 2.11). Usually this predicts the loss of the cell and the recording, thus is always excluded from the analysis. When the seal is practically lost, the resistance become constant and the voltage (V) is calculated just as a function of the current (I). This event is easily recognizable and opposite to the effect of barium.
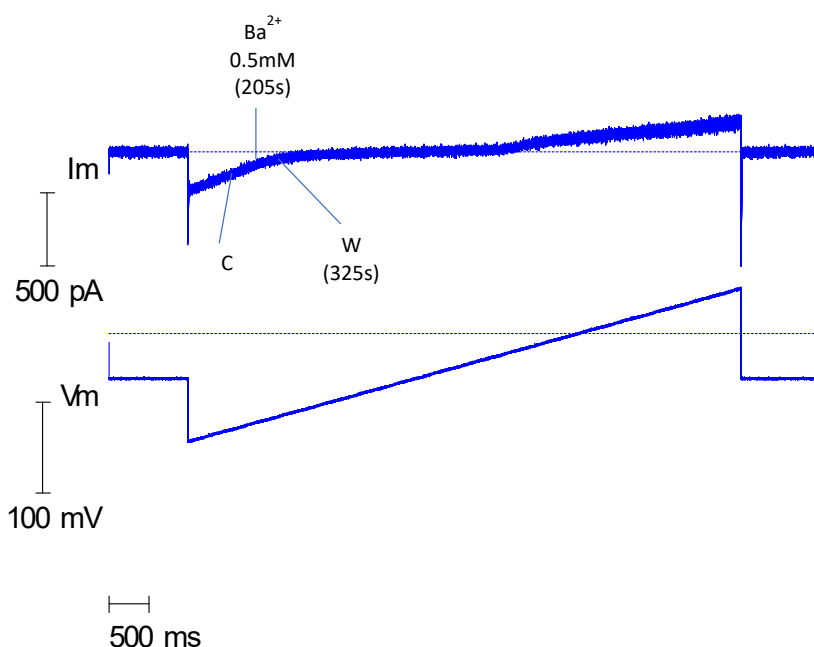
Figure 2.12 Absence of effect of BaCl₂ on K⁺ channels (rabbit left atrium).
Representative traces showing the effect of BaCl$_2$ (0.5 mM) during stimulation at 0.1Hz. C control, W washout, Ba^{2+} Barium Chloride. All the records are performed at physiological temperature (~37°C). Traces were generated using WinWCP 5.3.4.

A second validation of the effect of Ba^{2+} was obtained after washing the cell with control solution and observing, eventually, the reversibility of the drug effect. However, the effect of Ba^{2+} on cells was not always present, an example of which is shown in figure 2.12, and this depends on the cell biological variability. In that particular cell Ba^{2+} was applied after 205s and washed at 325s, thus I waited more than 2 min to ensure that no effect by Ba^{2+} could possibly be detected. In addition, the figure 2.12 is a perfect example of the stability of the recordings and the low level of electrical noise, which become extremely important, especially with small currents. However, an absence of effect was always included in the analysis and considered as the results of cell-to-cell variability, which is an extremely important concept to account for the study of different currents. Based on this background, several traces from both human right atrium and rabbit left atrium and ventricle myocytes were recorded. The barium had different effect among single cells, showing different response to the drug within the same chamber (Fig. 2.14-2.15) and among different species (Fig. 2.13), demonstrating that biological variability is an important factor to

consider even with such a predictable effect. Specifically, Barium 0.5mM reduced the peak current density from 38.9 ± 5.9 pA/pF to -12.9 ± 4.5 pA/pF (by 133 %), in 15 out of 16 (94%) rabbit left ventricle cells, from 20.3±4.2 to -11.6±2.9 pA/pF (by 157 %) in 23 out of 25 (92%) rabbit left atrial cells and from 4.3 ± 1.3 to 1.2 ± 0.2 (72%) in 11 out of 12 (92%) human right atrial myocytes. Overall, however, barium significantly reduced the current density at -115mV (Fig.2.16) and at -65mV (Fig. 2.17) in all species and chambers.
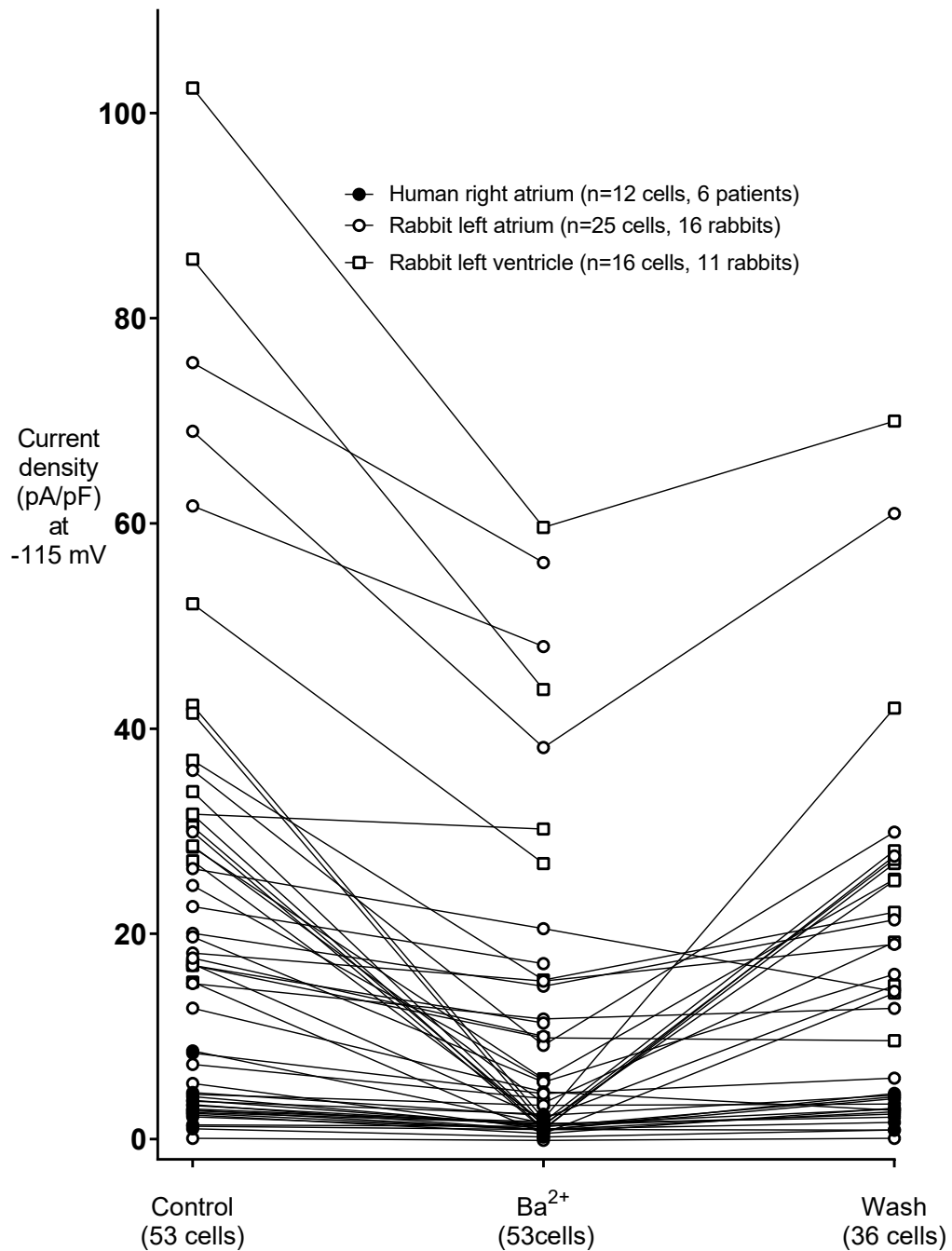
Figure 2.13 Heterogeneity of Ba^{2+} effect among cells from different rabbit left atrium and human right atrium.

Peak currents density recorded at -115mV for all conditions: control (C), barium (Ba^{2+}) and wash (W). Some wash records are missing due to cell death during recordings. Sample size: n=25 cells n=16 rabbits (rabbit left atrium); n=16 cells n= 11 rabbits (rabbit left ventricle); n=12 cells n=6 patients (human right atrium).
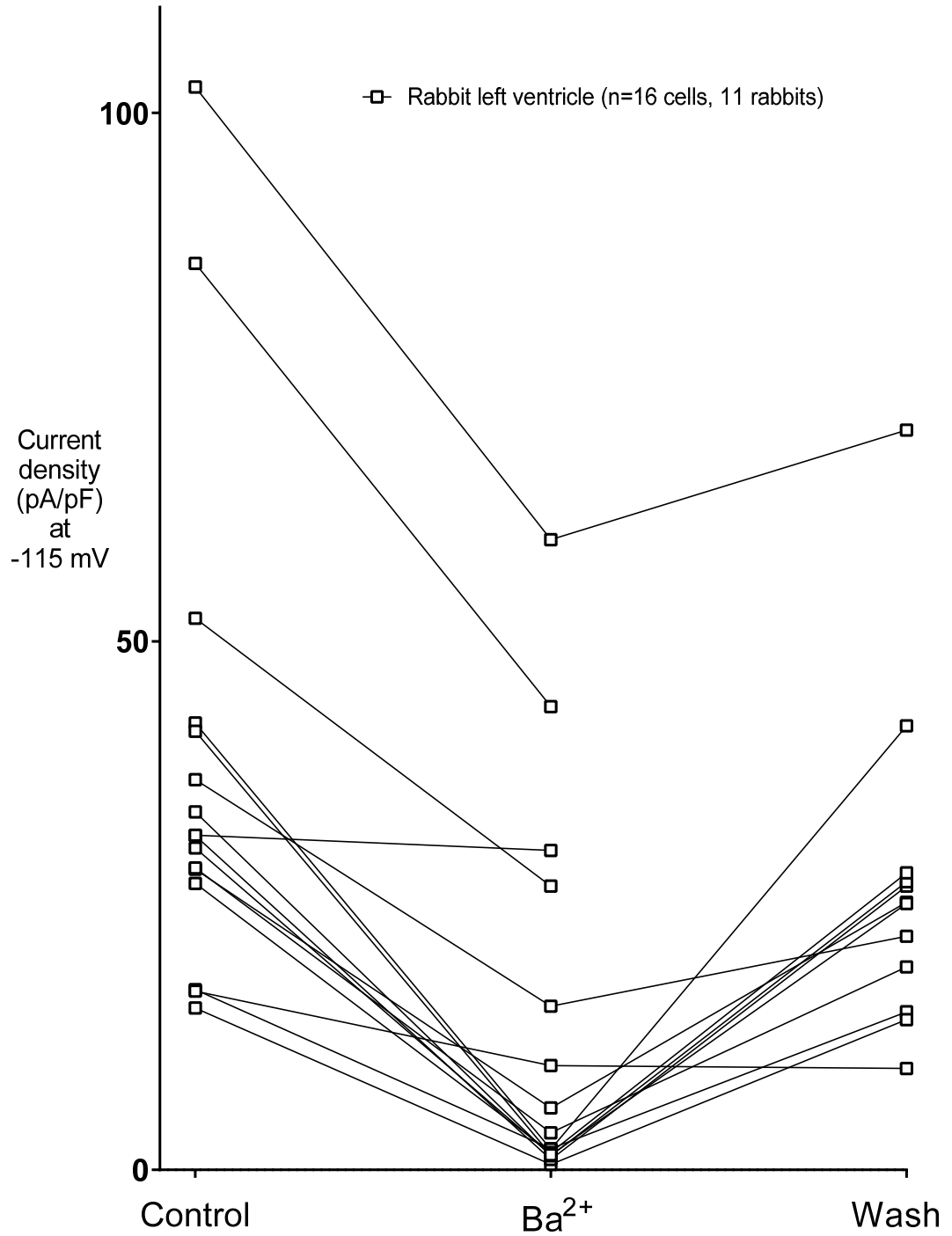
Figure 2.14 Heterogeneity of Ba²⁺ effect among cells from rabbit left ventricle.

Peak currents density recorded at -115mV for all conditions: control (C), barium (Ba²⁺) and wash (W). Some wash records are missing due to cell death during recordings. Sample size: n=16 cells n=11 rabbits.
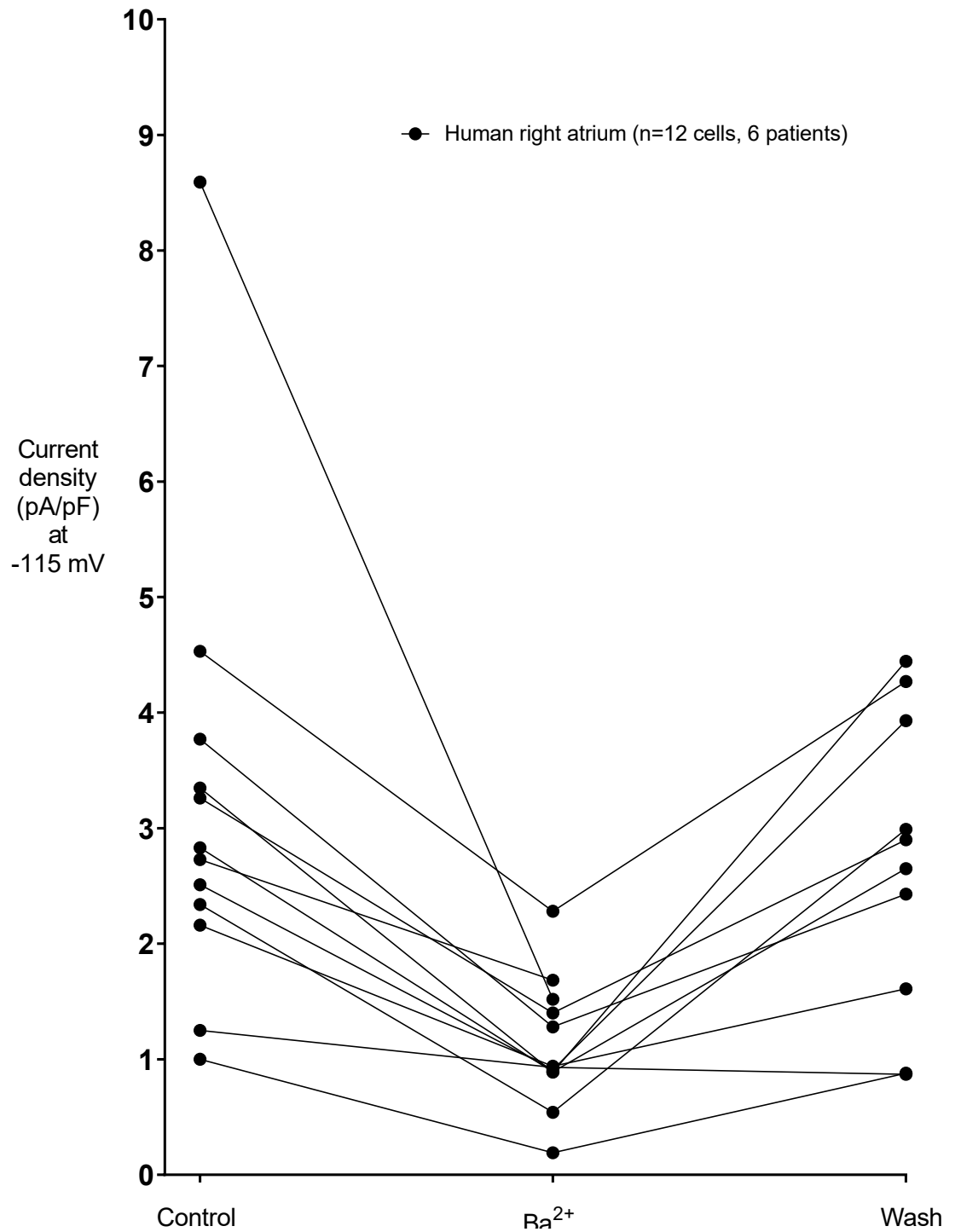
Figure 2.15 Heterogeneity of Ba^{2+} effect among cells from human right atrium.

Peak currents density recorded at -115mV for all conditions: control (C), barium (Ba^{2+}) and wash (W). Some wash records are missing due to cell death during recordings. Sample size: n=12 cells n=6 patients.
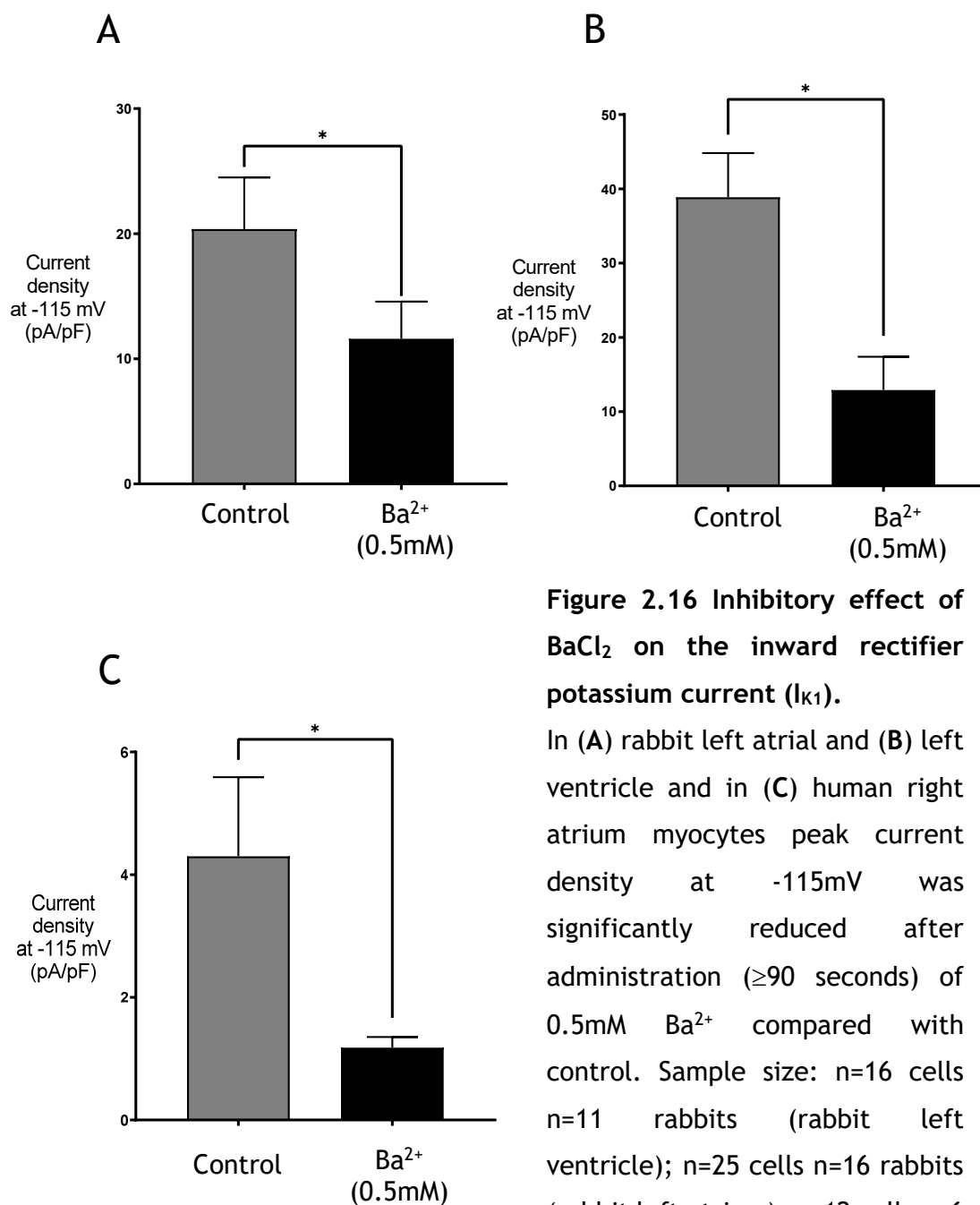
Figure 2.16 Inhibitory effect of BaCl$_2$ on the inward rectifier potassium current (I$_{K1}$).

In (**A**) rabbit left atrial and (**B**) left ventricle and in (**C**) human right atrium myocytes peak current density at -115mV was significantly reduced after administration ($\geq$90 seconds) of 0.5mM Ba^{2+} compared with control. Sample size: n=16 cells n=11 rabbits (rabbit left ventricle); n=25 cells n=16 rabbits (rabbit left atrium); n=12 cells n=6 patients (human right atrium). Currents are represented as positive values. The data are expressed as mean ± s.e.m. Values of P<0.05 (*) were considered significant.
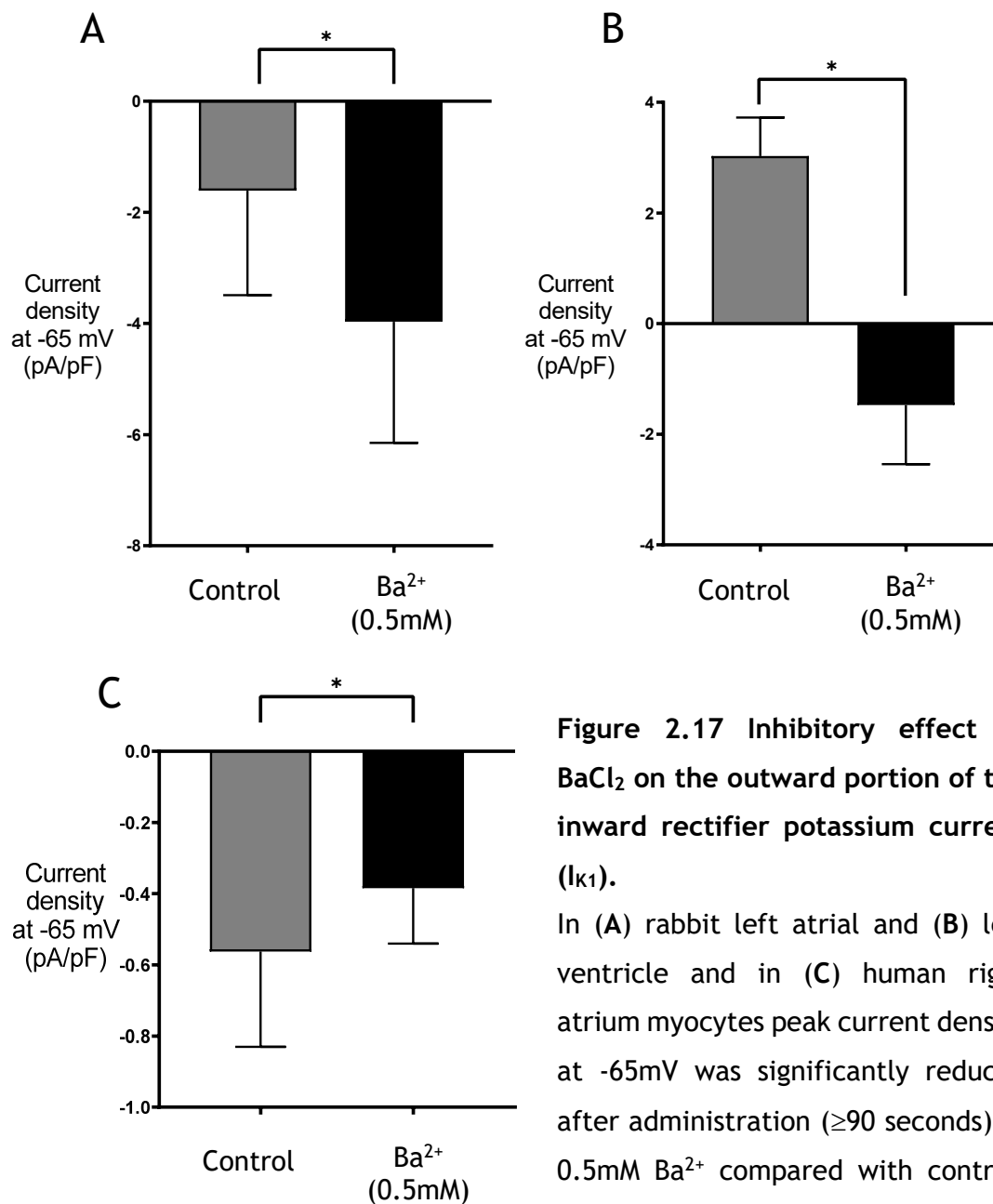
Figure 2.17 Inhibitory effect of BaCl$_2$ on the outward portion of the inward rectifier potassium current (I$_{K1}$).

In (**A**) rabbit left atrial and (**B**) left ventricle and in (**C**) human right atrium myocytes peak current density at -65mV was significantly reduced after administration (≥90 seconds) of 0.5mM Ba^{2+} compared with control. Sample size: n=16 cells n=11 rabbits (rabbit left ventricle); n=25 cells n=16 rabbits (rabbit left atrium); n=12 cells n=6 patients (human right atrium). The data are expressed as mean ± s.e.m. Values of P<0.05 were considered significant.

2.10.3 Measurement of I_{K1} in atrial cells, and comparison with ventricular cells.

I_{K1} makes an important contribution to APD in heart ventricular cells and the large inward rectification ensures the resting potential is stabilized close to EK (220).
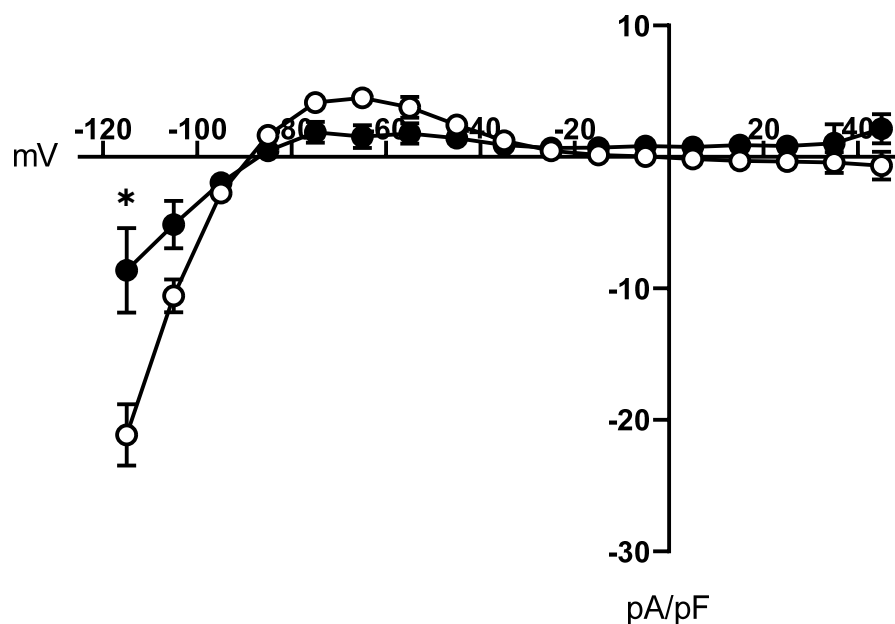
Figure 2.18 Comparison of current-voltage relationships of rabbit left atrial and left ventricular I_{K1}.

[O] LV I_{K1} has greater current density than [●] LA I_{K1}.Ventricular I_{K1} has a prominent negative slope conductance, which is significantly smaller in atrial I_{K1}. Curves are plotted as barium-sensitive current. Values are mean ± s.e.m and P<0.05 was considered significant, unpaired t-test, left atrial n=10 cells (n=6rabbits) vs left ventricle n= 12 cells (n= 6 rabbits).

As Fig. 2.18 shows, and as stated earlier, I_{K1} properties are markedly different in the atria compared to the ventricles. In fact, rabbit atrial I_{K1} was a third compared to ventricular I_{K1} current density, which explains the more

hyperpolarized resting membrane potential and faster phase 3 repolarization in the ventricles (220, 221).

In addition, the mean outward current at voltages more negative than -30 mV and more positive than -80 mV is characterized by an "n-shape" or negative slope conductance region, which is less evident in atrial I_{K1} (221).
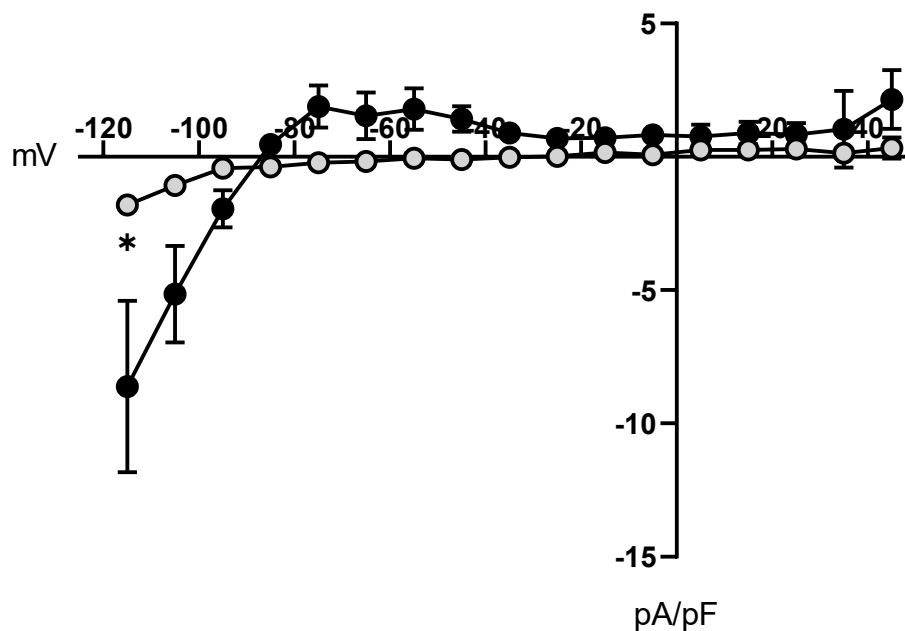
Figure 2.19 Comparison of current-voltage relationships of rabbit left atrial and human right atrial I_{K1}.

Comparison between [●] rabbit LA I_{K1} and [○] human RA I_{K1}. Rabbit left atrial I_{K1} has a greater current density than human right atrial I_{K1} for both inward and outward portion. Curves are plotted as barium-sensitive current. Values are mean ± s.e.m and $P<0.05$ was considered significant, unpaired t-test, right atrial n=9 cells (n= 5 patients) vs left atrial n=10 cells (n=6rabbits).

Peak inward I_{K1} was recorded at -115mV with a mean current density of 21.1 ± 2.3 pA/pF (n=12 cells, n=6 rabbits) for left ventricle and 8.6 ± 3.2pA/pF (n=10 cells, n=6rabbits) for left atrium. Peak outward I_{K1}, was recorded at -65mV with a mean current density of 4.5 ± 0.7 pA/pF (n=12 cells, n=6 rabbits) for left ventricle and 1.5 ± 0.9 pA/pF (n=10 cells, n=6rabbits) for left atrium. In human right atrial cardiomyocytes I_{K1} was almost a fifth smaller than I_{K1} recorded in rabbit left atrial cells. Peak inward current was recorded at -115mV with a mean current density of 8.6 ± 3.2 pA/pF (n=10 cells, n=6 rabbits) for rabbit left atrium

and 1.8 ± 0.3 pA/pF (n=9 cells, n=5 patients) for human right atrium. Peak outward I_{K1}, recorded at -65mV presented a mean current density of 1.5 ± 0.9 pA/pF (n=12 cells, n=6 rabbits) in left atrium and -0.2 ± 0.1 pA/pF (n=9 cells, n=5 patients) for human right atrium. However, the small amplitude of I_{K1} recorded in human right atrium is due to the presence of patient treated with β-blockers, which are reported to reduce the peak inward I_{K1} (at -120mV) (222).

2.10.4 High control current correlates with high Ba^{2+}-sensitive current

At the drug concentration used (0.5millimolar), and in a limited voltage range (approximatively from -115mV to-90mV), the Ba^{2+}-sensitive current displayed a marked inward rectification and behaved as expected for a pure K^+ current (at physiological $[K^+]_o$) suggesting that under these conditions the only current affected by Ba^{2+} was I_{K1}. Therefore, to verify the hypothesis that I_{K1} was the main component of the current recorded at -115mV, further analyses were performed. Firstly, the barium-sensitive current magnitude was compared among species and chambers. Figure 2.18 demonstrates that the current blocked by Ba^{2+} at -115mV is significantly bigger in ventricle (25.9 ± 3 pA/pF) compared to atrium (8.7 ± 1.9 pA/pF) in rabbit isolated myocytes, which is in accordance to the literature for I_{K1} (220, 221, 241). Moreover, the barium-sensitive current in rabbit left atrium was 4 times larger than the current recorded in human right atrium (2.1 ± 0.5 pA/pF). The barium chloride is a reasonable intervention to inhibit I_{K1}, even though it is probably not very selective for it (depending also on species and chamber); in fact, it targets all the potassium inward rectifier channels (IRCs) of the KCNJx gene family (247). Nevertheless, a relatively high concentration (0.5 mM) was chosen for these studies, especially because I could compare the results directly with previous data from human atrial cells (222). Interestingly, two different populations of cells were identified based on the response to barium (Fig.2.21 A), composed by the lowest half and the highest half of the barium sensitive current among all cells.
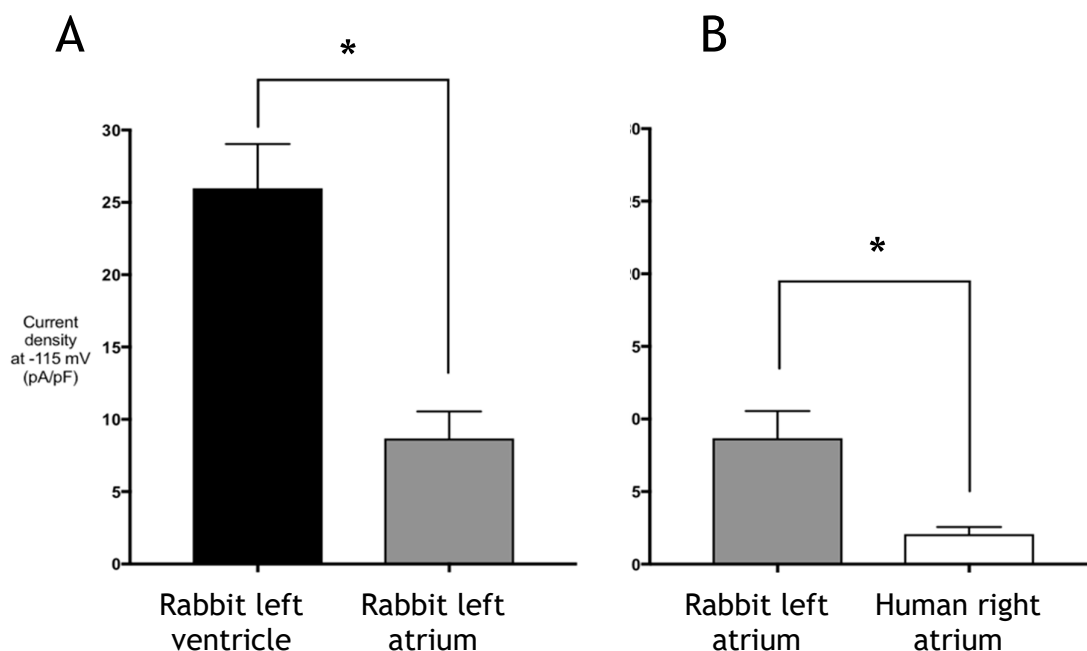
Figure 2.20 Comparison of barium-sensitive currents from rabbit left atrial and ventricle and human right atrial myocytes.

(A) Comparison of peak current density at -115mV between rabbit left ventricle and left atrium. Sample size: rabbit left ventricle n=16 cells (n=11 rabbits) vs rabbit left atrium n=25 cells (n=16 rabbits), unpaired t-test (B) Comparison of peak current density at -115mV between rabbit left atrium and human right atrium. Rabbit left atrium n=25 cells (n=16 rabbits) vs human right atrium n=12 cells (n=6 patients), unpaired t-test. The data are expressed as mean ± s.e.m. Values of P<0.05 were considered significant.

Moreover, it was noticed that most of current data from ventricle were included in the highest half. Consequently, it was found that these two populations were significantly different, confirming the variable sensitivity of Kir channels to Ba^{2+} among different heart chambers, and especially supporting the evidence that ventricular I_{K1} is greater compared to atrium (220, 221). In addition, the current component blocked by Ba^{2+} increased proportionally to the current amplitude, despite barium concentration, which was kept constant, verifying that 0.5 mM $BaCl_2$ is sufficient to block effectively I_{K1}, as confirmed previously by literature (222, 225) and that the barium-sensitive current is mainly composed by I_{K1} (225, 226). Figure 2.21 shows that the barium-sensitive current is very variable among cells and species, as supposed, and the degree of inhibition of barium increases with the increasing of the control current

amplitude. This is confirmed by the graph (B) that shows significant correlation among heart chambers and species between the barium-sensitive current and the control current at -115mV.
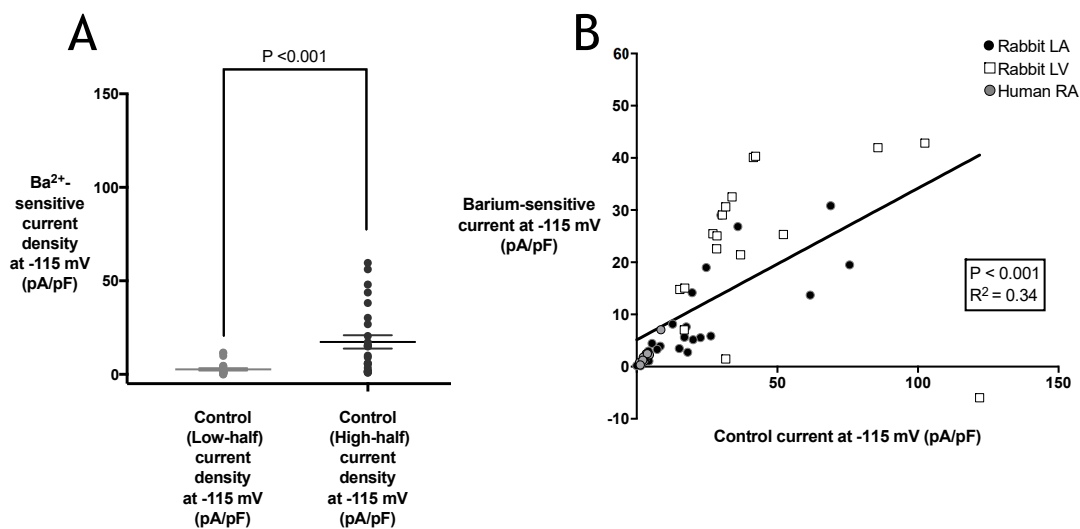
Figure 2.21 Relationship between high current in control condition and high effect of barium, in rabbit left atrial and ventricle and in human right atrium single cells.

A) The aligned dot-plot graph shows the comparison between Ba^{2+}- sensitive currents in two portion of cells: 1) the block provided by Ba^{2+} was small or not visible (● low-half) 2) the current blocked by Ba^{2+} was large (● high-half). B) The linear regression graph confirms the correlation between higher control current and high barium-sensitive current density. A linear regression line was used based on the equation Y = a + bX, where **X** is the explanatory variable (control current) and **Y** (barium-sensitive current) is the dependent variable. The slope of the line is **b**, and **a** is the intercept (the value of y when x = 0). Sample size: n=41 cells n=11-16 rabbits; n=13 cells n=6 patients (rabbit left atrium); n= 16 cells n=11 rabbits (rabbit left ventricle) n=12 cells n=6 patients (human right atrium). The data are expressed as mean ± s.e.m., Values of P<0.05 were considered significant.

2.11 Discussion

The experiments outlined in this chapter demonstrated validation of my patch-clamp technique (including appropriate voltage control), and of the temporal stability, timing and reversibility of a pharmacological intervention which will serve as positive control in the next experiments. In fact, the voltage protocol used, after validation, revealed the presence of a large current significantly blocked by 0.5 mM $BaCl_2$ in both human and rabbit which, based on previous literature (199, 222), was classified as I_{K1}. Also, I_{K1} amplitude was compared among heart chambers and species showing inter-cellular and inter-animal or patient variability.

2.11.1 Validation of voltage control

Prior to the experiments both the software and the patch clamp electrical components have been tested for correct voltage measurements and for background noise (test for electrical and vibration isolation), which were minimal, showing clean current and voltage traces (Fig. 2.7). Also, as described previously in this chapter, considering that I_{K1} is much larger in ventricle than in atrium and that this current in rabbit presents a bigger inward component compared to human, it was chosen to validate the voltage patch clamp technique in terms of voltage control in single rabbit left ventricle cells. I_{K1} reversal potential was measured and resulted equal to E_K calculated by Nernst equation, which confirmed that my recording conditions and technique are correct.

2.11.2 Biological variability

0.5 mM $BaCl_2$ was expected to have a large effect on the current in each cell, however, it was demonstrated that in some cells (~7%) the current was not affected by the drug. The percentage of cells that did not respond to the application of the drug did not significantly alter the results, on average, but proved that extreme inter-cellular and inter-animal or patient variability has to be considered. In fact, within the same chamber and species it was discovered that the response to 0.5mM $BaCl_2$ differed substantially (e.g. Fig. 2.14), even with such a predictable intervention. Considering the large magnitude of I_{K1}, the variation in drug effect was not masked by the average but represent an essential

component to be considered when it comes to study currents with small amplitude, such as I_{SK}.

2.11.3 Atrial vs ventricular I_{K1}: a comparison with other studies

In this study Ba^{2+} was shown to reduce I_{K1} at both -115mV and -65mV, with a mechanism of Ba^{2+} block that is probably of the "open channel block" type, at concentration lower than 1 mM, as suggested by the pronounced fast inactivation component of the resulting current (224). The major problem was represented by the identification of I_{K1} and its kinetics, which lies in the presence of other time dependent and time-independent components overlapping I_{K1} changes during voltage-clamp pulses (225). However, it was confirmed that the main component blocked by Ba^{2+}, at relatively high concentration, is represented by $I_{K1,}$ also confirmed by the literature (222, 225), verifying that the current block was directly proportional to the size of the current. Moreover, the size of I_{K1} was 3-10 times larger in ventricle compared to atrium in single rabbit cells in accordance with previous results by Giles et al. (199). Also, I_{K1} in rabbit left atrium was 4 times greater than in human right atrium, with current amplitudes of ~8.6 pA/pF vs 1.8 pA/pF, respectively. The average current density for I_{K1} is recognised to be small in human right atria cells from patients in SR (79). Also, considering that the average I_{K1}, recorded at -115mV in my experiments, results from both patient treated and not-treated with ß-blockers, which have been shown to reduce I_{K1} magnitude at -120 mV, it can be concluded that the current density value is very similar to the one reported by our lab in an earlier study (222).

Interestingly, dissimilarities in I_{K1} can be addressed also as a result of different isolation methods. For example, Hoshino et al., report that I_{K1} is strongly affected by the chunk method compared with the Langendorff perfusion procedure in myocytes isolated from mouse heart (248). However, it is not possible to utilise the perfusion procedure in human tissue, therefore, the hypothesis that the difference in I_{K1} magnitude recorded in myocytes isolated from patients can be caused by the utilization of the chunk method, cannot be ruled out.

To conclude, I successfully mastered the patch-clamp technique studying a well-known current as I_{K1}. Solid responses were obtained validating my patch-clamp configuration, reversal of intervention and software precision. Importantly, I have proved that the theoretical and the measured E_K were identical, confirming that the voltages I was commanding were correct. Lastly, I succeeded to create a positive control profile that will serve as a validation for the next experiments involving the study of I_{SK}.

Chapter 3 Fluorescence imaging of intracellular Ca^{2+}: calibration procedures and verification of [Ca^{2+}]$_i$ in vitro and in rabbit cardiomyocytes

3.1 Introduction

The SK current (I$_{SK}$), may change the cardiac atrial action potential shape in response to altered intracellular [Ca^{2+}], and thus may be a potential therapeutic target for treating atrial fibrillation (AF) (29, 174, 249-253). Specifically, cardiac SK channels are functionally linked to voltage-gated Ca^{2+} channels (174) and are expected to be activated during systole thereby participating in the repolarization of the cardiac action potential (AP). Previous studies have reported that Ca^{2+} entry through voltage-gated Ca^{2+} channels (VGCC), can trigger neuronal SK channels in mice. Furthermore, there is a unique specificity of coupling between L-type VGCCs and SK channels (172). However, the molecular mechanisms underlying the coupling of the Ca^{2+} channels and SK channels are not known. In conclusion, additional experiments are required to further define the roles of global versus local Ca^{2+} rise as well as the roles of sarcoplasmic reticulum Ca^{2+} in the SK channel activation in atrium (172, 254).

3.2 The importance of the calculation of [Ca^{2+}]: the relationship between Ca^{2+} and K$^+$

In addition to the background above, the investigation of I$_{SK}$ required aqueous media that mimic the physiological intracellular fluid and the adjustment of the free [Ca^{2+}]$_i$ in these media is of critical importance because of the essential role of Ca^{2+} in the regulation of K$^+$ efflux through the cell membrane (155, 249, 255). Moreover, it has been reported that, beside calcium, no diffusible second messengers or protein kinases appear to be necessary for SK-channel gating, and that gating reflects interactions between the channel and Ca^{2+} only (165). However, the concentration of calcium ions in physiological buffers is normally calculated using either tabulated constants or software (203, 256, 257). In fact, many papers cite the use of different programs to calculate the [Ca^{2+}]$_i$ or they simply mention the addition of CaCl$_2$, without mentioning

whether the final concentration of free-calcium described had been measured (29, 250, 251). McGuigan et. al showed that the ligand optimization method (258) was the most accurate when it comes to measuring the ionized concentration in buffer solutions (259). Therefore, this technique has been previously used to compare the measurements of the $[Ca^{2+}]$ in EGTA [ethylene glycol-bis (ß-aminoethylether)-N,N,N|,N|-tetraacetic acid] and BAPTA [1,2-bis (o-aminophenoxy) ethane- N,N,N|,N|-tetraacetic acid], buffers with calculated values (252). The results showed that the ionized concentrations $[X^{2+}]$ calculated using software programs or tabulated constants always differed from measured, and calculated values differed among themselves by a factor of at least 2 (252). These variations cast doubts on the published resting values for $[Ca^{2+}]$ in cells. The conclusion is that until buffer standards become internationally defined the measurements of $[Ca^{2+}]$ is more reliable than calculation (252).

3.3 Section Aims

It is clear that such calculations can be seriously misleading, and this has major repercussions for fields in which precise buffering of $[Ca^{2+}]$ is essential such as in patch clamping, measurement of intracellular $[Ca^{2+}]$, and molecular biology (256). Therefore, considering the crucial role that $[Ca^{2+}]$ plays in determining the behaviour of numerous physiologically vital proteins (260, 261), and the importance for measurement over calculation of this ubiquitous second messenger, the aim was to generate solutions with precise $[Ca^{2+}]_i$. Since submicromolar (0.3-0.5 µM) concentration of this divalent cation have been demonstrated to be sufficient to activate SK channels (175), due to their high Ca^{2+} sensitivity (165, 262), it was decided to perform accurate measurements of calcium and buffering, verified first in vitro then in cells, to ensure that during the current recordings the myocytes were experiencing the expected amount of intracellular free-calcium. This contrasts with general methods, where the $[Ca^{2+}]_i$ is estimated (165, 175, 203, 250, 256, 257) and the current measurements are limited by the use of unphysiological solutions or cell type (e.g. HEK cells, Xenopus oocytes) (29, 165, 251). Hence, the present goal was to design a protocol to generate calibration curves utilising EGTA-buffered solutions (253) and calcium imaging apparatus. Subsequently, to utilise the curves to replace EGTA with BAPTA in the solutions, in order to exploit its higher speed of interaction with calcium and its much less pH dependent affinity for calcium to

compensate for the intrinsic cell buffer power (263-265). The final objective consisted of the generation of 3 different known $[Ca^{2+}]_i$ (100, 300, and 500nM) BAPTA-based solutions. The hypothesis is that the utilization of these solutions will help determine the global $[Ca^{2+}]_i$ necessary to elicit SK current in left atrial rabbit and in human right atrial adult myocytes.

3.4 Methods

3.4.1 Fura-2 free acid: intracellular ratiometric calcium indicator

Fura-2-Pentapotassium (PP) salt (Fig. 3.1) has been widely used as a fluorescent probe, which binds to calcium and allows the quantification of $[Ca^{2+}]_i$. This fluorometric dye was become essential in the investigation of Ca^{2+} handling mechanisms and its role in multiple signalling pathways (266). Fura-2 provides some advantages over other fluorescent probes in the study of physiological properties and pathophysiological states of cells.
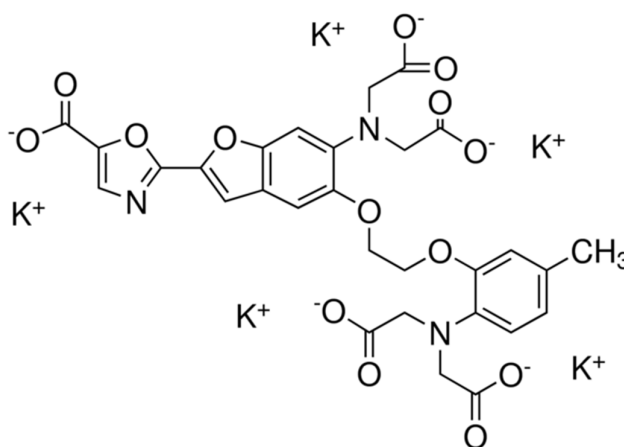
Fig 3.1. Fura-2 chemical structure (7).

Firstly, the fluorescence quantum yield, which is defined as the ratio of the number of photons emitted to the number of photons absorbed (267):

$$(1) \qquad \Phi(\lambda) = \frac{\#\ photons\ emitted}{\#\ photons\ adsorbed}$$

This value for fura-2 ranges up to ~0.5 with Ca^{2+}, which is typical of dyes normally considered to be highly fluorescent (Fig. 3.2)(7). In addition, this indicator's selectivity for Ca^{2+} is considerably better when compared to other dyes (7, 268) (table 2).
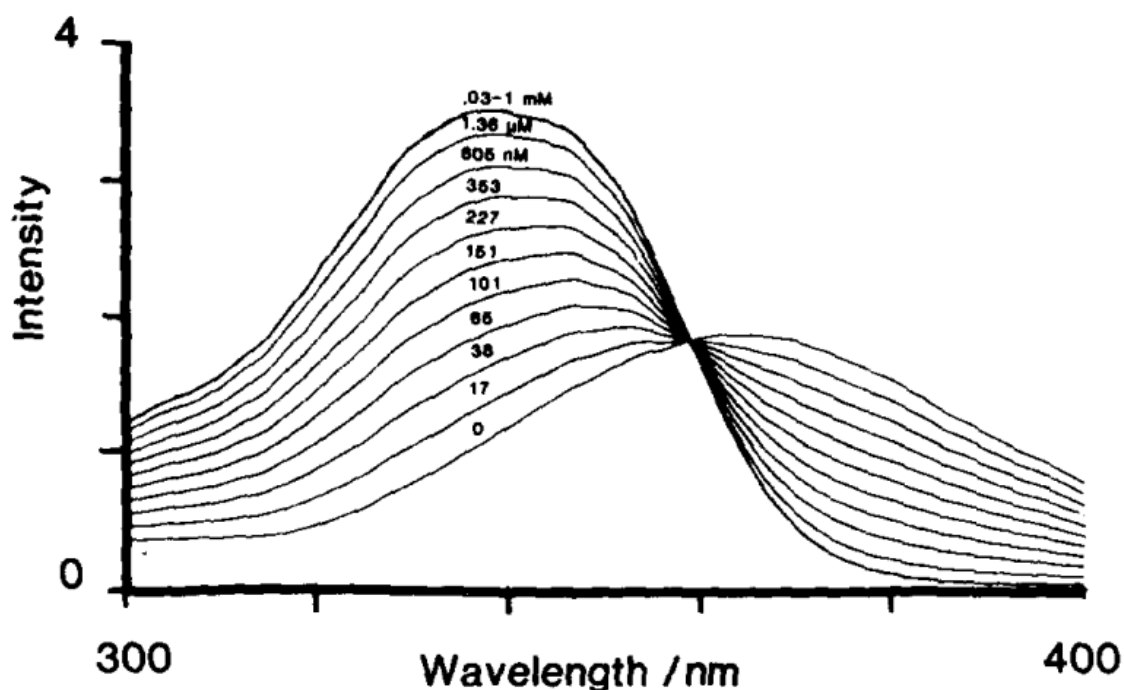
Fig 3.2. Excitation spectra for 1 µM fura-2 at 20˚C in buffers with free Ca^{2+} values ranging from <1 nM to >10µM.

An example of a set of excitation spectra for fura-2 in calibration buffers of varied $[Ca^{2+}]$. Given such calibration data, the $[Ca^{2+}]$ in an unknown solution containing the dye can be deduced from the shape of the excitation spectrum. The fluorescence excitation spectra shift to shorter wavelengths as $[Ca^{2+}]$ increases, much as the absorption spectra do. EGTA is buffering all the established free $[Ca^{2+}]$ values. Equality of Ca^{2+} and EGTA contents in the $K_2CaEGTA$ solutions was insured by titration of K_2H_2EGTA and $CaCl_2$. The excitation peak shifts towards 340 nm as $[Ca^{2+}]$ increases. Taken from Grynkiewicz et al (7).

Furthermore, this dye is more resistant to photochemical alteration (photobleaching) which can modify the outcome of the ratio method and, consequently, prevent accurate calcium concentration estimation. It has been

calculated that an 8% loss of total fluorescence intensity is sufficient to produce a large error (269). There are different classes of Indicators, which are characterized by their own advantages and limitations, but they can be simply divided into either single wavelength or ratiometric dyes. Each class requires specific lasers, filters, and/or detection methods that depend on their spectral properties.

Dye	Excitation Wavelength (nm)	Emission Wavelength (nm)	Apparent dissociation constant (K_d) for Ca^{2+} (nM)
Fura-2	340 & 380	500	224
Indo-1	340	405 & 485	250
Fluo-3	500	530	400

Table 2 Comparison of commonly used fluorescent indicators (268, 270)

Single wavelength indicators are generally very bright and optimal for Ca^{2+} detection while ratiometric indicators, where fluorescence is measured at two excitation wavelength (e.g. Fura-2, table 2), can be calibrated very precisely and they minimize the most common problems associated with chemical Ca^{2+} indicators: uneven dye loading, leakage, photobleaching, and changes in cell volume (271).

3.4.2 Buffering of intracellular Ca^{2+}

It has been demonstrated that large amounts of the fluorescent indicators, when loaded into the cells, can buffer the $[Ca^{2+}]_i$ and this results in lowering of $[Ca^{2+}]_i$ or blunting of Ca^{2+} transients (272) The fluorescent indicator Fura-2 has approx. 30-times more Ca^{2+}-dependent fluorescence intensity than some other dyes (7), therefore, it is possible to decrease intracellular dye loading, and consequent buffering, to obtain usable Ca^{2+}-dependent fluorescence signals (268, 273). Moreover, the absolute concentration of EGTA employed in the present solutions for the calibration procedures was not critical but could be

varied to set the ionic strength of these solutions at the level of interest. However, the absolute level of EGTA should be high enough that Fura-2 represents an insignificant Ca^{2+}-buffering contribution in comparison (EGTA:Fura-2 >>100:1) (274)

3.4.3 Fura-2 ratiometric wavelength dependency

Dyes that are characterized by low fluorescence intensities, present a shift of the peak excitation wavelength (when bound to Ca^{2+}) such as Fura2 and Fura-2-PP, but due to the long-wavelength end of their excitation spectrum, this shift cannot be directly related to intracellular Ca unless compared with the two spectra measured at high and low Ca^{2+}levels (7). For this reason, ratiometric property of the Fura-based dyes including fura-2-PP is very important, as it allows for calibration of $[Ca^{2+}]$ and obviates the need for experimental corrections for photobleaching, sample thickness variability, dye concentration, etc. in intracellular systems (275). As shown in fig.3.2 the binding of Ca^{2+} by Fura-2 shifts the wavelengths of the emission maxima much less than it shifts the excitation maxima. Basically, the 340nm excitation increases upon the formation of Ca^{2+} -Fura-2 complexes, while signal from 380nm excitation is reduced (7). This means that the ratio (R) of fluorescence emission intensity of this indicator (at two excitation wavelengths) allows, in principle, the use of standard calibrations to calculate $[Ca^{2+}]_i$ that is independent of dye concentration (276). However, It has been reported that solution viscosity influences the fluorescence properties of Fura-2, affecting the calibration of fluorescent signals in some cell types (277). Therefore, the in vitro calibration of Fura-2 needs to be performed in a solution that mimics the intracellular composition of the cells. In addition, the measurements of the fluorescent emission spectrum were obtained from increasing concentrations of Ca^{2+} (7) and the conversion of the resultant fluorescent ratio by plotting it as a function of the applied Ca^{2+} concentration. Furthermore, in the 90's Lattanzio et. al, showed that the probes have a reduction in binding affinity at acidic pH, and measured the appropriate K_d corrections (278). Therefore, when Fura-2 is used in a new cell type, the applicability of in vitro calibration must be checked by comparing in vitro and ex-vivo calibration curves (268). Finally, to ensure that the correct pH was used for physiological solutions, this was measured precisely with a pH electrode calibrated with commercially available, internationally defined standards.

3.4.4 Calibration procedures for Fura-2 measurement of free Ca^{2+}

As stated, K_d corrections are essential for the determination of precise [Ca^{2+}] measurements (278, 279). The majority of the literature has opted simply to refer to the original in vitro K_d determined by Grynkiewicz et al (7). However, to more precisely calibrate the fluorescence of Fura-2, it become necessary the use of the same cell type (280, 281), or at least the utilisation of the same optical system and experimental techniques with which the actual experiments were conducted, including any K_d correction (282-284). Therefore, following these guidelines, the relationship between excitation ratios (340nm:380nm), [Ca^{2+}]$_i$ and the dissociation constant (K_d) for Fura-2 were accurately determined through several calibration procedures utilising solutions of increasing [Ca^{2+}] at a given temperature, ionic strength and pH.

3.4.5 Conversion of fluorescence to [Ca^{2+}]

A dye species which is excited at two wavelengths, like Fura-2-PP, upon binding calcium shifts peak excitation wavelength and the resulting ratio values of the dye's fluorescence intensities, at just two excitation wavelengths, are sufficient to calculate [Ca^{2+}] (7). The sigmoidal relationship observed in Fig 3 can be explained by the following equation:

$$(2) \qquad [\,Ca^{2+}\,] \; = \; K_d * \left[\left(\frac{R - R_{min}}{R_{max} - R} \right) - 1 \right]$$

Where R_{min} is the ratio in the Ca^{2+}-free solution, R_{max} represents the ratio at a saturating Ca^{2+} concentration of the dye and K_d is the apparent dissociation constant (K_d app). The apparent K_d is linked to the real K_d by the equation:

$$(3) \qquad Kd\,(app) = Kd * \beta$$

Where β is the result of the ratio of the 380 fluorescence at Rmin divided by the 380 fluorescence at Rmax.

The filter system used presented a β value ranging from 10-12 (Godfrey Smith personal communication).

I availed of the software Origin version 7.5 to create a curve by fitting the data points generated with the logistic equation:

$$(4) \qquad R = R_{max} + (R_{min} - R_{max})/ (1 + (x/K_d))$$

With the same software the best fit for this curve was applied and after the substitution of R_{min} and R_{max} values to the equation (2) an intracellular estimation of Ca^{2+} was obtained.

3.4.6 Data recording, analysis and curve fitting

The output voltage from the PMT (photomultiplier tube) for the individual wavelengths (340nm and 380nm) and the ratio were saved on a hard disk for later evaluation. The interpretation of fluorescent ratio and channel data required the use of the software Origin version 7.5 and GraphPad Prism version 8. The calibration experiments were selected manually and for each experiment, potential artefact or noise, resulting from the chamber loading and stirring step, were removed. When inconsistencies concerning time length or reagents load timing were detected among readings, they were adjusted to be consistent across triplicates. Ratiometric data were converted into $[Ca^{2+}]$ adopting the parameters obtained from the Fura-2 calibration curves. Data are presented as mean values ± s.e.m. Unless otherwise stated, statistical significance was calculated using One-way ordinary ANOVA and statistical significance defined as $p < 0.05$.

3.4.7 The microscope

The selection of Fura-2-PP for this type of experiment was driven by the necessity of a ratiometric dye which allowed an accurate estimation on $[Ca^{2+}]_i$ with less susceptibility to possible movement artefacts (285), which can be experienced during recordings in cells. The signals were registered using an inverted microscope (schematic configuration in Fig 3.3) which greatly facilitates viewing living cells using a high numerical aperture oil-immersion objective (9). A xenon arc lamp (75W) was utilised, which are generally superior to mercury lamps for excitation ratioing, because xenon gives a broader and relatively uniform spectral output. The xenon lamp was utilised to excite Fura-2 every 100 milliseconds for the 380 nm channel and at every 50 milliseconds for the 340nm. Fluorescent data were collected at both wavelengths and processed with a PMT, which can give continuous records of fluorescent intensity, ratio signal and it allows a rapid time course of $[Ca^{2+}]_i$ changes (268). 500Hz rotating optical chopper and bandpass filters were utilized as the main system for selecting wavelengths. Thus, the total fluorescence of Fura-2 was recorded at 510nm (emission wavelength) after excitation by alternating 340nm and 380nm wavelengths. Finally, IonWizard (by IonOptix, LLC) software was employed for data acquisition and trace analysis (background subtraction, ratio and ion calculation).
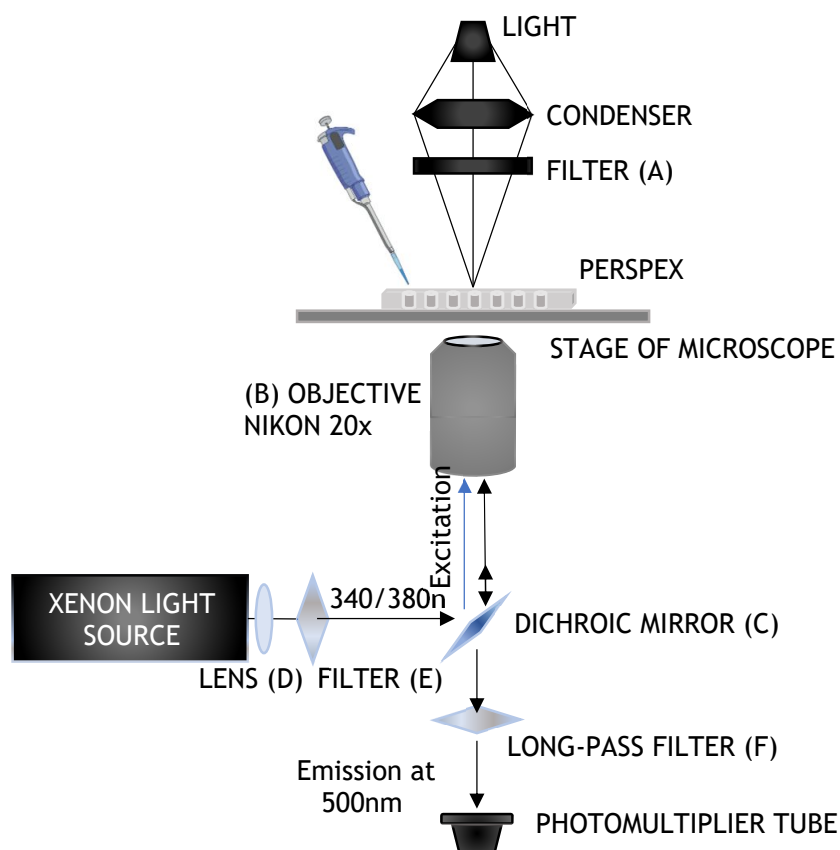
Figure 3.3 Apparatus used for measurement of [Ca^{2+}] with fluorescent indicator probes that binds free-Ca^{2+}.
(A) Bandpass filter to pass 730-770 nm infrared from the tungsten lamp above. (B) 20x Objective lens (Nikon Plan Flour w20 D). (C) Dichroic mirror to reflect below 405 nm and transmit above 405 nm. D) Convex lens to decrease the size of the projected image by focusing it less far outside the microscope. (E) Filter to contribute additional blocking of infrared wavelengths. (F) Long-pass barrier filter to block wavelengths below 420 nm or 455 nm. (adapted from Tsien et al. 1990) (9).

3.4.8 The Perspex block bath

To proceed to the calibration, firstly, a Perspex block bath (similar to a home-made Plexiglas multiwell, fig. 3.4) was prepared, with 12 wells which served as chambers for testing samples of different dilutions. A coverslip was attached underneath each well of the Perspex block using silicone grease.

Then, each one of the seven dilutions of EGTA/CaEGTA was loaded in 100 μl chambers with the fluorescent indicator and manually stirred with the aid of a pipette tip. Specifically, 2 μL of Fura-2PP (0.02 mM) were added to 98 μL of each solution to test and agitated to ensure interaction between Fura-2-PP and Ca^{2+}. Agitation was characterised by the pipette circularly moving, to ensure a homogeneous mixture.

Figure 3.4 Perspex block composed of 12 wells for the analysis of solution samples.

3.4.9 Calibration protocol using standard buffer solutions

The comparison between in vitro and in vivo is made possible by calibration of Fura-2 ratios that includes the preparation of solutions of known total ($[Ca]_T$) in the nM and µM range (276).

100mM EGTA solution			
Compound	Stock solution concentration (M)	Desired concentration (mM)	Volume of each compound to be added to make up 100mL solution (mL)
EGTA	0.1	10	10
KCl	1	100	10
NaCl	1	10	1
HEPES	0.5	25	5
$MgCl_2$	1	1	0.1
100mM CaEGTA solution			
Compound	Stock solution concentration (M)	Desired concentration (mM)	Volume of each compound to be added to make up 100mL solution (mL)
CaEGTA	0.1	10	10
KCl	1	100	10
NaCl	1	40	4
HEPES	0.5	25	5
$MgCl_2$	1	1	0.1

Table 3 List of chemicals used to make 10mM EGTA and 10mM CaEGTA from 100mM stock solutions for generation of the Fura-2 calibration curve. Stock solution were calibrated to pH 7 using KOH at 20-24°C. They were stored in the fridge for further use.

We adopted the ratio method (with Fura-2-PP) for the preparation of the buffer solutions. This method requires the use of two background solutions: one containing only ligand and the other containing Ca–ligand (Table 3). The two solutions are then mixed in the appropriate proportion to give the 7 buffer solutions, in which the $[Ca]_T$ is known but the ionized $[Ca^{2+}]$ needs to be measured (table 4). Sufficient KOH was substituted for KCl to compensate for the acidity of the ligands so that the pH of both the ligand solution and the Ca–ligand solution was just slightly more alkaline than pH 7.25. Both solutions were

titrated to pH 7.25 with 1M KOH. Buffer solutions were obtained through the creation of a series of mixed dilutions starting from stock solutions of 100mM EGTA and 100mM CaEGTA (table 3). Then, small aliquots of the resulting 10mM EGTA and 10mM CaEGTA solutions were added, in different proportions, to make a series of calcium calibration buffers (1 ml each) that exhibited different well-established free Ca^{2+} values with free calcium concentrations ranging from zero (10mM EGTA) to 60μM (10mM CaEGTA). The purity of the EGTA must be known, to maintain the calcium contamination at as low a level as possible (253).

EGTA:CaEGTA	Volume to be added (μL)		[Ca^{2+}] in M
	EGTA	CaEGTA	
1:0 (10mM EGTA)	1000	0	1E-09
10:1	900	100	4.18E-08
3:1	600	400	1.25E-07
1:1	500	500	3.75E-07
1:3	400	600	1.2E-06
1:10	100	900	4E-06
0:1 (10mM CaEGTA)	0	1000	6E-05

Table 4 Shows 7 different dilutions which were required to create the calibration curve for EGTA.

Seven different dilutions of EGTA/CaEGTA will represent the multiple points in the Fura-2 calibration curve. Dilutions commonly used are: 10mM EGTA, 10:1, 3:1, 1:1, 1:3, 1:10, 10mM CaEGTA. For each one of these solutions, the calcium values are already known (table 4). Intracellular [Ca^{2+}] concentrations were estimated using the React software (286). Values concerning the buffering capacity of EGTA were obtained from Smith and Miller (287). Importantly, the free [Ca^{2+}] is a function of the apparent Ca-EGTA association constant (K_{CaEGTA}) which will impact strongly on the K_d of Fura-2 and consequently on the [Ca^{2+}] measurements (276).Therefore, accurate pH adjustment (within 0.01 pH units) was adopted, due to the high sensitivity of EGTA to pH variations around 7.00 (276), and the calibration experiments were performed at a specified temperature.

3.4.10 BAPTA, tetrapotassium salt: when faster kinetics are required.

In some circumstances BAPTA-tetrapotassium salt can have limitations, since it is not possible to get avoid the potassium which may be a requirement of certain experiments. In order to achieve zero potassium solution, normally the BAPTA-free acid buffer is required, because it gives more scope with chemistry. This is not the case, since my solution, required potassium for the detection of I_{SK}. The calcium buffering power of the cell is of the order of 100µM, depending on where its measured, so it must be countered with a higher buffer power (at least 3 times stronger, so in the order of mM) (265). BAPTA (tetrapotassium salt, cell impermeant) was chosen because is more selective for Ca^{2+} than EDTA, and its metal binding is also much less sensitive to pH (259, 288). In addition, BAPTA has a similar buffering range to EGTA for Ca^{2+}, but with faster kinetics (100-fold increase) (265). This is a very important feature, since there was the necessity to obtain a maximum buffer power close to the inner subsarcolemmal surface. So, it was needed to maximise the BAPTA level, and even though 1 mM would have been sufficient for the objective, the uncertainty of calcium contamination would have been high. Therefore, to be absolutely sure, 5mM BAPTA was used, which guaranteed the fastest calcium buffering envisaged in an experiment. K_d remains an important determinant for accurate $[Ca^{2+}]$ measurements, but since BAPTA is not pH sensitive (or very low) and the temperature and $[Ca^{2+}]_i$ achieved were constant, the K_d could be extrapolated. Therefore, no calibration curves was performed for BAPTA but instead the amount of calcium necessary to get to 100nM and 300nM was measured; this indirectly generated the K_d. More precisely, an internal check was performed calculating the amount of exogenous calcium that was added and the $[Ca]_T$ in the solution. The result of this calculation permitted extrapolation of the K_d for in vitro measurements and to compare it with the Kd obtained from ex-vivo measurements (in rabbit left atrial myocytes). In fact, during the course of the measurements, endogenous fluorescence may change the background fluorescence as the result of compounds and compartmentalized Fura-2 indicator (289) and consequently this artefact, un-corrected with suggest changes the BAPTA K_d values.

3.4.11 Creation of final intracellular solutions with BAPTA: PIP42

The protocol required the creation of new solutions, based on the intracellular solution PIP35 composition, to which BAPTA (5mM) was added, and to compensate for the potassium concentration reached in the solution KOH was used to bring the pH to neutral values. Then the ratio values needed, to achieve 100 nM, 300 nM and 500 nM $[Ca^{2+}]_i$ in my solutions, were established (with ± 5% of error) using the EGTA/CaEGTA calibration curve. The next step demanded precise measurement of volume for PIP42 (i.e. PIP35 with BAPTA) and the addition of small quantity of solution, from high $[Ca^{2+}]$ stock, to maintain the difference in volume negligible (<5%). Initially, only 120 μL of $CaCl_2$ from 1 M stock solution were added to 10 mL of PIP42, in order to reach a safe point of calcium concentration. At this point, the process of titration started with the addition of 1-2 μL of stock solution (1 M $[Ca^{2+}]_i$) each time. Every addition of $CaCl_2$ was monitored, using 98 μL of solution sample to which 2 μL of Fura-2 were added, and using the same apparatus described above, the ratio was measured to ensure that the right $[Ca^{2+}]_i$ was achieved (based on the ratio value obtained with Fura-2 calibration in EGTA). Values were originated from at least three technical replicates of 3. This procedure was repeated until the ratios that represented 100nM, 300nM and 500nM $[Ca^{2+}]$ were reached.

3.5 Results

3.5.1 Creation of calibration solution based on the pipette solution for ruptured patch-clamp

The first calibration experiment was carried out using standard buffer solutions (table 2). The resulting ratio (340:380) values are plotted against the calcium concentration in logarithmic scale (in M) (Fig. 3.5). This procedure was necessary to calibrate the apparatus and get the K_d values for Fura-2 at a certain temperature and ionic strength.
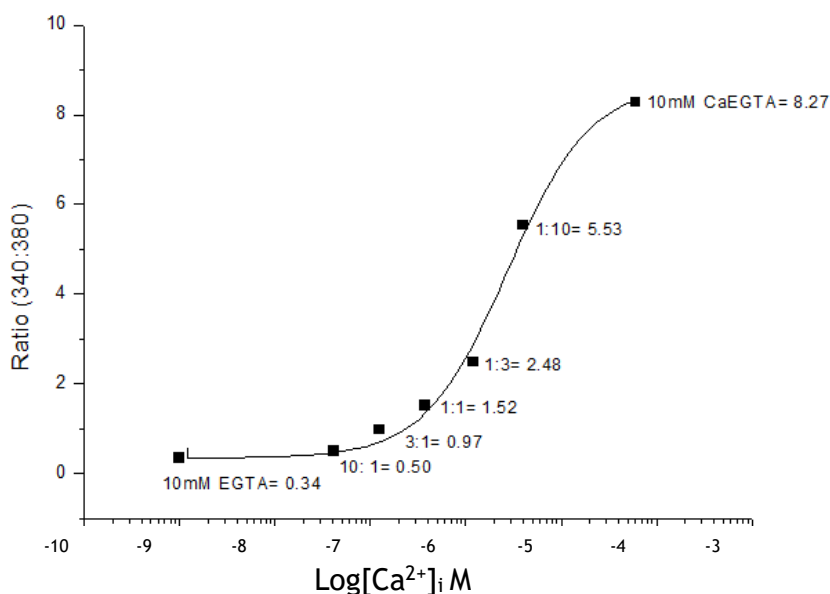
Figure 3.5: Calibration curve for Fura-2 pentapotassium based on mixtures of EGTA and CaEGTA using standard buffer solutions.

The ratio of the Fura-2 fluorescence was plotted against the LogCa (M) in order to generate a sigmoidal curve fitted according to the logistic function (equation: $y = A2 + (A1-A2)/(1 + (x/x0)^p)$) utilising an analysis program (Origin, Version 7.5) for nonlinear data. Rmin was calculated to be 0.34 ± 0.2, Rmax was equivalent to 8.27 ± 0.3 and, measured Kd was 2.7 µM ± 0.3 µM . Slope was equal 1. Data is represented as means ± s.e.m (n=6). Readings were performed in triplicate at 22-23°C. The value of each point represents the ratio recorded for that particular $[Ca^{2+}]_i$.

Once the calibration using standard buffer solutions was completed, the next step involved the use of a solution that reproduced the intracellular milieu used in cells, called "PIP35"(in mM): 130 K-aspartate, 15 KCl, 10 NaCl, 1 $MgCl_2(\cdot 6H_2O)$, 10 HEPES. The pH was set to 7.25 by back titration with 1M KOH. Based on this solution two background solutions were generated adding 10mM EGTA and 10mM CaEGTA from 100mM stocks. The compensation for the acidity and the potassium concentration was accomplished using KOH. An inverted microscope was used to detect fluorescence changes in the bath due to the binding of Fura-2 to free-Ca^{2+} present in different concentrations in each well. One by one, wells were positioned on the stand of the inverted microscope and the fluorescence ratios produced at 340nm and 380nm were recorded. A calibration curve of fluorescence ratio against the Ca^{2+} concentration (in M) was plotted in logarithmic scale (Fig. 3.5). This procedure was routinely used to calibrate the fluorescent signals. To proceed to the calibration, the first step involved the preparation of 500mL of a pipette solution for ruptured patch-clamp (PIP35) that was used throughout this project, with ionic concentration within mammalian physiological ranges, i.e. "PIP35" as used in previous studies from the Workman laboratory (58, 290). A 10 mL sample was used to run the protocol. The setup facilitated the access to each small well and permitted the following up of 340:380 dynamics, so that Fura-2-PP loading and stirring steps could be performed manually, without any physical impediments. Pipette tips were inserted perpendicularly all the way down to the centre of the bath chamber.

3.5.2 Results of calibration: advantages of self-prepared buffers

The calibration was performed with self-prepared buffer and calibration solutions, which can be tedious and time-consuming, and the measurements were taken between 60 and 80 minutes. However, the use of self-prepared calibration solutions, guaranteed a great control on the coefficient of variation (CV). An upper limit of ± 10% deviation from the mean value for [Ca^{2+}] is attainable if the CV is less than 5% (252, 256). This CV percentage can be reduced by increasing the accuracy of solutions preparation, pipetting and improving the control of pH in the buffer solution (256). Initially, the fluorescence of Fura-2 was measured in the solutions deprived of the standard buffer, in this way it was possible to calibrate the system for background fluorescence at the excitation wavelengths of 340 and 380nm. The initial stirring process is necessary for the

Fura-2 to not precipitate and being uniformly mixed. This was followed by withdrawing of the tip from the chamber. Then, fluorescence was recorded without external interference. Importantly, the microscope was focused to the bottom of the well to reduce the out-of-focus blur. At this point, the Perspex block with the different dilutions was positioned on the stage of the microscope, and one by one each well was tested for fluorescence emission. The calibration traces produced were recorded for 3 minutes, which was enough time to generate stable signals as EGTA bound to Ca^{2+} and reduced free $[Ca^{2+}]$. The optical train was converted to epifluorescence using a xenon arc excitation source and fluorescence emission detection with a photometer and photomultiplier tube (Cairn Research Ltd, Kent, UK). Subsequently, background measurements are subtracted from the in vitro measurements. Then, the obtained ratio (340:380 nm) of the two resulting measurements is calculated and, finally, ratio images are calibrated in terms of mean $[Ca^{2+}]_i$ (268) (Fig. 3.6 B).
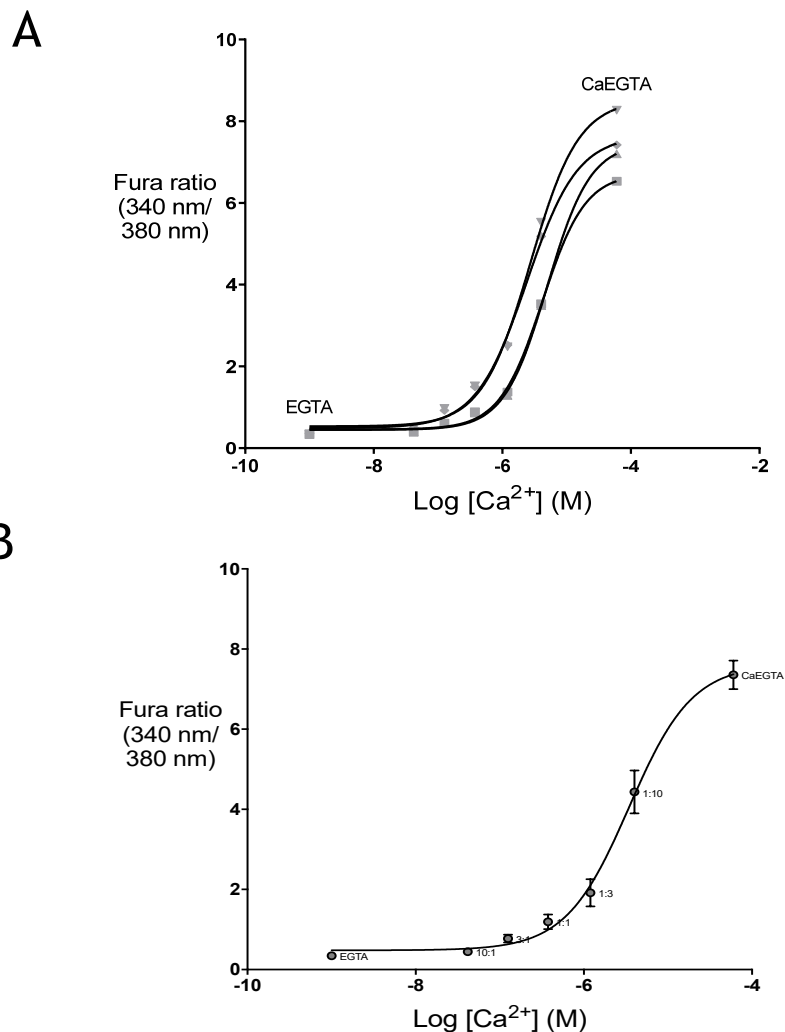
Figure 3.6   Calibration curves for Fura-2-PP based on mixtures of EGTA:CaEGTA.

A) Four independent calibration curves recorded on different days and B) the mean calibration curve. The ratio of the Fura-2 fluorescence was plotted against the Log $[Ca^{2+}]$ (M). Average Rmin was calculated to be 0.35 ± 0.01, Rmax was equivalent to 7.4 ± 0.4 and, measured Kd was 3.6 µM ± 0.6 µM. Slope was equal 1. Data is represented as means± s.e.m (n=4). Readings were performed in triplicates at 22-23°C. The value of each point represents the ratio recorded for that particular $[Ca^{2+}]_i$.

3.5.3 Estimation of Fura-2 dissociation constant for Ca^{2+}

The free Ca concentration can be estimated from the relative proportion of CaEGTA to EGTA in each of the solution mixtures. However, such estimations contain many sources of error, such as the value adopted for apparent affinity constant (K'_{Ca}) for EGTA association with Ca^{2+} or the actual total concentration of EGTA in a solution due to impurities and an unknown and a variable degree of hydration of EGTA. Importantly, this uncertainty spreads into the estimation of fluorescence ratio-[Ca^{2+}] relationship and the K_d for Ca/Fura-2 (274). Therefore, to bypass this issue the K_d of Fura-2 was extrapolated from the absorbance spectra measured in calibration solutions, in vitro. Single calibration curves (Fig. 3.6A) were obtained on different days from a series of replicates in order to test the consistency of K_d. The results of the analysis of these curves showed dissimilarity in K_d values from the same experimental setup (table 5). Rmax (CaEGTA) calibration points showed the main variability. These readings were performed at 22-23°C. Values for K_d were found to vary in some determinations. This could depend on the relationship between K_d and the ratio of the fluorescence intensity coefficient at 380 nm in the virtual absence of Ca^{2+} to that in the presence of an excess amount of Ca^{2+}, which is known as β. Although the β ratios give intermediate dynamic range on the [Ca^{2+}] dependence of R (340:380), the variations of ratios are large, especially at high Ca^{2+} concentrations, as shown in table 5. And this variation can affect the K_d in part because of the very weak fluorescence intensity for Ca^{2+}-bound Fura-2 at 380 nm and in part due to Fura-2 partial vulnerability to photobleaching (266, 269). However, the standard K_d obtained can be considered a reliable constant which is being regularly checked and, despite some discrepancies, Kd values are still within the acceptable range of variation. The average Kd in my experiments was 3.6 μM which, assuming the beta value of 12 (for the set of filter used), gives an apparent Kd of 0.3 μM (see eq. 2), which is not far from the value previously reported, if the differences in experimental conditions are considered (7). This dataset allowed the determination of the relationship between excitation ratio and Ca^{2+}, and for calculation of the K_d for Ca^{2+} Fura-2 in rabbit left atrial and human right atrial cardiomyocytes.

Calibration curve	Rmin	1:1	Rmax	K_d (M)
1	0.35	0.89	6.53	4.2 E-06
2	0.33	0.86	7.21	4.9E-06
3	0.34	1.52	8.27	2.7E-06
4	0.36	1.50	7.42	2.4E-06

Table 5 Summary of calibration parameters and Kd across multiple experiments. Values were originated from at least three technical replicates.

3.5.4 Verification of $[Ca^{2+}]_i$ in rabbit left atrial cells.

Concentration of 500nM $[Ca^{2+}]_i$ was considered borderline for patch-clamp recordings in cells. The reason lies on the fact that, usually, cells experiencing 500nM $[Ca^{2+}]_i$ continuously for a long period of time (>3 minutes) will contract, shorten (291) and lose the electrode seal. It is true that SK channel activity has been reported at higher $[Ca^{2+}]_i$ (~10µM) (257), but as stated in the beginning of this chapter, this was not measured in cardiac myocytes.

Therefore, it was decided to verify the calcium concentration in single rabbit left atrial cells loaded with Fura-2PP through the patch pipette, at 37°C, using a similar setup to the one used for Fura-2 calibration. However, due to the change of the apparatus and experimental conditions, many variables had to be considered. The limiting value of the apparent K_d of Fura-2PP is about a 4-fold increase in K_d when compared to that without proteins (266). Thus, on the hypothesis that K_d would be altered in cells, a set of calibration curves was plotted, based on three standardization points (Fig. 3.7). Figure 3.7 shows the results obtained from the calibration measurements of fluorescence in rabbit left atrial cells dialysed with 3 different $[Ca^{2+}]_i$ intracellular solutions loaded with Fura-2PP.
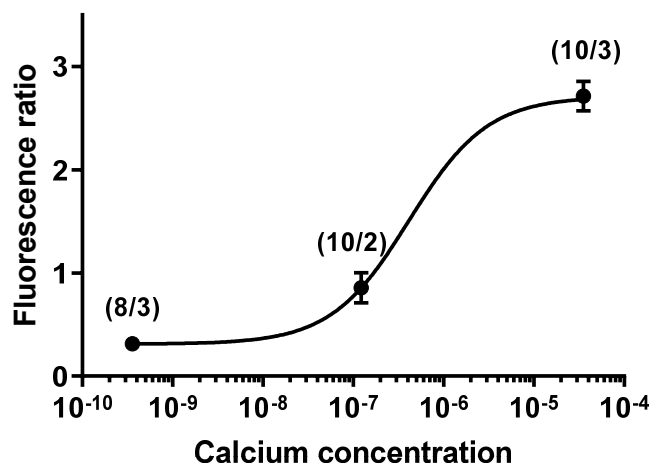
Figure 3.7 Mean calibration curve for Fura-2-PP based on PIP35.
The ratio of the Fura-2 fluorescence was plotted against the Log $[Ca^{2+}]$ (M) in order to generate a sigmoidal curve fitted according to the logistic function (equation: $y = A2 + (A1-A2)/(1 + (x/x0)^p)$) utilising an analysis program (GraphPad Prism version 8) for nonlinear data. Rmin was calculated to be 0.31±0.02; Rmax was equivalent to 2.71 ± 0.14 and, measured Kd was 2.03 µM ± 0.2 µM. Slope was equal 1. Data is represented as means± s.e.m (n=8-10 cells, 2-3 rabbits). Readings were performed in triplicate.

Each one of the three points represent the individual average measurement (fluorescence ratio) for single cells dialysed with 3 different $[Ca^{2+}]_i$ solutions. For each single cell it was possible to measure only one $[Ca^{2+}]_i$ at time, since the cells were loaded with the specific intracellular $[Ca^{2+}]_i$ solution and patched. These experiments were challenging and only three points were required to define the curve of a sigmoidal relationship, which was established based on the more extensive *in-vitro* calibration measurements. In addition, since K_d is reported to be strongly dependent on the ionic strength of a solution (7, 269, 292, 293) the variation was maintained sufficiently small in order to not affect K_d. The pH of solutions was kept within ± 0.01 pH unit and ionic strength was kept constant using KCl. Once the sigmoidal curve from calibration measurements in cells was obtained, the next step was to measure the ratio value of the actual $[Ca^{2+}]_i$ present in cells loaded with 3 different $[Ca^{2+}]_i$ solutions. Figure 3.8 shows the results obtained from the application of a BAPTA buffering system to intracellular solutions at 3 different $[Ca^{2+}]_i$ based on the

calibration curve shown in figure 3.7. Ratio values were recorded after cells were loaded with each one of the 3 designated $[Ca^{2+}]_i$ solutions containing 5 μM of Fura-2-PP (Thermo Fisher Scientific). Once correction for the variables mention above was achieved, the ratio value was converted to $[Ca^{2+}]_i$, in cells (figure 3.8 B) and compared with the one obtained in vitro (Fig. 3.8 A). Figure 3.8 A shows that BAPTA based solutions are routinely producing consistent $[Ca^{2+}]_i$ measurements in vitro compared to the $[Ca^{2+}]_i$ expected. Whereas, Figure 3.8 B shows that the same measurements in cells produced similar results to the one in vitro, but much more variable data were observed. This was probably due to the inability to precisely measure the background fluorescence (at 340 and at 380). Small errors in these type of measurements will result in larger errors in ratio measurements in cells. Also, the biological variation and compartmentalization of Fura-2 indicator (289) in cells has to be considered. However, a significant step increasing $[Ca^{2+}]_i$ was observed between 100 nM $[Ca^{2+}]_i$ solution (95 μM ± 18 μM, mean ± s.e.m., unpaired data, Fig. 3.8 B) and 300 nM $[Ca^{2+}]_i$ solution (357 μM ± 77 μM, mean ± s.e.m., unpaired data, $p<0.05$ Fig. 3.8 B). Also, a significant increase was observed between 300 nM $[Ca^{2+}]_i$ solution (357 μM ± 77 μM, mean ± s.e.m., unpaired data, Fig. 3.8 B) and 500 nM $[Ca^{2+}]_i$ solution (479 μM ± 98 μM, mean ± s.e.m., unpaired data, $p<0.05$ Fig. 3.8 B).
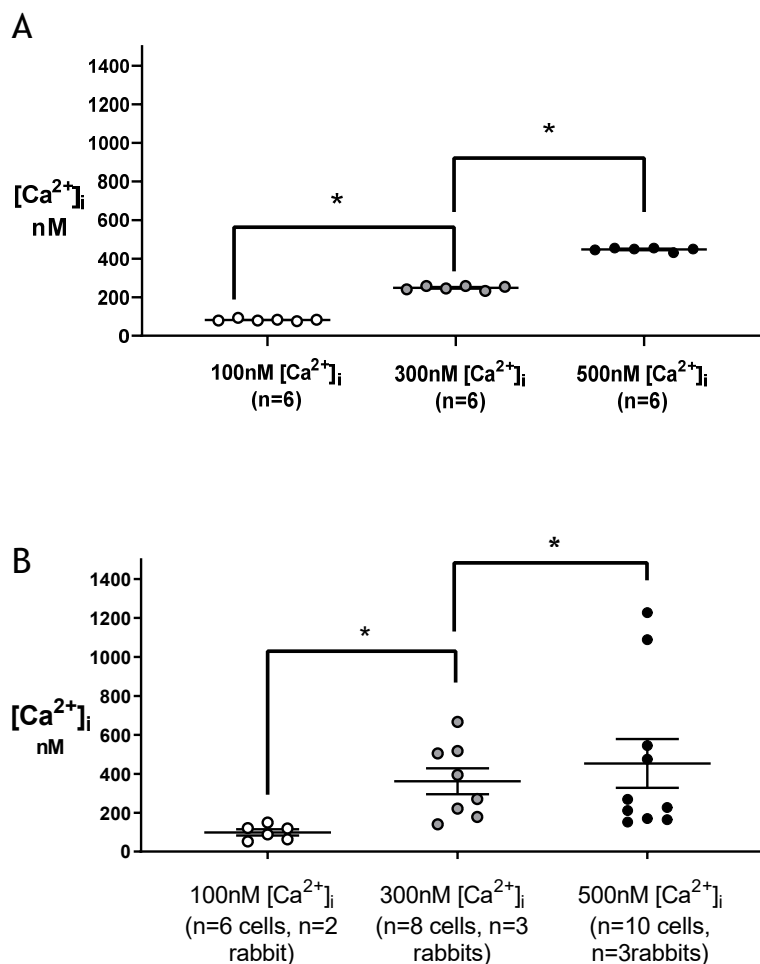
Figure 3.8 Comparison between [Ca^{2+}]$_i$ recorded in vitro and in cells, using a patch clamp apparatus optimized for calcium imaging.

Dot-plot showing 3 different increasing [Ca^{2+}]$_i$ solution measurements A) in vitro and B) in cells. Each point represent single recording A) in vitro and in B) single rabbit atrial cells. B) sample size 100nM: n=6 cells, n=2 rabbits; 300nM: n=8 cells, n=3 rabbits; 500nM: n=10 cells, n=3 rabbits. All values are mean ± s.e.m. A value of p<0.05 was considered statistically significant.

The results of these measurements confirms that the 3 different [Ca^{2+}]$_i$ solutions used successfully allowed the achievement of 3 significantly increasing [Ca^{2+}]$_i$ in cells. Interestingly, at the highest expected concentration (500nM) it was possible to appreciate the variability among the estimated [Ca^{2+}]$_i$ values measured inside cells, which reached values up to 1.23 µM [Ca^{2+}]$_i$ (figure 3.8 B). These values were also achieved during experiments, due to the high BAPTA

concentration (5mM), which immediately clamped the calcium inside the cell, minimizing the possible errors due to biological variability. The range of values estimated represents the technical problems of distinguishing Fura-2 fluorescence from background fluorescence measurements particularly at the higher calcium concentrations.

3.5.5 Additional verification of increased $[Ca^{2+}]_i$ in cells

Excitation-contraction coupling in heart muscle is triggered by an increase in the concentration of intracellular calcium (294). A discrete increase of $[Ca^{2+}]_i$ fuses into a peripheral 'ring' of elevated $[Ca^{2+}]_i$, followed by propagation (via calcium-induced Ca^{2+} release, CICR) to the cell centre, resulting in contraction (295). Therefore, the effect of raising the $[Ca^{2+}]_i$ from physiological range to 500nM, was tested by monitoring the cell length time course (Fig. 3.9 B).We expected a partial contraction of the cell as a consequence of globalising calcium through dialysis of 500nM $[Ca^{2+}]_i$, present inside the pipette, into the cytosol after rupture (291). The cell length was monitored before the seal (resting cell) and every 20s after the rupture by the patch-clamp pipette tip, for >3 minutes. As a result, 500nM global $[Ca^{2+}]_i$ resulted in a contraction of the cell, which reduced the cell length by ~8% compared to the resting state. In addition, the variations in cell length were compared between cells dialyzed with 100nM and 500nM $[Ca^{2+}]_i$ (Fig. 3.9 A), which showed a shortening of 7.3% at the highest calcium concentration. The cells were simultaneously stimulated using a voltage-ramp protocol at 0.1Hz (increasing from -120mV to +50mV, Holding potential of -50mV). These measurements provide an additional confirmation of the significant increase in $[Ca^{2+}]_i$. In fact, a shorten cell length indicates chronic contraction of the microfilaments due to activation by calcium. Under the conditions of the voltage clamp experiments the $[Ca^{2+}]_i$ was buffered at 3 precise values based on BAPTA solutions described previously. The step-wise increase in calcium inside the cells was confirmed by the chronic cell shortening, which was monitored. The increase in cell shortening confirmed that calcium inside the cell was increased from diastolic (i.e. 100nM).
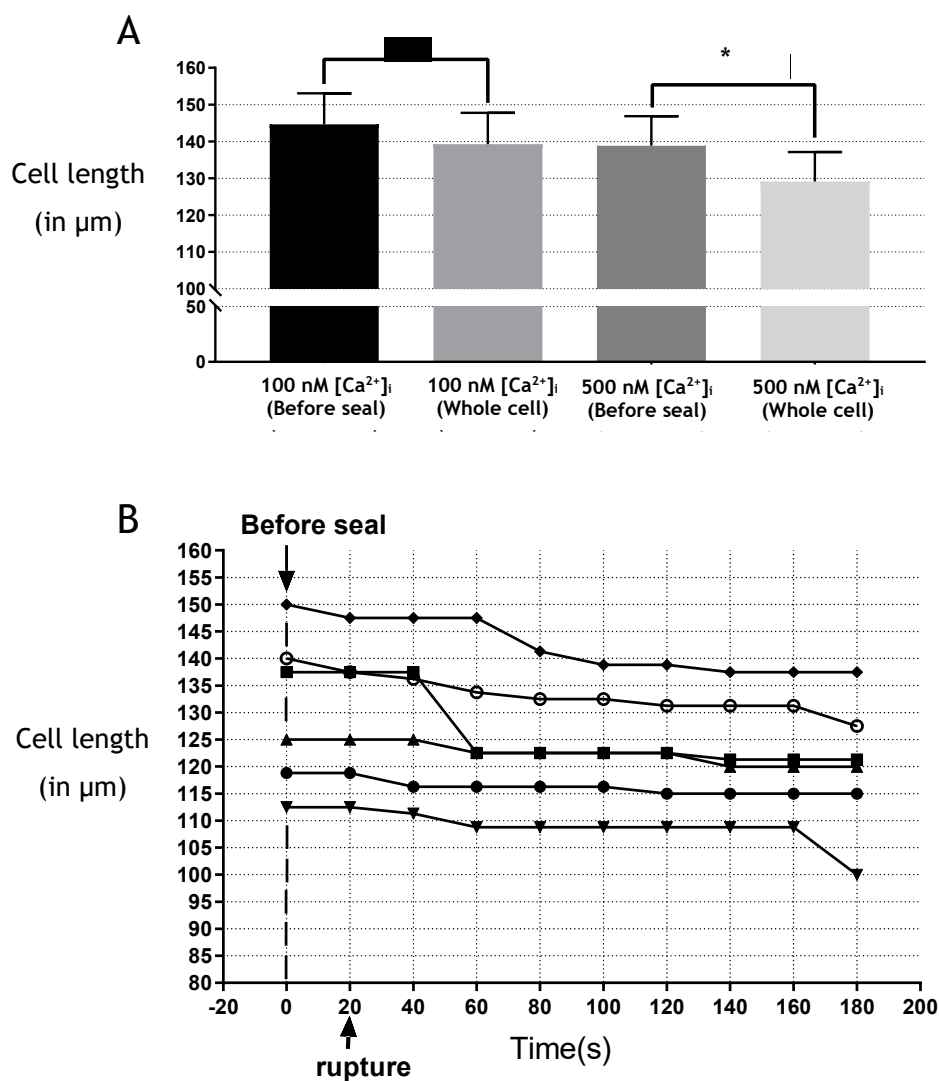
Figure 3.9 Cell length measurements at increasing [Ca^{2+}]$_i$.

A) Average cell length at 2 different [Ca^{2+}]$_i$ before and after rupture. B) Cell length time course before seal and after rupture at 500nM [Ca^{2+}]$_i$. Measurements were performed simultaneously to cell stimulation. Cell length was only analysed for atrial myocytes that displayed a prominent linear contraction. Sample size for 100nM [Ca^{2+}]$_i$: n=7 cells, n=5 rabbits; 500nM: n=9 cells, n=5 rabbits.

3.6 Summary

In this chapter are described the calibration procedures carried out in self-prepared buffers, which guarantee a total control on the main variables (ionic strength, K_d, and buffering power) that characterise every $[Ca^{2+}]_i$ measurement (274). The precision reached during these calibrations permitted to ensure the right $[Ca^{2+}]_i$ in cells and the substitution of EGTA with an alternative and faster calcium chelator: BAPTA. The injection of calcium buffers into the cells is an important method for controlling cytosolic calcium (296) and BAPTA permits fast calcium buffering (~100 times faster than EGTA), essential to control any immediate calcium variation inside the cell (263, 265). Therefore, BAPTA has frequently been used for patch-clamp experiments due to its speed of clamping calcium during physiological exchange in the cells. Based on the fast diffusion constant of Ca^{2+} and BAPTA (297), it was assumed that after rupture the pipette solution would diffuse inside the cell and rapidly clamp Ca^{2+} to the desired concentration. However, differently from other studies (203, 298), I decided to measure the calcium concentration inside the cells, since this may not fully equilibrate with the pipette solution. In fact, it was discovered that the $[Ca^{2+}]_i$ was not exactly the one expected (especially at 500nM). Nevertheless, a statistically significant difference among each concentration in cells was achieved as reported by mean values for expected 300 nM (357 µM ± 77 µM) and for expected 500nM (479 µM ± 98 µM) $[Ca^{2+}]_i$ solution. The $[Ca^{2+}]_i$ achieved in cell was, therefore, considered to be sufficient to generate an increment in the I_{SK} current, if present in rabbit left atrial or human right atrial myocytes.

The implication of this part of the work are that, for the investigation of I_{SK} and its $[Ca^{2+}]_i$-sensitivity in the next chapters, I have developed a reliable way of setting and keeping constant the $[Ca^{2+}]_i$ at values between 100 and 500 nM, verified firstly in glass tubes, then in the cells to be patched themselves. In conclusion, the solutions generated by the designated method represent a fundamental step toward the investigation of the $[Ca^{2+}]_i$-sensitivity of atrial I_{SK} within $[Ca^{2+}]_i$ typical of global diastolic-to-systolic values.

Chapter 4 Investigation of the relationship between SK3 current amplitude and intracellular [Ca^{2+}] using inside-out patch technique

4.1 Introduction

Ionized calcium (Ca^{2+}), the most common signal transduction element in cells, regulates many cellular processes. Especially, upon cardiac myocyte membrane depolarization, Ca^{2+} enters the cytosol mainly via voltage dependent L-type Ca^{2+} current (I$_{CaL}$), which triggers Ca^{2+} release from the sarcoplasmic reticulum (SR) via Ca^{2+} channels or ryanodine-receptors (RyR), a process termed Ca^{2+}-induced Ca^{2+} release (CICR) (299, 300). This is one of the main processes that through a complex system of transmembrane molecules, channels, pumps and exchangers, maintain global intracellular Ca^{2+} concentrations at very low levels (10–100 nM) (301). Different classes of ion channels, such as SK channels, are gated by intracellular Ca^{2+} ions. The superfamily of Ca^{2+}-activated K$^+$ channels (KCa) is composed of the group of small (KCa2.1–2.3), intermediate (KCa3.1) and large-conductance (KCa1.1) channels. These channels play a crucial role in hyperpolarizing the membrane potential and modulate calcium signalling cascades in both excitable and non-excitable cells (302). In the last few years SK channels have been much better characterised and studied for their possible involvement in AF (196, 206, 303), due to their crucial role in the cardiac repolarization in both rabbit and human models (304-306). It is generally accepted that CaM has a role in the gating of all SK2 and SK3 channels (161, 307-309). KCa2 and KCa3.1 channel opening begins via Ca^{2+}-binding to the N-loops of calmodulin (CaM) constitutively attached to a calmodulin binding domain (CaMBD) located in the proximal intracellular C terminus (165, 307). The energy of the ensuing conformational change is transferred to the transmembrane (TM) regions to open the gate. The small and intermediate-conductance channels are closely related for structure and function, in fact, KCa2 and KCa3.1 channels are both inward-rectifying, voltage-independent, and activated solely by submicromolar concentrations of intracellular Ca^{2+} (161). KCa2 and KCa3.1 channels share 25-35% sequence homology and they have similar activation mechanisms, but they can be found in different tissues. (310, 311). In fact,

KCa3.1 subunits are components of IK channels, which are mainly expressed in blood and epithelial cells, and in some peripheral neurons, whereas KCa2 channels are predominantly expressed in the nervous system (161). Importantly, few years ago SK1 and SK2 transcripts were found to be more abundant in atria compared with ventricle, while similar SK3 expression levels were found in both atria and ventricle (27, 28). In addition, KCNN3 gene, encoding SK3, in mice, is one of the few genes directly linked to clinical AF, indicating that Ca^{2+}-activated SK channels are important in human atria (206, 303). It has already been demonstrated, using calcium activation curves of SK channels, that all three SK subtypes share similar gating mechanisms and calcium sensitivities, with calcium concentration between 0.3 and 0.7 µM being sufficient to achieve half-maximal activation of the SK channels at 22-23°C (165, 186, 262, 298, 308, 312-315). However, since the majority of the published studies on the relationship between $[Ca^{2+}]_i$ and I_{SK} amplitude used sub-physiological temperatures and a variety of experimental conditions, and a single study (316) suggested that using physiological temperature, which is more clinically relevant, may change this relationship, it is important to clarify this issue by systematically comparing the $[Ca^{2+}]_i$-sensitivity of I_{SK} between physiological and sub-physiological temperatures. Hence, the following aims.

4.2 Section aims

With this study I aimed to test a range of Ca^{2+} concentrations, which would reproducibly augment $I_{KCa2.3}$, at both 22-23°C and 37°C. Accordingly, it was decided to compare the EC_{50}, obtained from calcium-dose relationship curves for $I_{KCa2.3}$ at 22°C and 37°C. The data obtained from recordings at physiological temperature will improve the knowledge about the sensitivity of the hSK3 channel to calcium.

4.3 Hypothesis

That the data acquired from the calcium-dose relationship curves in inside-out patches of HEK293 cells, will support that the $[Ca^{2+}]_i$ achieved in the solutions previously created using BAPTA (tetrapotassium salt, cell impermeant) will be sufficient to activate SK channels at physiological temperature.

4.4 Methods

4.4.1 Inside-out patch clamp technique

The study of the nature of ion channels can be also performed on a section of membrane attached to the pipette. This can be achieved using cell-attached (single channel) or inside-out macropatch recording technique, which examine channels that are localized in a small area ($<10\mu m^2$) of the membrane rather than from the entire cell: whole-cell patch clamp. For this study, I exploited the inside-out macropatch configuration which allowed me to measure the current arising from the channels which are located within the diameter of the tip of the recording pipette (Fig. 4.1). This technique as well as HEK293 cell culture protocols were taught to me during my secondment at Acesion Pharma (ApS) in Copenaghen (where the experiments outlined in this chapter were performed) by Rafel Simó Vicens and Bo Hjorth Bentzen to complement the studies on I_{SK} at University of Glasgow.
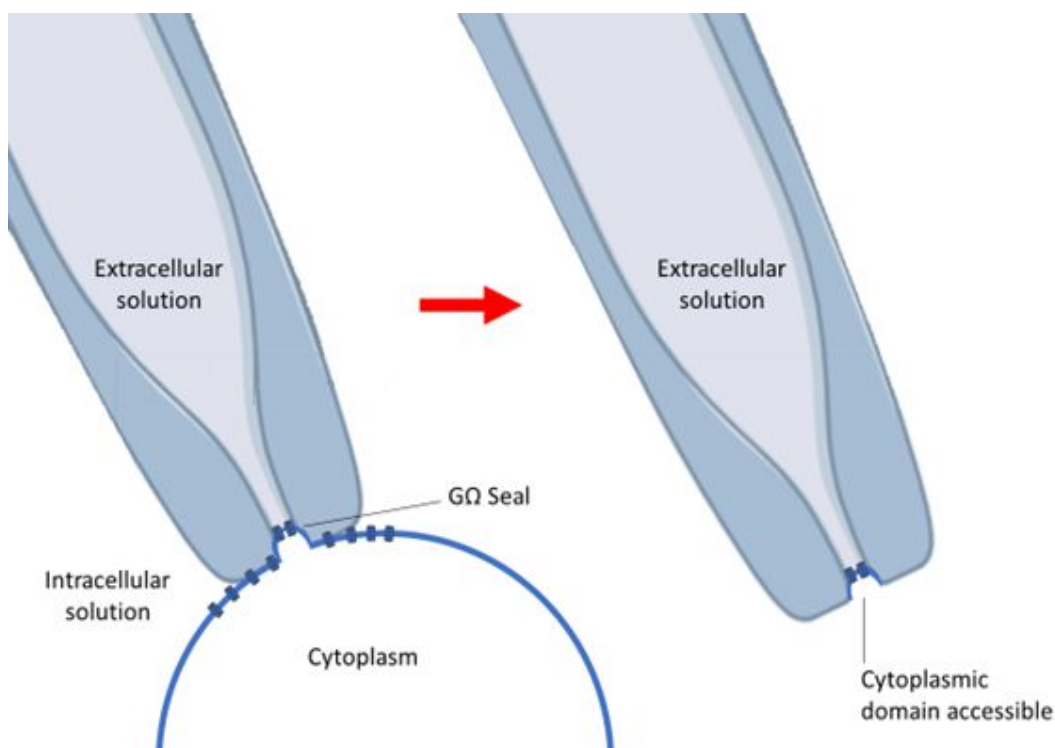
Figure 4.1 Illustration showing the procedure to achieve single channel inside-out patch clamp configuration.
Based on Ackerman et al., 1997 (3)

The inside-out recording configuration was achieved by gently withdrawing the electrode from the cell (which is firmly attached to the cover slip) after obtaining GΩ seal, excising the patch inside the pipette tip. With the internal aspect of the cell membrane now exposed to the bath solution, changes in the solutions on the inner facing channel can be readily achieved. This configuration is especially effective for studying the outcome of the application of different intracellular environments on ion channel function.

4.4.2 Cell culture and preparation

All experiments were performed on one stable HEK293 cell line expressing hKCa2.3 channels obtained from NeuroSearch A/S (Ballerup, Denmark). The cell line was established as described in Strøbæk et al., 2004 (317). The cells were cultured in DMEM (DMEM1965, Thermo Fisher Scientific) supplemented with 26.2 mM $NaHCO_3$, 25 mM HEPES, 10 mL/L Glutamax (Gibco, Gaithersburg, Maryland, USA), 10% fetal bovine serum (Biowest, Nuaillé, France) and 100 U/mL of penicillin/streptomycin (Sigma-Aldrich, Munich, Germany). In the case of the stable cell lines, 100 µg/mL geneticin (Gibco, USA) was added to the medium. On the day of the experiment, when cells were 80-90% confluent, they were detached from the flask using 1mL of Detachin™ (Amsbio, Abingdon, UK). After being washed with free calcium and magnesium phosphate-buffered saline (PBS), the cells were plated on 5 mm diameter coverslips. In the case of inside-out patch clamps, the cover slips were treated overnight at 37°C with 50 mg/mL1 poly-L-lysine (Sigma-Aldrich) to get firmer cell attachment.

4.4.3 Solutions

Patch-clamp experiments with hKCa2.3 channels were conducted using symmetrical K^+ solutions. In addition, to study the activation of the channels, a range of intracellular solutions containing different free Ca^{2+} concentrations (0.01–10 µM) was used. The extracellular solution contained (in mM): 0.1 $CaCl_2$,3·$MgCl_2$,154·KCl, 10 HEPES and 10 glucose (pH 7.4and 285–295 mOsm). The intracellular solution contained (in mM): 8.106 $CaCl_2$ (final Ca^{2+} concentration of 400nM) 1.167 $MgCl_2$, 10 EGTA, 154 KCl, 10 HEPES, 31.25/10 KOH/EGTA and 15 KOH (pH7.2). Excised patches were exposed to free $[Ca^{2+}]_i$ in the range from 0.01 to 10 µM to cover the dynamic range of SK channel activation (as described in

Strøbæk et al., 2006). The osmolarity of the intracellular solutions was adjusted using sucrose (Sigma-Aldrich) to match the extracellular solutions. A gravity flow-based perfusion system was employed to introduce onto a patched cell with free calcium concentrations solutions; the application was manually controlled. The temperature of the solutions was regulated (for experiments at 37°C) by a heater placed along the last portion of the tubing and by a 4 sides heated bath. Patched cells were challenged with at least 60s exposure to each different $[Ca^{2+}]_i$. A liquid-liquid junction potential (LLJP) correction was not applied during recordings. However, the problem was minimized by using equimolar (and concentrated) KCl solutions. KCl is chosen because K^+ and Cl^- have almost equal ionic mobilities, and, as a consequence, liquid junction potentials are in the range of 1mV or smaller.

4.4.4 Statistics and data analysis

4.4.4.1 Calculation of the half maximal effective concentration (EC_{50})

Data were extracted from PATCHMASTER (HEKA Elektronik, Harvard Bioscience, inc.) version 2x90.5 and analysed using GraphPad Prism 7. Current amplitudes were measured at−80 mV, and the mean of the last three recordings during each application was used for further analysis. To calculate the EC_{50} of calcium, the values were normalized using the current recorded at the lowest calcium concentration (0.01 μM) for total inactivation and used as baseline, while the current recorded at the highest calcium concentration (10 μM) was used as the maximum activation of the channel. Individual EC_{50} values for each experiment were calculated using the equation (Eq.1):

Eq.1
$$Y = Y_{min} + \frac{(Y_{max} - Y_{min})}{1 + 10^{(logEC_{50} - X) \times Hill\ slope}}$$

Where X is the logarithm of the dose of calcium and Y is the normalized measured current with variable Hill slope. Individual EC_{50} values were calculated for each experiment and then used to determine the final EC_{50}. The final results are summarized as means ± s.e.m of the individual values . Values of $P<0.05$ were considered significant.

4.4.5 Electrophysiology and analysis

Patch-clamp recordings were made using a HEKA EPC9 amplifier and the Patchmaster software (HEKA Elektronik, Ludwigshafen, Germany) at both 22-23°C and 37°C. Patch pipettes (Drummond Scientific; diameter: ∅ 3.5") were pulled using a horizontal DMZ Universal Puller (Zeitz, Germany) with resistances of 2.2±0.6 MΩ for inside-out patch clamp. $K_{Ca}2.3$ currents were elicited every 2s using a 200ms voltage ramp ranging from −80 (held for 10ms) to +80mV from a holding potential of 0 mV (Fig. 4.2). Current at -80 mV was analysed for the creation of the activation-curves at both 22-23°C and 35-37°C. Data were sampled at 10 kHz. Series resistance values were 5.4 ± 0.6 MΩ with 80% of compensation. Two Bessel filters of 10 and 2.9kHz were used to avoid background noise. Statistical analyses were performed using GraphPad Prism 8. Single comparison of means was conducted using standard 2-tailed t-test (paired where appropriate). For parametric data, one-way ANOVA followed by multiple comparison tests were used to compare three or more groups of data.
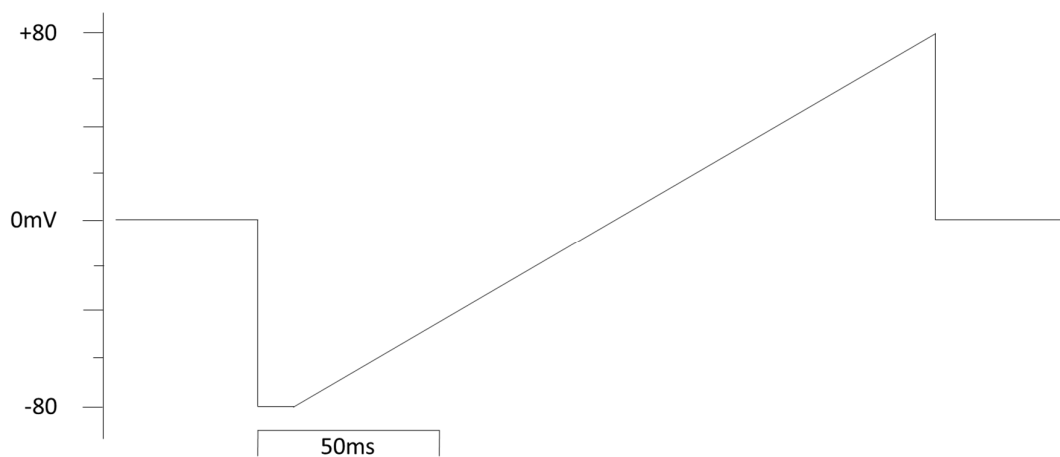
Figure 4.2 The voltage protocol used to elicit I$_{KCa2.3}$.

4.5 Results

4.5.1 0.5 μM [Ca^{2+}]$_i$ is sufficient to activate hKCa2.3 channel current in HEK cells

I used the inside-out manual macropatch voltage clamp technique, on HEK cells stably expressing the hKCa2.3 channel, to test up to 8 different increasing [Ca^{2+}]$_i$ solutions to generate a [Ca^{2+}]$_i$-I$_{SK}$ curve. The patch was excised and the inner side of the HEK cell membranes were exposed to the intracellular solution, which contained a range (from 0.01 to 10 μM) of free Ca^{2+} concentrations that were applied individually in increasing order. I waited for the hK$_{Ca}$2.3 current to stabilize before applying each different solution. Up to eight increasing concentrations of [Ca^{2+}]$_i$ between 0.01 and 10 μM (Fig. 4.3B) were applied and perfused by gravity flow on the patch. In symmetrical intracellular and extracellular K$^+$ solutions, hK$_{Ca}$2.3 currents displayed a characteristic inwardly rectifying current–voltage relationship (Fig. 4.3A and 4.4A). Current values recorded at -80 mV were plotted against time in Figure 4.3 B and 4.4 B. Calcium was able to elicit hK$_{Ca}$2.3 channel current in a concentration-dependent fashion at both room (22-23°C) and physiological (35-37°C) temperature (Fig. 4.3B and 4.4B). Current was recorded every 4s at -80 mV and plotted against time for both room (Fig. 4.3B) and body (4.4B) temperature. The activation started at 0.5 μM [Ca^{2+}]$_i$ and total activation was reached at 3 μM [Ca^{2+}]$_i$ (Figure 4.3B and 4.4B). This was true at both 22-23°C and 35-37°C. Superfusion with 0.5 μM [Ca^{2+}]$_i$ solution provoked an increase in hK$_{Ca}$2.3 current of 75 ± 7% at 22-23°C (n=10) and of 83 ± 8% at 35-37°C (n=8).
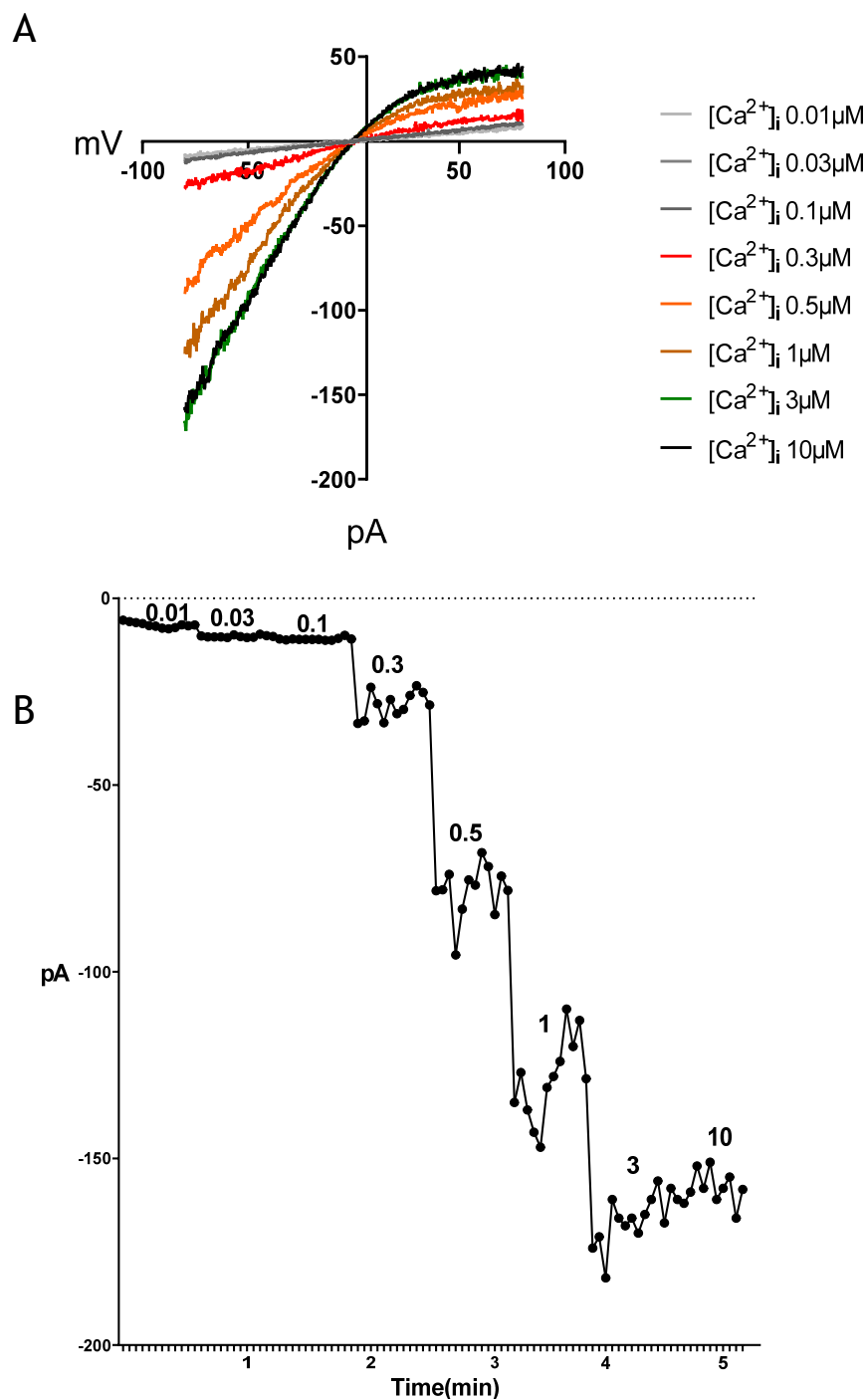
Figure 4.3 Absolute current at increasing $[Ca^{2+}]_i$ measured at 22-23°C and obtained by inside-out patch clamp on a single HEK cell macropatch stably expressing the hKCa2.3 channel.

A) Representative current–voltage plots and (B) their corresponding current–time plots of activation by calcium (current amplitude was measured at -80mV).
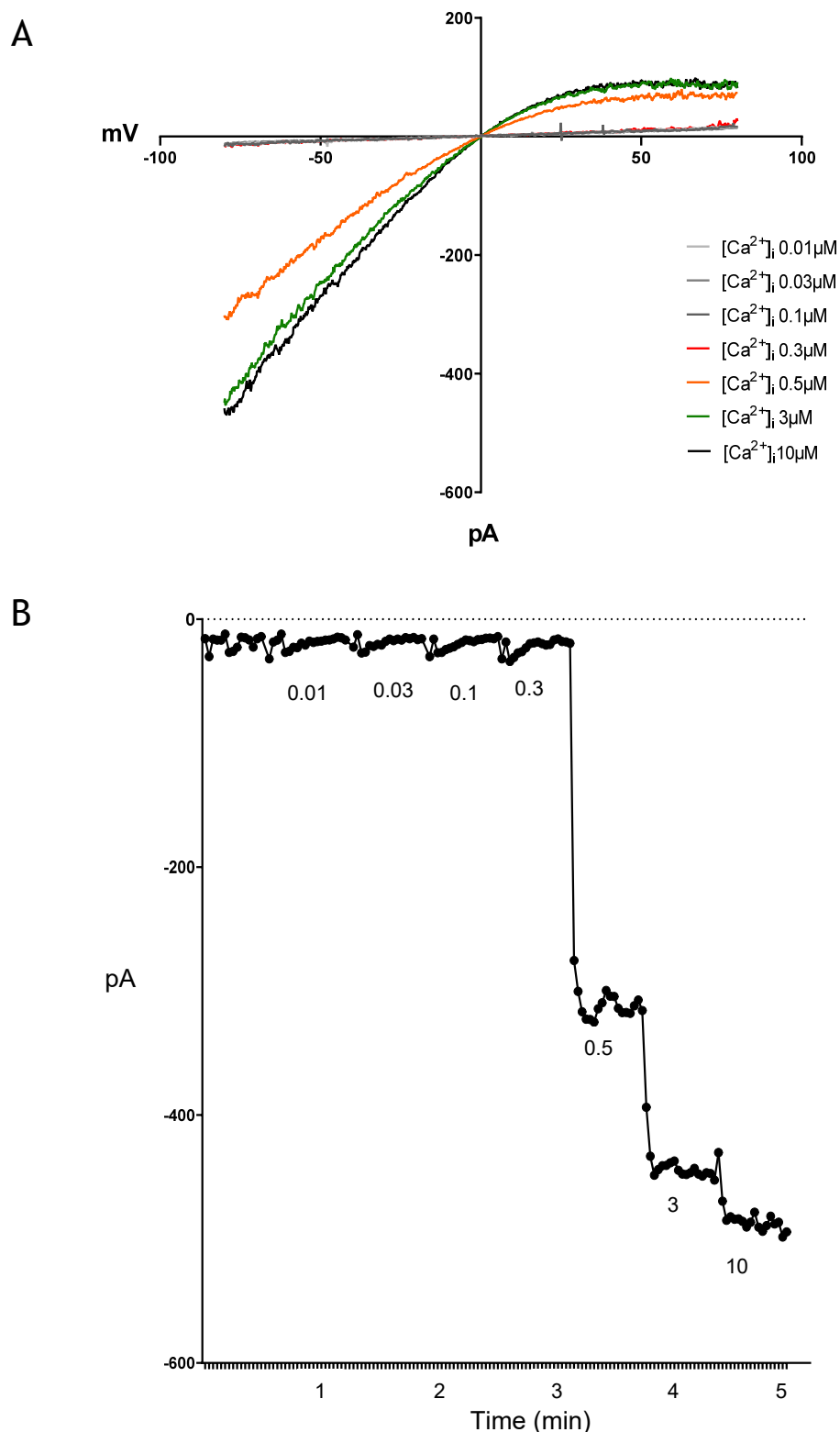
Figure 4.4 Absolute current at increasing [Ca^{2+}]$_i$ measured at 35-37°C and obtained by inside-out patch clamp on a single HEK cell macropatch stably expressing the hKCa2.3 channel.

A) Representative current-voltage plots and B) the corresponding current–time plot (current amplitude was measured at -80mV).

Subsequently, the values of the current were normalized to create a calcium dose-response curve, using the analysis program GraphPad Prims. The values for EC_{50} were extrapolated from the curves and resulted as 0.39 ± 0.02 μM and 0.29 ± 0.03 μM for 22-23°C and 35-37°C, respectively (Fig 4.5). The reduction in EC_{50} that occurred during the shifting from perfusing with solution at 22-23°C to solutions at 35-37°C, describes an increase in hKCa2.3 channel sensitivity to Ca^{2+} with a significant leftward shift of SK calcium activation curves at 35-37°C, as shown in figure 4.6.
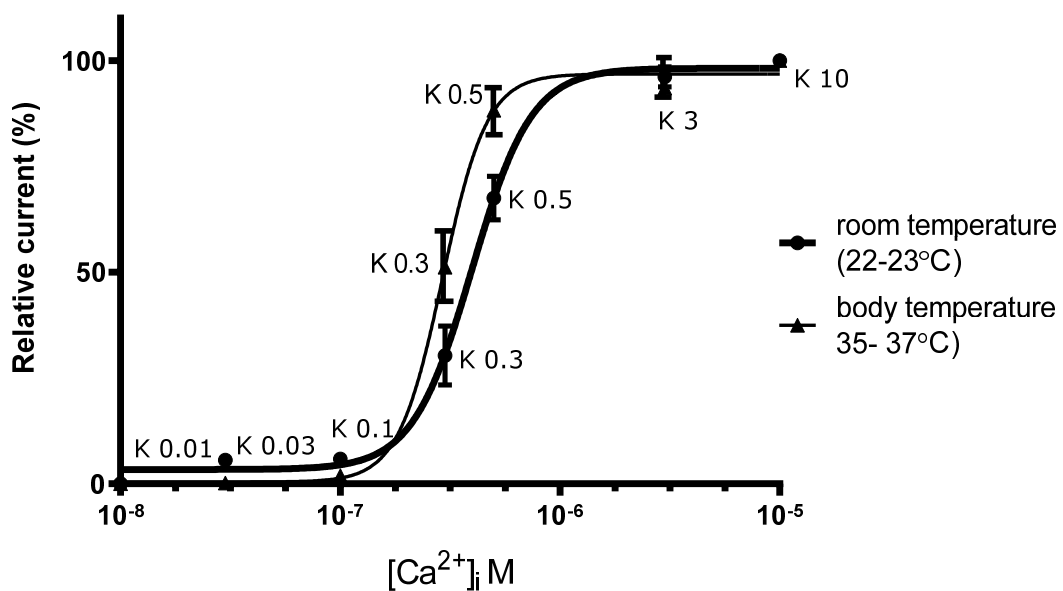
Figure 4.5 Comparison of calcium-activation curves of SK channels obtained at 22-23˚C and 35-37˚C.

Sigmoidal curves were fitted according to the logistic function:

$Y = Y_{min} + (Y_{max} - Y_{min})/(1 + 10^{\wedge}((LogEC50 - X) * HillSlope))$ utilising an analysis program (GraphPad prism7) for nonlinear fitting of transformed data (normalized). Data were obtained from inside-out patch clamp experiments performed on a stable HEK293 cell line expressing the human SK3 channel. The Hill slope was 3.2 at 22-23˚C and 4.3 at 35-37˚C. Data is represented as means ± s.e.m. Sample size: n=10 patches, n= 10 cells (for 22-23˚C); n=8 patches, n=8 cells (for 35-37˚C).

Moreover, at 35-37˚C the Ca^{2+} dose–response curves showed that the Hill slope for Ca^{2+} gating was increased from 3.2 (at 22-23˚C) to 4.3. The half maximal effective concentration (EC_{50}) was significantly lower at 22-23˚C

compared with that at 35-37°C (Fig.4.6), while the Hill slope of the curve at 35-37°C was increased. Thus, lower calcium concentrations were required to activate the channels at physiological temperature.
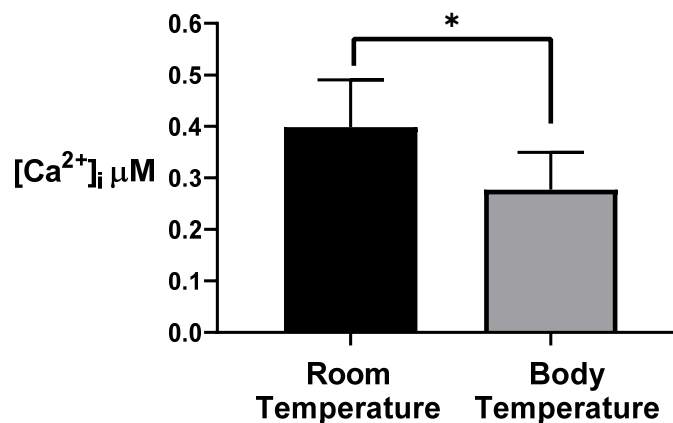
Figure 4.6 Comparison between EC50 at both room and 35-37°C in HEK293 cells.

The calcium's EC50 was 0.39±0.02µM at 22-23°C (n=10 patches, n=10 cells) and 0.29±0.03µM at 37°C (n=8 patches, n=8 cells). All values are mean ± s.e.m, P<0.05 (unpaired student's t-test)

4.6 Discussion and conclusion

These experiments aimed to improve the understanding of the calcium sensitivity of SK channels and contributed to expanding knowledge about SK channel activation at physiological temperature. The use of HEK cells stably expressing just the hKCa2.3 channel can just provide an estimation of the current behaviour when compared with my previous data obtained from rabbit left atrial and human right atrial cardiomyocytes. However, it was demonstrated that calcium activation of one of the major SK isoforms is taken to diastolic calcium range at 37°C. This is particularly important, considering that SK3 is one of the isoforms that is expected to be associated with lone AF (206). Furthermore, SK calcium-activation curves present steep slopes with Hill coefficients ranging from 3 to 4, suggesting positive cooperativity during calcium binding (165, 262, 298, 308, 312-314, 318). These results show that I_{SK} half maximal effective calcium concentration is in the range of diastolic values, also confirmed by the literature. Ilse et al. performed inside-out macropatch voltage clamp ramps at 23°C and 37°C and observed a pronounced leftward EC_{50} shift at 37°C (from 0.53 ± 0.07 µM to 0.23 ± 0.02 mM) for $hK_{Ca}2.3$ channels. The recording solutions and condition used for this experiment are not provided in the abstract (316). However, these values show a more marked leftward EC_{50} shift to the one observed in my experiment. $[Ca^{2+}]_i$ response-curves from inside-out macropatch recordings in HEK293 cell line stably expressing WT $hK_{Ca}2.3$ channels made by Jenkins et al., showed EC50 values of 0.48 µM ± 0.05 µM and Hill coefficients of 4.8 ± 1.0 at room temperature (22-23°C) using symmetrical K^+ solutions (310), which are consistent with the conditions used in my experiments, although the hill coefficient is higher compared to mine at room temperature. On the other side, these data, taken together with mine obtained from HEK cells support the hypothesis that this current should be detectable in rabbit and human myocytes, even at low $[Ca^{2+}]_i$. Nevertheless, this study was limited due to the unphysiological $[K^+]$ used, which was equivalent for the extracellular and intracellular solutions. These arrangement were necessary to reach high current amplitudes in HEK cells and shift the reversal potential to 0mV. However, in human cardiomyocytes the current is expected to be small and difficult to detect (29), even at high $[K^+]$ and Ca^{2+} concentration in the range of EC_{50} calculated during this study. In conclusion, the results obtained provided a better insight of

SK channel calcium-sensitivity and will aid the investigation of I_{SK} under physiological conditions.

Chapter 5 Investigation of SK (ICA-sensitive or apamin-sensitive) current in rabbit and human atrial cardiomyocytes using 3 different $[Ca^{2+}]_i$

5.1 Background

5.1.1 The disputed role of cardiac SK channels

Circumstantial evidence for the presence of Ca^{2+}-activated K^+ channels in cardiac muscle was initially reported more than 40 years ago (319) but was later disputed following contradictory views in 1983 by Eisner et al (198). However, later in 1999, Wang et al renewed the interest in these channels, describing the presence of SK3 mRNA in H9c2 cells derived from embryonic rat ventricle, as well as the Ca^{2+}-dependency, K^+-selectivity and susceptibility to blockade by apamin of I_{SK} (320). This work was followed by a series of elegant studies that confirmed the presence of functional SK2 channels in human and mouse cardiac myocytes, from which this channel subtype was then cloned (27). Moreover, the same group, 2 years later, first described the presence of the three different isoforms of SK channels in the heart and the differential expression of these channels between mouse atria and ventricle (28). 5 years later, these studies in combination with the first evidence for an association of variants in the KCNN3 gene (encoding SK3) and risk of AF in man (206), boosted the interest for these channels in the field.

The characteristics of the superfamily of KCa channels have been described earlier in this thesis, focusing on the critical role that SK may have in cardiac repolarization. This may be crucial during atrial fibrillation (AF), which is characterized by adaptation and remodelling of the atrial myocardial electrical and mechanical activity in response to a variety of cardiac disease conditions and Ca^{2+} handling abnormalities (321, 322). In particular, in the general introduction, the role played by single- and multiple-circuit reentry in AF has been widely discussed, as well as the importance of the atrial effective refractory period (aERP) in the determination of reentry during irregular and rapid atrial electrical activity (14). The atria remodelling, led by episodes of AF,

shortens the aERP and the atrial action potential duration (APD), promoting and maintaining AF (77). Thus, the identification of new drugs that could lengthen specifically the aERP and the APD in the atria become essential in the treatment of AF.

SK1 and SK2 channels have been found predominantly distributed in human and mouse atrial compared to ventricular myocytes (27, 28). In fact, under normal physiological conditions, there seems to be a general consensus that SK channels play a negligible - if any - role on ventricular tissue compared to atria (27, 196, 203). Therefore, in recent years an increased focus has been given to SK channels because they might constitute a new atrial-selective target in the treatment of AF (27, 28, 30, 200, 211). However, at present, the function of SK channels in the human myocardium remains unclear and is not well known whether the activation of these channels produces antiarrhythmic or proarrhythmic effects (27, 306, 323-325). Diness et al. described a reversion of atrial fibrillation by inhibition of SK channel, which prolonged atrial effective refractory period (aERP), in rat and rabbit model of paroxysmal AF (196). Whereas, Hsueh et al., described a possible proarrhythmic effect of SK channels blockade by promoting APD heterogeneity in the canine left atrium.

Additionally, as previously described, the Ca^{2+}-sensitivity of SK channels is conferred by the calcium-binding protein calmodulin (CaM) that cooperatively opens these channels with high Ca^{2+} -sensitivity (EC_{50} ~100-400nM) (165, 168, 318, 326, 327). Recently, Fan et al. reported an increase in calcium-sensitivity and current density of human I_{SK} during chronic AF, with the downregulation of expression of mRNA and protein levels of all the SK subtypes compared to sinus rhythm patients. They concluded that this current rise, associated with increased atrial SK channel sensitivity to $[Ca^{2+}]_i$ in AF patients, is due mainly to the Ca^{2+}/calmodulin-dependent protein kinase II (CaMKII) phosphorylation and $[Ca^{2+}]_i$ elevation (30). Given the relevance of this publication to the present study, it could have been used to inform the rationale of the present experiments, but due to its recent date of publication (May 2018), this was not possible. Nevertheless, discrepancies among the results and methods used were discovered when compared to the present work and are discussed later in this chapter. Besides, part of the findings made by Fan et al. is in contrast with

previous studies by Yu et al. who demonstrated that chronic AF decreases I_{SK} density compared to sinus rhythm, along with downregulation of protein and mRNA expression levels of SK1 and SK2 (211). Skibsbye et al., hypothesize an initial up-regulation of SK channels expression followed by down-regulation during long-lasting AF (29). Thus, it seems that the different expression levels of these channels, along with the current elicited, depend on the duration of AF, which is associated with extensive structural and electrical remodelling of the atria (79, 211, 328). In fact, increased SK current density has also been described in atrial myocytes from patients in persistent AF (213). However, how the expression level of SK channels changes and how this impact on I_{SK} in sinus rhythm versus AF is not clear. On the other hand, it can be supposed that, based on their high calcium-sensitivity and relatively weak voltage-dependence, SK channels have a significant functional role in the direct connection between calcium handling and cardiac repolarization also under physiological conditions. Therefore, in theory, I_{SK} could activate upon the abrupt atrial rate increase (which should also increase $[Ca^{2+}]_i$) of new-onset or paroxysmal AF, i.e. in un-remodelled atrium. In this chapter the aim was to stimulate, in un-remodelled atrial cells, the intracellular calcium overload that distinguishes this particular arrhythmia (84, 329), which could potentially trigger SK channels during systole and make them participate in the cardiac repolarization. Thus, utilizing solutions with precise $[Ca^{2+}]_i$ typical of global diastolic-to-systolic values, the aim was to simulate the calcium overload present at rapid stimulation frequency in AF which could cause the activation of I_{SK}. Many previous studies have addressed the investigation of SK current using a voltage-clamp protocol in whole-cell configuration availing of solutions with increased $[Ca^{2+}]_i$. For example, Xu et al. found an apamin-sensitive current using $[Ca^{2+}]_i$ of 500 nM and just 50 pM of the toxin, which based on the data reported blocked almost 15% of the current in atria (27). On the other hand, in a study from 2009 by Nagy et al., 100 nM apamin, which is 2000 times higher compared to the one used by Xu et.al, failed to alter the I-V curve in ventricle with $[Ca^{2+}]_i$ of 900nM (203). Despite this single study, apamin was found effective in different investigations of SK current. In a recent study by Fan et al, an apamin (100 nM)-sensitive current recorded at $[Ca^{2+}]i$ of 500 nM was found greater in patients with AF compared to sinus rhythm. In contrast, a few years earlier, Skibsbye et al., showed significant current reduction caused by the selective blocker ICAGEN at the concentration of 1 µM

with 300 nM $[Ca^{2+}]_i$ in atrial myocytes from patients in sinus rhythm but not in AF (29). However, the latter study used un-physiological $[K^+]_o$ (20 mM) to shift the reversal potential of the current, which, considering the small effect of ICAGEN, limits extrapolation of their data to more physiological conditions. Therefore, it is clear that some discrepancies have emerged about the presence or not of SK current and its relevance under pathological or physiological condition. In this chapter, therefore, the investigation regarding the presence of I_{SK} was performed only under physiological conditions, availing of 3 "tools":

- The same voltage protocol used to test the positive control in chapter 2;
- High $[Ca^{2+}]_i$ solutions, used to potentially trigger I_{SK} at physiological temperature;
- Two specific SK blockers: apamin and ICAGEN.

5.1.2 Two SK channel blockers in comparison: a conventional peptide (apamin) and a new neutral small molecule (ICAGEN)

Among the variety of compounds claimed to inhibit SK channels (183, 330-332), numerous studies identified apamin as a state-of-the-art blocker of SK, and it has been used extensively as a key tool to investigate SK function in different tissues including skeletal muscles (333-337). This peptide, proposed as SK blocker firstly by Habermann (338), is a small peptide containing 18 amino acids present in honey bee venom (Fig. 5.1) which targets all SK subtypes (179). The homogeneous substance was called apamin, from apis, the bee (338). Apamin acts as a negative allosteric modulator, binding to both the outer pore region residues and the S3-S4 extracellular loop to inhibit channel activity (188). The bond at the loop is supposedly the basis of SK subtypes disparity in apamin sensitivity

HQQCRRACLATEPAKCNC

Apamin

Figure 5.1 Aminoacidic sequences of the insect peptide toxin apamin. Brackets are used to show disulphide bridges.

Modified from Hamid S. Kachel et. al. (4)

(table 6), which is useful for determining the expression pattern of SK channel subtypes in native tissue (179).

	SK1 IC$_{50}$ (nM)	SK2 IC$_{50}$ (nM)	SK3 IC$_{50}$ (nM)
Apamin	0.7-8 (169, 179, 339, 340)	0.06-0.14 (318, 340)	0.63-1 (340, 341)

Table 6 Inhibitory concentration of apamin for each SK subtype.

On the other hand, recently, a new chemical class of SK blockers has been reported by Gentles et al. exploiting the apamin binding site (183). This class is represented by the ICAGEN compound (Fig. 5.2), 2-aminothiazole N-(pyridin-2-yl)-4-(pyridin-2-yl) thiazol-2 amine, also known as ICA (IC50 = 0.3/0.5 µM)
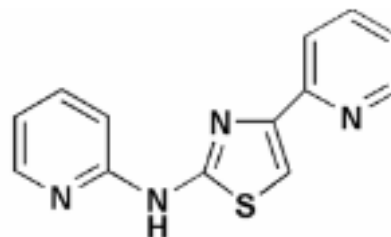
Figure 5.2 Chemical structure of ICAGEN

which inhibits all SK subtypes with equal potency (29, 183). This new molecule displays excellent potency as a K$_{Ca}$2 blocker and has been previously tested both ex-vivo and in vitro (29, 196, 197). Given its apamin-displacing nature, it is believed to share a similar mechanism of action with apamin, therefore, ICA was chosen over other compounds which present similar or lower potencies (183, 196).

5.2 Section Aims

To my knowledge, only a single recent study (published after completion of my experiments) cited above, from Fan et al, reported the effect of a conventional I$_{SK}$ blocker, apamin, on the apamin-sensitive potassium current (I$_{KAS}$) under physiological conditions and measured [Ca^{2+}]$_i$ in single human atrial myocytes (30). On the other hand, many studies that show a significant effect of different I$_{SK}$ blockers report [Ca^{2+}]$_i$ calculated using a software (27) or the use of unphysiological conditions (e.g. high external K$^+$ concentration) (29, 213, 298). In addition, few publications have documented the role of cardiac I$_{SK}$ in rabbit and only one have studied it also in single rabbit left atrial cells (304). Therefore, given the wide range of results and contradictions in the literature, the aim was to investigate I$_{SK}$ in atrial myocytes from human and rabbit, under physiological

conditions. By this means, 3 different and precisely measured $[Ca^{2+}]_i$ solutions (100 nM to 500 nM) as previously described (chapter 3), and two SK channels blockers (Apamin and ICAGEN) were used (183, 342) to determine $[Ca^{2+}]_i$ sensitivity of atrial I_{SK}. Additionally, given its weak voltage sensitivity, SK current should be activated in a wide range of membrane potential (27, 320). Therefore, SK current was directly measured in voltage-clamped single cells from rabbit and human myocytes.

5.2.1 Subsidiary aim

To measure I_{SK} in a small number of cells from rabbit with myocardial infarction (MI), considering that MI has been associated with a significantly increased I_{SK} density and altered I_{SK} sensitivity to intracellular Ca^{2+} (343).

5.3 Methods

5.3.1 Measurement of intracellular free Ca^{2+} concentration: 3 different increasing $[Ca^{2+}]_i$ solutions

Rabbit atrial cells were firstly loaded with 5 µM of fluorescent Ca^{2+} indicator Fura-2-PP (Thermo Fisher Scientific). Then, Intracellular solutions free Ca^{2+} concentration was measured previous to electrical recordings. The resulting ratio values were converted to $[Ca^{2+}]_i$ as previously described in this thesis, aiming for intracellular free calcium concentrations of 100, 300 and 500nM.

5.3.2 Drugs and solutions

In general, the perfusate, or external solution (EPSS2: extracellular physiological salt solution), was composed of: 140 mM NaCl, 4 mM KCl, 1.8 mM $CaCl_2(\cdot 2H_2O)$, 1.0 mM $MgCl_2(\cdot 6H_2O)$, 11 mM glucose, 10 mM HEPES, with the pH adjusted to 7.4 with 1 M NaOH. The internal (PIP35: pipette solution) solution, contained: 130 mM K-aspartate, 15 mM KCl, 10mM NaCl, 1mM $MgCl_2$ ($\cdot 6H_2O$), 10 mM HEPES, 5mM BAPTA, pH adjusted to 7.25 with 1M KOH. Based on the internal solution (PIP35) composition, the 3 different $[Ca^{2+}]$ solutions were created as described in chapter 3. The external perfusate could be collected to measure drug concentrations, as well as the intra-pipette solution to verify $[Ca^{2+}]_i$. All

experiments were performed at 37°C. Unless otherwise mentioned, all the chemicals used were of analytic grade and were obtained from Sigma-Aldrich. Apamin was dissolved in distilled water (344). 2-aminothiazole N-(pyridin-2-yl)-4-(pyridin-2-yl) thiazol-2 amine (ICA) was synthesized at NeuroSearch A/S, Ballerup, Denmark, and was dissolved in DMSO (183, 186). All substances were added directly to the organ bath. Apamin was applied for ~180s and ICA for 180-200s based on previous data regarding drug peak effect on I_{SK} (27, 29)

5.3.3 Electrical recordings and analysis

Electrophysiological signals were recorded from single cardiac myocytes in the whole-cell ruptured patch clamp configuration using AxoClamp 2B patch-clamp amplifier and WinWCP 5.3.4 software (University of Strathclyde, UK). For current recordings, patch pipettes (2.5-5MΩ filed with intracellular solution) were pulled from borosilicate glass capillaries 1.2ODx0.69x100L mm (Harvard Apparatus, USA) with a gravity puller (model PP-83, NARISHIGE, USA). A liquid-liquid junction potential of +9 mV (bath relative to pipette) was compensated for *a priori* (79, 238). Voltage-dependent activation of I_{SK} was measured by stimulating cells at 0.1 Hz from a holding potential (HP) of −50 mV, with voltage ramps of 7s duration increasing from −120 to +50 mV (Fig. 5.3). The voltage protocol is identical to that used in the positive control experiments (Chapter 2). This protocol shares similarities to voltage ramps used in previous studies (27, 29, 203). The access resistance changed substantially in 3 cells, so these were excluded from the analysis. The peak current at -115mV and at -65mV were considered for the analysis of the inward and outward current, respectively. The external and pipette solutions reproduced the physiological milieu as described above and previously used by our laboratory (58). I_{SK} amplitude was calculated as the I_{KAS} (apamin-sensitive potassium current) at -115mV or -65mV to avoid current artefacts immediately after the start of the ramp. Data were analysed using WinWCP 5.3.4 software and the graphs were created using GraphPad 7.05 software. Currents were normalized for each cell capacitance as described in Chapter 2 (section 2.5). Statistical analyses were performed using GraphPad Prism 8. Single comparison of means was conducted using standard 2-tailed t-test (paired where appropriate). For parametric data, one-way ANOVA followed by multiple comparison tests were used to compare three or more groups of data.
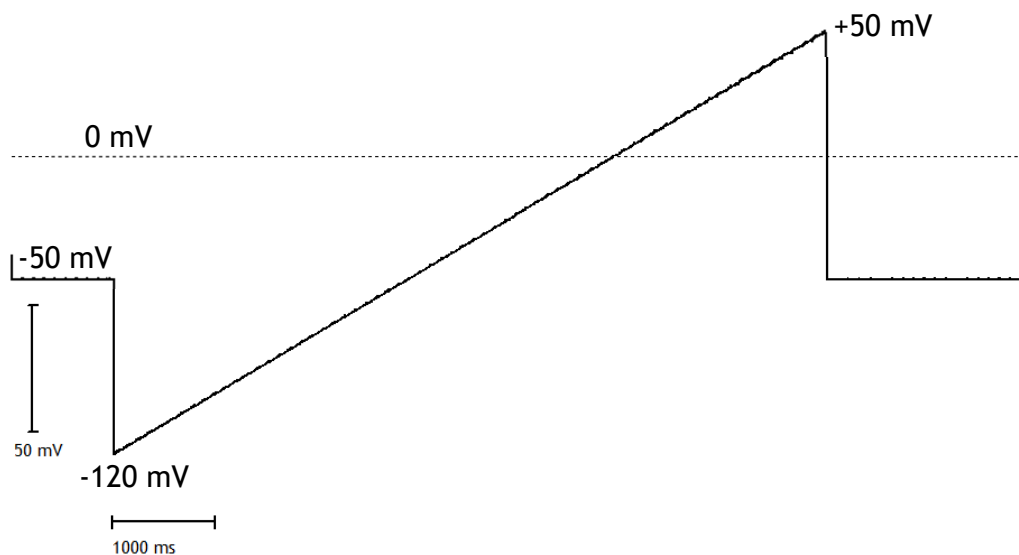
Figure 5.3 Voltage pulse (ramp) protocol used during recordings of I$_{SK}$

5.3.4 Atrial cell Isolation and experimental condition

Myocytes from stock and MI rabbits left atrium or from sinus rhythm patients' right atrial tissues were isolated and superfused with solutions as previously described (See Methods 2.3.1-2.4.1). Experiments were performed using ruptured whole-cell patch clamp (See Methods section 2.6-2.8) in voltage-clamp mode whereby pre-specified voltage pulses are applied to the myocyte and the resultant current is recorded. In this study, for the rabbit model of MI, the ligation of the left descending coronary artery (LAD) of the rabbit was used. The vessel is permanently ligated, and the heart is harvested 8 weeks after ligation. This model provides consistent apical LV infarct formation and early stages of cardiac remodelling, comparable to what is often encountered in humans post MI, such as cellular hypertrophy, decreased ejection fraction and APD prolongation. Importantly, the cells obtained from the model of MI and used in this experiment were available from an isolation performed for another study (kindly donated from Sara Dobi, PhD student at University of Glasgow) and just a small number of cells were tested from that single rabbit model of MI.

For human experiments, only myocytes isolated from the right atrial appendage were used. The atrial appendage was available for investigation as it constitutes the most accessible location for sampling human myocardial tissue (345). Also, the human right atrial (RA) appendage is more accessible for sampling than the left atrial (LA) appendage (345). Therefore, only the RA appendage was suitable to obtain a sufficient number of human samples. However, rabbit LA was also used, since it may be more relevant as source of ectopic activity (346, 347), possibly due to the location of the pulmonary veins in the left atrium, which appear to have a highly significant role (38) or consequent to the shorter atrial refractory period (ARP) compared to the RA, which could favour re-entry (348).

5.3.5 Statistics

Data are expressed as mean values ± s.e.m. Student t-test for paired data was used to compare results, if not otherwise stated. Results were considered significant when P was less than 0.05.

5.4 Results

5.4.1 Changes in $[Ca^{2+}]_i$ showed no effect on control quasi-steady-state current-voltage relationship

Chapter 2 describes in detail the protocol used as a positive control to test temporal stability, timing, and reversibility of the I_{K1} block obtained by the application of $BaCl_2$. Once its validity was confirmed, an identical protocol was employed for the investigation of I_{SK}. The validation step was essential, since the current blocked by apamin was expected to be difficult to detect due to its low density, even at high extracellular $[K^+]$ (20mM) (29). Also, as previously stated, the goal was to study I_{SK} under physiological conditions, including intracellular and extracellular $[K^+]$. Thus, I_{SK} density was assumed to be even smaller. Besides, the aforementioned study by Nagy et al., also showed that apamin (100nM) failed to alter either atrial or ventricular action potential duration (APD) from rat, dog and human multicellular preparations as well as in single cells under physiological conditions (203). So, with these premises, firstly the mean control "steady-state" current-voltage relationships among the different calcium concentrations (100,300 and 500nM) in rabbit and human were compared to each relative positive control, which are shown in Fig. 5.4. This will allow a better investigation of any possible change in the current due to drug application, especially at negative potential (-115mV).
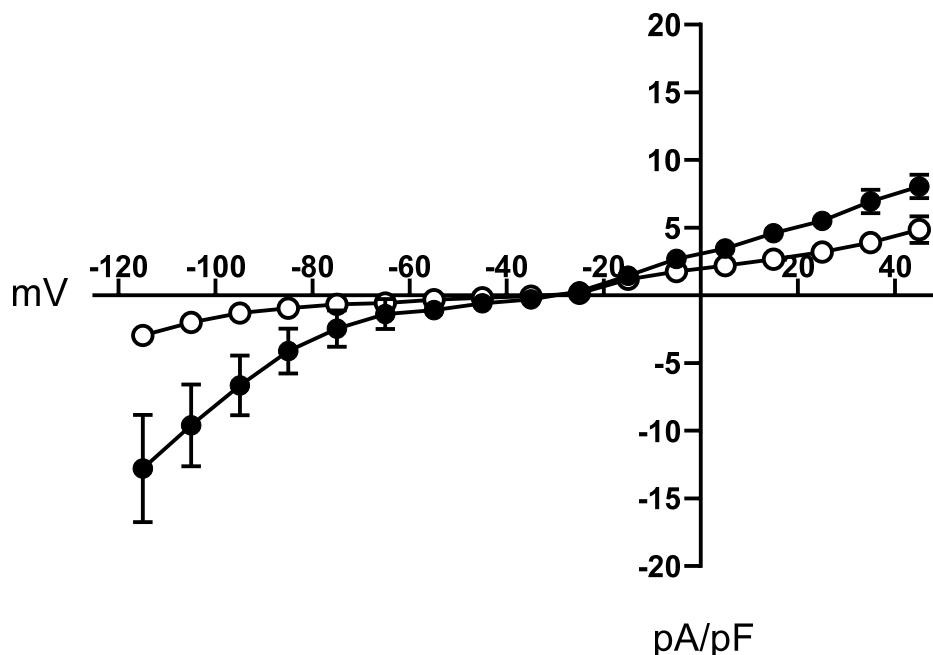
Figure 5.4 Comparison of mean current-voltage relationships of rabbit left atrial and human right atrial myocytes, under control conditions.
Comparison between [●] rabbit LA and [○] human RA control currents. Rabbit left atrial current has a greater current density than human right atrial for both inward and outward portion. Curves are plotted as control current (pA/pF) against voltage (mV). Values are mean ± s.e.m. Human right atria n=9 cells, n= 5 patients; rabbit left atria n=10 cells, n=6rabbits.

5.4.1.1 Rabbit control

In rabbit left atrial myocytes, the ramp current I-V relationship obtained in the presence of $[Ca^{2+}]_i$ of 100 nM (i.e. typical of global diastolic level, Fig. 5.5), was observed to be similar as for the positive control (Fig. 5.4). Thus, showing inward rectification at voltages negative to the resting potential (~-80 mV), and a relatively small outward current at positive potentials (Fig 5.5). In different atrial cells, with the $[Ca^{2+}]_i$ increased to 300 nM, and also to 500 nM (anticipated to substantially activate I_{SK}) there was no difference in the current profile compared to that recorded with 100 nM $[Ca^{2+}]_i$ (Fig. 5.5).

5.4.1.2 Human control

Similar conclusions can be drawn from the comparison between the positive control (Fig. 5.4) and the ramp current I-V relationship obtained at $[Ca^{2+}]_i$ of 100 nM (Fig. 5.6), in human right atrial myocytes. This is true also for the ramp current recorded at each other $[Ca^{2+}]_i$ (i.e. 300 and 500 nM, Fig. 5.6) which shows no significant difference when compared to the positive control. Also, no significant difference was observed among currents recorded at different $[Ca^{2+}]_i$ in the same chamber and species. The only difference is represented by the general amplitude of the current between rabbit LA and human RA, which has been addressed earlier in this thesis, and reported to be smaller in human RA compared to rabbit LA due to a reduction in I_{K1} density (222).

Rabbit left atrium
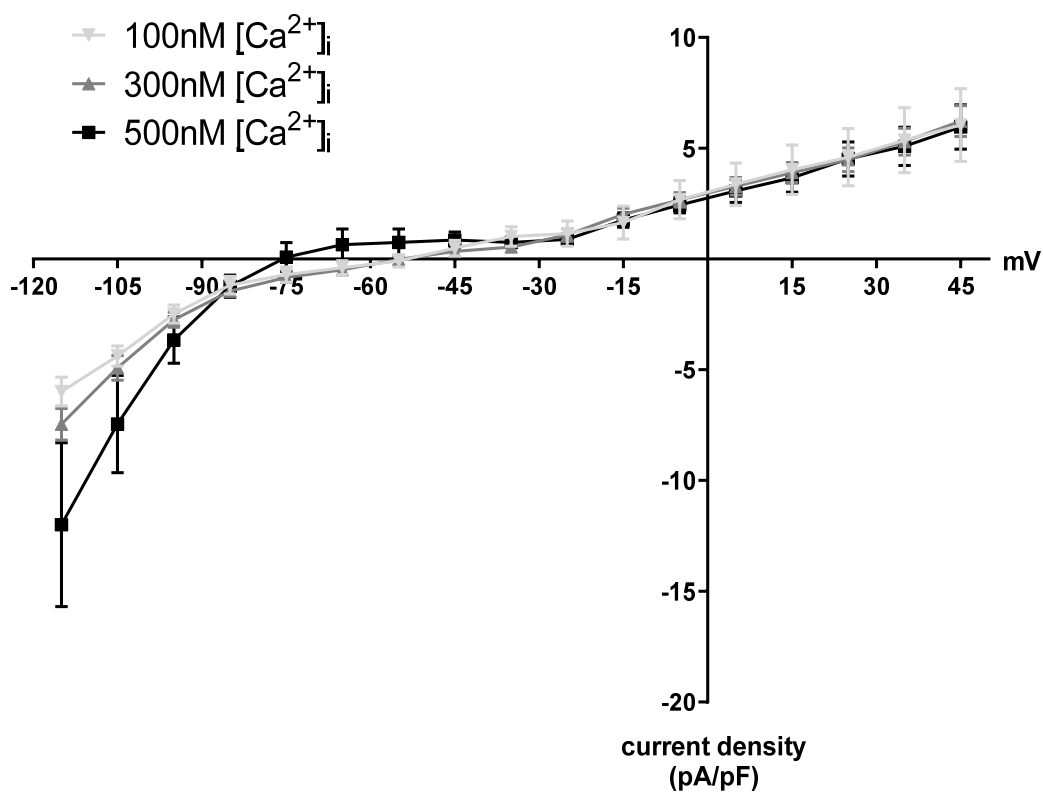
Figure 5.5 Control current-voltage relationships of rabbit left atrial myocytes at 3 different [Ca^{2+}]$_i$.

Steady-state current–voltage relations were obtained by plotting the end-pulse membrane current as a function of the respective membrane potential (Vm). Values are mean ± s.e.m and $P<0.05$ was considered significant. 100nM [Ca^{2+}]$_i$: n= 12 cells, n=9 rabbits; 300nM [Ca^{2+}]$_i$: n= 23 cells, n=11 rabbits; 500nM [Ca^{2+}]$_i$: n= 13 cells, n= 8 rabbits.

Human right atrium
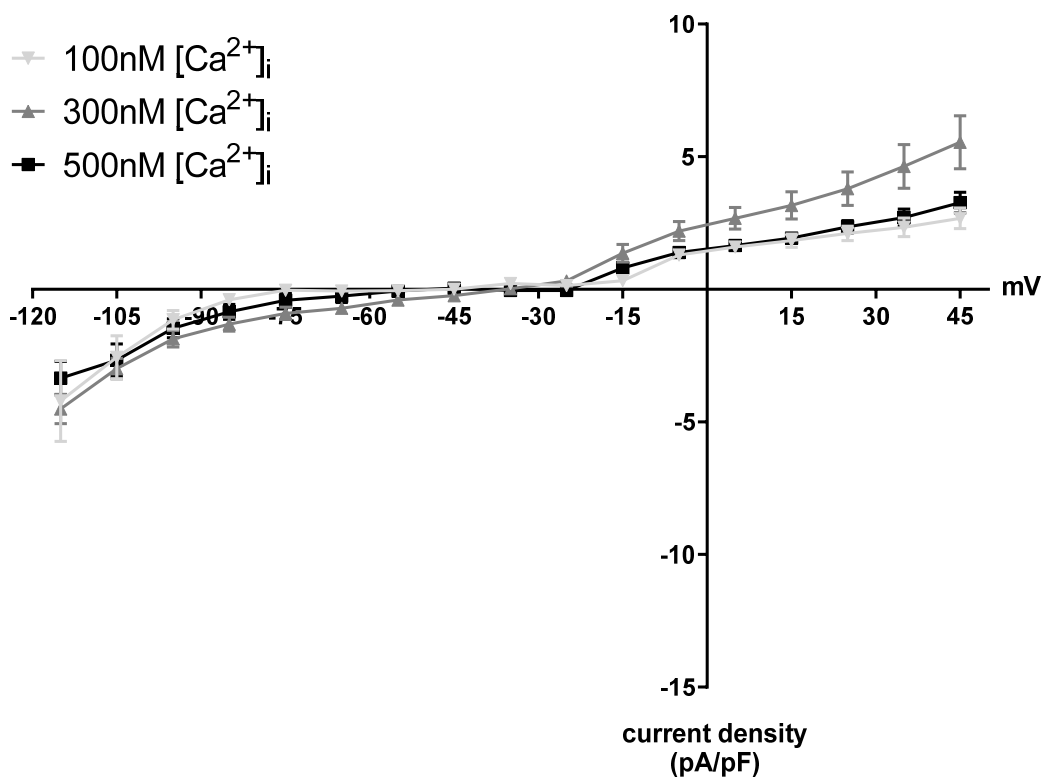
Figure 5.6 Control current-voltage relationships of human right atrial myocytes at 3 different [Ca²⁺]ᵢ.

Steady-state current–voltage relations were obtained by plotting the end-pulse membrane current as a function of the respective membrane potential (Vm). Values are mean ± s.e.m and P<0.05 was considered significant. 100nM [Ca²⁺]ᵢ: n= 5 cells, n= 3 patients; 300nM [Ca²⁺]ᵢ: n= 12 cells, n= 6 patients; 500nM [Ca²⁺]ᵢ: n= 8 cells, n= 5 patients.

5.4.2 Investigation of the effect of apamin on ion currents recorded in single human right atrial and rabbit left atrial cells

The identical protocol described in the previous section (5.4.1 and 5.3.3) was employed with the whole-cell configuration of the patch clamp technique to detect the effect of 100 nM apamin on SK current in single cells and to measure the apamin-sensitive current in isolated human right atrial and rabbit left atrial myocytes. Although this peptide does not always provide a complete inhibition of SK channels (171), it remains the most widely used peptidic blocker of SK channels and its specificity is especially important for characterising these channels (156, 340). Therefore, in the following experiments the neurotoxin was used to investigate I_{SK} current in myocytes isolated from rabbit left atrium and human right atrium using the whole-cell patch clamp technique. The concentration of 100nM for apamin was chosen in order to block most of the SK current, based on previous literature (30, 169, 211, 213, 340).

Under whole-cell conditions, the free Ca^{2+} concentration in the pipette solution was set to 100, 300 or 500 nM in these experiments with the intention of induce maximal activation of SK channels. These pipette Ca^{2+} concentrations approximate the global diastolic to systolic Ca^{2+} level which normally occurs in cells, during systole (not to peak $[Ca^{2+}]_i$ levels) or diastole (349, 350). Under this condition the $[Ca^{2+}]_i$ was highly elevated as compared to the diastolic Ca^{2+} level. In addition, I aimed to apply a range of increasing $[Ca^{2+}]_i$ to possibly test the Ca^{2+}-sensitivity of $I_{KAS.}$ After achieving whole-cell configuration, I waited approximately 50-60s to allow the dialysis of the pipette solution with the intracellular space; a duration found to be sufficient to reach the desired $[Ca^{2+}]_i$. Also, it has been demonstrated that a substantial difference in $[Ca^{2+}]_i$ could produce a significant change in the cell length (Chapter 3).

5.4.2.1 Absence of effect of 100 nM apamin in rabbit left atrial myocytes

Firstly, the conventional blocker apamin (100nM) was tested on the inward peak current at -115mV (Fig. 5.8 A) and the outward current at -65mV (Fig. 5.8 B) in rabbit left atrial myocytes. However, at 100nM $[Ca^{2+}]_i$ the current was not significantly changed before and after the application of the drug, neither at -115mV (control current -4.8 ± 0.6 pA/pF vs -4.7 ± 0.6 pA/ pF following 100

nM apamin, mean ± s.e.m., paired data, Fig. 5.8 A) nor at -65mV (0.4 ± 0.4 vs 0.7 ± 0.3 pA/pF, mean ± s.e.m., paired data, Fig. 5.8 B). With 300 nM $[Ca^{2+}]_i$, apamin also had no effect on inward (-6.3±0.5 vs -6.2±0.4 pA/pF, mean ± s.e.m., paired data, Fig. 5.8 A) or outward current (-1.15 ± 0.2 vs -0.95 ± 0.3 pA/pF, mean ± s.e.m., paired data, Fig. 5.8 B). When $[Ca^{2+}]_i$ was set to 500 nM, apamin again showed no effect either on inward (-13.4 ± 5.2 vs -13.3 ± 5 pA/pF, mean ± s.e.m., paired data, Fig. 5.8 A) or on outward (1 ± 0.7 vs 1.2 ± 0.7 pA/pF, mean ± s.e.m., paired data, Fig. 5.8 B) currents. Finally, during the analysis of the effect of 100nM apamin on the inward current in rabbit (Fig. 5.8 A) the control current at 500nM $[Ca^{2+}]_i$ was found to be significantly higher than the one at 300nM $[Ca^{2+}]_i$. However, the hypothesis that this was a true result was rejected, which was confirmed by one-way ANOVA test, that increased the statistical power (351). In addition, two very high current values (hid by the mean) recorded in two different cells were noticed. In the event of exclusion of those values from the analysis the mean control current was 9.3±4.3 pA/pF, which re-enters into the expected range. Those values were not dismissed from the final analysis, because they are part of the biological variability and were considered valid recordings. Interestingly, Nagy et al. report a $[Ca^{2+}]_i$-dependent augmentation of the Ba^{2+}-sensitive current (I_{K1}) in canine and human ventricular myocytes (352), which may be the cause of these outstanding current values recorded from two different rabbit left atrial myocytes, but this eventuality was not further investigated.

Below, typical original traces obtained with WinWCP software are shown, demonstrating absence of effect of apamin at all voltages tested and stability of the recordings in rabbit left atrial myocytes (Fig. 5.7). Raw traces for 100, 300 and 500 nM $[Ca^{2+}]_i$ are shown.
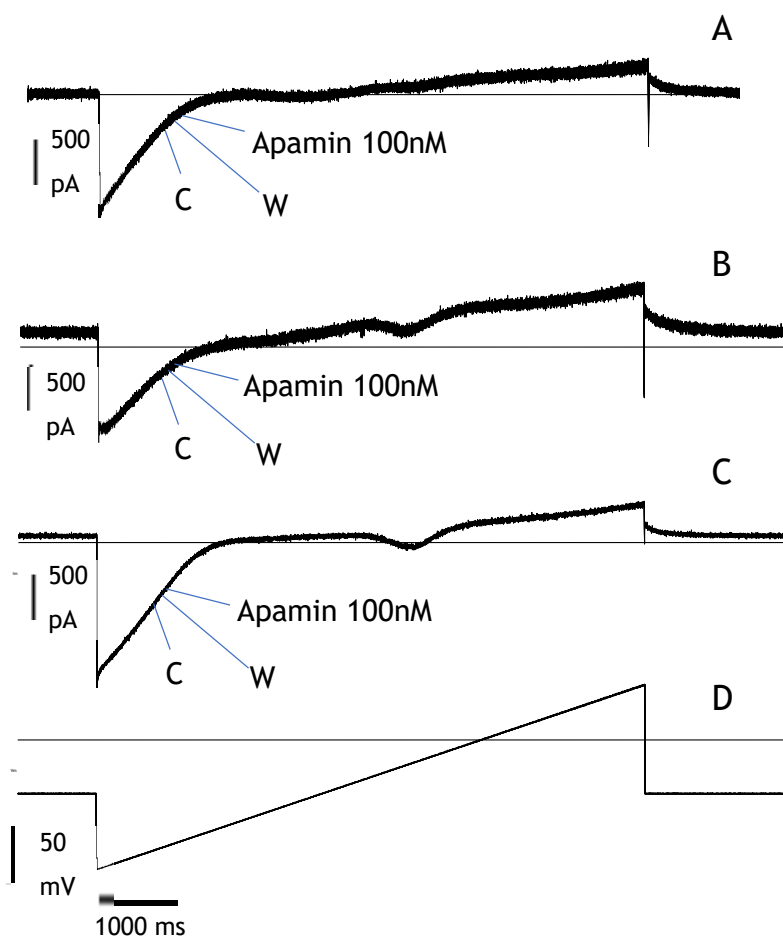
Rabbit left atrium

Figure 5.7 Representative superimposed traces obtained at 3 different [Ca^{2+}]$_i$, before and after acute administration of 100 nM apamin, in rabbit atrial myocytes.

Raw traces recorded in rabbit left atrial myocytes with A) 100 nM [Ca^{2+}]$_i$, B) 300 nM [Ca^{2+}]$_i$ and C) 500 nM [Ca^{2+}]$_i$, showing stability of the recordings and absence of effect of apamin. D) Represent the protocol already described in section 5.4.1 and 5.3.3. C= control, W= wash; the figure shows 15 (5 for each condition) superimposed recordings. Figures were created with WinWCP V 5.1.6 software.
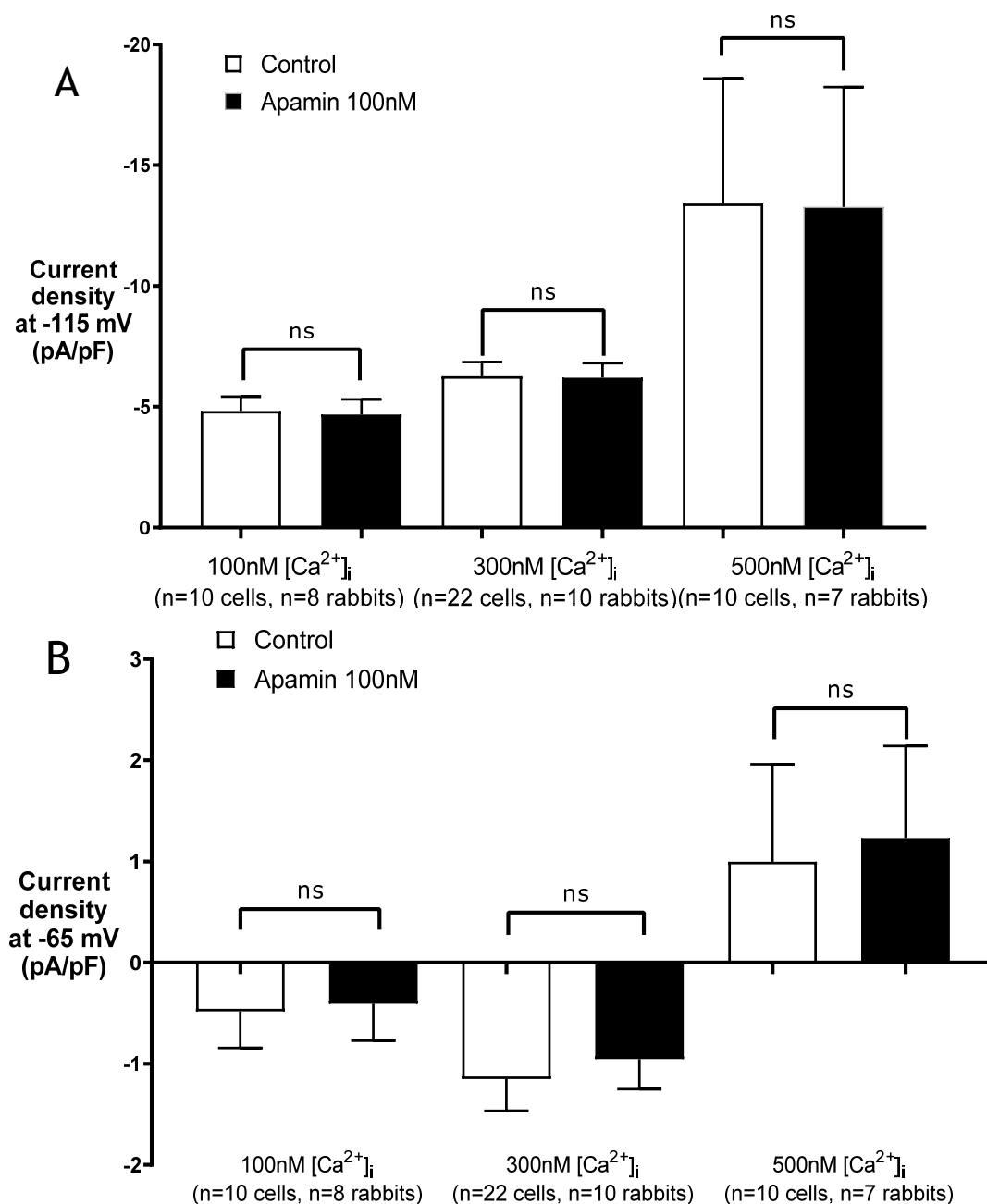
Figure 5.8 The effect of apamin (100nM) on both inward (A) and outward (B) membrane currents from voltage clamped rabbit left atrial myocytes.

A) Current densities at -115mV and B) at -65mV were measured before and after ($\geq$120 seconds) the application of 100 nM apamin. The currents were recorded at 3 different increasing $[Ca^{2+}]_i$ as a consequence of pipette solution buffered to 100, 300 and 500 nM by BAPTA. The free-Ca^{2+} was previously measured in cells. During the experiments a different degree of cell shortening could be observed. Values represent mean $\pm$ s.e.m. Also, one-way ANOVA was employed in the analysis. Sample size is noted below X axis.

5.4.2.2 Absence of effect of 100 nM apamin in human right atrial myocytes

The protocol was repeated also in myocytes from human right atrial tissue, using only 300nM $[Ca^{2+}]_i$ buffered solution, but the currents recorded at -115mV (control current -4.4 ± 0.9 vs -4.6 ± 0.9 following 100 nM apamin, mean ± s.e.m., paired data, Fig. 5.10 A) and -65mV (0.49 ± 0.1 vs 0.54 ± 0.1, mean ± s.e.m., paired data, Fig. 5.10 B) before and after the exposure to 100nM apamin were similar, indicating that the peptide failed again to block any current at those voltages and at the frequency used (0.1Hz).

Below, typical original traces obtained with WinWCP software are shown, demonstrating absence of effect of apamin at all voltages tested and stability of the recordings in human right atrial myocytes (Fig. 5.9). Human right atrial cells were tested only for 300 and 500 nM $[Ca^{2+}]_i$.

Human right atrium
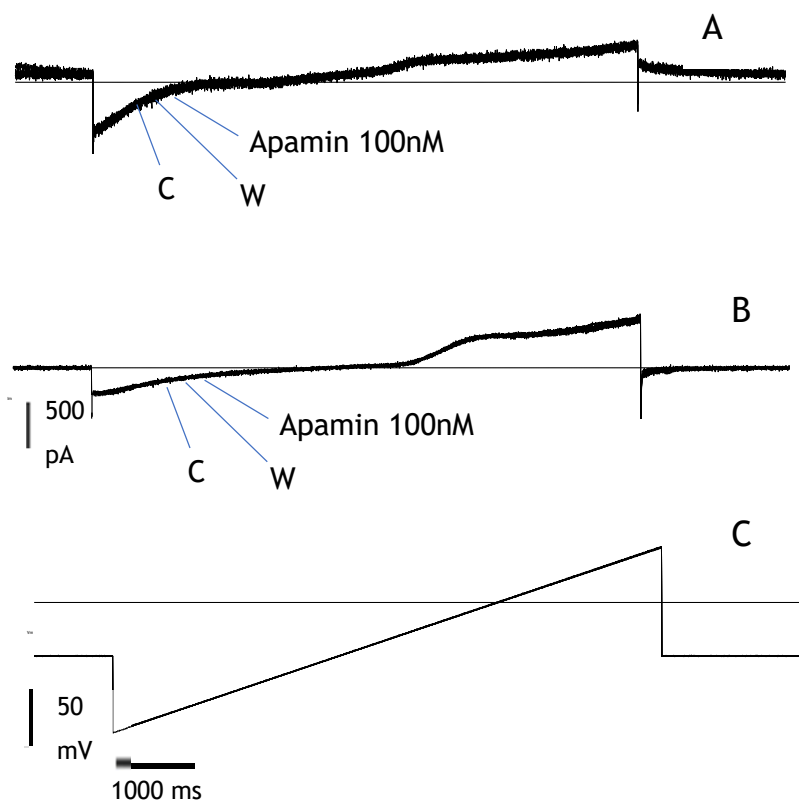
Figure 5.9 Representative superimposed traces obtained at 2 different [Ca^{2+}]$_i$, before and after acute administration of 100 nM apamin, in human atrial myocytes.

Raw traces recorded in human right atrial myocytes with A) 300 nM [Ca^{2+}]$_i$ and B) 500 nM [Ca^{2+}]$_i$, showing stability of the recordings and absence of effect of apamin. C) Represent the protocol already described in section 5.4.2 and 5.3.3. C= control, W= wash; the figure shows 15 (5 for each condition) superimposed recordings. Figures were created with WinWCP V 5.1.6 software.
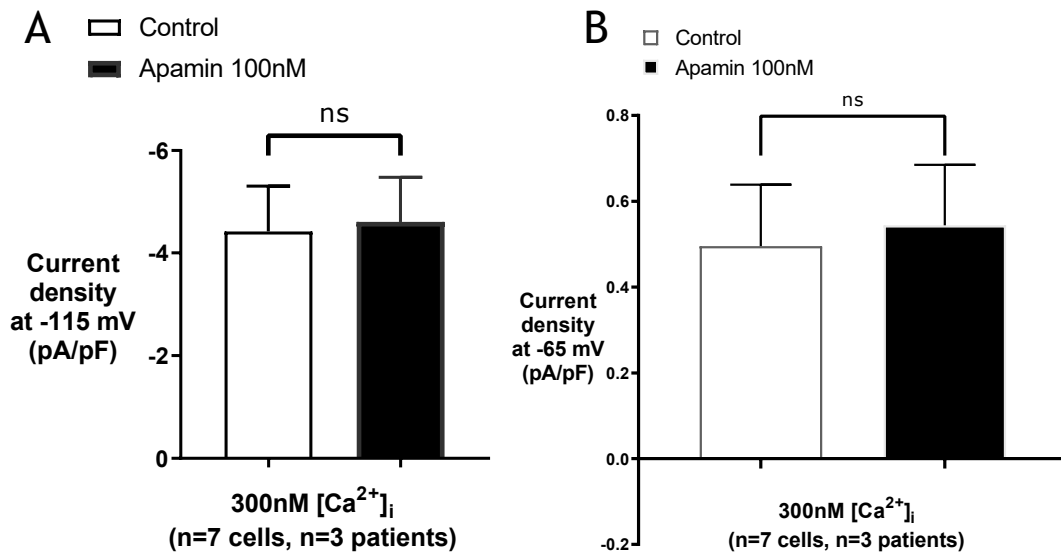
Figure 5.10 The effect of apamin (100nM) on both inward (A) and outward (B) membrane currents from voltage clamped human right atrial myocytes. (A) Current density at -115mV was measured before and after (≥120 seconds) the application of 100 nM apamin. The currents were recorded at elevated $[Ca^{2+}]_i$ as a consequence of pipette solution buffered to 300 nM by BAPTA. The free-Ca^{2+} was previously measured in cells. During the experiments a different degree of cell shortening could be observed. Values represent mean ± s.e.m and P<0.05 was considered significant. Sample size is noted below X axis.

5.4.3 Investigation of effect of ICAGEN on ion currents recorded in single human right atrial and rabbit left atrial cells

Apamin has shown lack of effect, especially in cardiac tissues (171, 353) due to uncertain reasons. Dale et al., report that SK channels can be partially apamin-sensitive and leave almost half of the SK currents unblocked despite a supramaximal concentration (1µM) of the peptide being used in Chinese hamster ovary cells. The explanation remains unclear, but may rely on some post translational modification of SK channels (340). Also, the existence of an apamin- and scyllatoxin-insensitive isoform of the human SK3 channel has been reported

(354). In light of these findings, and after the presented negative results, it was decided to replicate the protocol using a different drug: the putative selective blocker ICAGEN (ICA). This small molecule is a SK channel pore blocker acting at the apamin binding site (187), but with lower potency (183). However, ICA has already been tested both ex-vivo and in vitro. Diness et al. report that AF was reversed in 100% of hearts perfused with 1 µM ICA and could not be reinduced, while 1 µM apamin had no effect (196). In addition, Skibsbye et al., showed prolongation of APD in myocytes from sinus rhythm patients, but not in AF myocytes, after inhibition of putative I_{SK} by 1µM ICA (29). Nevertheless, the latter one is the only publication that shows positive results in human single cells using ICA at different concentrations (1-10 µM). Moreover, unphysiological experimental conditions have been used (e.g. 20mM $[K^+]_o$), the $[Ca^{2+}]_i$ has been calculated with a computer program rather than measured and they were not able to wash out the drug effect.

Therefore, using the whole-cell configuration of the patch clamp technique, the effect of a relatively high concentration of ICA (1 µM) on ion current in single cells was investigated and the ICAGEN-sensitive current in isolated human right atrial and rabbit left atrial myocytes was measured. Following the protocol used for apamin, the free Ca^{2+} concentration in the pipette solution was set to 100, 300 or 500 nM in these experiments with the intention of inducing maximal activation of SK channels.

5.4.3.1 Absence of effect of 1 µM ICA in rabbit left atrial myocytes

In rabbit left atrial myocytes the results showed no effect of 1 µM ICA at any $[Ca^{2+}]_i$ used. Specifically, at 100 nM $[Ca^{2+}]_i$ acute administration of the putative selective SK blocker ICA did not affect either inward (control current -7.4 ± 1.3 pA/pF vs -7.3 ±1.3 following 1 µM ICA, mean ± s.e.m., paired data, Fig. 5.12 A) or outward (0.4 ± 0.3 pA/pF vs 0.3 ± 0.4, mean ± s.e.m., paired data, Fig. 5.12 B) currents. The inward peak current at -115mV (-7.7 ± 2.1 pA/pF vs -8.8 ± 2.2, mean ± s.e.m., paired data, Fig. 5.12 A) and the outward current at -65mV (0.8 ± 0.5 pA/pF vs 0.2 ± 0.7, mean ± s.e.m., paired data, Fig. 5.12 B) were also not affected by ICA at $[Ca^{2+}]_i$ of 300 nM. The absence of effect of ICA was observed also at $[Ca^{2+}]_i$ of 500 nM on both inward (-5.5 ± 0.8 pA/pF vs

-6.0 ± 0.7, mean ± s.e.m., paired data, Fig. 5.12 A) and outward (0.3 ± 0.2 vs 0.4 ± 0.3, mean ± s.e.m., paired data, Fig. 5.12 B) currents. Finally, figure 5.12 A shows a significant increase of the inward current at -115mV with 300nM $[Ca^{2+}]_i$, after the application of 1µM ICA, which was considered a false positive due to rundown of the current (on average) which drifts in the opposite direction compared to a potential effect of the drug. The rundown during analysis never compromised the detection of any possible drug effect.

In figure 5.11 typical original traces obtained with WinWCP software are shown, demonstrating absence of effect of ICA 1 µM at all voltages tested and the stability of the recordings in rabbit left atrial myocytes. Raw traces for 100, 300 and 500 nM $[Ca^{2+}]_i$ are shown.
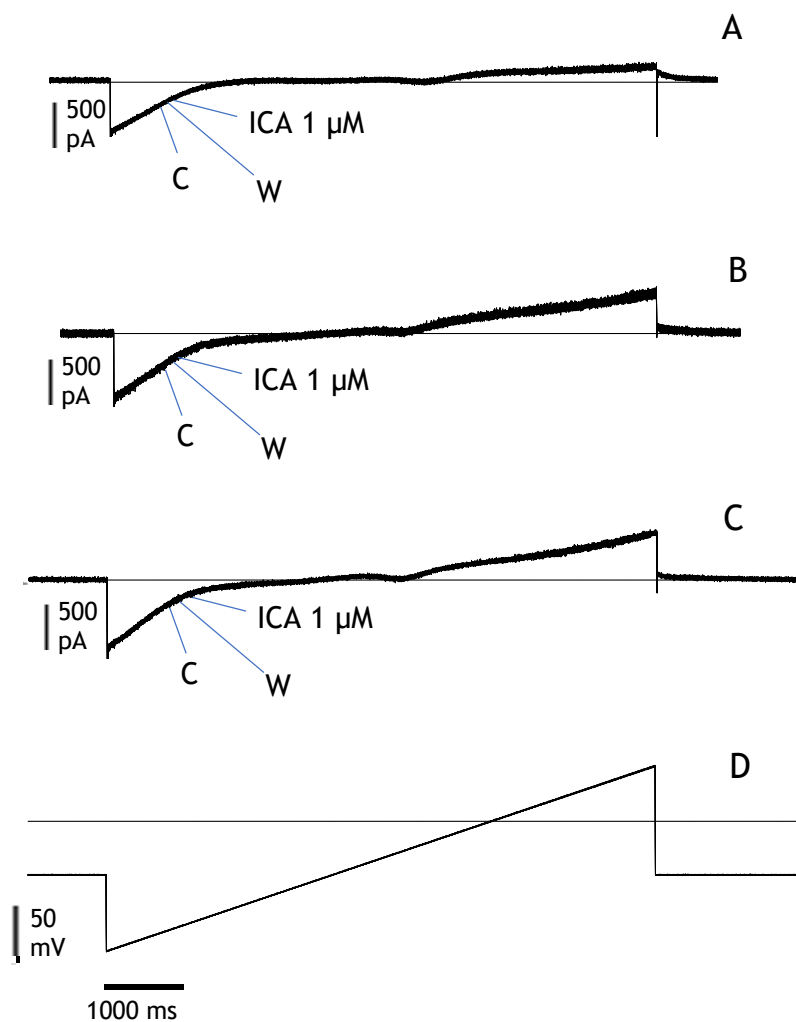
Rabbit left atrium

Figure 5.11 Representative superimposed traces obtained at 3 different [Ca^{2+}]$_i$, before and after acute administration of 1 μM ICA, in rabbit atrial myocytes.

Raw traces recorded in rabbit left atrial myocytes with A) 100 nM [Ca^{2+}]$_i$, B) 300 nM [Ca^{2+}]$_i$ and C) 500 nM [Ca^{2+}]$_i$, showing stability of the recordings and absence of effect of ICA. D) Represent the protocol already described in section 5.4.2 and 5.3.3. C= control, W= wash; the figure shows 15 (5 for each condition) superimposed recordings. Figures were created with WinWCP V 5.1.6 software.
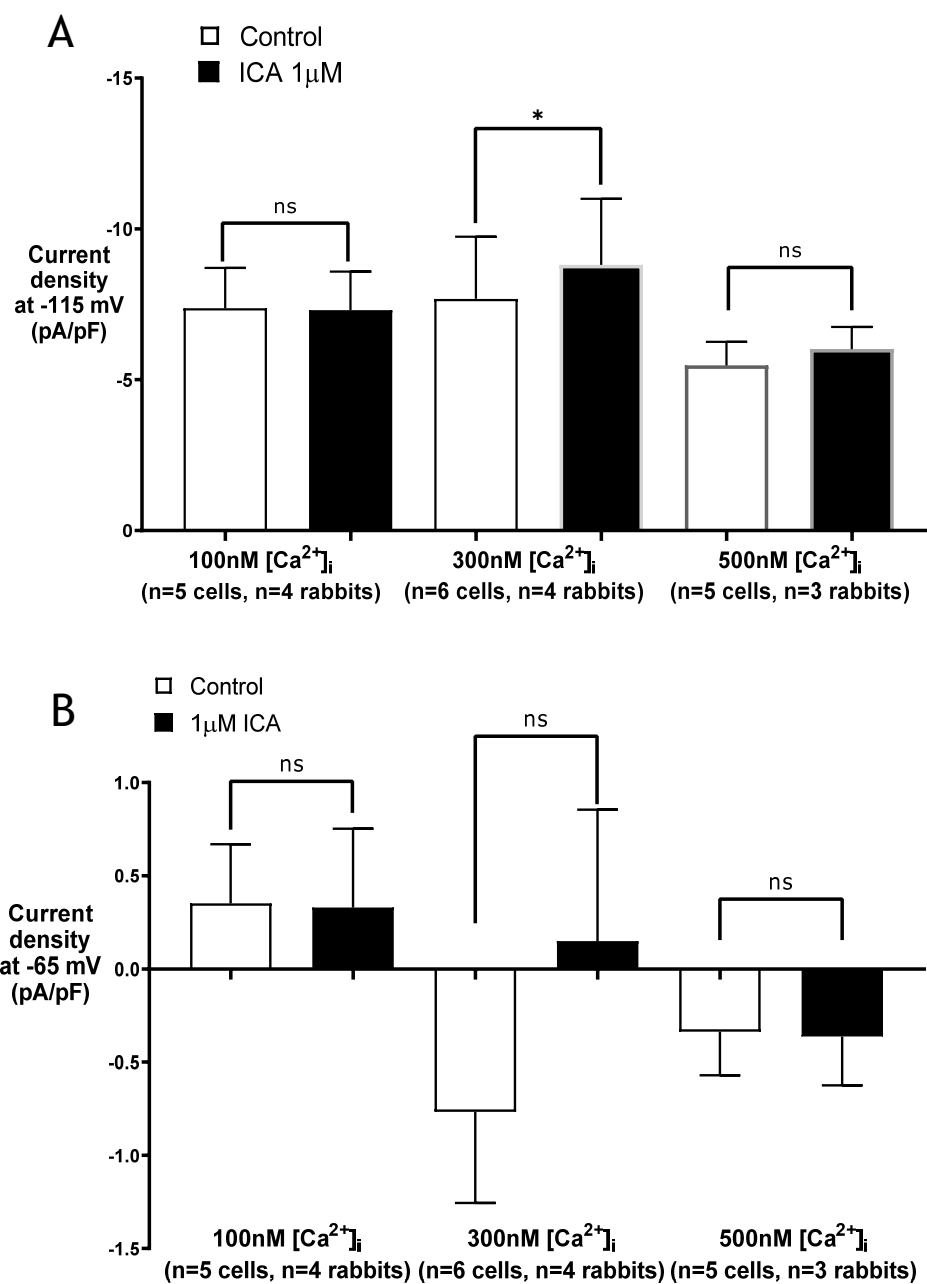
Figure 5.12 The effect of ICA (1µM) on both inward (A) and outward (B) membrane currents from voltage clamped rabbit left atrial myocytes.

A) Current densities at -115mV and B) at -65mV were measured before and after (≥120 seconds) the application of 1 µM ICA. The currents were recorded at 3 different increasing $[Ca^{2+}]_i$ as a consequence of pipette solution buffered to 100, 300 and 500 nM by BAPTA. The free-Ca^{2+} was previously measured in cells. During the experiments a different degree of cell shortening could be observed. Value represent mean ± s.e.m and $P<0.05$ was considered significant. Also, one-way ANOVA was employed in the analysis. Sample size is plotted below X axis.

5.4.3.2 Absence of effect of 1 μM ICA in human right atrial myocytes

The protocol was replicated in human right atrial myocytes with similar results. At $[Ca^{2+}]_i$ of 100 nM the currents recorded at -115 (control current -2.8 ± 0.5 pA/pF vs -2.6 ± 0.4 following 1 μM ICA, mean ± s.e.m., paired data, Fig. 5.14 A) and -65mV (0.08 ± 0.1 pA/pF vs 0.1 ± 0.05, mean ± s.e.m., paired data, Fig. 5.14 B) remained unchanged before and after the exposure to 1 μM ICA. Also, at $[Ca^{2+}]_i$ of 300 nM ICA had no effect either on inward (-3.4 ± 0.3 pA/pF vs -3.6 ± 0.3, mean ± s.e.m., paired data, Fig. 5.14 A) or outward (0.5 ± 0.2 pA/pF vs 0.6 ± 0.2, mean ± s.e.m., paired data, Fig. 5.14 B) currents. Finally, at $[Ca^{2+}]_i$ of 500 nM the acute administration of ICA failed to alter both inward (-2.9 ± 0.4 pA/pF vs -2.8 ± 0.4, mean ± s.e.m., paired data, Fig. 5.14 A) and outward (0.2 ± 0.2 pA/pF vs 0.2 ± 0.2, mean ± s.e.m., paired data, Fig. 5.14 B) currents. Thus, even the putative selective SK channel blocker failed to block any current at those voltages and at the frequency used (0.1Hz).

In figure 5.13 typical original traces obtained with WinWCP software are shown, demonstrating absence of effect of ICA at all voltages tested and the stability of the recordings in human right atrial myocytes. Raw traces at 100, 300 and 500 nM $[Ca^{2+}]_i$ are shown.

Human right atrium
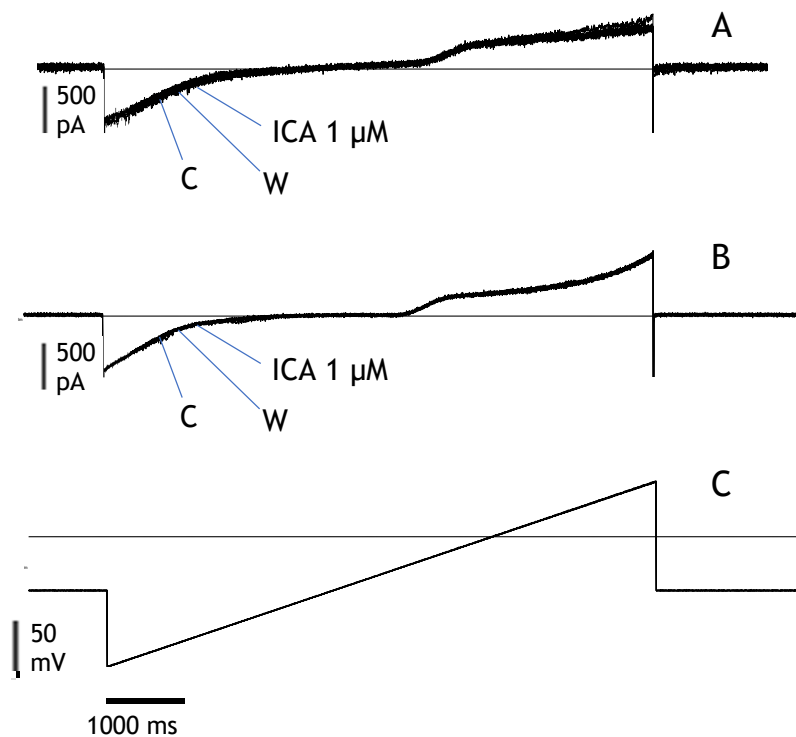
Figure 5.13 Representative superimposed traces obtained at 2 different [Ca^{2+}]$_i$, before and after acute administration of 1 μM ICA, human atrial myocytes.

Raw traces recorded in human right atrial myocytes with A) 300 nM [Ca^{2+}]$_i$ and B) 500 nM [Ca^{2+}]$_i$, showing stability of the recordings and absence of effect of ICA. C) Represent the protocol already described in section 5.4.2 and 5.3.3. C= control, W= wash; the figure shows 15 (5 for each condition) superimposed recordings. Figures were created with WinWCP V 5.1.6 software.
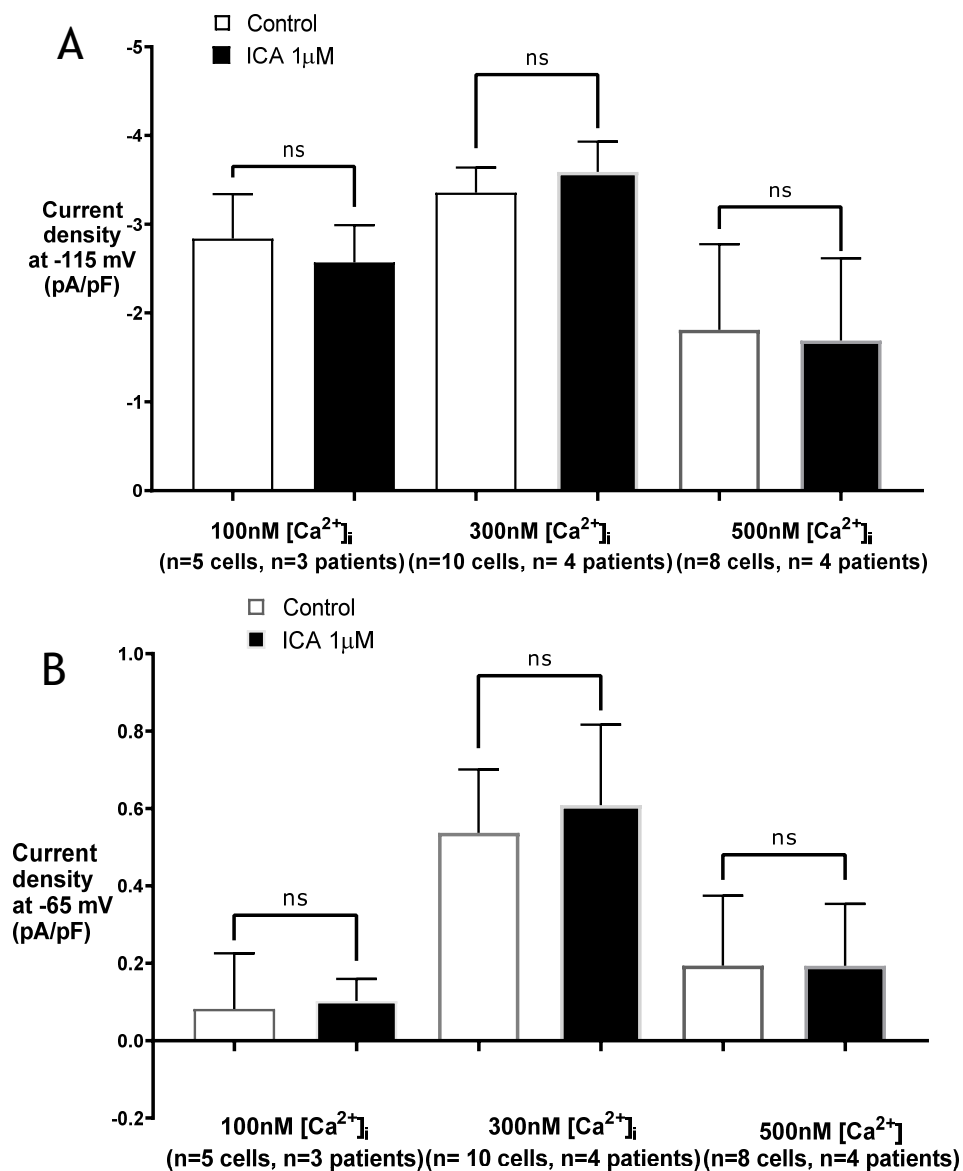
Figure 5.14 The effect of ICA (1μM) on both inward (A) and outward (B) membrane currents from voltage clamped human right atrial myocytes.

A) Current densities at -115mV and B) at -65mV were measured before and after (≥120 seconds) the application of 1 μM CA. The currents were recorded at 3 different increasing $[Ca^{2+}]_i$ as a consequence of pipette solution buffered to 100, 300 and 500 nM by BAPTA. The free-Ca^{2+} was previously measured in cells. During the experiments a different degree of cell shortening could be observed. Value represent mean ± s.e.m and $P<0.05$ was considered significant. Sample size is plotted below X axis.

5.4.4 Some "hidden" results

Although neither apamin nor ICA significantly affected mean inward or outward current at any $[Ca^{2+}]_i$ in either species, I noticed a slight reduction of the current at -115mV in a few cells (as specified below) after the application of 100nM apamin at 300nM $[Ca^{2+}]_i$. The requirement for a positive control was previously expressed in this thesis since I_{SK} was expected to be difficult to detect due to its low density. Temporal stability, timing, and reversibility of K^+ current (I_{K1}) block by Ba^{2+} were tested. Thus, considering that I_{SK} might occur in only a small proportion of myocytes, potentially masked by cell averaging, data were checked for any individual cell I_{SK}-blocker effects. This event, named from now on as candidate drug effect (CDE), is defined as any current reduction at -115mV or -65mV compatible with the positive control onset profile, including reversal upon washout of intervention. Below, are shown representative superimposed raw traces captured by the WinWCP (version 5.3.4) software, which display the possible effect of 100nM apamin on the inward portion of the current at 300nM $[Ca^{2+}]_i$ (Fig. 5.15 B) and the total absence of effect after application of apamin at 100nM $[Ca^{2+}]_i$ (Fig. 5.15 A). In figure 5.15 A each condition (control, drug or wash) is represented by 29 (290s) overlapped traces which show total absence of effect at 100nM $[Ca^{2+}]_i$, whereas figure 5.15 B shows 5 superimposed traces (50s of recording), for each condition, which are compatible with the temporal stability and onset profile of the positive control. The reduction observable in figure 5.15 B was obtained ~90s after the application of 100nM apamin and was stable in time. Besides, the reduction had a characteristic slope, as already observed in the previous experiments with Ba^{2+} on I_{K1}, which was stable but not reversible (washable). Therefore, considering the stability over time of an absence of effect, and the compatibility with the positive control profile of those current reductions, those events, albeit rare, were classified as true drug effects, and this required a systematic scrutiny of each cell. Out of 84 cells from either species or drug, 5 CDEs occurred which required further investigation. The CDEs were observed only in rabbit left atrial cells, at $[Ca^{2+}]_i$ of 300 or 500nM and not 100nM, but only with 100nM apamin. It must be mentioned that, therefore, no CDEs were observed in human right atrial cells with either drug, nor with apamin in either species.
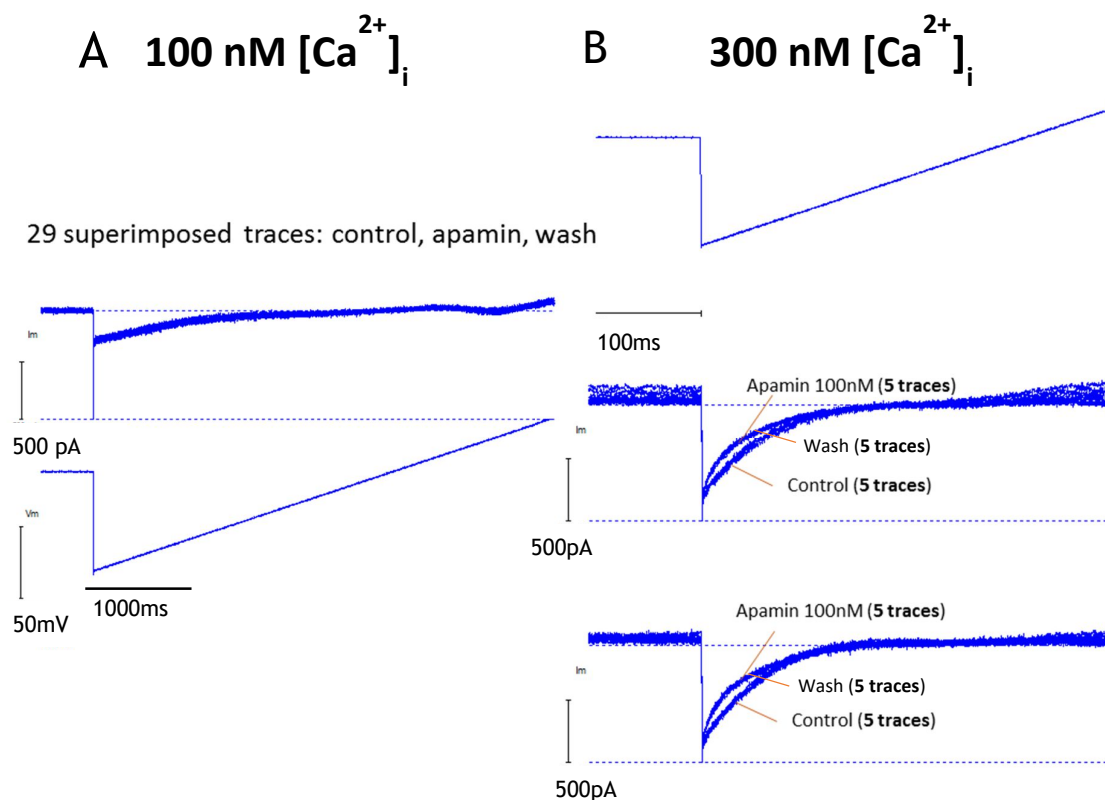
Figure 5.15 Raw current traces from single rabbit left atrial cells:

A) shows an absence of effect of the drug, represented by the maintenance of the "steady-state" through every condition (control, 100nM apamin and wash) at 100nM (diastolic) $[Ca^{2+}]_i$ B) shows traces from 2 different cells extrapolated from a subset (6/15) of cells where it can be appreciated the effect of apamin on the current at -115mV during 300nM (systolic) $[Ca^{2+}]_i$. Traces were generated by WinWCP 5.3.4 software.

Figure 5.16 shows current density of single rabbit left atrial cells at each $[Ca^{2+}]_i$. The cells were classified individually by any intervention occurring. The voltage ramp protocol shown in figure 5.15 was used and I_{SK} was estimated from the difference in current as a result of the addition of apamin (100 nM). This difference was measured at -115 mV. Specifically, the current values were investigated in single left atrial cells from rabbits undergoing sham ischemia procedure or stock animals. In addition, a sub-classification was made for usage of either bovine serum albumin (BSA at 0.01%) to avoid apamin adherence during single cell perfusion or 2,3 butanedione monoxime (BDM) during cardiomyocytes isolation procedure (30mM), which is an effective, quick-acting, and reversible

inhibitor of cardiac contractility (355-357) and it can protect myocardium from hypoxia and from the calcium paradox (358). Initially the scrutiny was driven by the identification of 2 cells (18.01.10 a, b) from the same tissue (with BMD used during isolation), which were characterized by high current. However, the use of BDM was not considered the reason behind the CDEs observed from the same tissue. Also, in regard to the subsidiary aim, few left atrial cells obtained from MI rabbits (n=4 cells n=1 rabbit) were examined after administration of 100 nM apamin (MI rabbits were not used for ICA experiments) (Fig.5.17), but no clear effect was observed in this preliminary study and, therefore, no further investigations were performed. Among the various conditions tested no significant pattern attributable to the occurrence of these CDEs was observed. In summary, only 6% of cells were classified as CDEs with an average current density values of 1.2 ± 0.3 pA/pF.
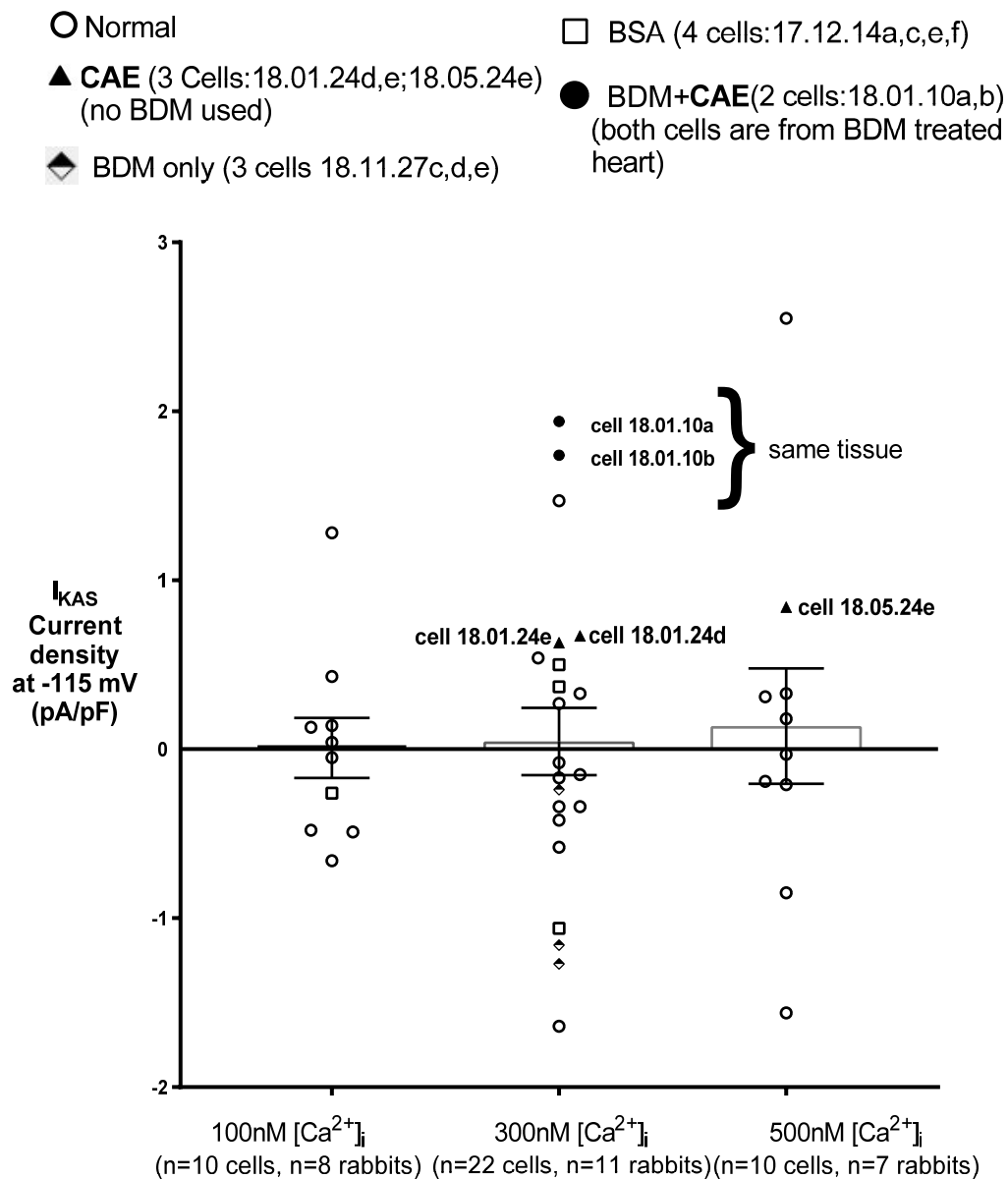
Figure 5.16 Comparison of apamin-sensitive current among different [Ca²⁺]ᵢ: scrutiny of single rabbit left atrial cells.

The scatter plot with bars displaying I_{SK} density for each single cell. The legend above the graph describes all the condition under which the cells were classified. Bovine serum albumin (BSA), 2,3 butanedione monoxime (BDM), candidate apamin effect (CAE). For the identification, each single cell is reported as year.month.day.alphabet letter. Values are mean ± s.e.m.

◆ MI (1 cell:18.11.22a) (no BDM used)

◇ BDM+MI (3 cells:18.11.22b,c,d)
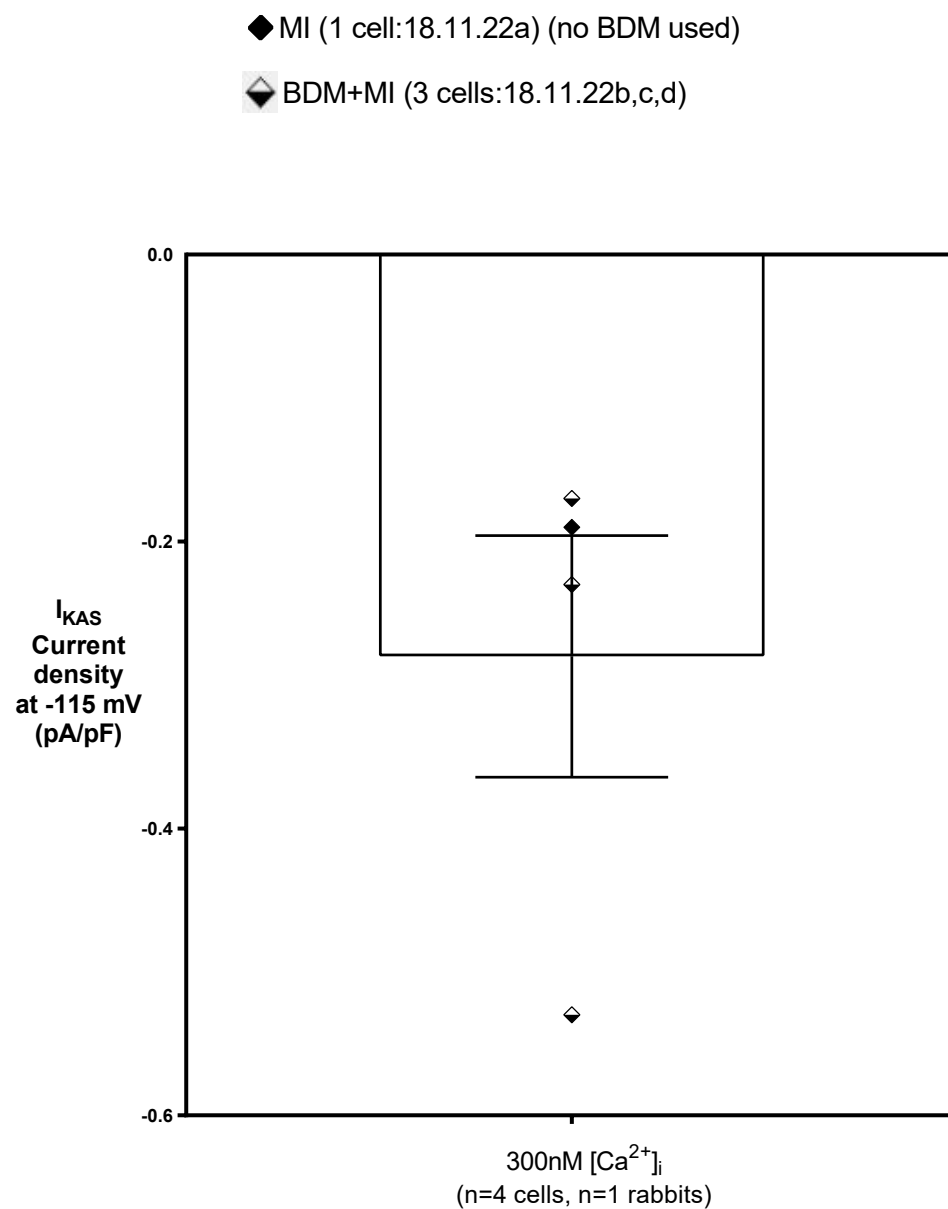
Figure 5.17 Apamin-sensitive current recorded at 300 nM [Ca²⁺]ᵢ: scrutiny of single left atrial cells from rabbit underwent myocardial infarction (MI).

5.5 Discussion

Two potent and highly selective I_{SK} blockers, acting with similar mechanism on the SK channels, have been demonstrated to be ineffective even at typically-reported mean global systolic $[Ca^{2+}]_i$ levels (i.e. 500 nM), in contrast with many published studies (27-30), but not all (203, 340). Therefore, the apparent discrepancies between the findings herein reported and those previous publications (27-30) require scrutiny and discussion, as follows.

5.5.1 Inter-study differences of I_{SK} with respect to heart chamber, cell type, recording solutions, and other experimental conditions.

Apamin was firstly chosen due to its proven selectivity for SK channels and the substantial number of studies showing its potency on these channels. However, given the aforementioned limitation of the toxin in cardiac tissue, in addition to its possible adhesiveness to the perfusion tubes, which could have resulted in a lower concentration present in the cell bath, it was decided to use it in addition to a second SK blocker, ICAGEN. This blocker, being a small neutral molecule that acts at the channel's outer pore, with equal potency on all subtypes, could represent a more reliable tool for addressing whole-cell studies, although it blocks SK channels less potently than apamin. Moreover, a recent study showed apamin had high-affinity for voltage dependent Kv1.3 (IC_{50} =13 nM) channels which are frequently coexpressed with SK channels (359), thus questioning the specificity of this peptide. Therefore, the comparison between the effect of a well-known neurotoxin and a new SK blocker in voltage-clamp experiments was considered the optimal condition to obtain solid results and avoid possible misleading interpretation.

Nevertheless, part of the explanation for the unexpected results could rely on variations in K^+ currents and calcium handling, attributable to interspecies differences in mammalian cardiomyocytes. In fact, previous studies show effect of either apamin or ICA in different tissues or cell type (e.g. HEK293 cells, Xenopus oocytes) (29, 197, 210), but to my knowledge only another preliminary study (abstract) from our laboratory, described APD prolongation by 1µM ICA in both rabbit whole heart and single left atrial cells (360). This limits the possibility to compare with the literature the effect of ICA. On the other

hand, the measurements were also performed in human atrial myocytes, where SK channels have been widely demonstrated to be functionally present and successfully blocked by either apamin or ICA (27, 29, 30). In addition, there are discrepancies regarding the apamin-sensitive current amplitude recorded among these studies. Xu et al., reported an I_{KAS} density of ~2 pA/pF (at -115mV) in mice atrial myocytes with just 50pM apamin and a calculated $[Ca^{2+}]_i$ of 500nM (27). Conversely, Nagy et al. showed absence of effect with 100nM apamin and 900nM $[Ca^{2+}]_i$ (calculated) in rat atrial myocytes (203), which share very similar action potential morphology and calcium handling with mice (361). Moreover, Fan et al., found I_{KAS} to be ~3 pA/pF in atrial myocytes from patients with sinus rhythm with 500nM $[Ca^{2+}]_i$. While they report measurements by epifluorescence of $[Ca^{2+}]_i$ for diastolic levels in both sinus rhythm and AF patients, the 500nM $[Ca^{2+}]_i$ used during current recordings appears to be obtained with addition of a calculated amount of $CaCl_2$ in the pipette solution; which contrasts with the conditions used in the present study. By this means, they used a calculation program to estimate the final $[Ca^{2+}]_i$ inside the patch pipette. This would result in approximation of the real $[Ca^{2+}]_i$ present inside the cells. Besides, they report the use of EGTA (5 mM) which, as discussed in chapter 3, represents a much slower buffer compared to BAPTA (used in my experiments) and this will not ensure a precise intracellular calcium concentration in cells. Therefore, given the lack of precision of $[Ca^{2+}]_i$ levels used and the discrepancies observed among the previous studies, it is difficult to explain with any certainty the lack of significant effect, by either apamin or ICA, in the presented voltage-clamp experiments. Although it should be acknowledged that I found a small effect of apamin in a very small sub-set of rabbit atrial cells, the overall finding is a general absence of detectable I_{SK} in rabbit or human atrial myocytes.

5.5.2 Role of $[Ca^{2+}]_i$ on SK blockers effect

Given the wide range of $[Ca^{2+}]_i$ used in previous studies (300-900nM) (27, 29, 203), not measured but rather calculated by programs, the present experiments were designed to better study the role of Ca^{2+} on the effect of apamin or ICA. The fluorometric measurements (chapter 4) confirmed that the highest $[Ca^{2+}]_i$ levels reached values up to 1 μM globally. Therefore, since submicromolar (0.3-0.5 μM) concentrations of this divalent cation have been demonstrated to be enough to activate SK channels (165, 168, 175, 318, 326,

327), the results achieved during the experiments described here were not expected. In fact, no difference in the effect of either apamin or ICA was seen as a function of $[Ca^{2+}]_i$ levels. However, in contrast to previous findings (203), it can be ruled out that $[Ca^{2+}]_i$ levels were not sufficiently high to activate SK channels, due to the previous measurements in cells.

5.5.3 Perforated versus ruptured patch clamp configuration

The possible big impact, on the activation of I_{SK}, of different patch-clamp configurations was also taken into consideration. In fact, Xu et al, used perforated patch clamp in isolated murine myocytes, while the present study used ruptured patch-clamp, which is probably not the best option to investigate minor current changes on account of some drawbacks. In fact, processes that depend on soluble intracellular biochemicals rapidly run down after the rupture and this can lead to disruption of endogenous cellular Ca^{2+} buffering mechanisms (362). However, Xu et al., showed an effect of a very low concentration of apamin (50pM) even with whole-cell (ruptured) patch clamp configuration, with a calculated $[Ca^{2+}]_i$ of 500nM. In contrast, Nagy et al. performed the experiments with both techniques but no effect of 100nM apamin was seen, even where $[Ca^{2+}]_i$ was highly elevated (supposed 900nM). Thus, it seems that the use of different patch clamp configurations does not compromise the investigation of I_{SK}.

5.6 Limitations

The use of the buffer BAPTA allowed to reach $[Ca^{2+}]_i$ that mimic the normal systolic levels. This $[Ca^{2+}]_i$ was expected to elicit SK channels and allow the detection of I_{SK}. However, the use of BAPTA could be limited by its capacity of disrupting the coupling between SK channels and L-type calcium channels, which has been reported to cause the loss of SK channel activity in pyramidal neurons (172). This, was confirmed by a more recent study in the same cell type, where the use of 10 mM BAPTA occluded the effect of 100nM apamin (363). Nevertheless, this mechanism has never been showed in cardiomyocytes. In addition, the scope of the present study was not to fully clamp the intracellular calcium but to use this mobile buffer to maintain a global systolic $[Ca^{2+}]_i$ which, therefore, allowed 300 to 500 nM intracellular free-calcium concentration.

The "chunk" method used for cell isolation in human could, in theory, disrupt ion currents. In support, in dog atrial cells, the "chunk" method reduced significantly the size of the delayed rectifier K^+ current (I_K) and the percentage of cells in which this current was detected in canine atria compared to the perfusion method (364). However, no differences of either apamin (100nM) or ICA (1µM) effect on current morphology were observed between human and rabbit (cell isolated by perfusion method), thus excluding a possible implication of different isolation method on the absence of effect of the drug.

5.7 Conclusion

To summarize, the data herein reported challenge previous findings about the pharmacology and physiological $[Ca^{2+}]_i$-sensitivity of I_{SK}, and potential reasons behind the apparent discrepancies have been discussed. However, the possibility that these channels might activate under special pathophysiological circumstances (such as conditions of ischemia or atrial fibrillation), which were not addressed in this study, cannot be excluded. Furthermore, the low stimulation frequency used in this study, which had been adopted following the protocol described in Chapter 2 and the highly buffered $[Ca^{2+}]_i$ with BAPTA, although it reaches very high values (close to systolic), might not allow some activation kinetics of SK channels. Some of these questions will be addressed in the next chapter.

Also, more recently, evidence supporting the existence of two distinct populations of SK channels in both human and mouse atria have been presented. One of these populations consists of homomeric SK2 channels and present sensitivity to apamin, while a second heteromeric SK2-SK3 channel population is apamin-insensitive and it is considered the only one activated during the falling phase of the action potential (AP) (365, 366). Nevertheless, while on APs apamin showed little or no effect, during voltage-clamp experiments it has been shown to reduce outward current in myocytes from both human (365), in contrast with the present results, and mouse (366) atrial tissue,

However, It is important to emphasise that, of the numerous published reports of cardiac I_{SK} being detectable in normal tissue (27-30, 365, 366), none of them employed physiological conditions (considering solution composition and

temperature) in atrial cells. Therefore, the consensus, based on the present whole-cell-currents data along with the most relevant available data already published (30, 365), is that it is presently debatable whether, and to what degree, I_{SK} may flow under physiological conditions in atrial myocytes, and further studies are warranted to clarify the debate. Nevertheless, according to the findings described in this chapter, it must be concluded that I_{SK} is either non-existent or rare, in rabbit and human atrial cardiomyocytes, at $[Ca^{2+}]_i$ typical of global diastolic-to-systolic values.

Chapter 6 Does the small conductance Ca^{2+}-activated K^+ current (I_{SK}) flow during atrial action potential repolarisation under physiological conditions?

6.1 Background

6.1.1 SK channels involvement in atrial action potential late-phase repolarization and AF

Action potential duration (APD) is determined by the fine equilibrium between inward and outward currents. The alteration of this balance, which may be compromised in several cardiac disorders, may cause shortening or prolongation of the action potential. In particular, the atrial cardiac electrical and mechanical remodelling that occurs in response to a variety of diseases can predispose to AF, which is characterised by a rapid and irregular atrial rate that causes an adaptation of the atrial electrical activity and promotes AF in turn. This process is known as "AF-induced atrial electrophysiological remodelling" (77, 80, 367) caused by shortened effective refractory period (ERP), slowed conduction velocity or both, which reduce the wavelength (λ) duration and can cause re-entry. Specifically, the tenfold (400-600 min^{-1}) increase in atrial rate during AF provoke a considerable $[Ca^{2+}]_i$ rise through I_{Ca} (84) which has been shown to be indirectly (e.g. through atrial contractile disfunction) involved with both short (92, 100) and long-term atrial tachycardia (89). On the other hand, this increase in $[Ca^{2+}]_i$ could be crucial for the activation of the SK channels, which may represent a direct link between calcium and atrial late phase repolarization. The first evidence that SK channels may be directly linked to AF was presented by Ellinor, et al. in 2010 in a study of common generic variants of KCNN3 which was found to be associated with lone AF (206) and confirmed later by other studies (207, 208). Also, additional evidence of the involvement of SK channels in atrial myocyte repolarization, was provided by Xu, et al., showing the presence of an apamin-sensitive current involved in the late phase of the action potential repolarization (APD90), which directly correlates with ERP duration, functionally expressed at higher level in human and mouse atrial cardiac myocytes compared to ventricle and that was significantly increased at

1µM $[Ca^{2+}]_i$ (27). These findings were confirmed by the same group, showing the presence of all three SK channel isoforms in mouse and rat hearts and the important role played by the SK2 isoform in human atria (28). Also, later Li et al. in 2009 published more direct evidence for a role of I_{SK} in AF, showing that atrial myocytes isolated from mice lacking $K_{Ca}2.2/SK2$ upon genetic knockout had prolonged atrial APD (200). In addition, SK channels have been shown to be functionally coupled to central molecules dominating the intracellular Ca^{2+} signalling, like L-type Ca^{2+} channels (LTCCs) in neurons (172) and in rabbit myocytes (368) and a downregulation of LTCCs has been associated to a decreased expression of SK2 channel subtype (174). Therefore, since these channels have been shown to be voltage-insensitive and activated solely by internal calcium ions, in chapter 5 the interaction between SK current and $[Ca^{2+}]_i$, near to systolic values (0.3-0.5 µM), was investigated using a voltage pulse (ramp) protocol at low stimulation frequency, and I expected to obtain an effect with either apamin (100 nM) or ICA (1 µM), both highly selective SK blockers (27, 168, 183, 201, 369). However, these molecules equally failed to alter either the inward or the outward current. Among the various hypotheses for these negative results, it was considered the possibility that the calcium signalling necessary to activate these channels could be disrupted by the use of the calcium buffer BAPTA (172, 363). Therefore, in this chapter the objective was achieve by testing the putative selective SK blocker ICAGEN (ICA) on action potentials. This extends the experiments with ICA on ramp-evoked currents (chapter 5), since $[Ca^{2+}]_i$ may be expected to be raised physiologically to higher levels during the AP, albeit transiently, compared to clamped free-Ca^{2+} used in voltage clamp experiments, and possibly activate I_{SK}.

6.1.2 Rationale to use increasing concentration of ICAGEN

ICA, as mentioned earlier in this thesis, is one of the new class N-(4-methyl-pyridin-2-yl) derivates, which display excellent potency as $K_{Ca}2$ channels blockers (183). This compound presents no significant selectivity among SK subtypes, inhibiting all with equal effectiveness. Given the demonstrated absence of effect of ICA at 1 µM in the previous voltage-clamp experiments (Chapter 5), a higher concentration (10 µM) of this compound was also tested in the following studies. Albeit limitations exist with 10 µM ICA, due to possible unspecific block of other currents (29, 197), this concentration was chosen with

the purpose of looking for acute responses to the compound that could be detectable, under physiological conditions and using the identical setup used for previous patch-clamp experiments. In fact, by using a 10-fold higher concentration, which is still lower than the lowest IC_{50} reported (I_{TO}, $IC_{50}=21\mu M$) (29) for other cardiac relevant ion currents, I aimed to confirm that the drug was active, and it was reaching the cell in the bath while remaining selective for the SK channel target. By this means, the aim was to support previous findings, which demonstrate absence of effect of the SK blocker ICA at a selective concentration of 1 μM.

6.2 Aim section

Therefore, considering the disputed role of SK channels in atrial repolarization and the unclear reason behind these different findings, the aims were as follows:

- Firstly, create a positive control by testing temporal stability, timing, and reversibility of the already demonstrated effect of 2 mM 4-aminopyridine (4-AP) on transient outward K$^+$ current (I_{TO1}) (79) in rabbit atrial myocytes in order to validate my current clamp recordings

- Investigate the effect of the putative selective SK blocker ICA at 1 or 10 μM on APD30, APD70 and APD90 in current clamped single rabbit left atrial (LA) and human right atrial (RA) myocytes at 1 Hz, with short period of stimulation at 3 Hz in order to possibly activate I_{SK}

- Study the possible contribution of SK current to the frequency-dependent adaptation of APD governed by changes in $[Ca^{2+}]_i$ as a consequence of increased stimulation rate (2-3Hz) in single human right atrial myocytes

6.3 Methods

6.3.1 Current Clamp: action potential recordings

The traditional method for recording the cell interior potential is the current-clamp technique, known also as "Bridge" recording. This technique is more challenging than voltage clamping and allows to recreate the response of a myocyte to electrical stimulation or depolarisation in vivo, thus, the generation of action potentials. It works under bridge mode and allows to perform current-clamp experiment, where a known constant or time-varying current is applied and the change in membrane potential caused by the applied current is measured. This type of experiment mimics the myocytes membrane voltage response to a current input, which causes a depolarization in vivo and eventually provokes the firing of an action potential. After the isolation, the myocytes experienced a period of rest after which they were found to be markedly depolarized, therefore, a small holding current was used to clamp cells to a diastolic potential of -80 mV. Only those cells which required a holding current (cells where Vm was markedly depolarized) of <0.15 nA immediately after establishing the whole cell configuration were used, which was a standard limit adopted and once set, the negative current was kept fixed during the full recording. The software programme utilised, WinWCP (J. Dempster, Strathclyde University) on a microcomputer (Gateway microcomputers with Pentium III microprocessor) permitted simultaneous stimulation and recording. Current and voltage data were low passed filtered at 5 kHz and digitised at a rate of 10 kHz (Digidata 1200 A-D converter, Axon instruments) prior to storage on compact discs and sampling interval was 0.02 ms.

6.3.2 Cell isolation methods and solutions

Atrial myocytes from stock rabbits or sinus rhythm patients' tissues were isolated and superfused with solutions as previously described (See Methods 2.3.1-2.4.1). Experiments were performed using ruptured whole-cell patch clamp (See Methods section 2.6-2.8) in current-clamp mode whereby a constant or pre-specified time-varying current is applied to the myocyte and the resultant change in membrane potential, the action potential, is recorded. The same

external and internal solutions described in method section 2.4.1 were used. All experiments were performed at 35-37°C.

6.3.3 Protocols

6.3.3.1 Current pulse used in the investigation of the effect of 4-AP

A cycle length of 1s with a single current stimulus per cycle was used for the experiments to test the effect of 4-AP on APD. At the start of each cycle, with 50 ms delay, a 3 ms current pulse of 1.8 nA was adopted as standard threshold to stimulate the firing of an action potential. If this amperage was not sufficient, the stimulus threshold was increased repetitively by 100-500 pA increments (depending on the cell response to the stimulus) until a regenerative action potential was stimulated (Fig. 6.2). Once an action potential firing occurred, the amplitude of the current pulse was maintained constant throughout the experiment in that cell. The APD was calculated as the interval between the action potential upstroke and repolarisation to the level of 30% (APD_{30}), 50% (APD_{50}), 70% (APD_{70}) and 90% (APD_{90}) of the upstroke amplitude (see figure 6.1) using the software program WinWCP (J. Dempster, Strathclyde University). The effect of 2 mM 4-AP on the RMP or the maximum diastolic potential (MDP) as well as on the upstroke velocity (dV/dt_{max}) was also examined. Examples of measurements made on action potentials to calculate plateau phase characteristics and repolarisation are shown in figure 6.1
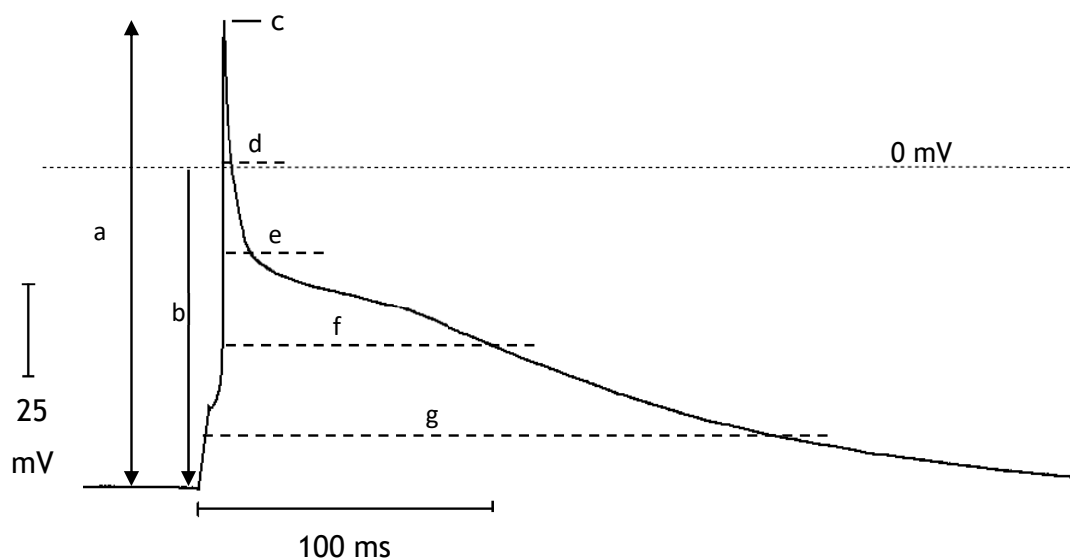
Figure 6.1 Representation of measurements in raw human atrial isolated myocyte action potential trace.

a= amplitude, b= RMP, c= overshoot (0% repolarization), d= APD_{30}, e= APD_{50}, f= APD_{70}, g= APD_{90}.
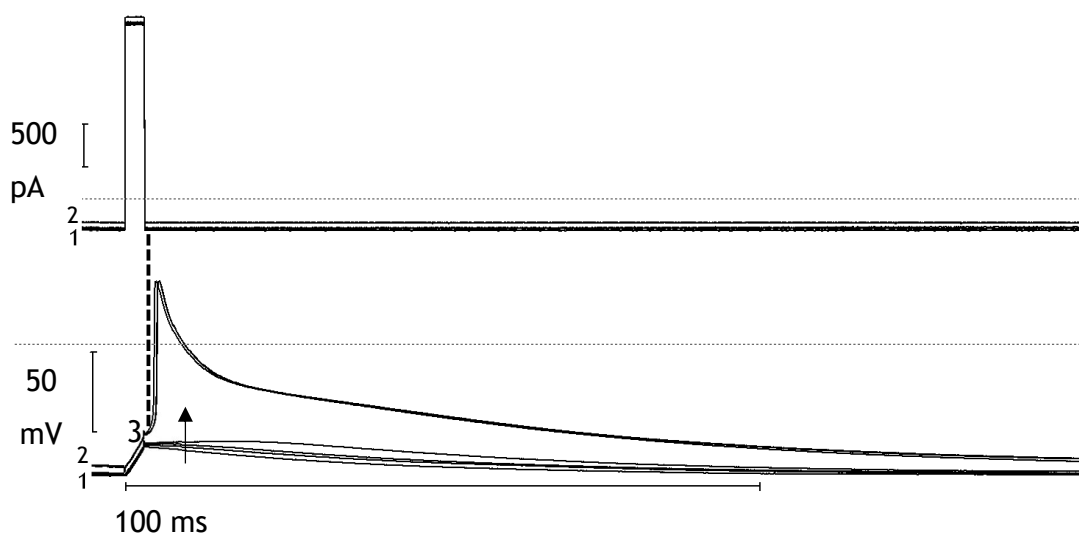
Figure 6.2 Raw traces representing the firing of 3 action potentials (below) succeeding the current pulse stimulus (above) under control conditions in rabbit left atrial myocytes.

A slightly less negative current was applied on this occasion to bring the MDP from -90mV (1) to -79 mV (2). Once the threshold (3) was reached an action potential firing occurred. The arrow shows the direction of the time course of 4 failed initiations and 3 consecutive action potentials. The dotted line indicates the end of the current pulse. The image was created using the WinWCP software.

6.3.3.2 Current pulse used in the investigation of the effect of ICAGEN (ICA)

Trains of action potentials were obtained by stimulation at 1 and 3 Hz during the same protocol in rabbit left atrial and human right atrial myocytes (Fig. 6.3). This protocol was characterized by two trains of APs at 1 Hz followed by 2 trains at 3 Hz, then 15 trains of APs at 1 Hz followed by 3 trains at 3 Hz, after which all the sequences of trains were repeated (Fig. 6.4). In addition, human right atrial myocytes were stimulated at 2 or 3 Hz with different current clamp protocols (Fig. 6.5). An identical current stimulus described above for the measurements with 4-AP and an identical increment method for the stimulus was adopted. However, at 2Hz and 3Hz trains of 18 (at 2Hz) and 27 (at 3Hz) stimuli were delivered at basic cycle length (S1-S1) of 500ms or 333ms, respectively. Figures 6.3 and 6.4 show 3 superimposed trains of action potentials (under control condition) recorded in the middle of the train at 1Hz (after the 3rd AP), at 2Hz (after the 6th AP) and at 3Hz (after the 9th AP) for both human and rabbit. Also, no mark change in action potential shape over the duration of the experiments was observed. The entire train of stimulated action potentials was monitored using the software program (WinWCP). The APD was calculated as the interval between the action potential upstroke and repolarisation to the level of 70% (APD$_{70}$) and 90% (APD$_{90}$) of the upstroke amplitude. APD$_{70}$ and APD$_{90}$ were analysed to investigate the effect of ICA (1 or 10µM) on the AP plateau (relevant to non-reentry) and on the ERP (relevant to reentry), respectively. In addition, in order to further investigate the effect of ICAGEN on the phase 2 of the action potential, the repolarization to the level of 30% (APD$_{30}$) was analysed. During this phase triggered I$_{Ca}$, with peak in few milliseconds, and consequent increase in [Ca^{2+}]$_i$, could activate I$_{SK}$.

The possible effect of ICA on RMP or MDP as well as on the upstroke velocity (dV/dt_{max}) was also examined. Action potential protocols were performed under control conditions and following acute administration of 4-AP (2 mM) or ICA (1µM or 10µM) as soon as a stable series (20 singles or 2 trains) of action potentials occurred. Succeeding exposure to 4-AP for 90s was based on the time required to reach peak effect on I$_{TO1}$ (~30s, Fig. 6.8) and ICA for 180-200s was based on previous data regarding drug peak effect on I$_{SK}$ (29), assuming stable action potential recordings were observed. Then the control solution was re-

administrated to the superfusate in order to observe possible wash (reversibility) effect (Fig. 6.6).
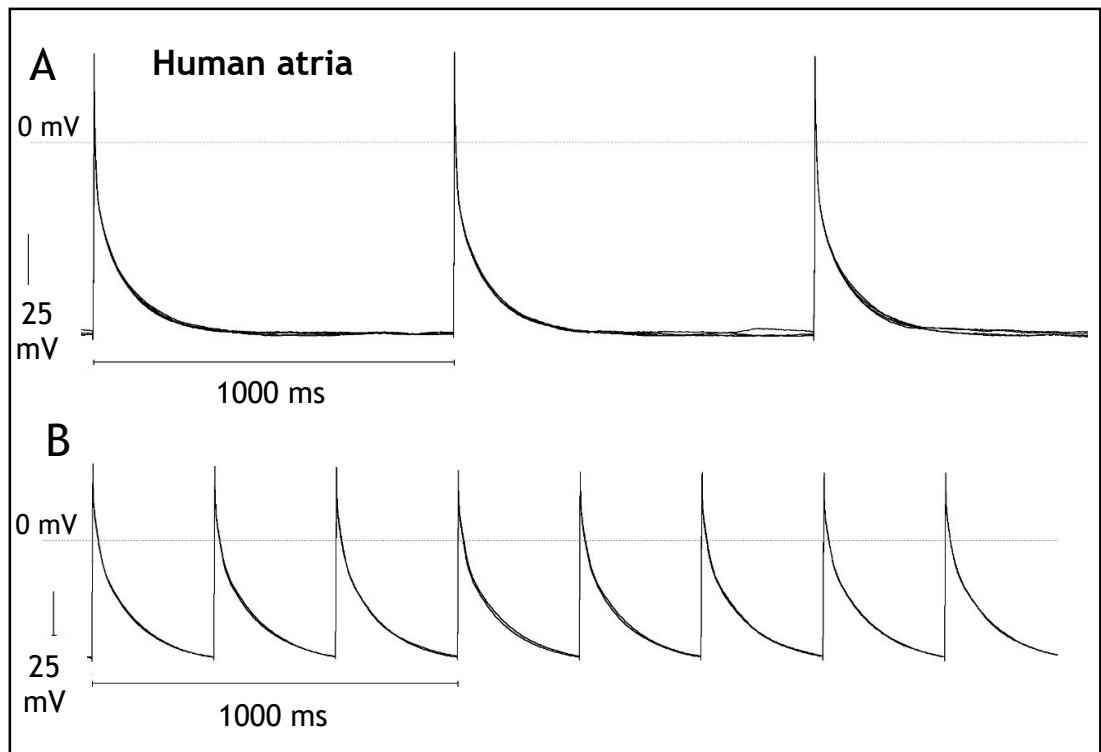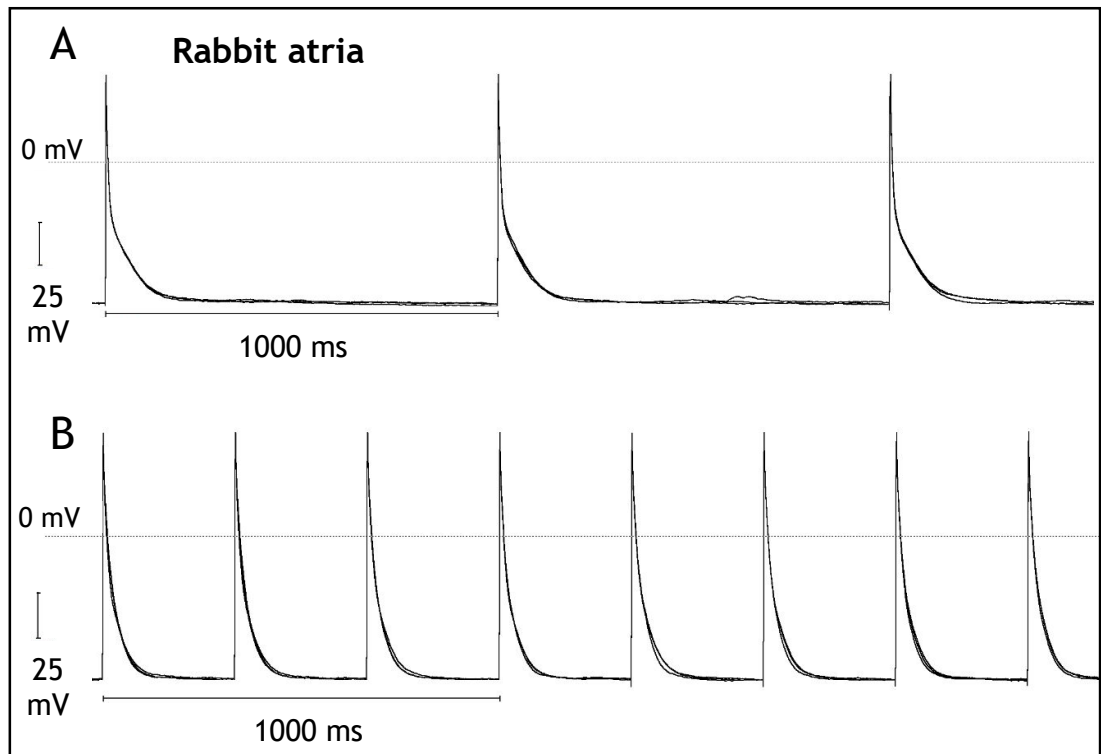
Figure 6.3 Three superimposed trains of action potentials from a rabbit left atrial (above) and a human right atrial (below) myocyte at stimulation frequency of (A) 1 Hz and (B) 3 Hz.

A) 9 superimposed action potentials and B) 24 superimposed action potentials are shown as an example.
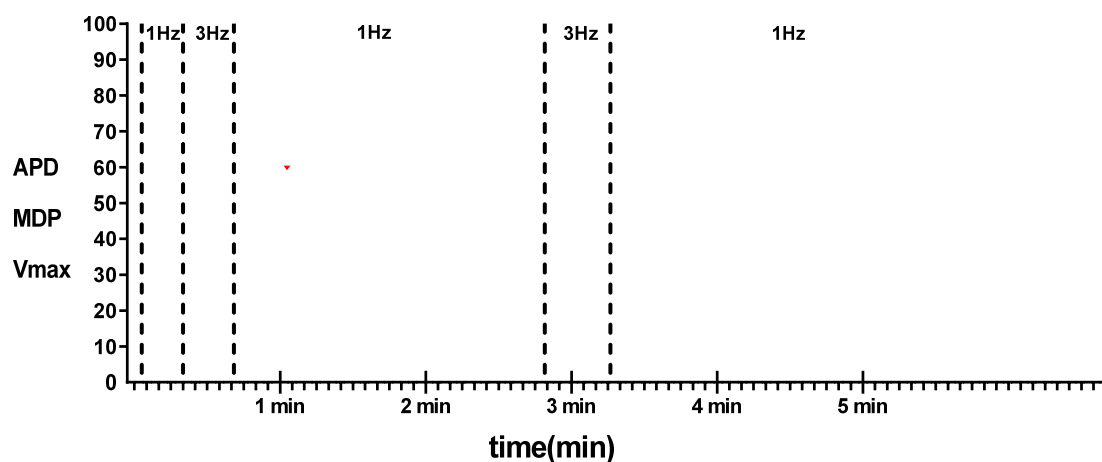
Figure 6.4 Schematic representation of the protocol used in human and rabbit atrial myocytes to stimulate action potential during acute superfusion with ICA (1-10 μM).
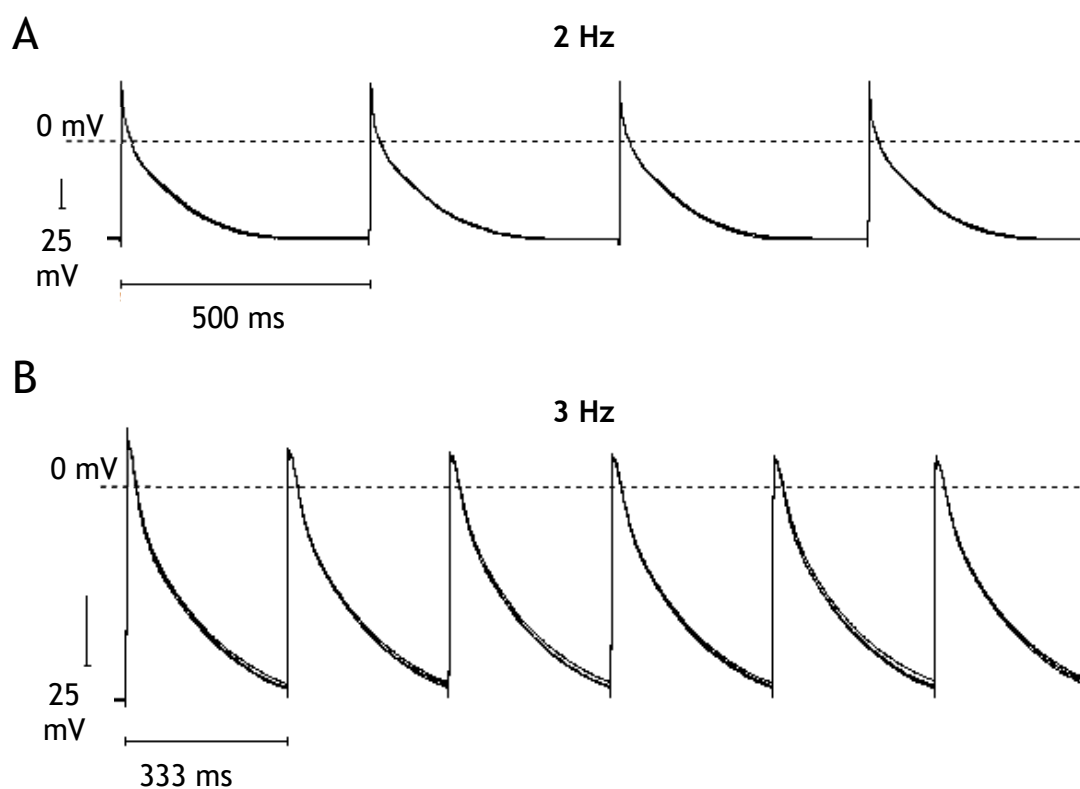
Figure 6.5 Representative superimposed trains of action potentials from human right atrial myocytes at stimulation frequency of (A) 2 Hz and (B) 3 Hz.

A) 12 superimposed action potentials and B) 18 superimposed action potentials are shown as an example.
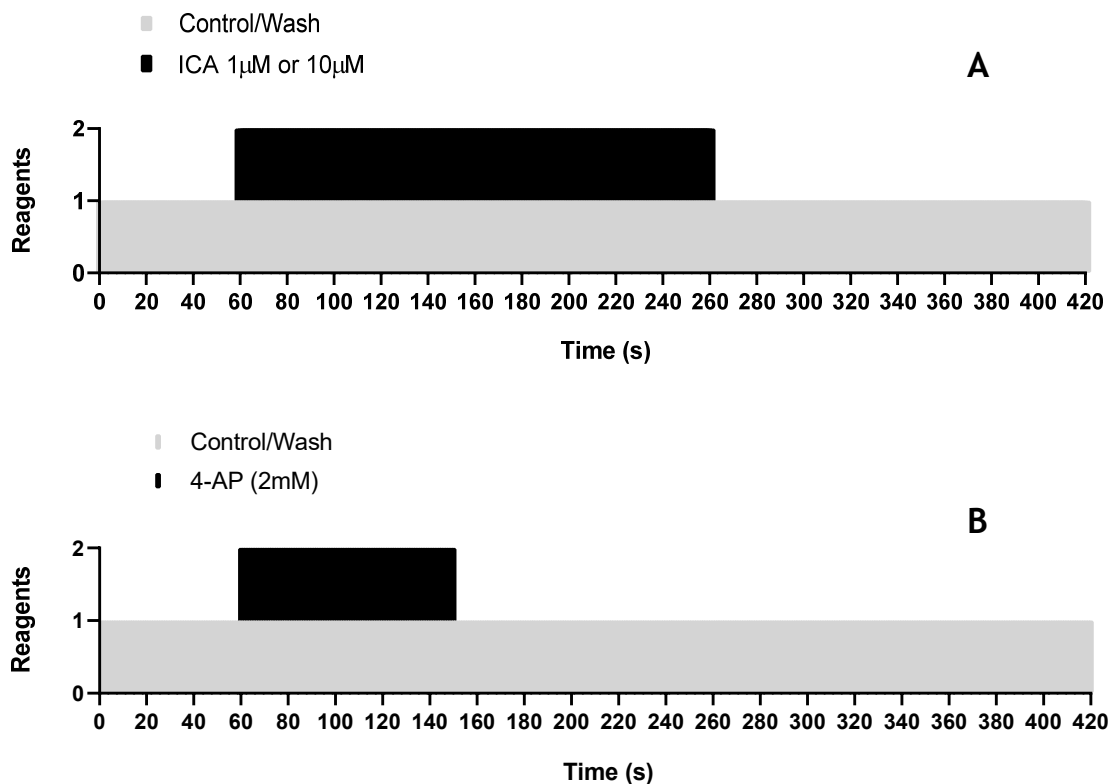
Figure 6.6 Schematic representation of the order and timing of recordings of human and rabbit atrial isolated myocyte action potentials during acute superfusion with A) ICA (1 μM or 10 μM) or B) 4-AP (2 mM).

6.3.4 Statistics & data analysis

Raw data pertaining to individual myocyte action potential traces were analysed by WinWCP waveform analysis tool. Raw data were then transferred to Excel Microsoft Word program and then used to generate graphs and statistics on GraphPad Prism. Data relating to APD, RMP, MDP and Vmax were expressed as mean ± standard error of the mean (s.e.m.) with number of cells studied and number of patients or rabbits from whom these cells were obtained. When superfusing cells with drugs, multiple action potentials were analysed (average of 3 APs) during control (once stability of the recording was achieved), 90s after drug addition, and again at 90s intervals after drug removal until the reversal of any drug effect was confirmed. The action potential characteristics of the entire dataset followed a normal distribution and therefore parametric statistic (Student t-test, one-way ANOVA) was employed to determine the degree of

difference between samples under control conditions and drugs. Statistical significance was predetermined at a level of P < 0.05. Figure 6.7 shows the results of a normality test performed on APD_{90} values obtained from human right atrial myocytes APs analysis. The two graphs confirms the normality of the APD_{90} data. In addition, several normality tests were performed, and showed consistency with a Gaussian distribution (i.e. P-value > 0.05), however D'Agostino & Pearson test was conventionally used.
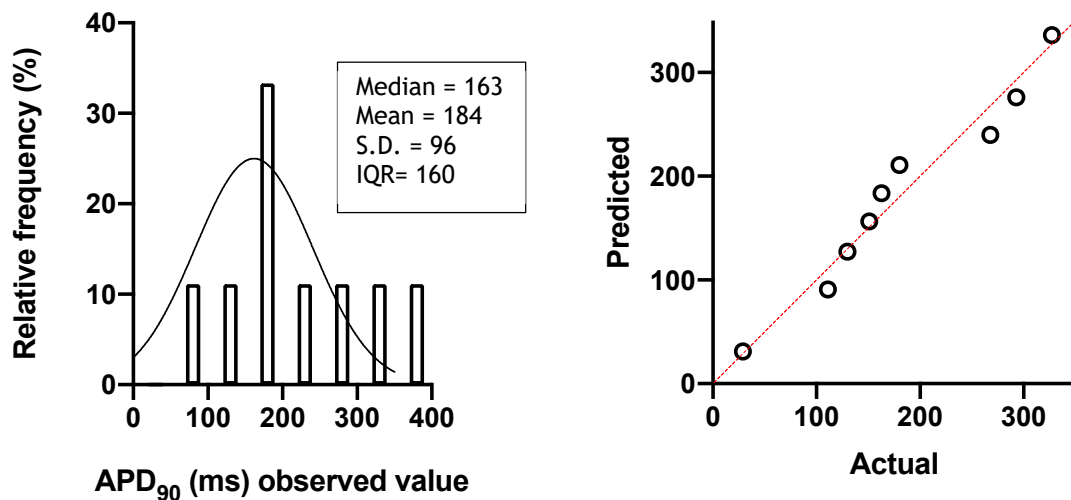
Figure 6.7 Results of normality test for APD_{90} values obtained under control conditions from human right atrial APs analysis.

A) Gaussian non-linear fit of the frequency distribution of APD_{90} values. B) Quantile-quantile (QQ) plot of APD_{90} values. The linearity of the points suggest normal distribution. P-value results from normality testing (D'Agostino & Pearson normality test) on populations of APD_{90} measurements; S.D.= standard deviation, IQR = interquartile range; n=9 cells, n=4 patients; P-values >0.05 were considered consistent with a Gaussian distribution.

6.4 Results

6.4.1 Action potentials morphology in human and rabbit atrial myocytes

A triangular action potential morphology (low-or no-dome) with prominent phase 1 in control, was the most frequently observed in recordings from myocytes from human right atrial appendage (Fig. 6.8 A). Whereas, under control condition APs from rabbit left atrial myocytes presented, typically, a pronounced phase 1 repolarization and low amplitude plateau (Fig. 6.8 B). In addition, most human atrial cells required a small (0.27 $\pm$ 0.04 pA/pF, n= 9) constant hyperpolarising current to gain $\sim$−80 mV resting Vm, as previously (79) stated and contrary to the majority of rabbit atrial cells.
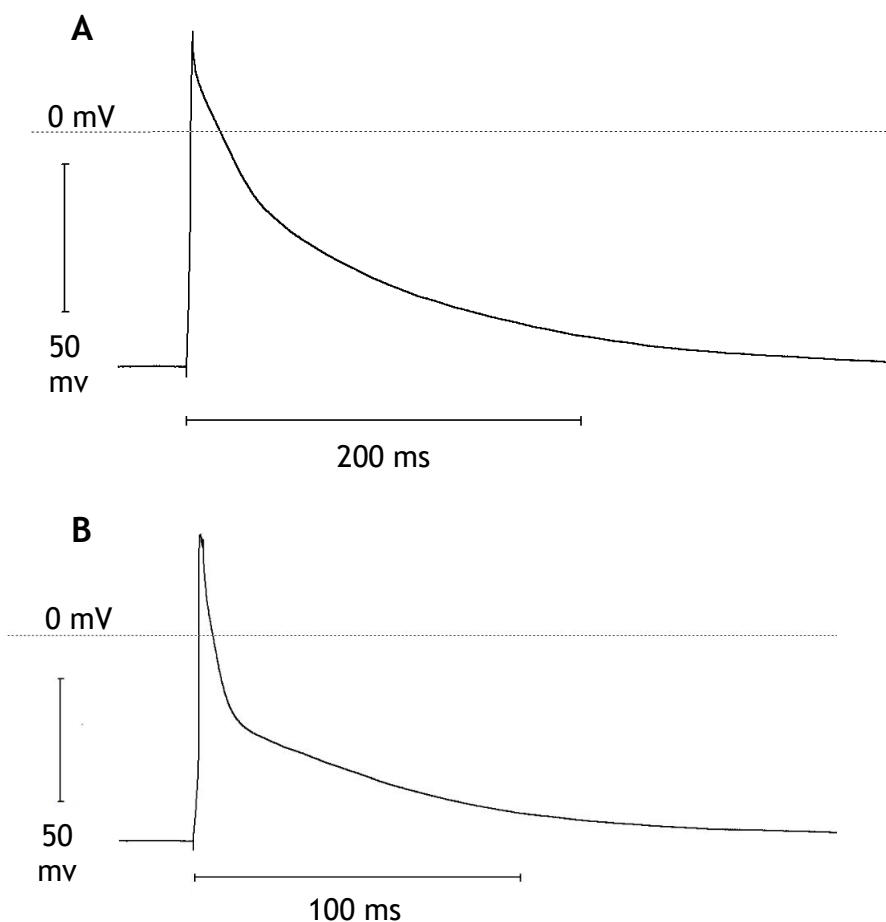
Figure 6.8 Representative (A) human right atrial and (B) rabbit left atrial isolated myocyte action potential recordings made under control conditions.

6.4.2 Effect of 2 mM 4-AP alone on rabbit atrial isolated myocytes action potentials: the positive control

The effect of acute administration of 2 mM 4-AP was tested on action potentials from rabbit left atrial myocytes at a cycle length of 1 second. 4-AP significantly suppressed phase 1 of the action potential and substantially prolonged subsequent repolarisation as illustrated in figures 6.9-6.11. All drug responses were rapid ($\leq$30 s), stable in all cells and reversable in 5 of 6 cells studied. Specifically, the mean APD_{30} under control conditions was 3.6 ± 0.3 ms, whereas acute superfusion with 2 mM 4-AP increased the duration by 72% to 6.2 ± 0.6 ms (n= 6 cells, n=2 rabbits, mean ± s.e.m., paired data, p< 0.05, Fig. 6.9). The typical time course of the effect of 4-AP on APD_{30} is represented in figure 6.10. Also, 4-AP prolonged APD_{50} and APD_{70} by 73% (control APD_{50} 6.6 ± 0.7 ms vs 11.4 ± 1.3 ms following 2 mM 4-AP n= 6 cells, n=2 rabbits, mean ± s.e.m., paired data, p< 0.05, Fig. 6.11) and by 31% (16 ± 3.0 ms vs 21± 3.6 ms , n= 6 cells, n=2 rabbits, mean ± s.e.m., paired data, p< 0.05, Fig. 6.11), respectively. APD_{90} was not significantly affected (44 ± 8.5 ms vs 54 ± 13 ms, n= 6 cells, n=2 rabbits, mean ± s.e.m., paired data, Fig. 6.11). The mean natural MDP (before application of hyperpolarizing current) was -56 ± 6.5 mV (n= 6 cells, n=2 rabbits, mean ± s.e.m., Fig. 6.12). Interestingly, the administration of 2 mM 4-AP provoked a significant increase in action potential amplitude (albeit moderate, 5.4%) while the MDP (after hyperpolarizing current, control MDP -79 ± 0.4 mV vs -79 ± 0.5 mV following 2 mM 4-AP, n= 6 cells, n=2 rabbits, mean ± s.e.m., paired data), and the maximal rate of depolarization (Vmax)(Control Vmax 0.41 ± 0.04 V/s vs 0.39 ± 0.02 V/s following 2 mM 4-AP, n= 6 cells, n=2 rabbits, mean ± s.e.m., paired data) were not affected (Fig. 6.12). The mean action potential amplitude under control condition was 115.7 ± 3.8 mV compared to 122 ± 5.7 mV during superfusion with 2 mM 4-AP (n= 6 cells, n=2 rabbits, mean ± s.e.m., paired data, p< 0.05, Fig. 6.12).
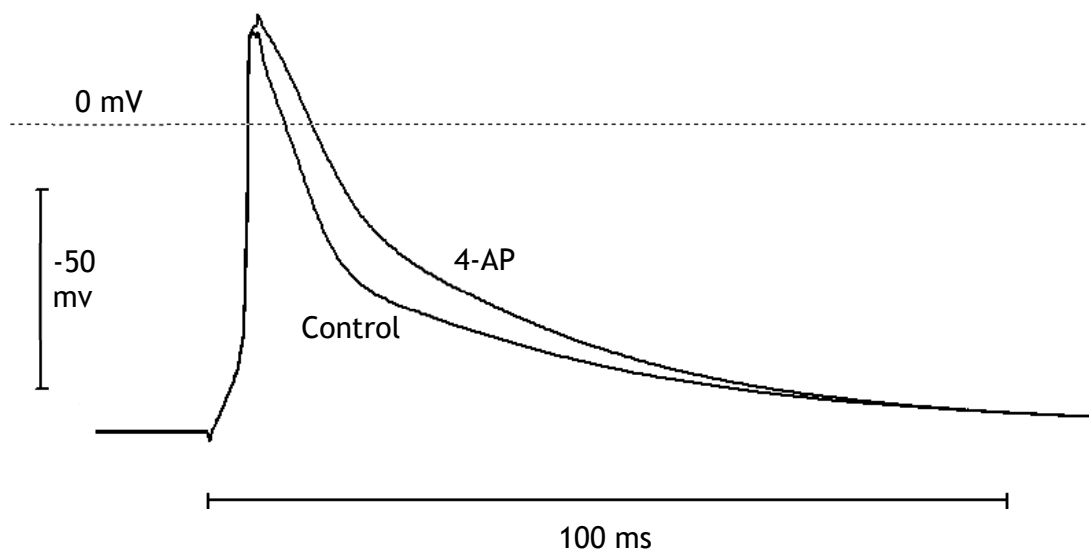
Figure 6.9 Representative raw traces showing the effect of acute superfusion with 2 mM 4-AP on a rabbit left atrial isolated myocyte action potential waveform.
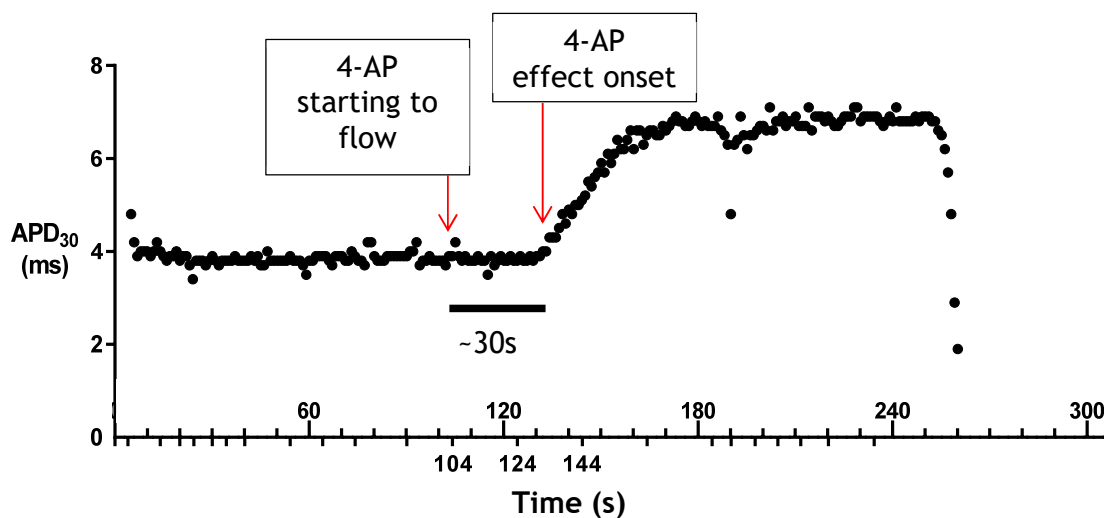
Figure 6.10 Representative time-course of the effect of 4-AP on APD$_{30}$ recorded in a rabbit left atrial myocyte: the positive control.
Each single point represents APD$_{30}$ data analysed every second of recording. Cell died around 250s which prevented the administration of control solution to test reversibility of effect. Note that the typical delay (~ 30s) between drug flow starting and drug effect onset is due to low flow (necessary to avoid cells washing away) and bath exchange time, consequent to the bath diamond shape (section 2.7.11, chapter 2) and the small "dead space" in the perfusion line.
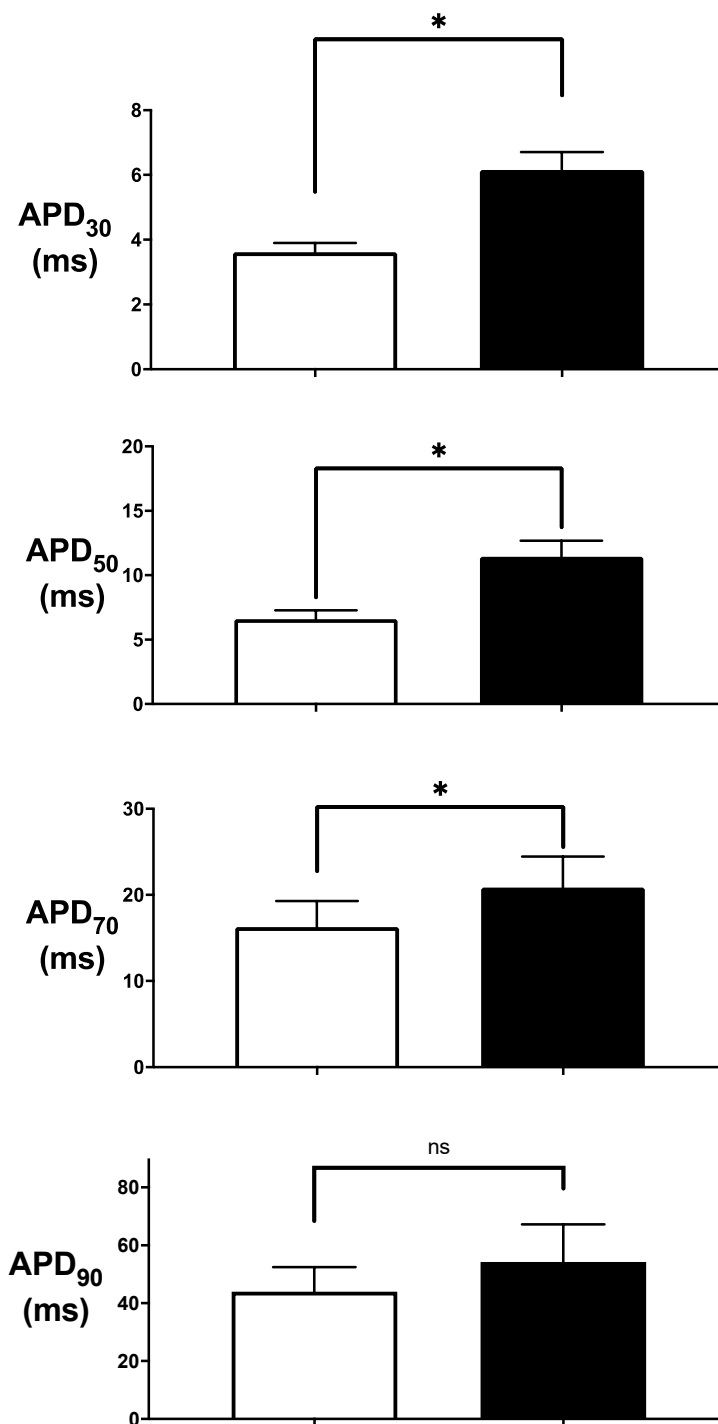
Figure 6.11 Effect of acute superfusion with 2 mM 4-AP on action potential repolarisation characteristics of rabbit left atrial isolated myocytes.

□= control ■= 2 mM 4 Aminopyridine (n= 6 cells, n=2 rabbits, paired data). Values are mean± s.e.m., values of p< 0.05 (*) were considered statistically significant.
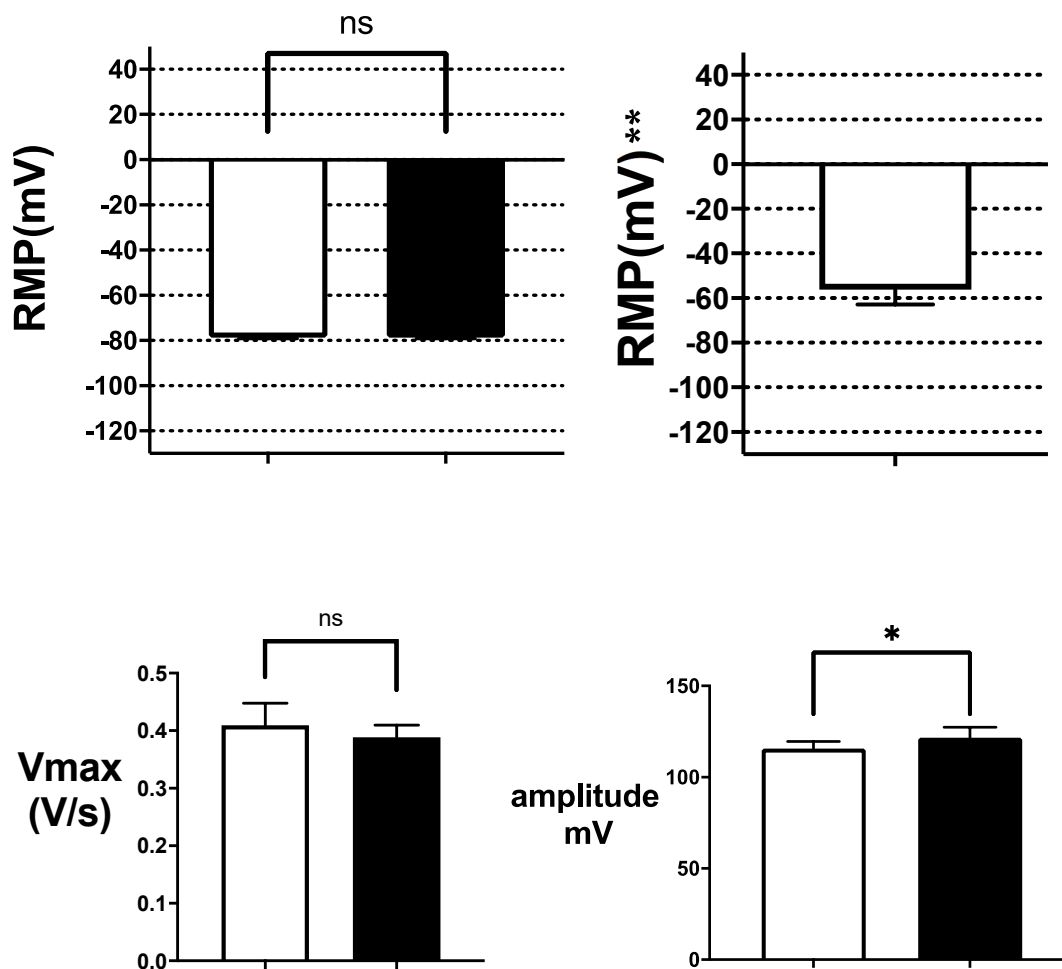
Figure 6.12 Effect of acute superfusion with 2 mM 4-AP on resting membrane potential and phase 1 and 0 action potential characteristics of rabbit left atrial isolated myocytes.

☐= control ■ = 2 mM 4-AP (n= 6 cells, n= 2 rabbits, paired data). Values are mean ± s.e.m., values of p< 0.05 (*) were considered statistically significant. ** Mean natural RMP, i.e. before application of the hyperpolarizing current.

6.4.3 Rabbit atrial APs: lack of effect of 1 μM ICA on action potential characteristics

In rabbit left atrial myocytes APs the acute administration of ICA 1μM failed to alter the APD at any percentage of repolarization at stimulation frequency of 1 or 3 Hz. There were no significant differences in APD_{30} (Control APD_{30} 3.7±0.6 ms vs 3.4±0.7 ms following 1μM ICA, n=10 cells, n=4 rabbits, mean ± s.e.m., paired data, Fig. 6.14), APD_{70} (32±8 ms vs 27±9 ms, mean ± s.e.m., paired data, Fig. 6.14) or APD_{90} (87±11 ms vs 82±14 ms, mean ± s.e.m., paired data, Fig. 6.14). Below, typical original action potentials obtained with WinWCP software are shown for control, 1 μM ICA and wash in rabbit left atrial myocytes (Fig. 6.13).
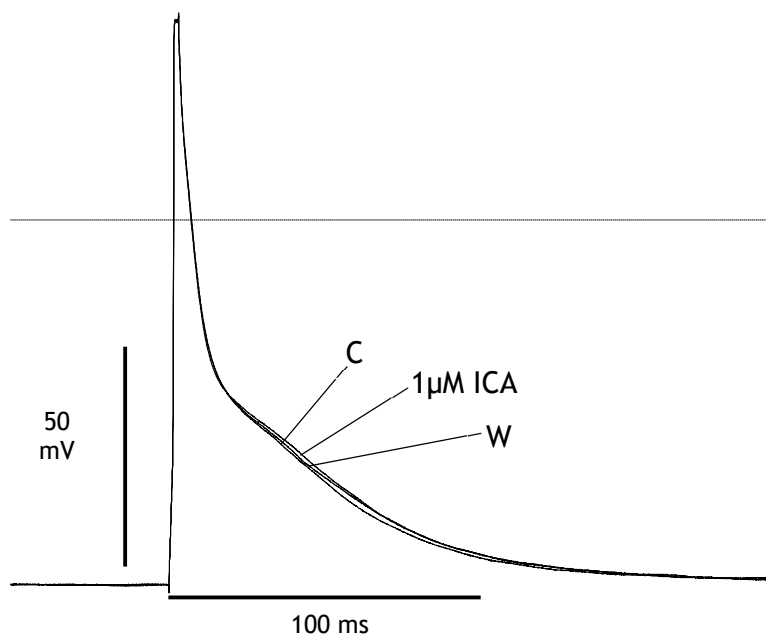
Figure 6.13 Representative action potential traces recorded from rabbit left atrial myocytes showing the absence of effect of 1 μM ICA.
Superimposed action potential waveforms recorded during control (C), 1μM ICA and Wash (W)
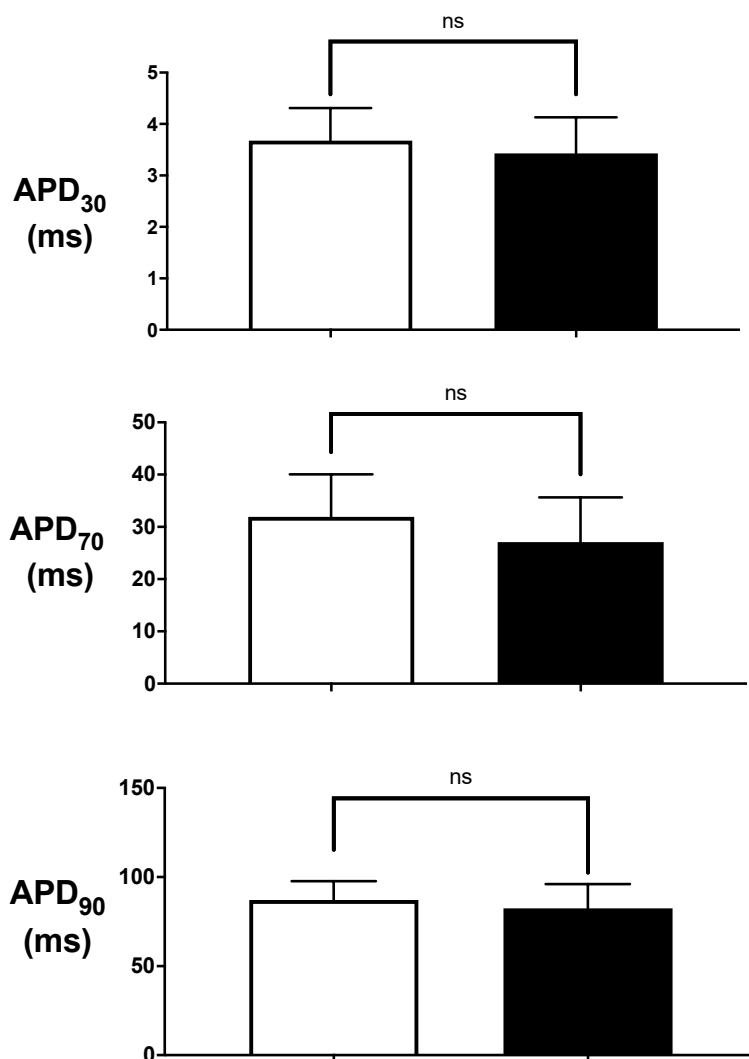
Figure 6.14 Lack of effect of acute superfusion with 1 μM ICA on action potential repolarisation characteristics of rabbit left atrial isolated myocytes.

☐ = control ■ = 1 μM ICA (n= 10 cells, n=4 rabbits, paired data). Values are mean± s.e.m.

I_{Ca} run-down during action potential recordings can cause a shortening of the APD by reducing the plateau phase within 5 minutes (370). Therefore, since this mechanism could mask a possible ICA-sensitive component, APDs were tested against time matched control (TMC) run-down. Figure 6.15 shows two representative time-course of APD_{90} recorded in two different single myocytes

from rabbit left atrium. In figure 6.15A APD_{90} was measured every 2s seconds and every second for 1Hz and 3Hz, respectively, and plotted against time. The data plotted in the graph shown in figure 6.15A show the time-course of the APD_{90} during control conditions. This permits the visualization of the run-down, mentioned above, of I_{Ca} and the effect exerted on the action potential duration over the course of the experiment. Whereas, the data plotted in the graph shown in figure 6.15B result from the analysis of each action potential recorded over the course of that experiment. The representative time-course of APD_{90} (Fig. 6.15B) shows the absence of effect 1μM ICA.
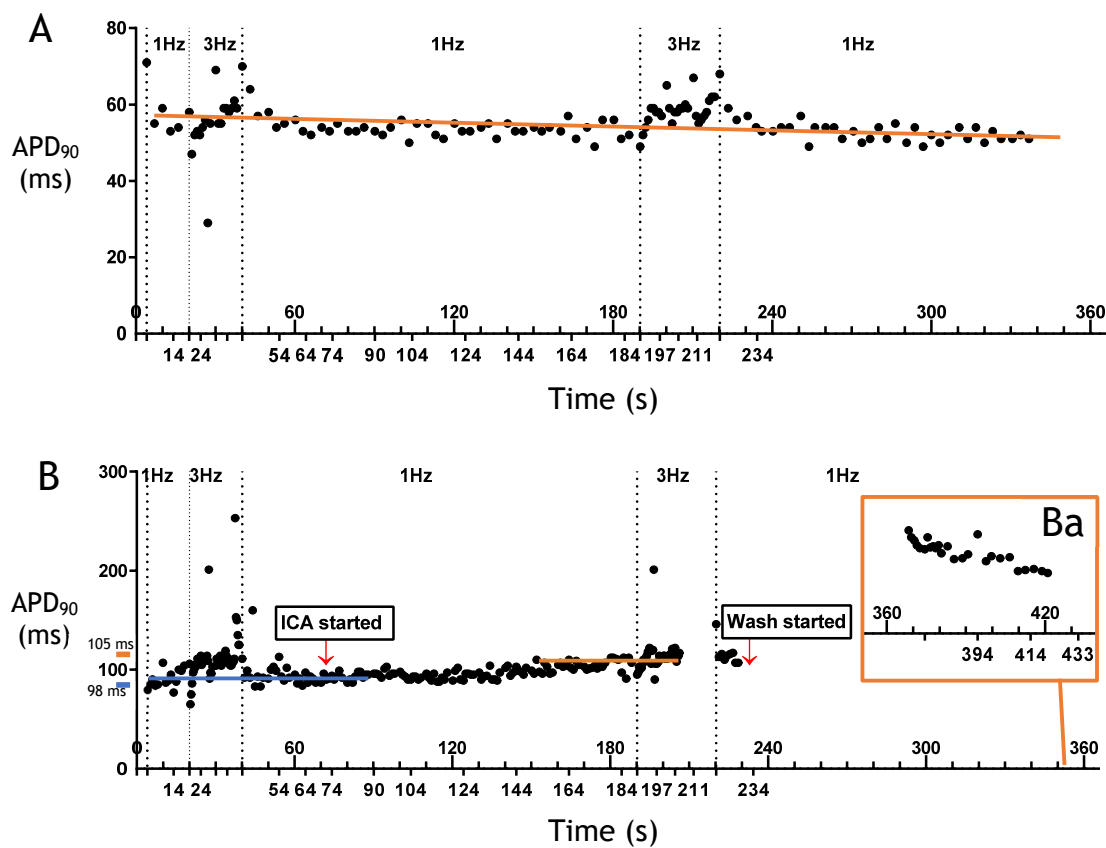
Figure 6.15 Representative APD$_{90}$ time-courses of APs recorded in two different rabbit left atrial myocytes.

A) Time-course of run-down of APD$_{90}$ recorded under control conditions (i.e. TMC). **B)** Time-course of APD$_{90}$ during control and 1 µM ICA present in the superfusate; APD$_{90}$ was analysed again at 370s for wash detection, but it was not included in the figure for sake of quality. Ba) Represents run-down during wash (control solution); cell died around 430s. Dotted lines divides the different stimulation periods at 1 or 3 Hz. Red arrows indicate the moment at which the different solutions (drug or control) started to flow. Lines represent the trend of the APD$_{90}$ during time.

For the following analysis, the ICA-sensitive component was estimated from the difference in APD as a result of the addition of ICA (1 μM). While the TMC was calculated as the difference in APD at the beginning of the recording and after 5 mins (300s) of recordings.

ICA-sensitive APD_{30} was -0.25 ± 0.2 ms (n=10 cells, n=4 rabbits) compared to -0.41 ± 0.1 ms (n=6 cells, n=3 rabbits) of TMC (mean ± s.e.m., unpaired data) as shown in Fig. 6.16. This was true also for APD_{70} (-4.8 ± 2.9 ms, n=10 cells, n=4 rabbits vs -1.8 ± 0.73 ms, n=6 cells, n=3 rabbits, mean ± s.e.m., unpaired data, Fig. 6.16) and APD_{90} (4.74 ± 5.7 ms, n=10 cells, n=4 rabbits vs 1.7 ± 1.8 ms, n=6 cells, n=3 rabbits, mean ± s.e.m., unpaired data, Fig. 6.16).

Moreover, the action potential depolarization characteristics were unaltered regardless of the presence of 1μM ICA in the superfusate. Neither the maximum diastolic potential (MDP) (control MDP -69 ± 5 mV vs -71 ± 5 mV following 1 μM ICA, n=10 cells, n=4 rabbits, mean ± s.e.m., paired data, Fig. 6.17) nor Vmax (control Vmax 365 ± 73 mV/s vs 363 ± 68 mV/s following 1 μM ICA, n=10 cells, n=4 rabbits, mean ± s.e.m., paired data, Fig. 6.17) were affected by the drug at the concentration of 1 μM.
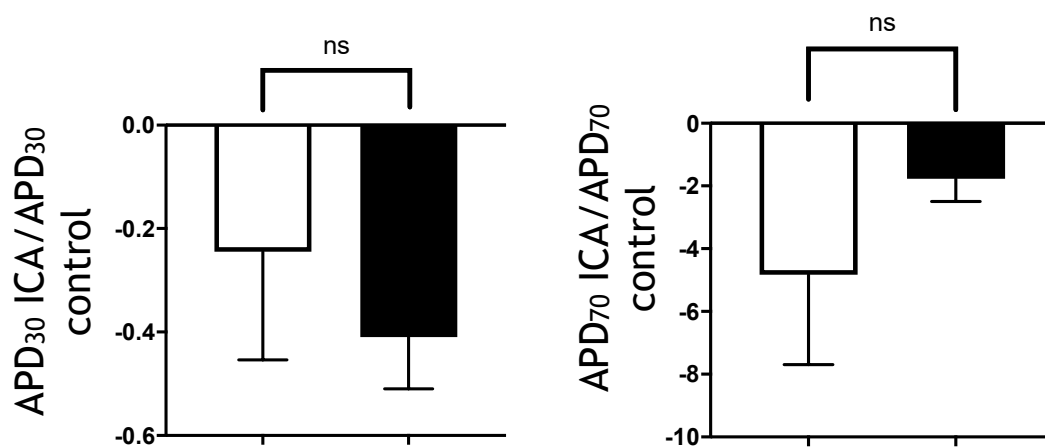
Figure 6.16 Comparison of the effect of 1 μM ICA on APD to the corresponding time matched control (TMC) in rabbit left atrial myocytes.

□=APD (ICA-sensitive component) (n= 10 cells, n=4 rabbits, paired data).

■ = TMC (n=6 cells, n=3 rabbits, paired data). Values are mean ± s.e.m.
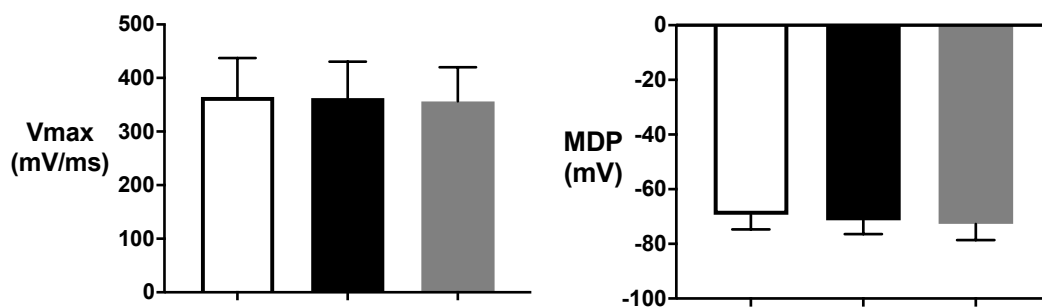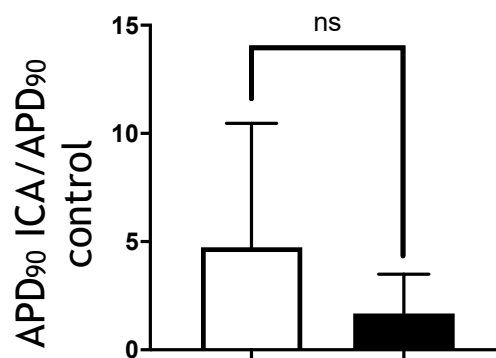
Figure 6.17 Lack of effect of acute superfusion with 1 μM ICA on maximum diastolic potential (MDP) and on maximum rate of depolarization (Vmax) of action potentials from rabbit left atrial isolated myocytes.

□ = control ■ = 1 μM ICA ▨= wash (n=10 cells, n=4 rabbits). Values are mean± s.e.m.

6.4.4 Rabbit atrial APs: effect of 10 µM ICA on action potential characteristics

Figure 6.18 shows a representative time-course of APD$_{90}$ recorded in a single myocytes from rabbit left atrium. The data plotted in the graph, shown in figure 6.18, are the result of the analysis of each action potential recorded over the course of that experiment. The representative time-course of APD$_{90}$ (Fig. 6.18) shows the typical time-course of the effect of 10µM ICA.
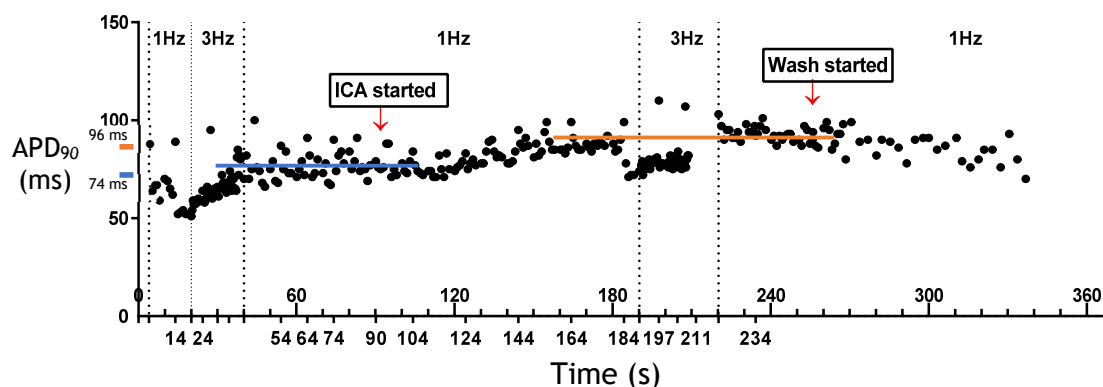
Figure 6.18 Representative APD$_{90}$ time-courses of APs recorded in rabbit left atrial myocytes.

Time-course of APD$_{90}$ during control and 10 µM ICA present in the superfusate. Dotted lines divides the different stimulation periods at 1 or 3 Hz. Red arrows indicate the moment at which the different solutions (drug or control) started to flow. Lines represent the trend of the APD$_{90}$ during time.

Below, typical original action potentials obtained with WinWCP software are shown for control, 10 µM ICA and wash in rabbit left atrial myocytes (Fig. 6.19).

The utilisation of a higher ICAGEN concentration, considered potentially non-selective for I$_{SK}$ (29), significantly prolonged the action potential duration in rabbit left atrial myocytes, when compared with relative TMC, while it did not affect either MDP or Vmax.
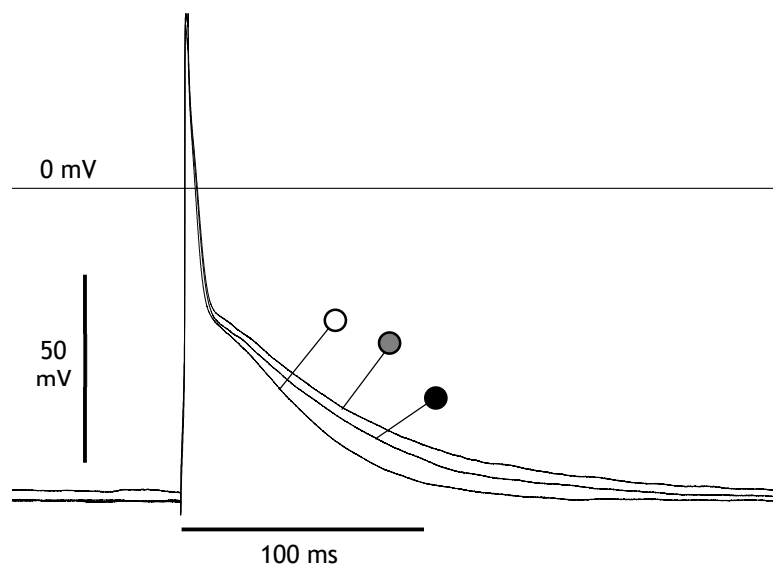
Figure 6.19 Representative action potential traces recorded from rabbit left atrial myocytes showing the effect of 10 µM ICA.
Superimposed action potential waveforms in absence of a drug (○), during superfusion with 10 µM ICA (◉) and after wash (●).

Under control condition APD_{70} and APD_{90} were 17.9 ± 5.6 ms and 89.4 ± 14.9 ms (n=7 cells, n=3 rabbits, mean ± s.e.m., paired data, Fig. 6.20) respectively, and following acute superfusion of rabbit left atrial myocytes with 10 µM ICA APD_{70} was observed to be 20.8 ± 5.9 ms, while APD_{90} was 111.7 ± 23.8 ms (n=7 cells, n=3 rabbits, mean ± s.e.m., paired data, Fig. 6.20). The MDP (control MDP 80 ± 1.2 mV vs 79 ± 1.6 mV post ICA, n=7 cells, n=3 rabbits, mean ± s.e.m., paired data, Fig. 6.21) and Vmax (control Vmax 538.6 ± 54.8 mV/s vs 452.4 ± 100 mV/s post ICA, n=7 cells, n=3 rabbits, mean ± s.e.m., paired data, Fig. 6.21) were not significantly affected by exposure to 10 µM ICA.

Although the values reported above describe APD prolongation occurring during superfusion with 10 µM ICA, the overall difference compared to control was not significant for either APD_{70} (n=7 cells, n=3 rabbits, paired data, p=0.06, Fig. 6.20) or APD_{90} (n=7 cells, n=3 rabbits, paired data, p=0.06, Fig. 6.20).
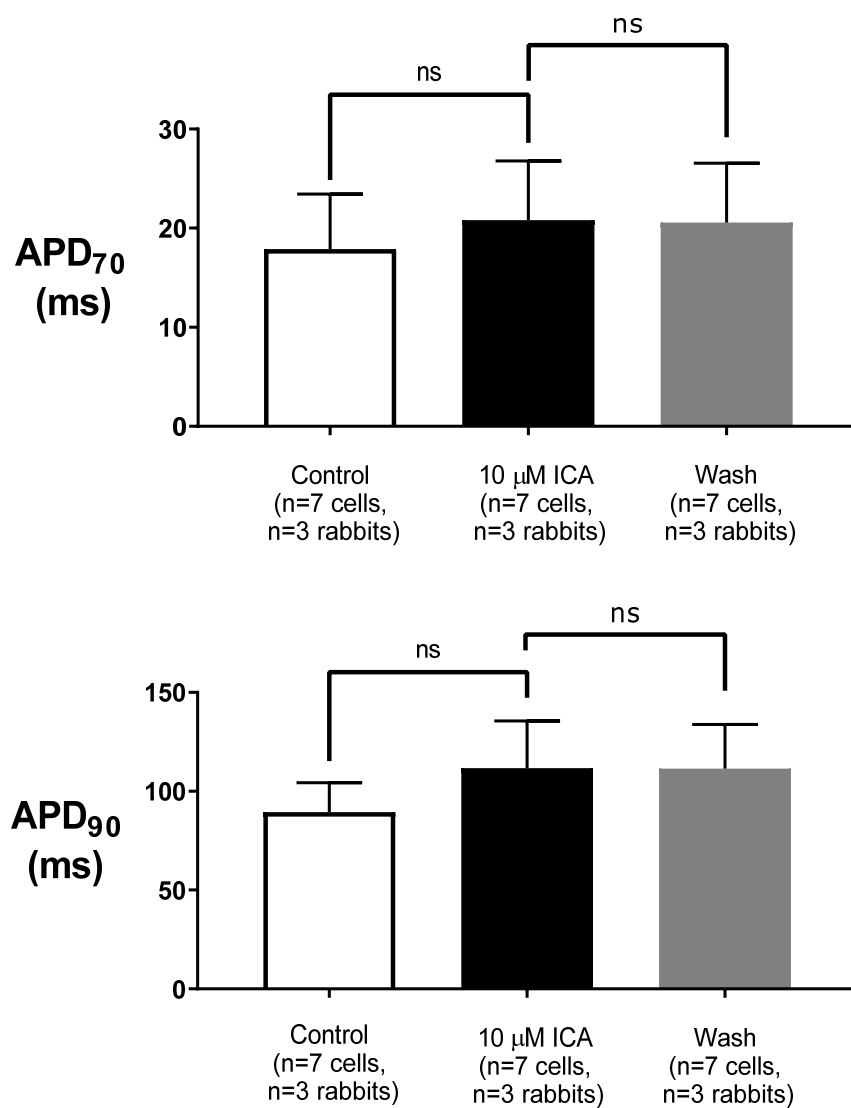
Figure 6.20 Lack of effect of acute superfusion with 10 µM ICA, vs paired control, on action potential repolarisation characteristics of rabbit left atrial isolated myocytes.

Lack of effect of 10 µM ICA on both APD_{70} (above) and APD_{90} (below).

☐ = control ■ = 10 µM ICA ▪ = wash (n=7 cells, n=3 rabbits). Values are mean± s.e.m.
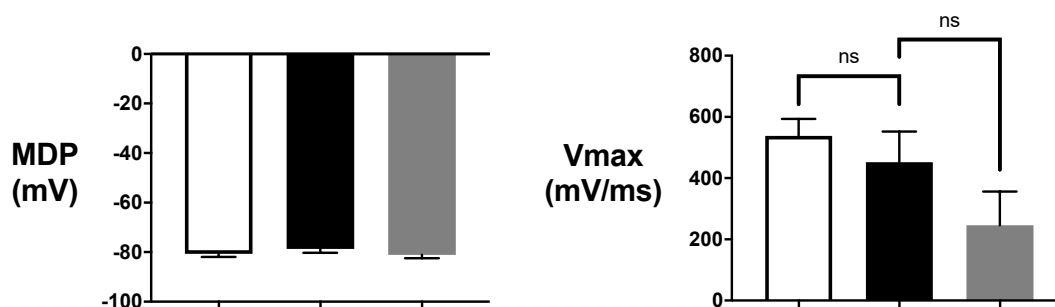
Figure 6.21 Lack of effect of acute superfusion with 10 µM ICA on maximum diastolic potential (MDP) and on maximum rate of depolarization (Vmax) of action potentials from rabbit left atrial isolated myocytes.

☐= control ■ = 10 µM ICA ☐ = wash (n=7 cells, n=3 cells). Values are mean± s.e.m.

Nevertheless, when the ICA-sensitive component was compared to the corresponding TMC a statistically significant prolongation at 70% and 90% of AP repolarization was observed. For the following analysis, the ICA-sensitive component was estimated from the difference in APD as a result of the addition of ICA (10 µM). While the TMC was calculated as the difference in APD at the beginning of the recording and after 5 mins (300s) of recordings.

APD_{70} of the ICA-sensitive component was 2.9 ± 1.2 ms (n=7 cells, n=3 rabbits, mean ± s.e.m., Fig. 6.22) compared to -1.8 ± 0.7 ms of TMC (n=6 cells, n=3 rabbits, mean ± s.e.m., unpaired data, p=0.01, Fig. 6.22). APD_{90} of the ICA-sensitive component was 22.3 ± 9 (n=7 cells, n=3 rabbits, mean ± s.e.m., Fig. 6.22) compared to -3.9 ± 2.1 ms of TMC (n=6 cells, n=3 rabbits, mean ± s.e.m., unpaired data, p=0.03, Fig. 6.22). MDP and Vmax were also analysed against the respective TMC, but no significant differences were observed (Fig. 6.23).
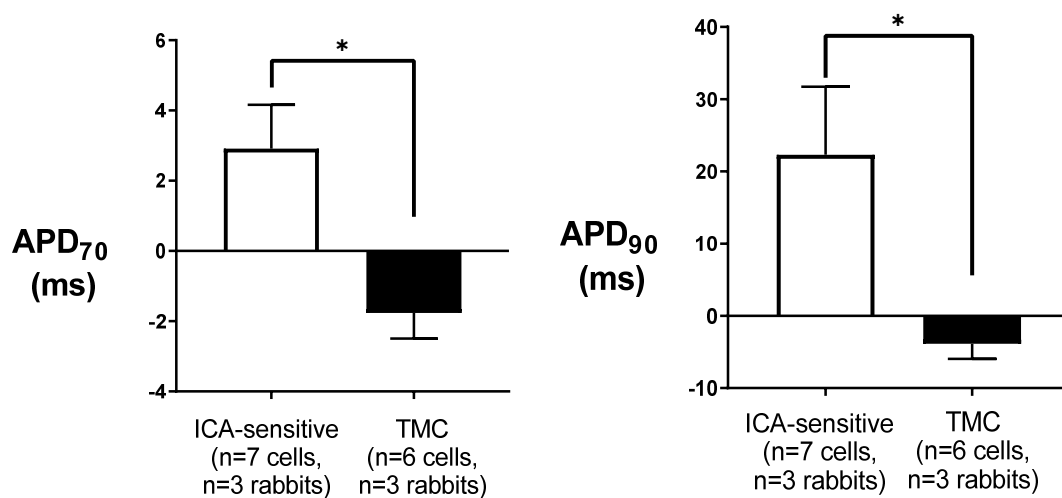
Figure 6.22 Comparison of the effect of 10 μM ICA on APD compared to the corresponding TMC in rabbit left atrial myocytes.

□ = ICA-sensitive component, ■ = TMC (n=6 cells, n=3 rabbits). Values are mean ± s.e.m. Values of p< 0.05 (*) were considered statistically significant.
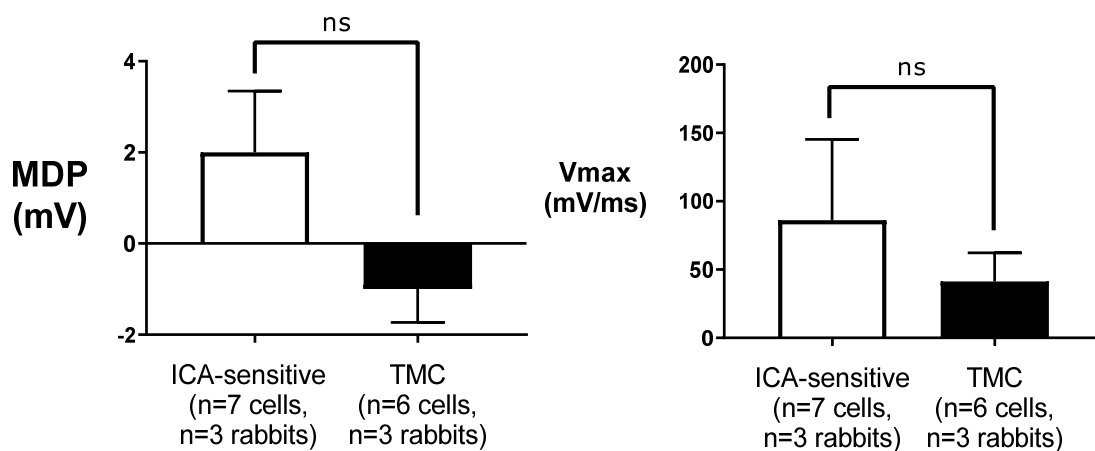
Figure 6.23 Comparison of the effect of 10 μM ICA on MDP and Vmax compared to the corresponding TMC in rabbit left atrial myocytes.

□ = ICA-sensitive component, ■ = TMC. Values are mean ± s.e.m.

6.4.5 Human atrial APs: lack of effect of 1µM ICA on action potential characteristics

Furthermore, the same action potential characteristics were analysed in human right atrial myocytes, but no significant effect of 1µM ICA was detected. Below, typical original action potentials obtained with WinWCP software are shown for control, 1 µM ICA and wash in human right atrial myocytes (Fig. 6.24).
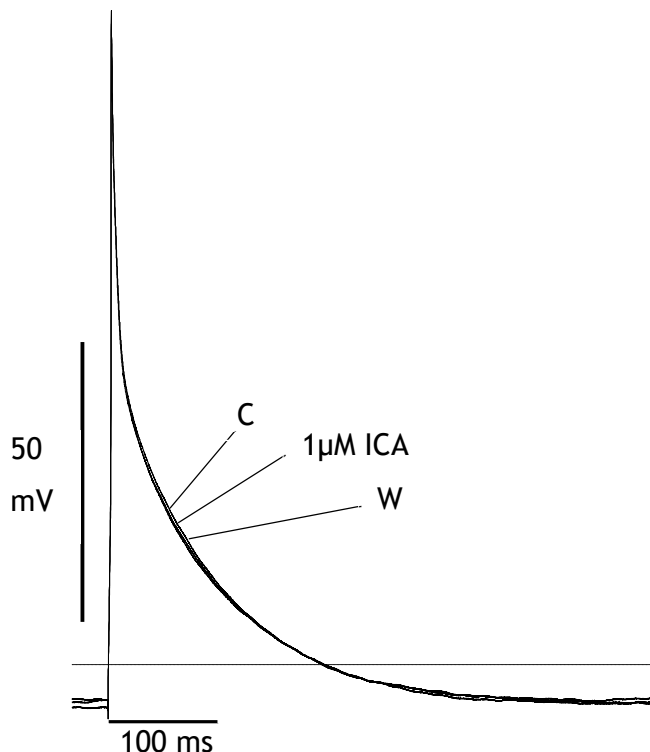
Figure 6.24 Representative action potential traces recorded from rabbit left atrial myocytes showing the effect of 1 µM ICA.
Superimposed action potential waveforms recorded during control (C), 1µM ICA and Wash (W).

Neither APD_{30} (6.9 ± 1.8 ms vs 7.2 ± 1.7 ms; n=9 cells, n=4 patients, mean ± s.e.m., paired data, p=0.74, Fig. 6.25) nor APD_{70} (66.7 ± 12.4 ms vs 62.7 ± 12.8 ms; n=9 cells, n=4 patients, mean ± s.e.m., paired data, p=0.45, Fig. 6.25) nor APD_{90} (183.6 ± 31.9 ms vs 170 ± 29 ms; n=9 cells, n=4 patients, mean ± s.e.m., paired data, p=0.23, Fig. 6.25) were affected by the acute administration of 1µM ICA. Additionally, the MDP under control conditions was -77 ± 1.3 mV as compared to 79.7 ± 2.1 mV during exposure to ICA, showing no statistically

significant difference (n=9 cells, n=4 patients, mean ± s.e.m., paired data, Fig. 6.26). Finally, also Vmax was unaltered following the superfusion with 1μM ICA (control Vmax 282 ± 35 mV/s vs 305 ± 36 mV/s following 1 μM ICA, n=9 cells, n=4 patients, mean ± s.e.m., paired data, Fig. 6.26). Wash traces were analysed for MDP and Vmax of both rabbit and human APs showing the stability and robustness of the experimental protocol over time for all sets of experiments.
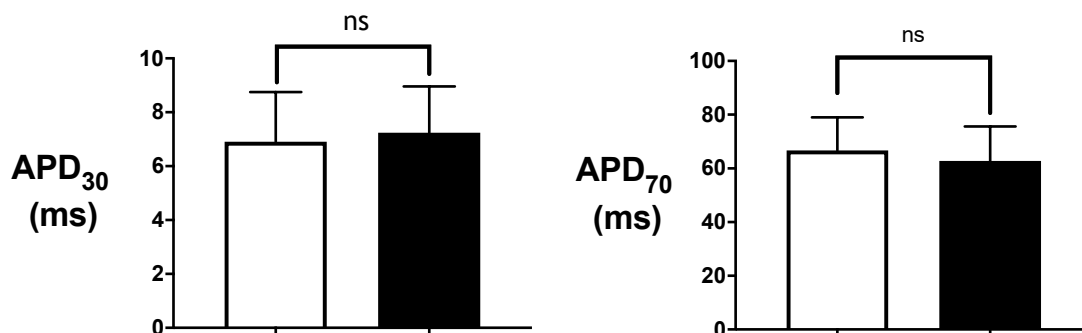
Figure 6.25 Lack of effect of acute superfusion with 1 μM ICA, vs paired control, on action potential repolarisation characteristics of human right atrial isolated myocytes.

□ = control   ■ = 1 μM ICA (n=9 cells, n=4 patients). Values are mean± s.e.m.
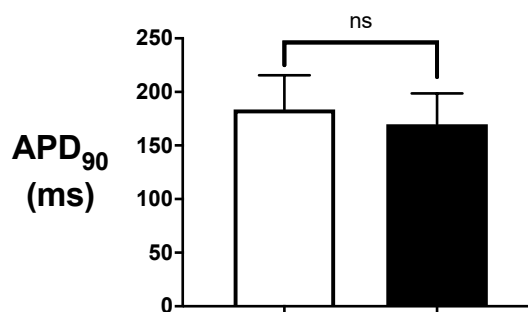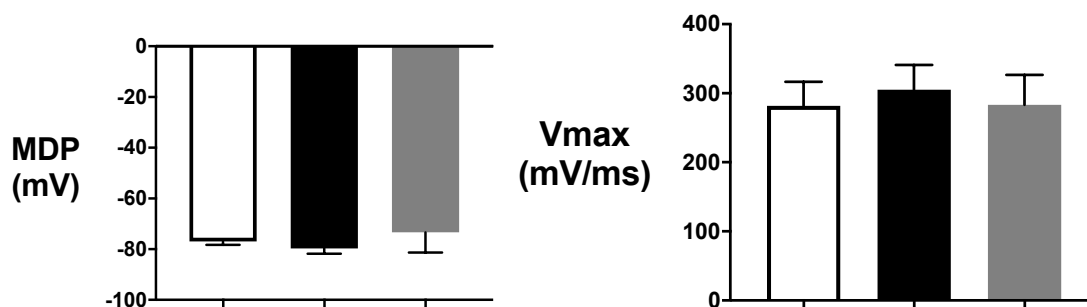
Figure 6.26 Lack of effect of acute superfusion with 1 µM ICA on maximum diastolic potential (MDP) and on maximum rate of depolarization (Vmax) of action potentials from human right atrial isolated myocytes.

□ = control ■ = 1 µM ICA □ = wash (n=10 cells, n=4 patients). Values are mean± s.e.m.

The ICA-sensitive component was compared to the corresponding TMC run-down, but no statistical prolongation at 30%, 70% and 90% of AP repolarization was observed (Fig. 6.27). APD_{30} of the ICA-sensitive component was 0.33 ± 0.1 ms (n=9 cells, n=4 patients, mean ± s.e.m., Fig. 6.27) compared to -0.8 ± 0.2 ms of TMC (n=4 cells, n=2 patients, mean ± s.e.m., unpaired data, p=0.48, Fig. 6.27). APD_{70} of the ICA-sensitive component was -3.8 ± 2.7 ms (n=9 cells, n=4 patients, mean ± s.e.m., Fig. 6.27) compared to -6.0 ± 1.9 ms of TMC (n=4 cells, n=2 patients, mean ± s.e.m., unpaired data, p=0.78, Fig. 6.27). Finally, the APD_{90} of the ICA-sensitive component was -16.9 ± 5.7 ms (n=9 cells, n=4 patients, mean ± s.e.m., Fig. 6.27) compared to -16.0 ± 5.9 ms of TMC (n=4 cells, n=2 patients, mean ± s.e.m., unpaired data, p=0.94, Fig. 6.27).
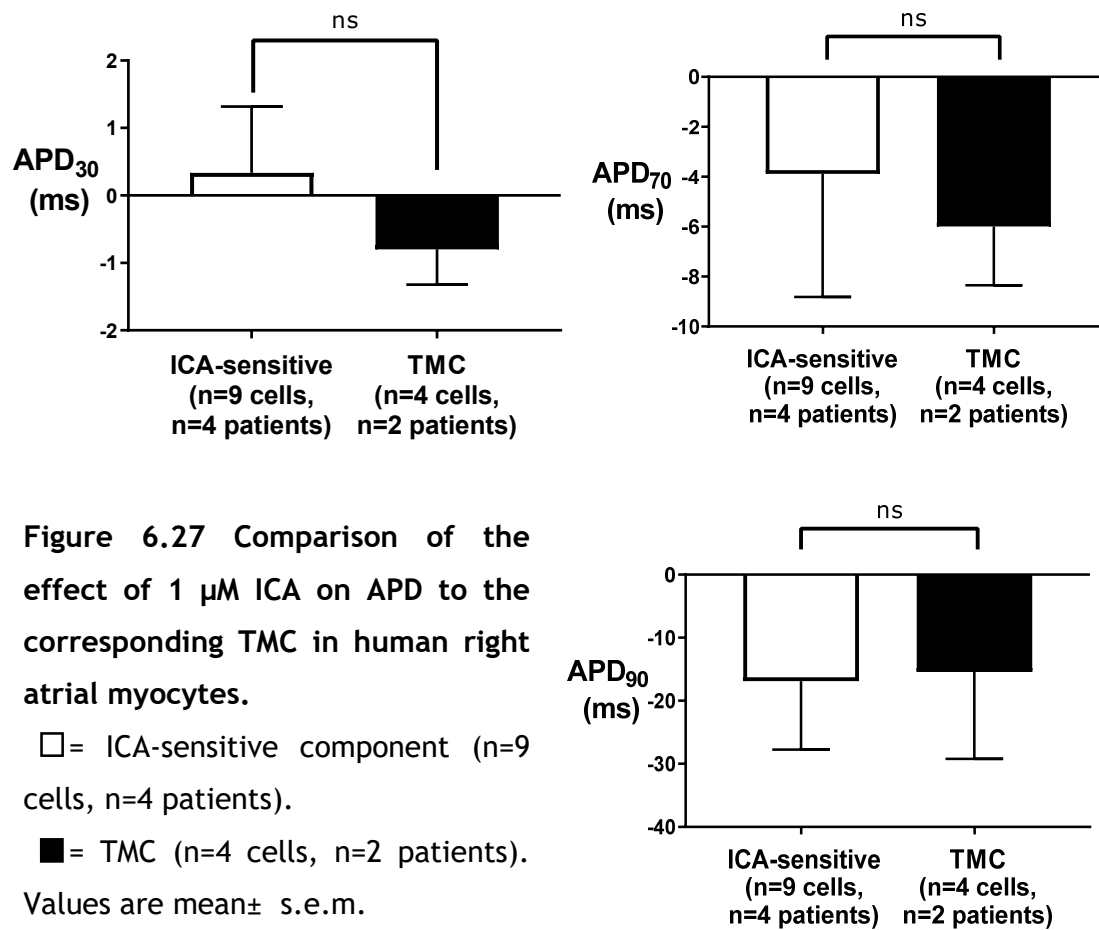
Figure 6.27 Comparison of the effect of 1 µM ICA on APD to the corresponding TMC in human right atrial myocytes.

□= ICA-sensitive component (n=9 cells, n=4 patients).

■= TMC (n=4 cells, n=2 patients). Values are mean± s.e.m.

6.4.6 Fast rate stimulation of human atrial cells: lack of effect of 1 µM ICA on action potentials

6.4.6.1 ICA (1 µM) on APs at 2Hz stimulation frequency

The experiments outlined in the following paragraphs aimed to test ICAGEN on action potentials stimulated at 2 or 3 Hz (bursts of 80-110 s) in order to increase systolic $[Ca^{2+}]_i$ and thus potentially enhance I_{SK}, in human right atrial myocytes. However, acute administration of 1 µM ICA, even under this conditions, failed to alter the APD at any level of repolarization. Under control condition, at 2 Hz stimulation frequency, APD_{30} was 9.3 ± 1.8 ms and APD_{70} was 70.4 ± 9.4 ms compared to 9 ± 1.7 and 64.7 ± 9.6 ms, respectively, following acute administration of ICA (n=10 cells, 3 patients, paired data, mean $\pm$ s.e.m. Fig. 6.28). Also, the APD_{90} was not significantly different under control conditions compared to during superfusion with 1 µM ICA (165.8 ± 18 ms vs 147.7 ± 18.4 ms, n=10 cells, 3 patients, paired data, mean $\pm$ s.e.m. Fig. 6.28). However, MDP was observed to be similar under control conditions (-78.9 ± 1.9 mV) compared to during superfusion with 1 µM ICA (-80.9 ± 2, n=10 cells, 3 patients, paired data, mean $\pm$ s.e.m. Fig. 6.29) and Vmax was not affected by the drug (control Vmax 218.2 ± 37.7 mV/s vs 277.5 ± 63.7 following ICA, n=10 cells, 3 patients, paired data, mean $\pm$ s.e.m. Fig. 6.29). The MDP (Control/ICA -2 ± 0.9 mV, n=10 cells, n=3 patients) and Vmax (Control/ICA 59.2 ± 30.6 mV/s, n=10 cells, n=3 patients) were compared to the respective TMC (TMC_{MDP} 0.5 ± 1 mV and TMC_{Vmax} 10.8 ± 27.4 mV/s, n=6 cells, 3 patients, unpaired data, mean $\pm$ s.e.m.), but no significant differences were observed (Fig. 6.30). Furthermore, APD parameters were compared to the relative TMC, only for 2 Hz stimulation frequency. However, neither ICA-sensitive APD_{70} (-5.7 ± 7.5 ms, n=10 cells, n=3 patients) nor ICA-sensitive APD_{90} (-18.1 ± 15.3 ms n=10 cells, n=3 patients) components were significantly different compared to the corresponding TMC (-9.2 ± 3.4 ms, n=6 cells, 3 patients, unpaired data, mean $\pm$ s.e.m. Fig. 6.30).
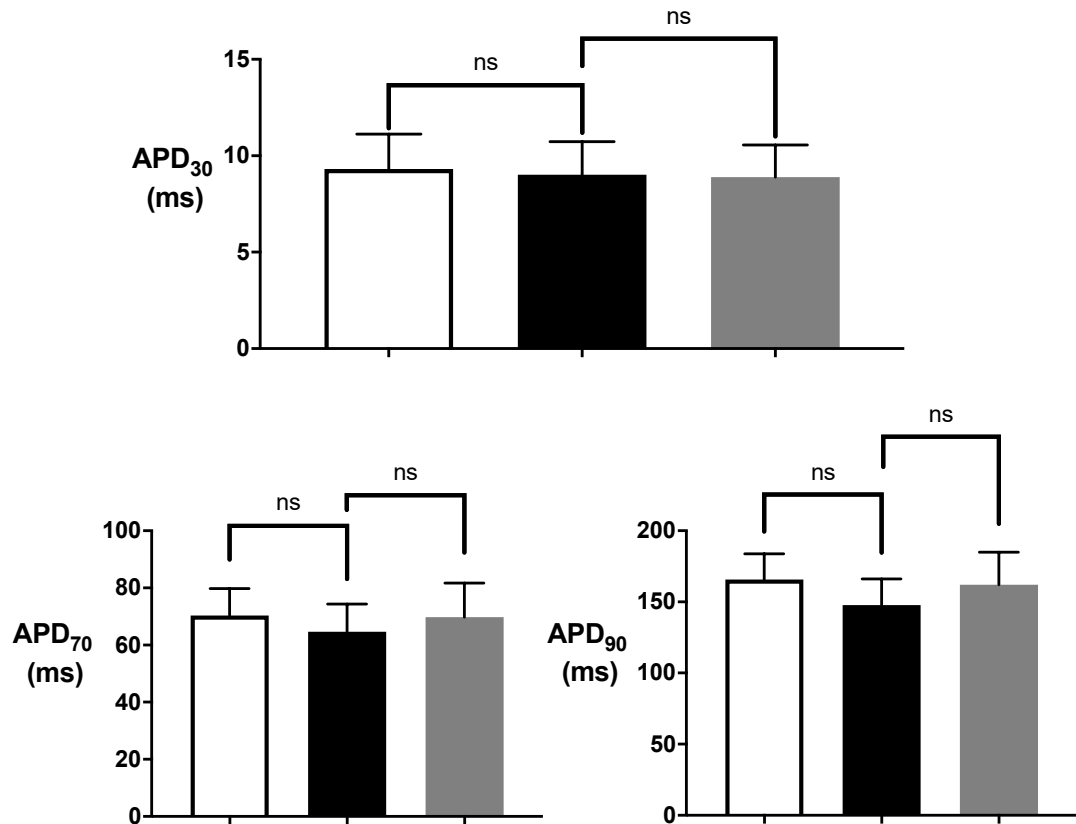
Figure 6.28 Lack of effect of acute superfusion with 1 μM ICA on action potential repolarisation characteristics of human right atrial isolated myocytes at stimulation frequency of 2 Hz.

□ = control   ■ = 1 μM ICA   ▨ = wash (n=10 cells, n=3 patients). Values are mean ± s.e.m.
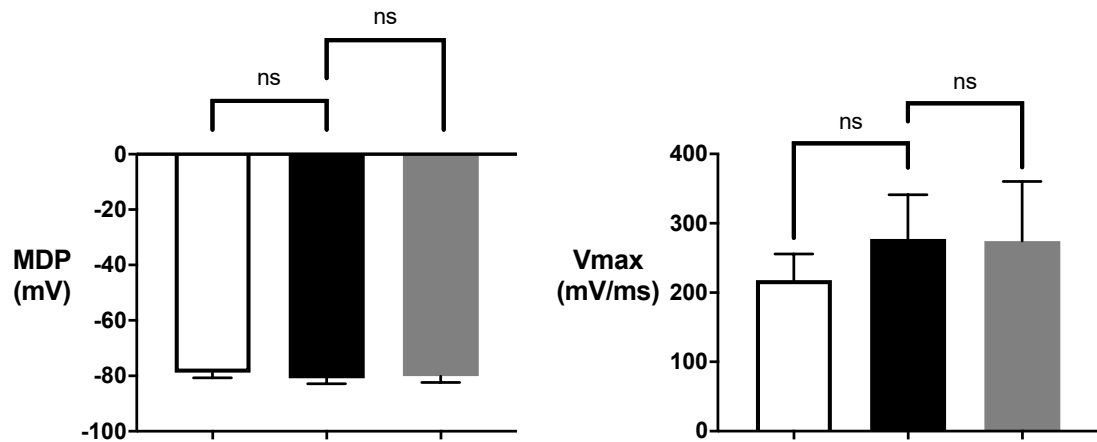
Figure 6.29 Lack of effect of acute superfusion with 1 μM ICA on maximum diastolic potential (MDP) and on maximum rate of depolarization (Vmax) of action potentials from human right atrial isolated myocytes at stimulation frequency of 2 Hz.

□ = control ■ = 1 μM ICA ▨ = wash (n=10 cells, n=3 patients). Values are mean ± s.e.m.
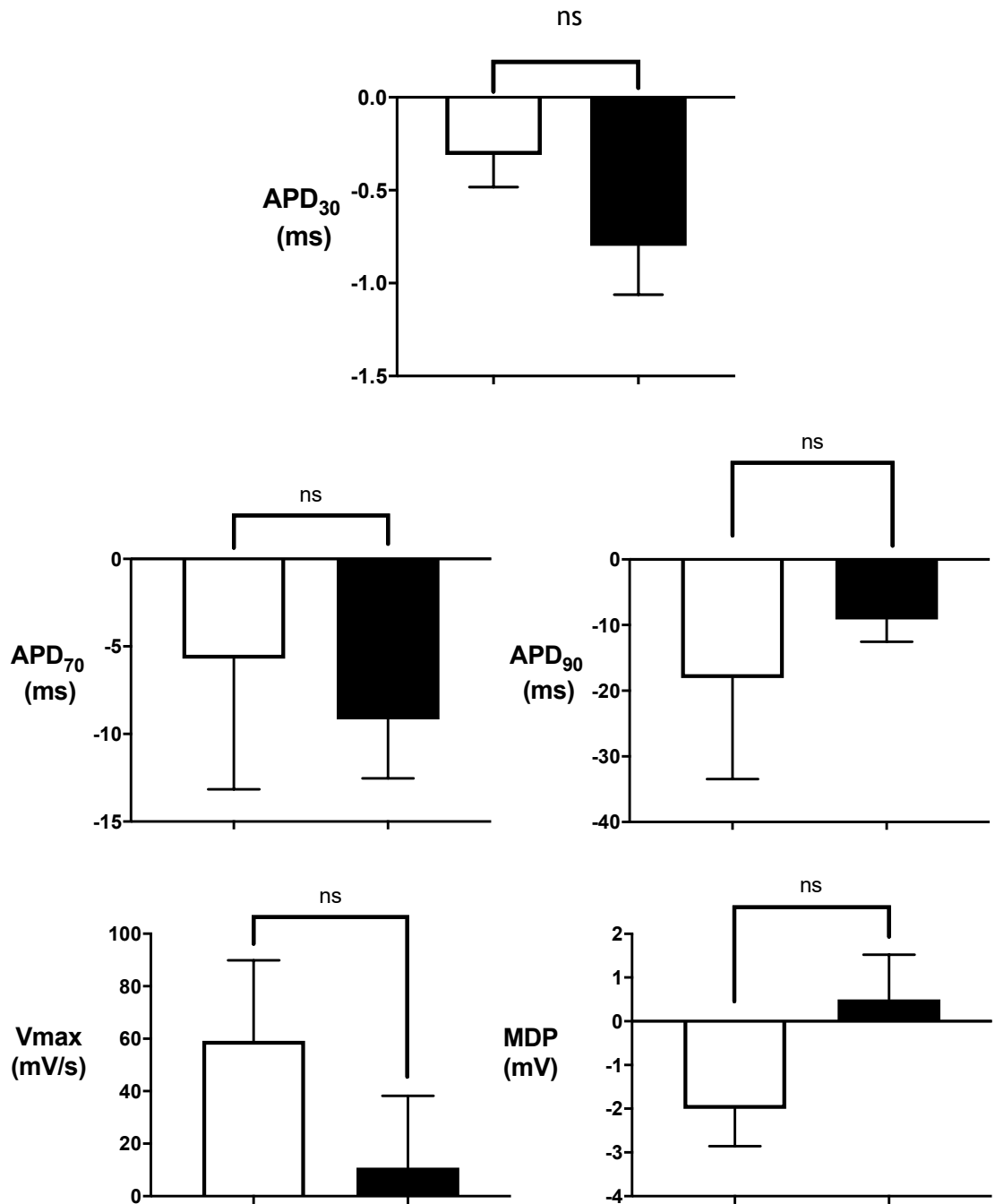
Figure 6.30 Comparison of the effect of 1 μM ICA on APD, MDP and Vmax to the corresponding TMC in human right atrial myocytes (2 Hz).

□ = ICA-sensitive component (n=10 cells, n=3 patients).

■ = TMC (n=6 cells, n=3 patients). Values are mean ± s.e.m.

6.4.6.2 ICA (1 µM) on APs at 3Hz stimulation frequency

Acute administration of 1 µM ICA failed to affect action potential morphology, at any percentage of repolarization studied, even at pacing frequency of 3 Hz in human right atrial myocytes. Under control conditions, neither APD_{30} (control APD_{30} 22.5 ± 4.9 ms vs 21.6 ± 4.9 ms following 1µM ICA; n=7 cells, n=3 patients, paired data, mean ± s.e.m.) nor APD_{70} (control 75.5 ± 15 ms vs 70.4 ± 13.4 ms post 1 µM ICA; n=7 cells, n=3 patients, paired data, mean ± s.e.m.) nor APD_{90} (control 144.7 ± 21.9 vs 135.7 vs 19.8 post 1 µM ICA, n=7 cells, n=3 patients, paired data, mean ± s.e.m.) were significantly affected by ICA (Fig. 28). Also, 1 µM ICA failed to alter both the resting membrane potential
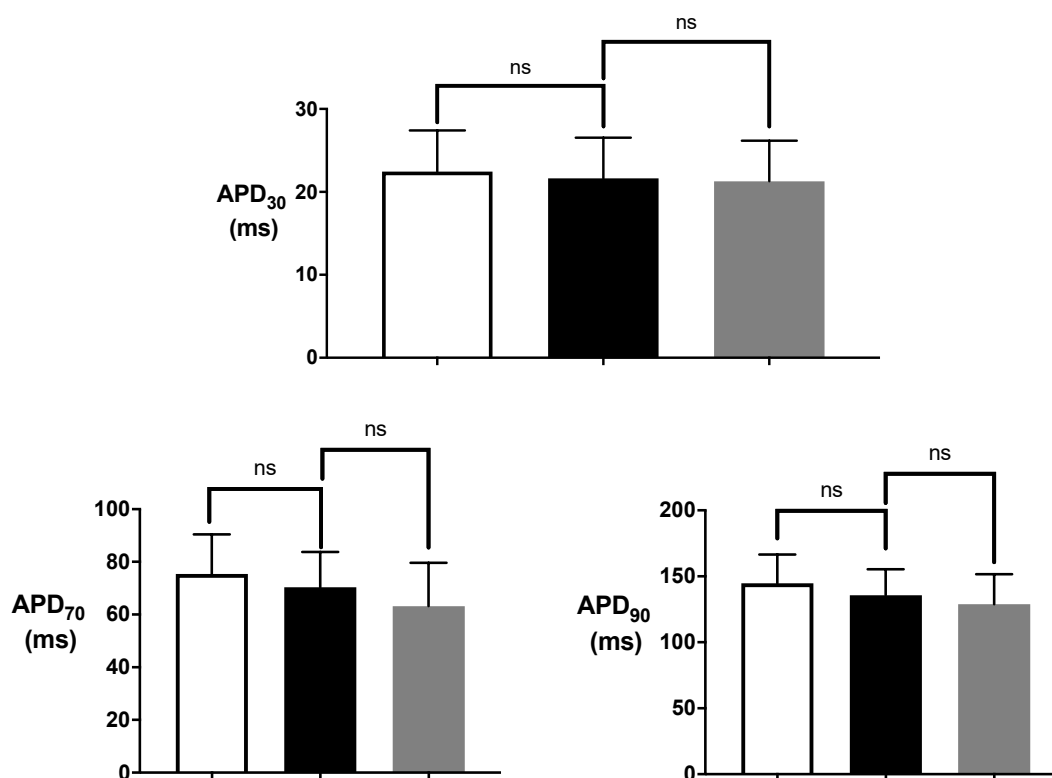
Figure 6.31 Lack of effect of acute superfusion with 1 µM ICA on action potential repolarisation characteristics of human right atrial isolated myocytes at stimulation frequency of 3 Hz.

☐ = control ■ = 1 µM ICA ▨ = wash (n=7 cells, n=3 patients). Values are mean ± s.e.m.

and the maximal rate of depolarization. Neither MDP (control -75.2 ± 3 mV vs -68.5 ± 8.5 mV post ICA, n=7 cells, n=3 patients) nor Vmax (control 204.6 ± 30 mV/s vs 226.5 ± 37 mV/s post ICA, n=7 cells, n=3 patients) was significantly different compared to during superfusion with 1 µM ICA at 3 Hz (Fig. 6.29).
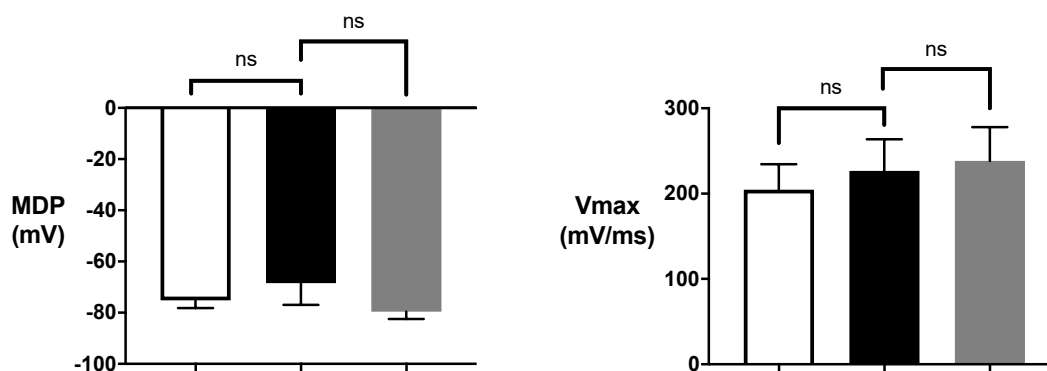
Figure 6.32 Lack of effect of acute superfusion with 1 µM ICA on maximum diastolic potential (MDP) and on maximum rate of depolarization (Vmax) of human right atrial isolated myocytes at stimulation frequency of 3 Hz.

□ = control ■ = 1 µM ICA ▨ = wash (n=7 cells, n=3 patients). Values are mean ± s.e.m.

6.5 Discussion

6.5.1 The validation of action potential recordings through a predictable pharmacological response

As a positive control for the subsequent ICA experiments, 2mM 4-aminopyridine was able to significantly prolong the APD at 30, 50 and 70% of repolarization and action potential amplitude (APA) in rabbit left atrial myocytes. The prolongation of the repolarization and the suppression of the phase 1 of the action potentials is attributed to the block of the transient (I_{TO}) and sustained (I_{KSUS}) outward potassium currents by 2 mM 4-AP (79). However, although 4-AP is considered the best currently available I_{TO} blocker, it is not completely selective at this concentration. In fact, previous studies proved the existence of two functionally distinct outward K^+ currents both sensitive to 4-AP (1-5 mM) (371).

Considering these caveats, the results reported are in accordance with previous findings about 4-AP inhibition, however, some discrepancies must be acknowledged. Surprisingly, 4-AP significantly increased the APA (albeit only moderately) while the MDP was unaltered, which is in contrast with previous findings (79, 372), and the reason behind it is not clear. In addition, the acute superfusion with 2 mM 4-AP did not significantly affect the late phase of repolarization (APD_{90}) in rabbit atria action potentials, which however can be explained as a consequence of the main influence of I_{TO} during the plateau and after the end of phase 1 (i.e. at around APD_{50-60}) (58). To be considered, I_{TO} presents interspecies variations in the rate dependence, which entail a different reactivation time-course between human and rabbit, causing this current to be strongly reduced at high rates (1-4 Hz) in the latter species (373). To conclude, validation of correct and stable drug effect recordings on action potential was performed successfully, demonstrating capability to proceed with I_{SK} studies.

6.5.2 Does ICAGEN represent a more reliable tool compared to apamin in the study of SK channels role on action potential?

The two SK blockers (ICA and apamin) utilised in this thesis, share a similar SK pore blocking mechanism (183), but apamin is considered a key tool and has been the most widely used in the investigation of SK channel function due to its high selectivity (179, 183). However, for unclear reasons this neurotoxin has been found to have low efficacy, especially in cardiac tissue (171, 353). Previous studies proposed the presence of apamin-insensitive heteromeric SK channels (366), confirmed by a more recent study showing negligible-if any- effect of the peptide on APs (365). Moreover, Nagy et. al in 2009 reported failure to alter APD under physiological conditions by apamin (100 nM), questioning the importance of SK channels in cardiac tissues and the efficacy of the toxin (203).

In contrast, ICA has been demonstrated to terminate AF both *in vivo* and *ex vivo* (29, 196, 197, 374). The ICA measured IC_{50} for SK channels has been reported to be 300/500 nM, which supports the rationale for employing a concentration of 1 μM, as used by previous studies (29, 196), in order to obtain a substantial block of these channels without compromising specificity. However, although the compound significantly prolonged action potential duration at 1 μM on human single cells (from sinus rhythm patients) in a previous study (29) it also showed an inhibitory effect, albeit minor, on I_{TO} (IC_{50} = 21 μM) and I_{K1} (IC_{50} >100 μM). Moreover, ICA showed indirect sodium channel inhibition due to a depolarization of the RMP by direct block of SK channels (29, 197). Nevertheless, in the experiment outlined in this chapter, 1 μM ICA showed no effect at any level on AP morphology in both rabbit and human atrial myocytes even when compared to TMCs. In contrast with previous results obtained by Skibsbye et al., which showed an effect of both 1 μM (significant only against TMCs) or 10 μM ICA on current (in voltage clamp experiments) and on APD_{90} (only with 1 μM ICA) in single human atrial myocytes from patients in sinus rhythm, while recordings from AF patients showed no effect of ICA at any concentration used (1 or 10 μM) on either current or APs (29). The pacing frequency used (0.5 Hz) and the free Ca^{2+} in the pipette (35 nM) differ from those used in my experiments on action potential and are far from being physiological. In addition, a recent publication suggests that, compared with other cardiac repolarizing currents, SK current

block is more effective at higher frequencies (366), which suggest that at the frequency used (1 Hz) in my experiments ICA effect on APs should have been even more prominent. Also, the magnitude of APD prolongation (~15%, compared to TMC) showed by Skibsbye et al., with 1 µM ICA in single human atrial cells (from sinus rhythm) stimulated at 0.5 Hz are higher than the one obtained in multicellular human atrial preparations at the same frequency with 10 times that drug concentration (13%, compared to TMC) (29). These data, combined with the use of high EGTA concentration (5 mM) which has been reported to prevent the detection of any Ca_i dependent current by previous studies (201, 375), cast doubts on the physiological relevance of the results and the selectivity of ICA. On the other hand, in the present study low EGTA (0.1 mM) concentrations were used, allowing free intracellular Ca^{2+} to rise physiologically during the AP stimulation. Nevertheless, no effect of the ICA compound at 1 µM was seen at any percentage of repolarization, confirming that I_{SK} plays no role in both rabbit and human cardiac repolarization, under physiological conditions. Therefore, it appears that the experimental conditions used in the present study are more physiologically relevant compared to those tested by Skibsbye et al., which to my knowledge is the only study showing an effect of ICA in single human atrial cells.

Nevertheless, at a concentrations of 10 µM, ICA provoked significant APD_{70-90} prolongation when compared with respective TMCs in my experiments. However, based on previous IC_{50} data, an unselective action of the compound at this high concentration cannot be ruled out. In fact, minor inhibitory effects on both I_{TO} and I_{K1} by ICA, as mentioned earlier, have been reported (29). Moreover, even though no effect of the compound at high concentrations was described on any other ion channels tested (29), it cannot be excluded that the results obtained with 10 µM ICA in the present study could depend on the block of other current rather than I_{SK}. For example, given the low IC_{50} for I_{TO} a possible block of this current by 10 µM ICA could lead to APD_{70} prolongation, as demonstrated by the positive control shown in section 6.4.2, or it could explain the late repolarization (APD_{90}) prolongation (79), which however was not observed in the positive control.

Interestingly, Skibsbye et al. also report a significant depolarization of the RMP at 1 Hz following 10 μM ICA administration, as well as significant decreased APA and Vmax (29). The reduction in upstroke velocity and amplitude was explained later by indirect I_{Na} inhibition trough accumulation of state-dependently inactivated channels, due to depolarization of the RMP (197). However, in the present study no effect was observed on either RMP or Vmax, demonstrating for the first time that under physiological conditions, high concentrations of ICA prolong late AP repolarization with no undirect effect on sodium currents.

6.5.3 1 μM ICA showed no effect on APs even at increased pacing frequency

The expression of SK channels has been hypothesised to strongly depend on the duration of AF and the consequent atrial remodelling (29, 211). On the other hand, previous studies reported increased apamin-sensitive current following enhanced trafficking of SK2 channels to the cardiomyocyte membrane leading to APD abbreviation as a response to intermittent burst pacing at the pulmonary vein region, possibly providing the basis for an arrhythmogenic substrate (201). The same group showed also that early stages of the remodelling process (within hours) depends on the site of ectopic activity, being effective in PV and coronary sinus (CS) but not in other regions. Furthermore, the burst pacing-induced APD shortening was found to be calcium-dependent and prevented by apamin (376). Additional evidence was given by Li, et al. in 2009 using SK2 knock-out mouse model, in which they reported prolongation of the atrial APD, which however, was hypothesised to be involved in the generation of atrial arrhythmias through different mechanisms, such as EAD (200). However, questions remain regarding the possibility of APD and ERP prolongation promoting inducibility of re-entry arrhythmias (377). All together, these studies suggest a crucial role played by SK channels in recent-onset AF and the importance of Ca^{2+} overload in early remodelling which could provoke the augmentation of I_{SK} (84). To test these hypothesis, myocytes isolated from human right atria were stimulated at 2 or 3 Hz in order to increase the $[Ca^{2+}]_i$. In fact, during action potentials $[Ca^{2+}]_i$ increases for short periods of time and at spatially restricted "Ca^{2+}signalling domains" known as nano/microdomains. The Ca^{2+} entry through Ca^{2+}-permeable channels is confined in this small spaces by the combination of different Ca^{2+}

buffer systems that limit its diffusion (378). L-Type channels, which plays the major role in generating this Ca^{2+} gradient, have demonstrated to be functionally coupled with SK channels. However, the rapid, high-affinity Ca^{2+} buffer BAPTA has been shown to reduce the coupling between these two channels (172). Since BAPTA was used in my previous voltage clamp experiments with apamin and ICA, which showed no effect on current, a correlation with the buffer and the absence of effect could not be excluded. Nevertheless, with unbuffered Ca^{2+} ions flowing during rapid (2-3 Hz) pacing frequency in human right atrial myocytes APs, neither repolarization nor MDP or Vmax were observed to be affected by the acute administration of 1 µM ICA. Although wash steps were performed, the data were also compared against corresponding TMCs (for 2 Hz) which, however, did not show any difference, contrary to previous published results by Skibsbye et al., who showed significant APD_{90} prolongation by ICA (1 µM) in single cells from sinus rhythm right atrial tissue (29). However, this study was performed at 0.5 Hz, which is a 4x slower pacing frequency compared to the one used in my experiments, and unphysiological free Ca^{2+} (35 nM) in the pipette solution. Moreover, clearly in contrast with the data herein presented, another study reported a greater percentage of APD_{90} prolongation following inhibition of I_{SK} at 2Hz when compared with 0.2 Hz, demonstrating a relatively larger contribution of I_{SK} at higher pacing frequencies (366). Nevertheless, a putative more potent blocker (UCL1684) compared to ICA and unphysiological temperature were used.

The present findings, therefore, obviously challenge previous publications and strongly suggest that I_{SK}, at physiological temperature and ion concentration, plays no role in the frequency-dependent modulation of APD, in single human atrial cells, even at supraphysiological rates of stimulation (up to 180 beats/min), which would have been expected to augment the current by elevation of $[Ca^{2+}]_i$ (31).

6.5.4 Potential limitations

The "chunk" method used for cell isolation in human atrial appendage could, in theory, disrupt ion currents. In support, in dog atrial cells, the "chunk" method reduced significantly the size of the delayed rectifier K^+ current (I_K) and the percentage of cells in which this current was detected in canine atria compared to the perfusion method (364). However, no differences of 1 µM ICA

effect on AP morphology were observed between human and rabbit (cell isolated by perfusion method), thus excluding a possible implication of different isolation method on the absence of effect of the drug. The effect of 10 μM ICA was not reversed by re-application of the control solution (wash), instead the TMCs were used to demonstrate the efficacy of the drug to fight run-down and the stability of the recordings. Importantly, throughout the present study action potentials were measured with standard whole-cell current clamp. This technique, also known as ruptured patch clamp configuration, presents some limitations (as previously mentioned, see section 5.5.3). These include potentially removing important intracellular substances, such as nucleotides or Ca^{2+} which regulate ion channels, particularly potassium channels (362) and this could have compromised the I_{SK} signalling. However, no published data are present in the literature regarding this possibility. Moreover, although perforated patch clamp configuration can prevent channel "run down" by avoiding the dialysis and maintain the integrity of many cytoplasmic components, it is more difficult than the standard method and potentially is not necessary. In fact, previous studies have reported the presence of I_{SK} in single cells from human and rabbit atrial tissue using standard (ruptured) whole-cell patch clamp configuration (29, 201, 211) or showed an absence of this current using both techniques (203).

During AF, the rapid and irregular activation of the muscular atrium wall in humans typically reaches 400–600 beats per minute (bpm) (14, 379). However, the highest frequency achieved during short bursts (1-2 minutes) used within the present study in human single atrial cells was 3 Hz (~180 bpm), which apparently is not sufficient to cause the pathological $[Ca^{2+}]_i$-elevation reputed to be necessary for I_{SK} activation. This is partially in contrast with previous findings in single mouse atrial cell APs measurements, which showed improved sensitivity to SK block at higher frequency (2 Hz) (366). Higher frequency (4 Hz) was tested only in one single human atrial myocyte, but the results were inconclusive given the difficulties in obtaining stable recordings and finally a decent sample size. Although a previous study in single human atrial myocytes showed that stimulations up to 600 bpm are achievable with current clamp technique (79), the focus of the present work was directed to obtain conclusive results (i.e. with proper sample sizes) at 2 and 3 Hz, which demonstrated that even with manipulation expected to increase $[Ca^{2+}]_i$, I_{SK} is still not detectable.

6.5.4.1 Limitation for the use of a holding current

The enzymatic isolation of human myocytes from atrial appendage tissue is recognized to depolarize the cell resting potential (Vm) (380, 381). Therefore, I current-clamped Vm to overcome this and prevent I_{Na} inactivation. The application of a holding current (also known as hyper-current) may be expected to exert a shortening influence on the APD. Instead of the characteristic spike and dome morphology, a more triangular shape with shorter APD was observed (fig. 6.12). The duration of the APs has been compared with the literature. The average APD_{90} reported in this chapter and recorded during my experiments in human cells (from SR patients) at 1Hz was 183.6 ± 31.9 ms, which, compared to the literature values of APD_{90} for cells from patients in SR, results 80-100ms shorter (29, 146).

However, the application of a holding current is an established and validated method, with accepted limitations (380, 381). The effect of the holding current, would be to shorten the action potential duration, because, while it helps retain the hyperpolarized membrane potential at rest, a continuous outward current applied by the patch-clamp amplifier during the action potential recordings, will tend to cause the membrane potential to repolarize quicker. On the other hand, this intervention was a constant effect throughout the experiment. By this means, I performed paired experiments (control and intervention in same cell) keeping the holding current unchanged throughout and I was controlling for the influence of the holding current on APD. In fact, the holding current used exerted the same influence for control and intervention. Moreover, APD_{90} with similar duration have been previously published by Workman et al. (APD_{90}: 193 ± 8 ms) (380).

Finally, the effect on the calcium signalling is thought to be minimal, assuming that the normal Vm of the cells is about -80 mV and the action potential has close to normal characteristics. The short APD_{90} observed in these experiments are, probably, mainly caused by the hyper-current, but the "low-dome" AP configuration (small or absent plateau) may result from a small I_{CaL} in these cells. If I_{CaL} is small, then that could be expected to produce a relatively shorter calcium transient. Cells showed transient shortening on each action potential, confirming that EC coupling was functional during this protocol.

Calcium transient shortens slightly because of the shortening of the APD. However, cells regularly showed transient shortening synchronous with the APD and calcium transient, the magnitude of which variate in a cell to cell basis.

6.6 Conclusion

ICAGEN effectiveness was observed only at high concentration (10 µM) which can be attributable to non-specific effects of the drug. In ruptured-patched current clamped rabbit or human isolated atrial myocytes, I_{SK}, assessed as any AP response to acute administration of 1 µM ICA, may not flow during AP stimulation at physiological pacing frequency (1Hz) with physiological temperature and ion concentrations. Furthermore, I_{SK} activation (and thus its potential pharmacological inhibition during AF) may require changes to cellular electrophysiology or cell signalling systems to develop a sensitivity to I_{SK} block, including pathological $[Ca^{2+}]_i$-elevation beyond that attainable by short bursts (1-2 mins) of supra-physiological ($\leq$180 beats/min) AP stimulation.

Chapter 7 Replication and modification of a protocol used to study NCX allosteric regulation: Is an extreme rise in $[Ca^{2+}]_i$ under controlled conditions, with physiological $[K^+]$, sufficient to trigger I_{SK}?

7.1 Background

7.1.1 Identification of a new protocol to raise global $[Ca^{2+}]_i$

In chapter 5 precisely measured $[Ca^{2+}]_i$ solutions were adopted to attempt to elicit I_{SK} and investigate the possible effect of two different SK blockers, but no effect was detected at any voltage studied. Note that this method of raising $[Ca^{2+}]_i$ requires constant, prolonged $[Ca^{2+}]_i$ elevation, which precludes the use of concentrations much above 500 nM because such conditions would lead to progressive cell contracture (see section 3.8.1) and death. Therefore, effects of ICA on APs were studied, where $[Ca^{2+}]_i$ also rises substantially, but only transiently. Then the use of APs at different stimulation frequencies, to raise $[Ca^{2+}]_i$ physiologically, did not produce any ICAGEN rate-dependent effect on repolarization, unless the ICA concentration utilised was increased to values considered non-selective for I_{SK} inhibition. Therefore, based on the assumption that SK channels are activated solely by Ca^{2+} ions (165), a different protocol which could transiently elevate $[Ca^{2+}]_i$ to values otherwise not achievable with the calcium solution method was utilised. This protocol, originally used by Weber et al., to study the allosteric regulation of the Na^+-Ca^{2+} exchanger (NCX) (382), was then modified by Quinn et al., for studies on NCX activity in rabbit ventricle myocytes (12). In my experiments the protocol from Quinn et al. has been repeated for validation in left ventricle myocytes and then modified by incorporation of physiological $[K^+]_i$ and $[K^+]_o$ solutions for the study of I_{SK}.

The rationale behind this protocol was that during the depolarizing phase of the protocol, calcium was brought into the cell via NCX, and causing a slow rise of intracellular calcium. Any subsequent activation of the calcium sensitive current, could be detected from the current traces in voltage clamp. Similarly, during the hyperpolarising phase this caused calcium extrusion from the cells via the NCX, and the corresponding decrease in any calcium sensitive currents. This

protocol is a convenient way to generate slow increases and decreases of intracellular calcium, which can be correlated with the corresponding current trace. The contribution of the SK current to the total current trace can be assessed by measuring the difference in current, resulting from the addition of ICA.

7.1.2 Exploitation of NCX to raise $[Ca^{2+}]_i$

The cardiac sarcolemmal Na^+/Ca^{2+} exchanger (NCX) is a bidirectional transporter that exchanges three Na^+ for one Ca^{2+} (383, 384) representing one of the main mechanisms of calcium extrusion during diastole (385, 386). The exchange direction of sodium and calcium ions depends on the membrane potential. Specifically, with membrane potential more negative than the equilibrium potential for NCX ($E_{Na/Ca}$) and in the presence of low $[Na^+]_i$ and high $[Ca^{2+}]_i$, inward NCX current ($I_{Na/Ca}$) and extrusion of Ca^{2+} will be electrochemically favoured ("forward mode") (2). Whereas, in the opposite conditions an outward $I_{Na/Ca}$ will be observed along with Ca^{2+} influx ("reverse mode") (382, 387). Importantly, NCX is allosterically regulated by Ca^{2+} in a counteractive manner to Na^+ and H^+ ions. A rise in $[Na^+]$ and a decrease in pH will deactivate $I_{Na/Ca}$, whilst an increase of $[Ca^{2+}]_i$ will increase $I_{Na/Ca}$ in opposition to the effect of $[Na^+]_i$ (388, 389). In fact, in patch-clamp recordings, a rise in NCX peak current represents $[Ca^{2+}]_i$-dependent activation of NCX (390). This mechanism was exploited by previous studies in order to measure the Ca^{2+} sensitivity of allosteric regulation of $I_{Na/Ca}$ in intact cardiac myocytes (12, 382). The voltage pulse protocol used in these studies refer to measurements of $I_{Na/Ca}$ under tightly controlled ions concentrations and composition, where the cell membrane was stimulated repetitively to provoke a progressive rise of $[Ca^{2+}]_i$ through reverse-mode $I_{Na/Ca}$. In this chapter the protocol modified by Quinn et al. was first replicated, i.e. utilising solutions K^+-free (replaced with equimolar $[Cs^+]$), designed to isolate I_{NCX}, and then validated using the setup described in section 2.3.8. (Chapter 2, methods), in rabbit left ventricle myocytes. Subsequently, the same protocol was replicated in the same cell type with solutions containing physiological $[K^+]$ (because I_{SK} is a K^+ current and so requires K^+ ions in the solutions to flow) to verify the capability and reproducibility of the protocol even under this condition. This represents a crucial transition step for the study of I_{SK} with ICA in any cell type. The hope was then, time-permitting, to test this modified

method in atrial cells; where SK channels have been shown predominantly expressed (27, 28). However, these would be challenging experiments, and if time would not permit for the study of atrial cells, novel and important data could nevertheless be obtained from this ventricular cell study alone.

7.1.3 Implication of rise in $[Ca^{2+}]_i$ on SK channel activity

The small conductance Ca^{2+}-activated K^+ channel family may play a role in integrating variations in intracellular Ca^{2+} with membrane potential, in excitable cells, thus contributing to cardiac repolarization. Recently, Torrente et al., described a rise in diastolic $[Ca^{2+}]_i$ of 41% in sinoatrial node (SAN) cells and intact SAN preparation from NCX knockout (KO) mouse model. This condition of Ca^{2+} overload could have enhanced SK current (recorded as apamin-sensitive current) which has been shown to cause long-lasting hyperpolarization in response to increased $[Ca^{2+}]_i$ and, therefore, gradually slowing the beating rate and reducing spontaneous activity in SAN (391). On the other hand, during AF, the acute rate - dependent atrial-cell Ca^{2+} load (1, 392) would be expected to increase SK current and might cause substantial hyperpolarization, which would shorten the APD and refractoriness. This mechanism could be contrasted by targeting SK channels and blocking them, resulting in prolongation of the atrial effective refractory period (aERP) and producing clear antiarrhythmic effects as others have previously described (196, 202, 209). Therefore, the rise of $[Ca^{2+}]_i$ is crucial for the activation of SK channels, albeit how they participate in APs repolarization remain disputed. However, the $[Ca^{2+}]_i$ has been poorly controlled in previous studies where the efficacy of SK channel blockade has been documented, as already described in chapter 3. Therefore, in this chapter, availing of the protocol cited above, the aim was to control, elevate and record the $[Ca^{2+}]_i$ and the resulting current simultaneously, trying to transiently elevate $[Ca^{2+}]_i$ (not buffered) higher than any other studies have documented in either rabbit left ventricle and atrium myocytes.

7.1.4 $I_{Na/Ca}$ "reverse-mode" on action potential

Measuring $I_{Na/Ca}$ without affecting other ion currents is challenging, since existing NCX blockers (e.g. Ni^{2+} or KBR7943) have limited selectivity and can block other channels (e.g. Na^+ and Ca^{2+} channels) which could change AP

morphology (393). Therefore, unphysiological conditions, such as those used in the experiments outlined in this chapter, are required to isolate and study $I_{Na/Ca}$. In a study by Armoundas et al., who used a different NCX blocker know as exchange-inhibitory peptide (XIP) and K^+-free solutions (which caused a very long APD), they successfully showed that in APs from ventricle myocytes of failing hearts in guinea pigs, the contribution of reverse-mode (I_{rev}) of NCX was higher compared to forward mode (I_{for}) at 10 and 15 mM $[Na^+]_i$, suggesting a net repolarizing influence of NCX at these levels of $[Na^+]_i$ (394). This could suggest a protective role of $I_{Na/Ca}$ in preventing excessive AP prolongation in heart failure where $[Na^+]_i$ has been shown to be elevated, as a result of higher diastolic Na^+ influx (395). However, it is well-known that $I_{Na/Ca}$ is in forward-mode for almost the entire AP and contributes with an inward current (Na^+ ions influx) to mid and late repolarization (396, 397). Therefore, inhibition of this depolarizing current should produce a shortening of the APD_{90}.

Based on this background, the APD_{90} prolongation caused by administration of 10 μM ICA in rabbit left atria APs, described in the previous chapter (Chapter 6), was retrospectively considered. In fact, although there are no published data about a possible, not negligible, direct effect of ICA at that concentration on non-SK currents, the lack of specificity of the compound at 10 μM has been hypothesised. In addition, Skibsbye et al. in 2014 reported data regarding the selectivity profile of ICAGEN, as previously cited in this thesis, albeit the SK pore blocker IC_{50} values were tested on different cardiac relevant ion currents (e.g. I_{TO}, I_{K1}, I_{Kur}, $I_{Ca,L}$), $I_{Na/Ca}$ was not among those. However, a non-selective block by 10 μM ICA on $I_{Na/Ca}$ cannot account for the APD_{70-90} prolongation observed in chapter 6, based on what has been explained above. On the other hand, ICA showed minor inhibitory effect only on I_{K1} (IC_{50} >100 μM) and I_{TO}, which presents an IC_{50} of 21 μM (29). Therefore, speculation was made, after the analysis of APs and before this set of experiments started, concerning a possible non-specific effect of 10 μM ICA and a consequent APD_{90} prolongation under physiological conditions.

7.2 Aims section

To summarise, the aims were as follows:

- Validate the protocol from Quinn et al. (12) by replicating the step-wise elevation of $[Ca^{2+}]_i$ and the Ca^{2+}-dependent activation of $I_{Na/Ca}$ by repetitively stimulating the isolated myocytes from non-failing rabbit left ventricle in K^+-free superfusate (substituted with Cs^+). During the validation step, also to investigate the effect of the putative selective SK blocker ICA at 10 μM and to compare with the effect of the NCX blocker Ni^{2+} (10 mM) on $I_{Na/Ca}$ in rabbit left ventricle myocytes.

- Replicate the protocol and Investigate the effect of ICA at 1 μM, the vehicle dimethyl sulfoxide (DMSO, 1 μM) and 10 mM Ni^{2+} in rabbit left ventricle myocytes, except this time with physiological $[K^+]$ solutions.

7.3 Methods

7.3.1 Voltage-clamp and $[Ca^{2+}]_i$ measurements

Isolated cardiomyocytes were superfused with Hepes-based solution at 35-37°C in a chamber mounted on the stage of an inverted microscope (see methods section 3.4.7). Voltage clamp was achieved a using an AxoClamp 2B patch-clamp amplifier (Axon Instruments) and WinWCP 5.3.4 electrophysiology software (J. Dempster, University of Strathclyde, UK). Pipette resistance was 2–4 MΩ for NCX, I_{SK} current density studies and for Fura-2 studies. Patch pipettes were pulled from borosilicate glass capillaries 1.2 OD x 0.69 x 100L mm (Harvard Apparatus, USA) with a gravity puller (model PP-83, NARISHIGE, USA). A liquid junction potential of –8.9 mV was compensated for prior to recordings. $[Ca^{2+}]_i$ was estimated from Fura-2 fluorescence using the dual-wavelength spectrophotometric method described in chapter 3. Cytosolic loading of Fura-2 was achieved by incubating cells with 5mM Fura-2-AM at 22-23°C for 10 min followed by 15 min in the absence of Fura-2-AM. The procedures used to convert Fura-2 fluorescence to $[Ca^{2+}]_i$ are detailed in chapter 3 (Methods section 3.3.6).

7.3.2 Isolation methods and experimental conditions

Ventricular and atrial myocytes from non-failing rabbit hearts were isolated as previously described (See Methods 2.3.1-2.4.1). Experiments were performed using ruptured whole-cell patch clamp (See Methods section 2.6-2.8) in voltage-clamp mode. All experiments were performed at 37°C.

7.3.3 External and internal solutions

The superfusion solution contained (mM): NaCl (140), CsCl (4), Hepes (5), $MgCl_2$ (1), $CaCl_2$ (1.8) and glucose (11.1); pH 7.4 with 1M NaOH. This solution was modified as appropriate for each experimental protocol. For NCX activity studies, the superfusate contained added (mM): 4-aminopyridine (5) (4-AP, to block K^+ currents), niflumic acid (0.1) (to block Ca^{2+}-activated Cl^-currents), strophanthidin (0.01) (to block Na^+/K^+ pump) and nifedipine (0.01) (to block $I_{Ca,L}$). Also, cells were pre-treated with 1 mM thapsigargin for 5 min to inhibit SR Ca^{2+} uptake. Then Caffeine (10 mM) was applied to provoke sarcoplasmic reticulum (SR) Ca^{2+} release, ensuring that it was empty, and its function disabled. The pipette solution contained (mM): Cs-Aspartate (100), CsCl (20), $MgCl_2$ (4.5, calculated free $Mg^{2+} \approx 0.9$ mM), Hepes (10), EGTA (0.01), tetraethylammonium chloride (TEACl, 20), disodium ATP (Na_2ATP, 4) and disodium creatine phosphate (Na_2CrP 1); pH 7.25 with CsOH. For I_{SK} studies, the perfusion and pipette solution were as for NCX activity studies, but Cs^+ was replaced with equimolar K^+ and no 4-AP was used in the external solution.

7.3.4 Electrophysiology protocol and $[Ca^{2+}]_i$ recordings

The protocol used to exploit NCX Ca^{2+}-dependent activation was based and modified from Quinn et al. (12). In the following experiments the voltage-protocol as well as the solutions were modified (after replication of the protocol to manipulate the reverse-mode $I_{Na/Ca}$ with the purpose of causing a rise of $[Ca^{2+}]_i$ and, if the allosteric regulation of NCX by $[Ca^{2+}]_i$ was present, this would initially increase also outward $I_{Na/Ca}$. Cardiomyocytes were held at -80 mV to lower $[Ca^{2+}]_i$ and then stepped 17 times to +100 mV and -100mV alternatively, with 250 ms intervals between each step (see Fig. 7.1). The duration of the voltage pulse, of 250ms, was chosen for each cell to produce a rise in $[Ca^{2+}]_i$ from global diastolic

to systolic values. The protocol was repeated in the presence of Ni^{2+} ($NiCl_2$, 10 mM) or ICAGEN (10 or 1 μM). For each cell was calculated the background fluorescence by confining the cell into a "box" created by regulation of a square diaphragm (Fig. 7.2). The area generated was then positioned on an empty (no cells or debris) space on the glass slide and the light was turned off during the recordings of background fluorescence. The background fluorescence recorded from the area of each cell was considered as R_{min} for each individual cell. While R_{max} was obtained by piercing the cell with the electrode all the way down (at the end of the recordings), which caused a massive release of Ca^{2+} and maximal rise in fluorescence. Individual R_{max} and R_{min} were used in the equation 2 (see Methods section 3.4.5).
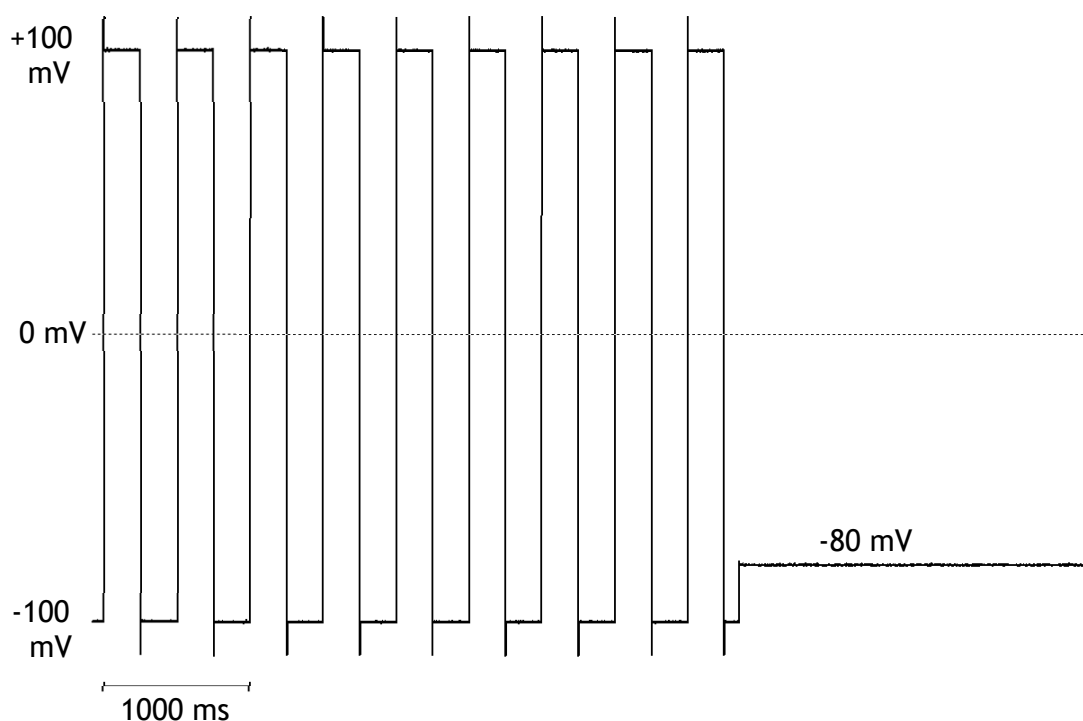
Figure 7.1 Representation of voltage pulse protocol. Image created using WinWCP 5.3.4 electrophysiology software.
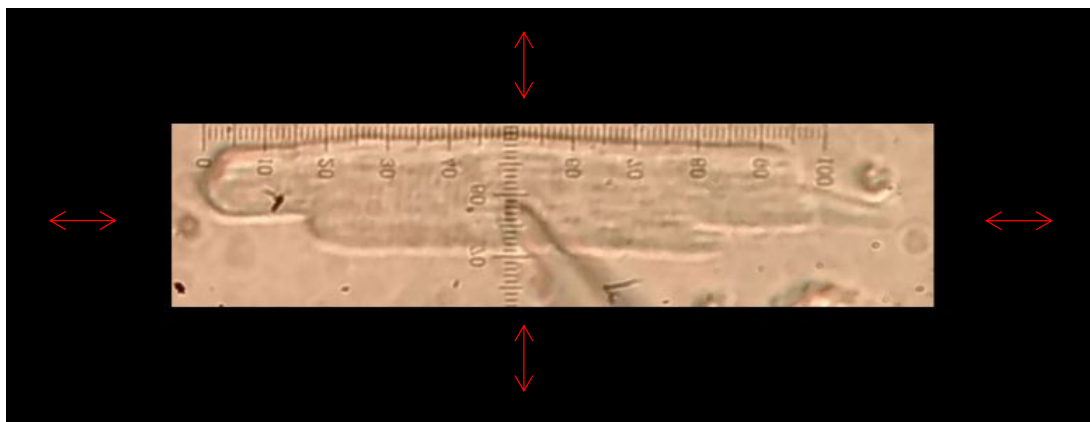
Figure 7.2 Photograph of a rabbit ventricle myocyte, delineated by the box, and modified to exemplify the "box". The red arrows show the possible direction of the 2 moving parts of the diaphragm. The whole "box" could be rotated to align with the cell.

7.3.5 Statistics & data analysis

Ion current and $[Ca^{2+}]_i$ data were compared using paired or unpaired Students' t-tests, as appropriate. Statistical significance was predetermined at a level of $P < 0.05$.

7.4 Results

7.4.1 Replication and validation of the protocol for Ca2+-dependent activation of NCX studies

As described in the methods section of this chapter, all currents were blocked (including $I_{Ca,L}$, Ca^{2+} dependent I_{Cl}, and Na^+/K^+ pump) except $I_{Na/Ca}$ which was the only one able to intrude and extrude Ca^{2+} in and from the cell during the replication of the protocol in myocytes from rabbit ventricle. Also, the SR was depleted of all the Ca^{2+} and blocked by thapsigargin. Therefore, under these controlled conditions the cell was able to exchange Ca ions only through NCX, which was repetitively stimulated with the voltage protocol described above. In figure 7.3 is shown a representative record from a single cell during control conditions (A) and after acute administration of 10 mM Ni^{2+} (B). Ni^{2+} almost completely blocked both outward and inward $I_{Na/Ca}$ (Fig. 7.3 Ac and Bc).

Additionally, the acute administration of Ni^{2+} prevented Ca^{2+} transient firing (Bb) and consequent cell contraction.
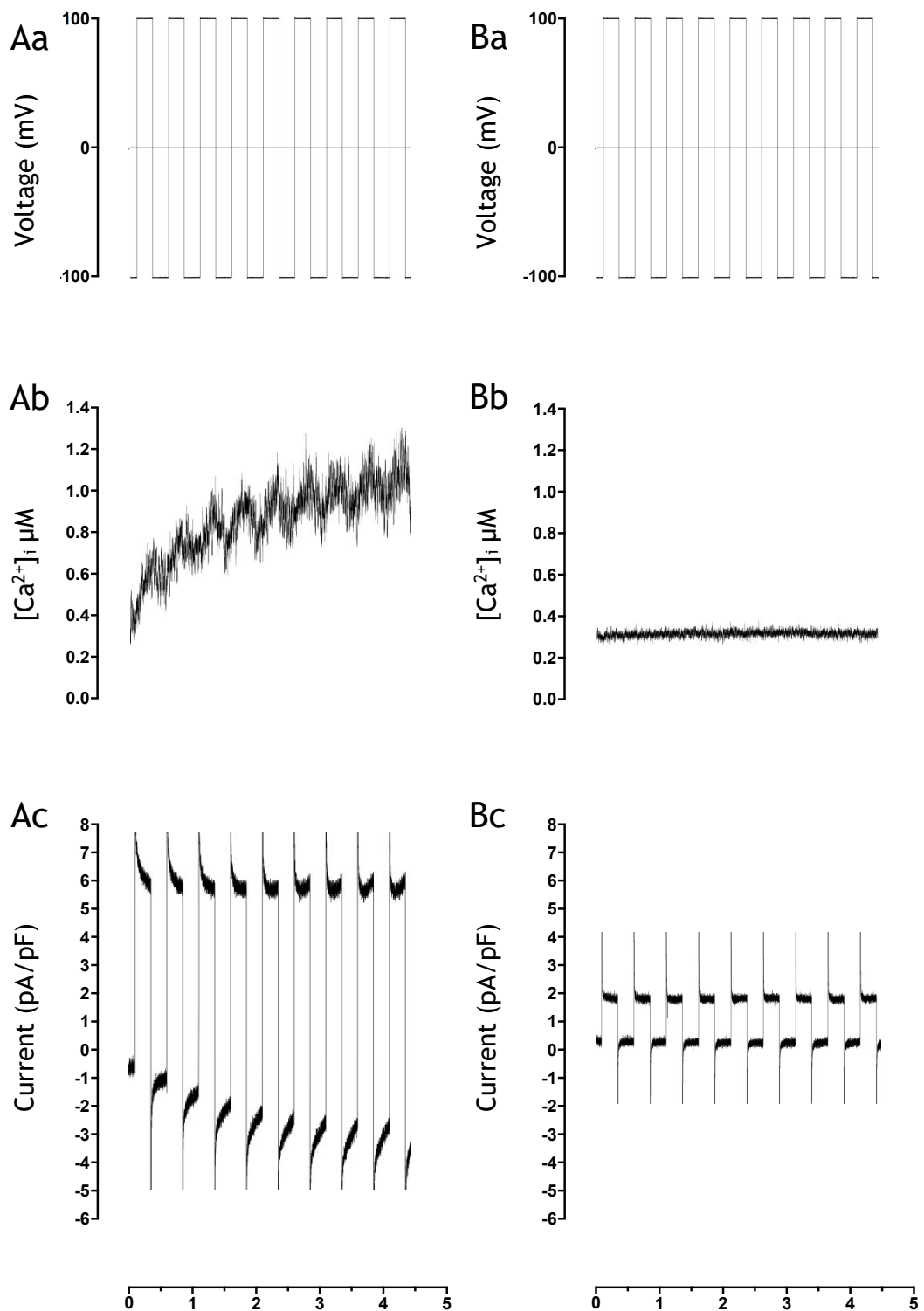
Figure 7.3 Representative current and $[Ca^{2+}]_i$ traces from a single rabbit ventricle myocyte.

Aa and Ba, Voltage-clamp protocol used to investigate the Ca^{2+}-dependent activation of NCX and to raise $[Ca^{2+}]_i$. The cardiomyocyte was alternately clamped at -100 and +100 mV, as described in methods. Ab and Ac, $[Ca^{2+}]_i$ and current traces recorded under control condition, whereas, Bb and Bc in the presence of 10 mM Ni^{2+}.

The protocol successfully allowed the control and measurements of $[Ca^{2+}]_i$ simultaneously to $I_{Na/Ca}$ current measurements. The outward $I_{Na/Ca}$ increase was attributed to allosteric regulation by Ca^{2+}, as explained, and was used to verify the presence of this mechanism in each cell. The raw Ca^{2+} traces illustrated in figure 7.3 (Ab) show a rise of $[Ca^{2+}]_i$ up to ~1.3 μM from ~0.4 μM in one ventricle cell. The diastolic $[Ca^{2+}]_i$ recorded in this experiment appears high if compared to the expected normal physiological values. However, the raw traces showed in figure 7.3 were obtained from the third train of voltage pulse, thus the increased $[Ca^{2+}]_i$ obtained during previous trains did not return to the initial diastolic values. This mechanism of "charging up" the basal cell calcium content was intentionally sought and essential for the study of I_{SK} further on. Interestingly, in one cell from rabbit left ventricle the maximal $[Ca^{2+}]_i$ achieved was of 2.8 μM (highest value recorded among all cells). Additionally, after subtraction, the resulting Ni^{2+}-sensitive current, which was considered pure $I_{Na/Ca}$, was plotted against $[Ca^{2+}]_i$ (Fig. 7.4). This showed that the responses in that single experiment shown in figure 7.3 are similar to the examples shown in Weber et al and Quinn et al. and confirm that the protocol used was working as expected in the ventricle cell showing a similar activation pattern to the one published by Quinn et al. (12). However, in that study they used mean values, and data were fitted using the equation from the model of Weber et al. They have chosen to model Ca activation as an instantaneous process and the simple model included all other non-blocked sources of Ca flux (sarcolemmal Ca pump, Ca background leak current) but no sarcoplasmic reticulum (SR) (382). On the other hand, in my experiments, a single representative myocyte from rabbit left ventricle was used and the data were fitted to a sigmoidal curve. The current values in the positive regions were fitted with a sigmoidal curve, which however resulted in a relatively low R^2, while the best fitting relationship for the current values in the negative sector was a straight line fit. Although, the fit was considered good enough to predict an increase in currents relative to $[Ca^{2+}]_i$, which confirmed the validity of the protocol. On the other hand, the use of the model from Weber et al. represents a further step to deeply study allosteric regulation of NCX, therefore, it was not employed in this chapter since the correct replication of the protocol and the obtainment of a substantial rise of $[Ca^{2+}]_i$ for I_{SK} studies was achieved and sufficient to the present purposes.
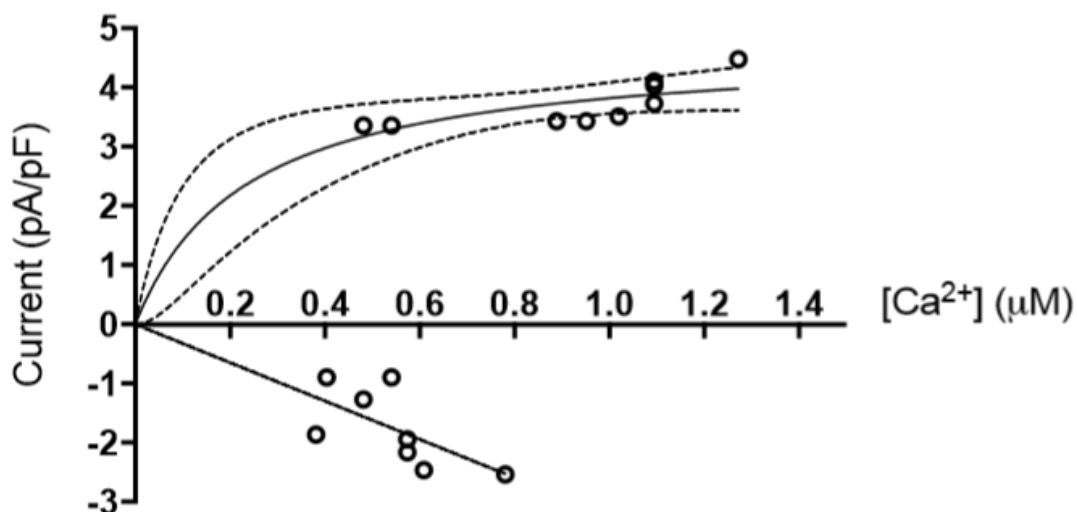
Figure 7.4 Representative Ni²⁺-sensitive current values plotted against [Ca²⁺]ᵢ.

Data were obtained by subtraction of current values in the presence of 10 mM Ni²⁺ from control current values. Data points represent outward and inward Ni²⁺ - sensitive current and derive from the same voltage protocol shown in figure 7.3. The points in the positive voltage sector were fitted to a sigmoidal curve (R^2= 0.46), while in the negative sector only a straight line fit was possible (R^2=0.43). The fit was based on the theoretical relationship described in Quinn et al. (12).

7.4.2 Effect of 10 µM ICA and 10 mM Ni²⁺ on both inward and outward I$_{Na/Ca}$ and [Ca²⁺]ᵢ in rabbit left ventricular myocytes with Cs⁺ based solutions

Throughout the whole analysis the last 2 pulses of the trains were used to collect data for currents and [Ca²⁺]ᵢ at both -100 and +100 mV for each condition, given the maximal rise in [Ca²⁺]ᵢ obtained during that 500 ms period. Below, representative current traces are show for control, ICA and Ni²⁺, showing the effect of 10 µM ICA and 10 mM NiCl₂ on both current and [Ca²⁺]ᵢ (Fig. 7.5).
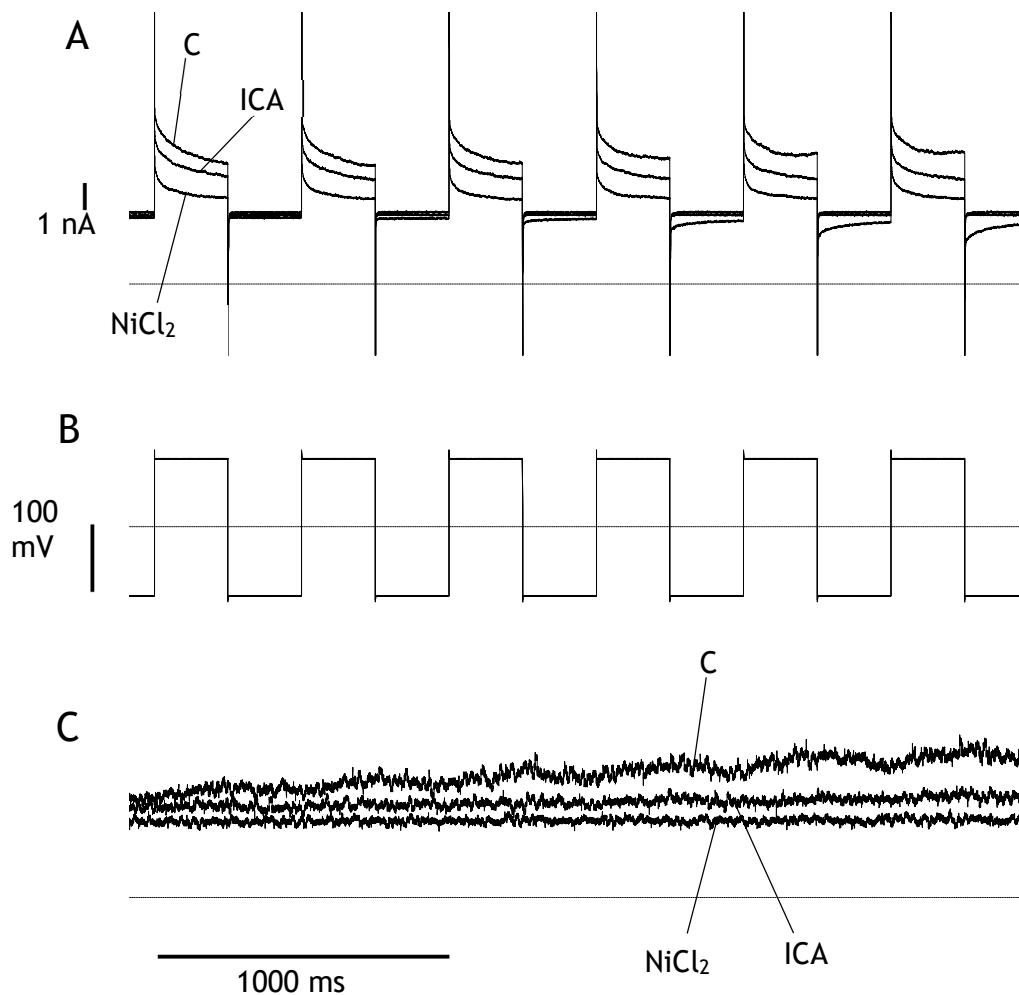
Figure 7.5 Representative current and $[Ca^{2+}]_i$ traces from a single rabbit ventricle myocyte.

A) Current traces showing the effect of 10 μM ICA and 10 mM $NiCl_2$ on both outward and inward current. C=control. B) Voltage-clamp protocol used to investigate the Ca^{2+}-dependent activation of NCX and to raise $[Ca^{2+}]_i$.

C) Raw ratio traces showing the effect of 10 μM ICA and 10 mM $NiCl_2$. Subsequently, ratio values were converted in $[Ca^{2+}]_i$ as explained in paragraph 3.4.5. Cardiomyocyte was alternately clamped at -100 and +100 mV, as described in methods.

Interestingly, 10 μM ICA significantly reduced both inward and outward $I_{Na/Ca}$ recorded at -100 and +100 mV respectively. Acute administration of 10 μM ICA provoked a reduction of 35% (control outward $I_{Na/Ca}$ 8.24 ± 1.53 pA/pF vs 5.38

$\pm$ 1.64 pA/pF following 10 μM ICA n= 4 cells, n=1 rabbit, mean $\pm$ s.e.m., paired data, p< 0.05, Fig. 7.6 A) and 49% (control inward $I_{Na/Ca}$ -2.86 $\pm$ 0.33 pA/pF vs -1.45 $\pm$ 0.55 pA/pF, n= 4 cells, n=1 rabbit, mean $\pm$ s.e.m., paired data, p< 0.05, Fig. 7.7 A) of mean outward and inward $I_{Na/Ca}$ compared to control, respectively. Whereas, subsequently applied 10 mM Ni^{2+} failed to further reduce outward or inward $I_{Na/Ca}$ compared to 10 μM ICA (Fig. 7.6 A and 7.7 A), consistent with ICA having already substantially blocked $I_{Na/Ca}$. $NiCl_2$ was applied only to 3 out of 4 cells, since one single cell did not survive the full protocol. Additionally, peak $[Ca^{2+}]_i$ was reduced in the presence of 10 μM ICA at both +100 mV and -100mV compare to control (Fig. 7.6-7.7 C), although only significantly at -100mV. Acute administration of 10 μM ICA provoked a 77% reduction of $[Ca^{2+}]_i$ at -100 mV (1.24 $\pm$ 0.23 μM vs 0.28 $\pm$ 0.03 μM n= 4 cells, n=1 rabbit, mean $\pm$ s.e.m., paired data, p< 0.05, Fig. 7.7 C) compared to control. Whereas, in the presence of 10 mM Ni^{2+} peak $[Ca^{2+}]_i$ was not significantly reduced compared to ICA at both voltages (Fig. 7.6 C-7.7C), also consistent with $I_{Na/Ca}$ inhibition by ICA. Subsequently, the Ni^{2+}-sensitive and ICA-sensitive component were measured by subtraction of the current in the presence of the drug to the current during control superfusion. In addition, the ICA-sensitive current was subtracted to the Ni^{2+}-sensitive current ($I_{Na/Ca}$), which resulted in a so called "ICA-sensitive non-$I_{Na/Ca}$" component, in order to show the magnitude of the difference between the latter and $I_{Na/Ca}$ (Fig. 7.8). By this means, the resultant current values, after the last subtraction, should represent a non-$I_{Na/Ca}$ ICA sensitive current, which was significantly smaller compared to Ni^{2+}-sensitive ($I_{Na/Ca}$) for both the outward ($I_{Na/Ca}$ 5.2 $\pm$ 1.1 pA/pF vs 2 $\pm$ 0.6 pA/pF non-$I_{Na/Ca}$ ICA-sensitive, n= 3 cells, n=1 rabbit, mean $\pm$ s.e.m., paired data, p< 0.05, Fig. 7.9 A) and inward (-2.2 $\pm$ 0.5 pA/pF vs -0.4 $\pm$ 0.3 pA/pF, mean $\pm$ s.e.m., paired data, p< 0.05, Fig. 7.9 B) portion.
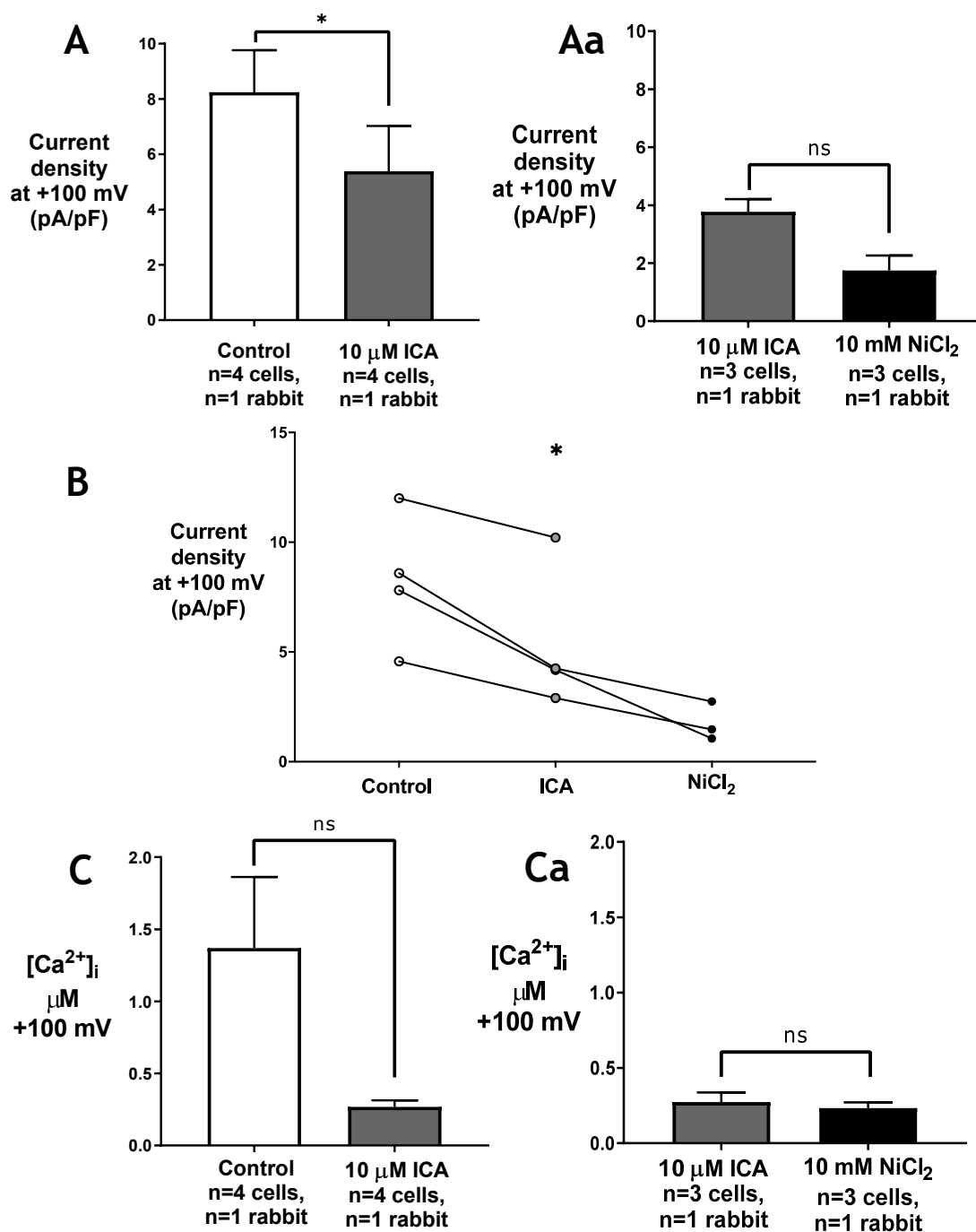
Figure 7.6 Effect of acute superfusion with 10 μM ICA and lack of effect of subsequent 10 mM Ni^{2+} on outward current and absence of effect of both drugs on [Ca^{2+}]$_i$ at +100 mV in rabbit left ventricle myocytes.

A) Effect of 10 μM ICA on outward current at +100 mV. Aa) Absence of additional current block by 10 mM Ni^{2+} when compared to 10 μM ICA. Ni^{2+} was applied only on 3 out of 4 cells. B) Dot-plot showing the current (at +100 mV) of each single cell for control, ICA and NiCl$_2$. C, Ca) Absence of effect of both drugs on [Ca^{2+}]$_i$. Values are mean± s.e.m., values of p< 0.05 (*) were considered statistically significant.
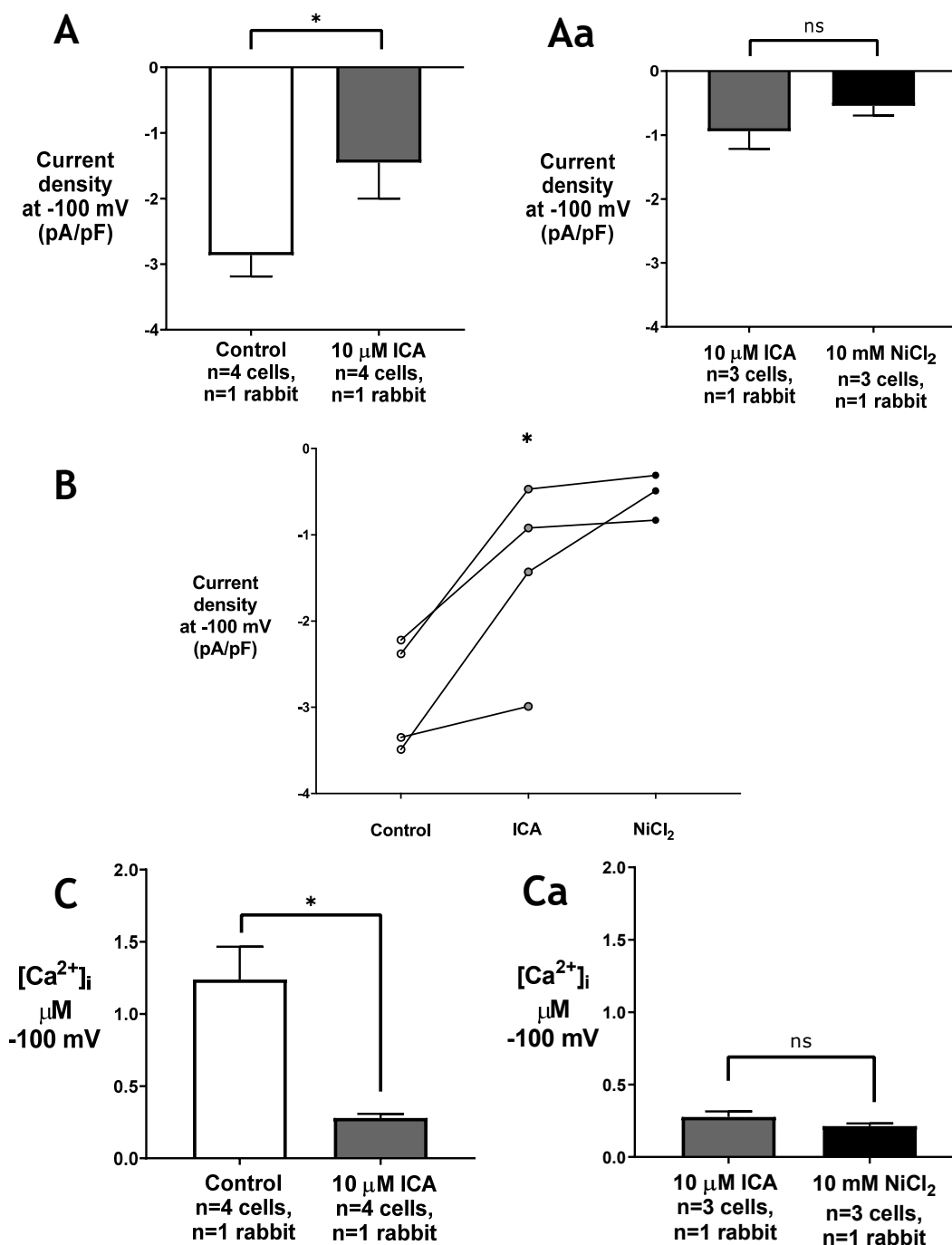
Figure 7.7 Effect of acute superfusion with 10 μM ICA on outward current and [Ca²⁺]ᵢ and lack of effect of subsequent 10 mM Ni²⁺ on outward current and [Ca²⁺]ᵢ at -100 mV in rabbit left ventricle myocytes.

A) Effect of 10 μM ICA on outward current at +100 mV. Aa) Absence of additional current block by 10 mM Ni²⁺ when compared to 10 μM ICA. Ni²⁺ was applied only on 3 out of 4 cells. B) Dot-plot showing the current (at -100 mV) of each single cell for control, ICA and NiCl₂. C) Effect of 10 μM ICA on [Ca²⁺]ᵢ. Ca) Lack of additional reduction of [Ca²⁺]ᵢ by 10 mM Ni²⁺ when compared to 10 μM ICA. Values are mean± s.e.m., values of p< 0.05 (*) were considered statistically significant.
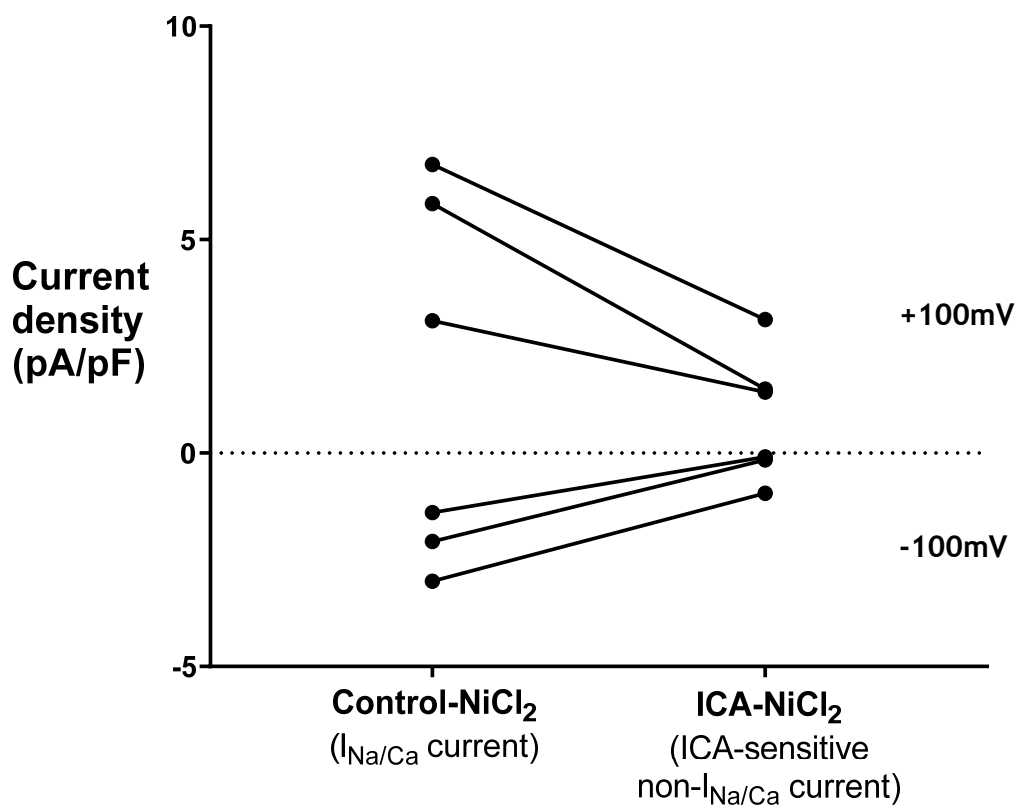
Figure 7.8 Comparison between Ni^{2+}-sensitive current (I$_{Na/Ca}$) and the subtracted ICA-sensitive current.

The resulting current is an ICA-sensitive non-I$_{Na/Ca}$. Each dot represent a single current value; n=3 cells n=1 rabbit.
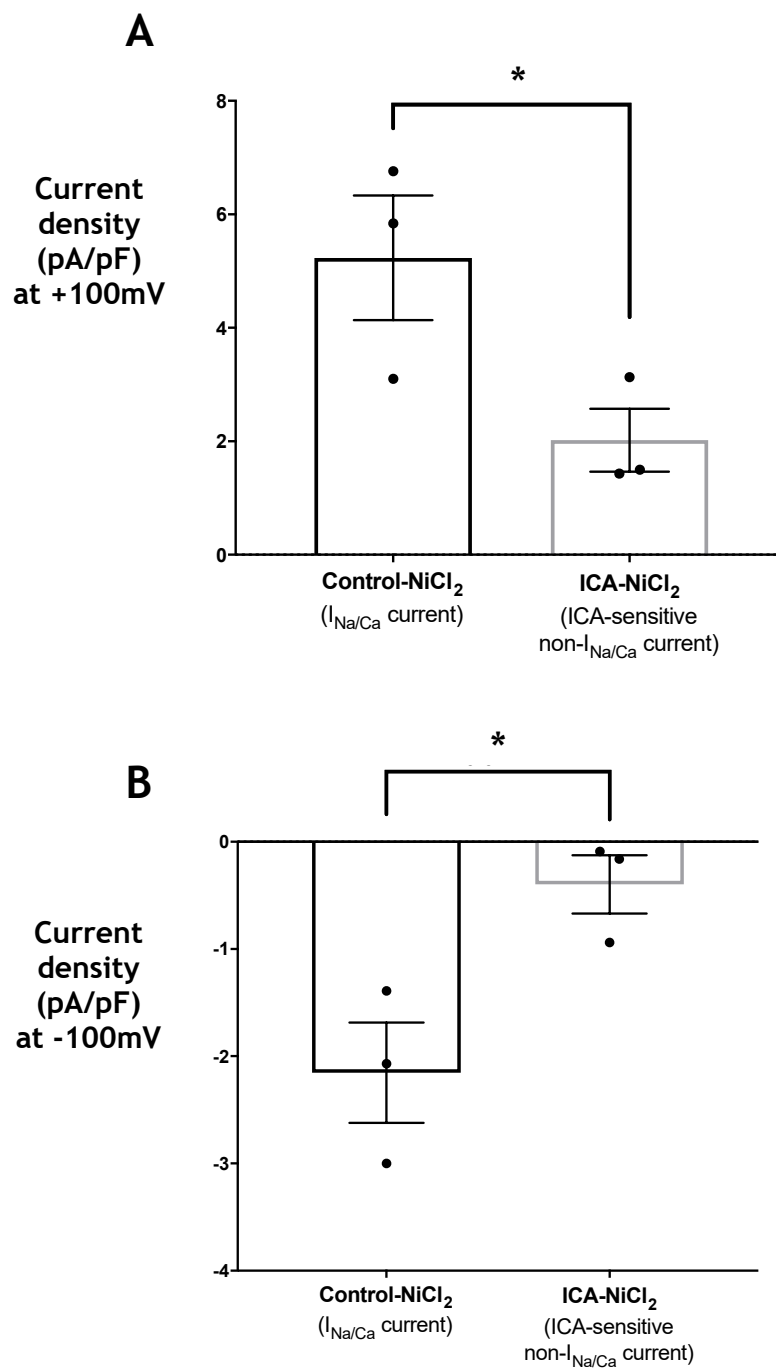
Figure 7.9 Comparison between A) outward and B) inward Ni^{2+}-sensitive current (I$_{Na/Ca}$) and the subtracted ICA-sensitive current in rabbit ventricular myocytes (n=3 cells, n=1 rabbit).

Values are mean ± s.e.m., paired data, values of p< 0.05 (*) were considered statistically significant.

7.4.3 Comparison among ICA, the vehicle DMSO and NiCl$_2$ on both outward and inward current in isolated rabbit left ventricle myocytes with physiological [K$^+$] solutions

ICAGEN was also tested at the concentration of 1 μM (selective for I$_{SK}$) and compared to the vehicle DMSO (1 μM) and to 10 mM Ni^{2+} in rabbit left ventricle myocytes. However, 1μM DMSO did not affect either outward (Control outward current 5.28 ± 0.55 pA/pF vs 5.14 ± 0.49 pA/pF following 1 μM DMSO; n=7 cells, n=2 rabbits, mean ± s.e.m., paired data, Fig. 7.10 A) or inward current (-1.73 ± 0.19 pA/pF vs -1.77 ± 0.16 pA/pF; n=7 cells, n=2 rabbits, mean ± s.e.m., paired data, Fig. 7.11 A) compared to control. Also, acute superfusion with 1μM ICA failed to significantly alter both outward (Vehicle outward current 4.95 ± 0.53 pA/pF vs 4.86 ± 0.49 pA/pF following 1 μM ICA; n=6 cells, n=2 rabbits, mean ± s.e.m., paired data, Fig. 7.10 A) and inward current (-1.72 ± 0.18 pA/pF vs -1.73 ± 0.18 pA/pF; n=6 cells, n=2 rabbits, mean ± s.e.m., paired data, Fig. 7.11 A) compared to the vehicle (DMSO). Nevertheless, acute administration of 10 mM Ni^{2+} significantly reduced both outward (ICA outward current 4.92 ± 0.76 pA/pF vs 2.44 ± 1.16 pA/pF following 10 mM Ni^{2+}; n=4 cells, n=2 rabbits, mean ± s.e.m., paired data, $p < 0.05$, Fig. 7.10 A) and inward current (-1.73 ± 0.28 pA/pF vs -0.69 ± 0.27 pA/pF; n=4 cells, n=2 rabbits, mean ± s.e.m., paired data, $p < 0.05$, Fig. 7.11 A). Increases in [Ca^{2+}]$_i$ were obtained also using the protocol with physiological [K$^+$] solutions, but no effect was detected on peak [Ca^{2+}]$_i$ during acute superfusion with either 1 μM DMSO or 1 μM ICA compared to control (Fig. 7.12 A and B). On the other hand, even in this case 10 mM Ni^{2+} provoked a significant 70% and 67% reduction of peak [Ca^{2+}]$_i$ at +100 mV (ICA peak [Ca^{2+}]$_i$ 0.82 ± 0.10 μM vs 0.25 ± 0.02 μM following 10 mM Ni^{2+}, n= 4 cells, n=2 rabbits, mean ± s.e.m., paired data, $p < 0.05$, Fig. 7.12 A) and at -100 mV (0.58 ± 0.06 μM vs 0.19 ± 0.01 μM, n=4 cells, n=2 rabbits, mean ± s.e.m., paired data, $p < 0.05$, Fig. 7.12 B), respectively, compared to ICA.
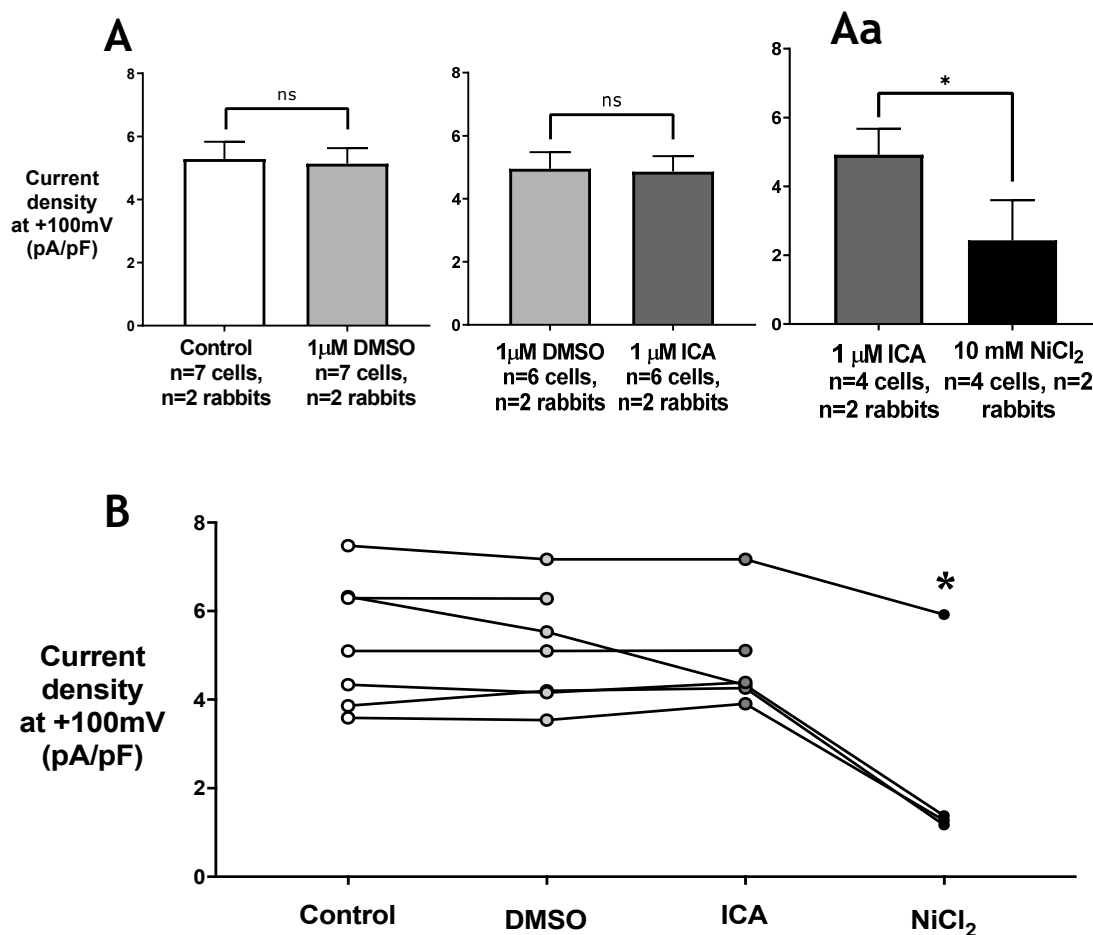
Figure 7.10 Comparison among the effect of different interventions on outward current (at +100 mV) in rabbit left ventricle myocytes. A) Histograms, B) dotted-lines shows the trend for each cell.

□= control ▨ =1 µM DMSO ▨ =1 µM ICA ■=10 mM Ni^{2+}. A) Absence of effect of 1 µM DMSO and 1 µM ICA on outward current. Aa) Effect of subsequent 10 mM $NiCl_2$ on outward current compared to the absence of effect of 1µM ICA. B) Single cell current values under each condition. Values are mean± s.e.m., values of p< 0.05 (*) were considered statistically significant.
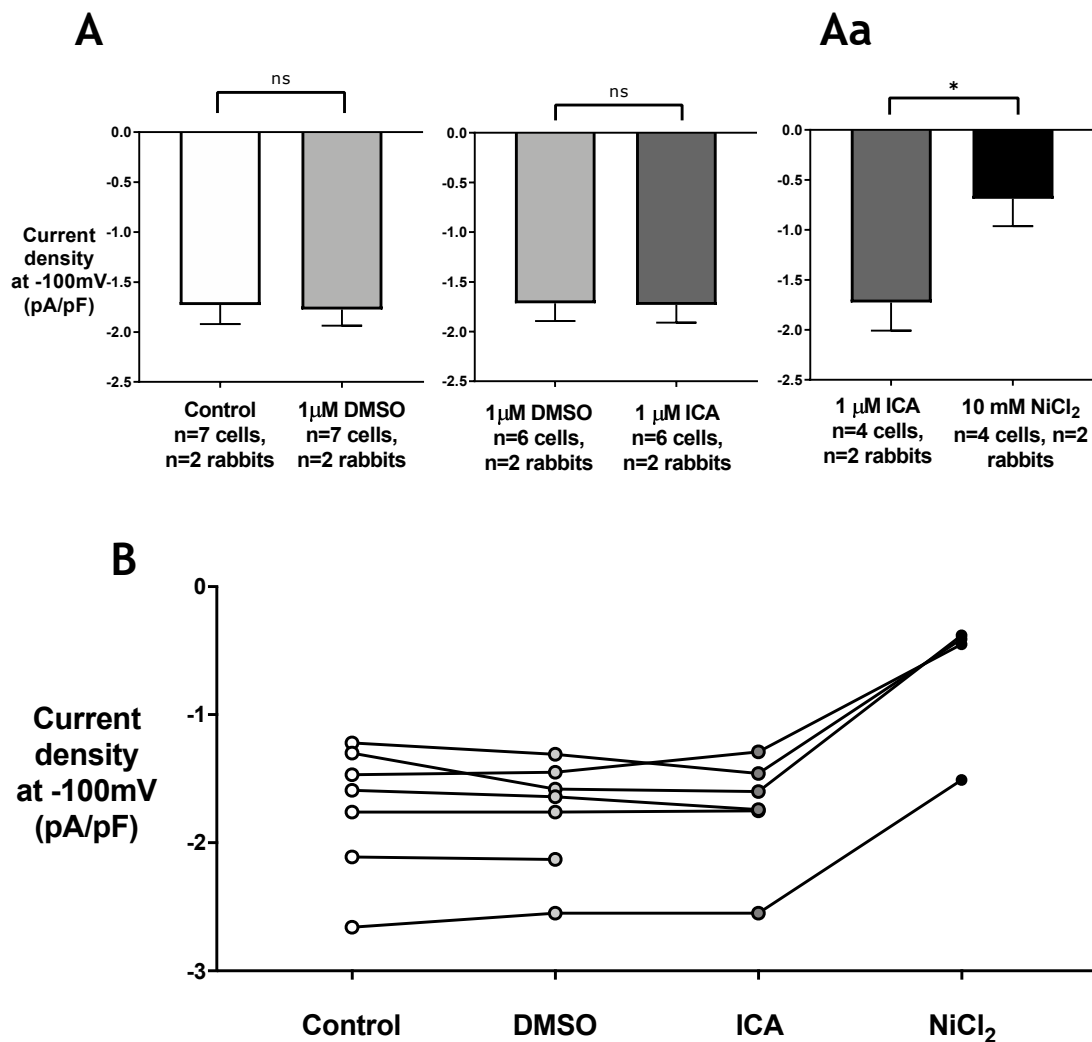
Figure 7.11 Comparison among the effect of different interventions on inward current (at -100 mV) in rabbit left ventricle myocytes. A) Histograms, B) dotted-lines show the trend for each cell.

□ = control ▨ =1 μM DMSO ▨ =1 μM ICA ■=10 mM Ni^{2+}. A) Absence of effect of 1 μM DMSO and 1 μM ICA on inward current. Aa) Effect of subsequent 10 mM $NiCl_2$ on inward current compared to the absence of effect of 1μM ICA. B) Single cell current values under each condition. Values are mean± s.e.m., values of p< 0.05 (*) were considered statistically significant.
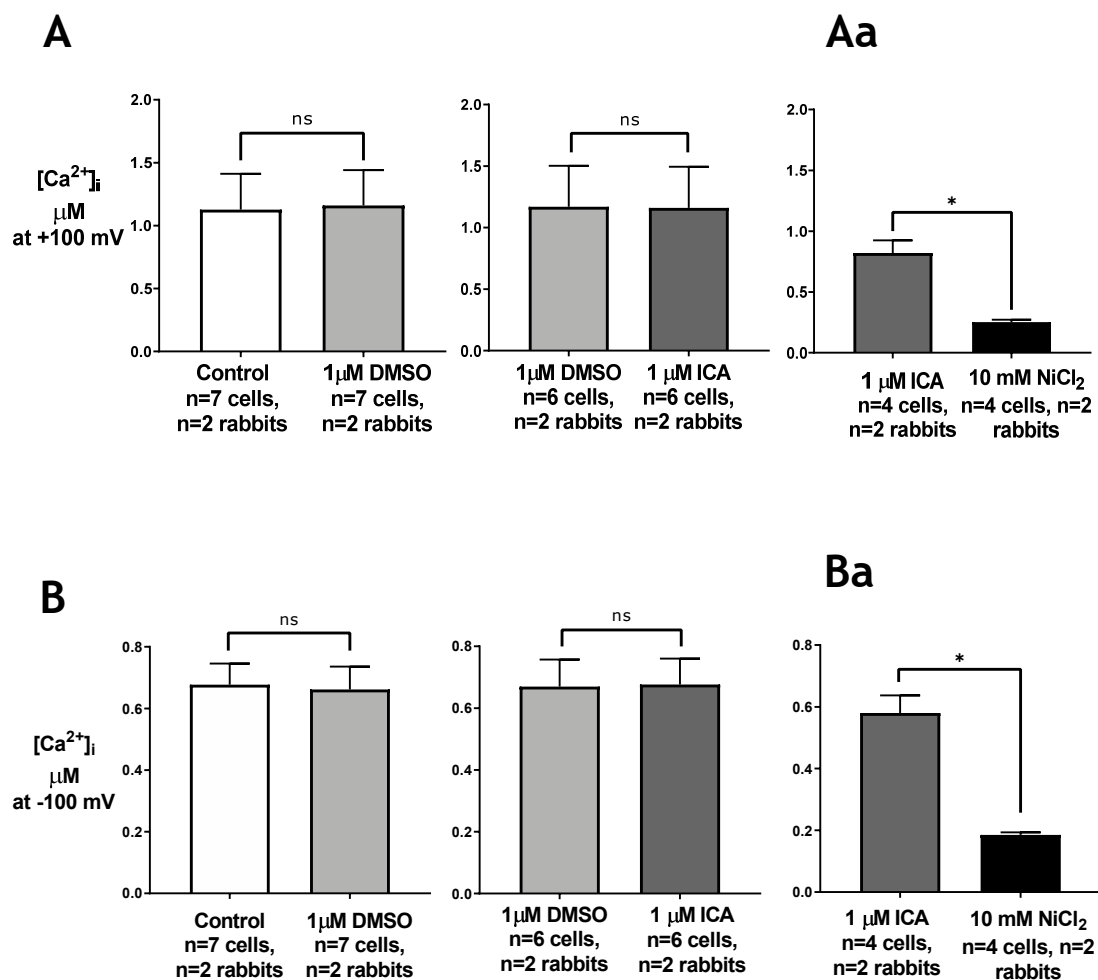
Figure 7.12 Lack of effect of acute superfusion with either 1 μM ICA or 1 μM DMSO and effect of 10 mM Ni^{2+} on $[Ca^{2+}]_i$ in rabbit left ventricle myocytes at both A) +100mV and B) -100 mV.

☐ = control ☐ =1 μM DMSO ■ =1 μM ICA ■ =10 mM Ni^{2+} . A) Absence of effect of 1 μM DMSO and 1 μM ICA on $[Ca^{2+}]_i$ at +100 mV. Aa) Effect of subsequent 10 mM $NiCl_2$ on $[Ca^{2+}]_i$ (at +100 mV) compared to the absence of effect of 1μM ICA. B) Absence of effect of 1 μM DMSO and 1 μM ICA on $[Ca^{2+}]_i$ at -100 mV. Ba) Effect of subsequent 10 mM $NiCl_2$ on $[Ca^{2+}]_i$ (at -100 mV) compared to the absence of effect of 1μM ICA. Values are mean± s.e.m., values of p< 0.05 (*) were considered statistically significant.

7.5 Discussion

The aims of the set of experiments outlined in this chapter were to investigate the possible effect of the putative selective SK channel blocker ICAGEN at two different concentrations (1 and 10 μM) under supra-physiological elevation of $[Ca^{2+}]_i$, and testing the possible unselective block of NCX by 10 μM ICA and the effect of 1 μM ICA on I_{SK} at elevated $[Ca^{2+}]_i$.

7.5.1 The replication of the protocol produced current and $[Ca^{2+}]_i$ values in accordance with the literature

As stated earlier in this chapter, the protocol used throughout these experiments, has been modified from Quinn et al. (12) who used it to measure the Ca^{2+} sensitivity of allosteric regulation of NCX. Since the objective of the experiments outlined in this chapter was mainly to achieve a rise in $[Ca^{2+}]_i$ to higher values than those obtained with buffered solutions (Chapter 5) and for longer period of time than during APs firing (Chapter 6), the protocol from Quinn et al. was exploited primarily for this purpose. However, given that ICAGEN has never been tested on NCX and given the contribution of $I_{Na/Ca}$ on action potential repolarization (394), the SK channel pore blocker has been tested also during the verification step of the protocol. Figure 7.3 A shows the protocol used to measure $I_{Na/Ca}$ at different values of $[Ca^{2+}]_i$ and illustrates the principle explained in the introduction regarding the Ca^{2+}-dependent activation of NCX. In fact, if allosteric regulation is absent the rise of $[Ca^{2+}]_i$ would electrochemically favour inward (forward mode) $I_{Na/Ca}$ over outward (reverse mode) $I_{Na/Ca}$. On the other hand, increases in outward $I_{Na/Ca}$ can only be attributed to allosteric regulation, since calcium activation would increase $I_{Na/Ca}$ in both directions (382). The period of stimulation at +100 and -100 mV was kept constant at 250 ms to maintain the rise in $[Ca^{2+}]_i$ for a longer interval, differently from Quinn et al (100-200ms). The focus of my experiment was to obtain a stable and strong rate of growth in $[Ca^{2+}]_i$ independently from each individual cell's Ca^{2+} content. By this means, cells that did not show a progressive transient rise in $[Ca^{2+}]_i$, dictated by the stimulation protocol, were excluded from the analysis. The values obtained for current density (pA/pF) and $[Ca^{2+}]_i$ were compared with previous studies. The $[Ca^{2+}]_i$ recorded during the first set of experiment reached higher values (up to 2.8 μM) compared to physiological systolic $[Ca^{2+}]_i$ (398, 399), and average NCX current

density in myocytes from rabbit left ventricle was found similar during control, when compared to Quinn et al., in sham animals (12). However, the slight difference could be explained by the application of a longer stimulation period, which maintained the cells at prolonged high $[Ca^{2+}]_i$. During the second set of experiments, where 1 μM ICA was tested, mean NCX current density values, in myocytes from rabbit left ventricle, were observed to be similar to those reported by earlier studies for both outward (~5 pA/pF) and inward (-2 pA/pF) currents (12, 382). In conclusion, I was able to control and measure the rate of rise in $[Ca^{2+}]_i$ while simultaneously measuring both inward and outward $I_{Na/Ca}$. Therefore, the protocol has been replicated successfully, ensuring the setup and measurement validation for the next steps.

7.5.2 Hypothesis for APD$_{90}$ prolongation due to a non-specific block provided by 10 μM

The concentration of 10 μM ICA was tested due to the results obtained in the previous chapter (Chapter 6) where a prolongation of both APD_{90} and APD_{70} was demonstrated. Therefore, considering the lack of effect of 1 μM ICA on APs morphology, it has been supposed the inhibition of different currents besides I_{SK}. 10 μM ICA was tested on outward and inward currents in rabbit ventricle myocytes during the validation of the protocol. Unexpectedly, ICA provided an equivalent reduction to the one produced by 10 mM Ni^{2+} on both currents and $[Ca^{2+}]_i$. However, the current reduction obtained by acute administration of Ni^{2+} was not significant compared to control, which can be due to different sample sizes and the diverse analysis method that have been shown to affect statistical power and error rates (400). In fact, the reduction obtained by Ni^{2+} on $[Ca^{2+}]_i$ confirms a block of NCX provided by the drug.

Interestingly, 10 mM Ni^{2+} did not produce a significant additional reduction of $I_{Na/Ca}$ compared to 10 μM ICA (see Fig. 7.5 A and 7.6 A). This is true also regarding $[Ca^{2+}]_i$, which was reduced to diastolic values during the superfusion with both drugs. These effects could result from a persistent block of ICA, which requires more time to wash out. However, single cell data (Fig. 7.5 B and 7.6 B) showed a possible reduction at least in two cells in the presence of 10 mM Ni^{2+}. Therefore, an additional block of Ni^{2+}, and thus an incomplete block by ICA cannot be ruled out. In fact, to verify this hypothesis, the outward and inward

Ni^{2+}-sensitive ($I_{Na/Ca}$) currents were then compared to the ICA-sensitive non-$I_{Na/Ca}$ currents, which were significantly smaller (Fig.7.9 A and B). Nevertheless, although 10 µM ICA did not block completely $I_{Na/Ca}$, which is virtually the only current flowing during the controlled conditions used, it provided a significant block which was of similar magnitude to the one of 10 mM Ni^{2+} compared to control. These data suggest a potential, albeit partial, block of both forward- and reverse-mode $I_{Na/Ca}$ by 10 µM ICA.

A non-selective block by 10 µM ICA on $I_{Na/Ca}$, as observed in this chapter, cannot possibly account for the APD_{70-90} prolongation produced by 10 µM ICA in chapter 6, for reasons mentioned in the introduction. On the other hand, given the selective profile of ICA (29), an alternative hypothesis was considered. Specifically, a possible block on I_{TO}, which is downregulated in AF (79), by 10 µM ICA under physiological conditions was considered, which could explain the APD_{70-90} prolongation observed in atrial cells from human and rabbit (58, 401) in the present study, and the absence of effect of this compound in cells from AF patients showed in a previous publication (29). However, this hypotheses was not further investigated.

7.5.3 Absence of effect of 1 µM ICA on I_{SK} in ventricle under high $[Ca^{2+}]_i$ and physiological $[K^+]$

The rationale behind experiments with 1 µM ICA in isolated myocytes from rabbit left ventricle was two-fold. First, determine whether I_{SK} was present during high $[Ca^{2+}]_i$ conditions in ventricle using ICA at putative selective concentration of 1µM and test the protocol with physiological $[K^+]$ before utilizing it in atria. Given that SK channels may be important during action potential repolarization in pathological conditions (e.g. cardiomyopathy and heart failure) associated with action potential (AP) prolongation combined with elevated $[Ca^{2+}]_i$ (203, 402, 403) the focus was to replicate a high $[Ca^{2+}]_i$ environment that could elicit I_{SK}. In fact, considering the coexisting conditions of intracellular calcium overload and upregulation of I_{SK}, Chua et al. showed that in failing hearts I_{SK} $[Ca^{2+}]_i$ – sensitivity was increased and apamin administration effectively prevented post-shock APD shortening, late phase 3 early after-depolarizations (EAD), and triggered activity and, therefore, prevented repetitive firing and recurrent spontaneous ventricular fibrillation (SVF). On the other hand I_{SK} played

little or no effect in APD regulation in normal ventricle (306). Numerous studies, as reported earlier in this thesis, have demonstrated that the presence of the apamin-sensitive K^+ current (I_{KAS}) is more abundant in cardiac atrial cells rather than in normal ventricular cells (28, 200, 201, 203). Although, a study by Xu et al. showed that the block of the apamin-sensitive current at high $[Ca^{2+}]_i$ (500 nM) provoked a moderate APD_{90} lengthening in normal ventricle with apamin concentration as low as 50 pM (27). It is true that this block was much greater in atria, but it has to be considered that the stated $[Ca^{2+}]_i$ was only of 500 nM. Also, they showed a significantly higher apamin-sensitive current at 1000 nM, which could explain the presence of apamin effect in ventricle. Therefore, the question about the activation of ventricular SK current in this chamber at high $[Ca^{2+}]_i$ remained open. In this chapter, this suspect has been addressed by monitoring the $[Ca^{2+}]_i$ and the current simultaneously in single myocytes from rabbit left ventricle, which has never done before to study I_{SK}, using a selective and neutral compound: ICAGEN. Nevertheless, no effect was seen by either this SK blocker or the vehicle (DMSO) at the specific concentration of 1 µM with high measured $[Ca^{2+}]_i$ (0.7-1.2 µM). Unfortunately, due to time constraints it was not possible to perform these challenging experiments in atria.

7.6 Conclusion

Elevation in $[Ca^{2+}]_i$ was obtained, within physiological range, to values up to ~6 folds higher than in buffered $[Ca^{2+}]_i$ solutions previously used (chapter 5). ICA, at a concentration putatively selective for I_{SK}, failed to block either outward or inward current in rabbit left ventricular myocytes at high $[Ca^{2+}]_i$. Surprisingly, 10 µM ICA significantly, albeit partially, blocked $I_{Na/Ca}$, providing some insights into a possible non-selective effect of this compound, but leaving unexplained the APD_{70-90} prolongation observed in the previous chapter. However, these last results must be taken with caution given the low sample size. To conclude, (1) I_{SK} probably did not flow in non-failing ventricular myocytes in the presence of supra-physiological $[Ca^{2+}]_i$, and (2) ICA at high (x20 IC_{50} for I_{SK}) concentration may partially inhibit $I_{Na/Ca}$.

Chapter 8 General Discussion

8.1 Summary

The data presented in this thesis aimed to test the possibility that SK channels may be involved in mediating the link between intracellular calcium handling and cardiac repolarization under physiological conditions, in human and/or rabbit atrial myocytes. This was accomplished by focussing, for the first time to my knowledge in atrial cells, on precisely controlled $[Ca^{2+}]_i$ changes and their possible link with I_{SK} activation, using two I_{SK} blockers having different modes of action.

Initially, having validated my technique and established relevant positive controls, intracellular solutions with $[Ca^{2+}]_i$ precisely buffered and measured in cells, in the range of global diastolic-to-systolic values, were used during voltage-clamp experiments. I found that there was no effect of either SK blocker, apamin or ICA, on the I_{SK}-sensitive I-V curve, at any $[Ca^{2+}]_i$ with low pacing frequency.

Therefore, a second group of experiments involved recording action potentials, using higher pacing frequencies ranging from 1Hz to 3 Hz, intended to elevate $[Ca^{2+}]_i$ physiologically to systolic values sufficient to trigger I_{SK}. However, even under these conditions, the selective SK blocker ICA failed to alter the APD (measured at multiple levels of repolarisation) at any frequency tested, in either rabbit or human atrial myocytes. Nevertheless, ICA, at a concentration putatively non-selective for I_{SK} (10 µM), produced a significant, albeit moderate, APD increase at 1 Hz in rabbit atrial myocytes.

The last set of experiments utilised a specific protocol where $[Ca^{2+}]_i$ was progressively, transiently increased further, to supra physiological levels in ventricular cells, by repetitive stimulation of reverse-mode $I_{Na/Ca}$. Even at this high $[Ca^{2+}]_i$ ICA (1 µM) alone failed to reduce either outward or inward current, although the higher concentration of this blocker showed a significant reduction

of both outward and inward currents, as well as of peak $[Ca^{2+}]_i$ at -100 mV, likely by inhibiting $I_{Na/Ca}$.

8.2 Predictable pharmacological response as a positive control

The work outlined in the second chapter describes the development of a positive control and its verification which, as predicted, would be crucial in the study of I_{SK}. That chapter gives a detailed account of the whole-cell patch clamp technique, which the majority of the experiments are based on. The primary aim of chapter 2 was to validate the voltage protocol which was then used in I_{SK} studies and to provide a positive control, which was tested for temporal stability, timing and reversibility of a well-known pharmacological intervention. The results obtained served as a foundation for the subsequent studies on I_{SK}.

The magnitude of the current, I_{K1}, studied during this set of experiments to test the voltage protocol and the pharmacological response to barium, was expected to be greater than that of I_{SK}. By this means, the confirmation of the correct voltage/current measurements and the timing of response to the administration of a drug in my setup, was fundamental to validate any future result, especially when studying a current expected to be characterized by small amplitude, such I_{SK} (29).

The timing of the delay between the opening of the perfusion valve, which let the solution flow, and the effect of barium (i.e. when it reached the bath) on current, which was ~45 s, allowed me to create a timing profile for any intervention applied with that apparatus. This helped define the inclusion criteria for any deviation on the current trace in the next experiments, thus, avoiding misleading results.

In addition, the biological variability observed among current values in cardiomyocytes, isolated from the same chamber, indicates that even an expected large pharmacological effect can fail to occur in a small percentage of cells (7%). This can be extremely important during electrophysiological experiments with the patch-clamp technique, where the quality and fragility of the cells can further reduce the already low throughput. Therefore, considering

these aspects, the results obtained from the investigation of I_{SK} were deeply scrutinized to ensure high quality data.

8.3 I_{SK} is either non-existent or rare at systolic $[Ca^{2+}]_i$ in rabbit and human atrial myocytes

Given that SK channels are gated solely by intracellular Ca^{2+} ions and possess weak voltage sensitivity (27, 168, 320) the optimized voltage-pulse protocol, at high $[Ca^{2+}]_i$, allowed the investigation of I_{SK} among a wide range of membrane potentials at which I_{SK} should, in theory, be active.

However, the results obtained showed that both SK blockers, apamin or ICAGEN, failed to alter the I-V curve at any voltage studied, despite the presence of elevated $[Ca^{2+}]_i$ (0.3-0.5 µM), indicating that I_{SK} might not be active in human and rabbit atrial myocytes at $[Ca^{2+}]_i$ typical of global systolic values. Importantly, this was verified in statistically sound group sizes, at different drug concentrations, in both rabbit and human atrial cells. The results obtained in HEK293 cells (chapter 4) demonstrated that transfected SK channel $[Ca^{2+}]_i$ - sensitivity -at least for SK3 subtype- is increased at 35-37°C when compared to room temperature (22-23°C), and the $[Ca^{2+}]_i$ EC$_{50}$ at physiological temperature (0.39 ± 0.02 µM) confirmed that the atrial cell studies were conducted within an optimal $[Ca^{2+}]_i$ range for I_{SK} activation. Although comparison of these transfected I_{SK} data to freshly isolated mammalian atrial cardiomyocytes should be made with caution, the data certainly helped in the design of the atrial $[Ca^{2+}]_i$ - sensitivity experiments. Nonetheless, the present rabbit and human atrial findings are clearly in contrast with the majority of the literature, which shows significant effect of both blockers. For example, Xu et al., in early 2003 described a greater apamin-sensitive current in atria compared to ventricle in myocytes from both human and mouse tissues, which was blocked by concentration as low as 50pM of the peptide. This effect was seen at 500 nM $[Ca^{2+}]_i$ and the fraction of apamin-sensitive current increased along with $[Ca^{2+}]_i$ (up to 1µM) (27). Nevertheless, the results from my experiments at 500 nM $[Ca^{2+}]_i$ show no effect of the toxin on the I-V curve. The reason behind this difference is still not clear but could depend on the technique adopted. In my experiments the ruptured-patch clamp technique was used, while Xu et al. used perforated-patch clamp technique, during APs recordings, which prevents excessive dialysis

of the intracellular milieu and could better preserve calcium signalling (404, 405). Also, they used 2,3-butanedione monoxime (BDM) to inhibit cardiac contractility during the isolation (406-408). On the other hand, they did not measure $[Ca^{2+}]_i$ in cells, rather calculating this with titration software, and the recordings were performed at room temperature. Nevertheless, as mentioned before, apamin has been shown to have low efficacy in cardiac tissue (171, 209, 353), and a recent paper by Hancock, et al. suggests a population of heteromeric SK2-SK3 channels which are apamin-insensitive (366). However, they also show that a second population of apamin-sensitive homomeric SK2 channels are active, together with the heteromeric population, during whole-cell voltage clamp recordings (366), which contrasts with the findings described in this thesis. However, importantly, most of the publications, as described earlier, did not precisely measure $[Ca^{2+}]_i$ but rather inferred from calculation programs, which could lead to misleading results. By contrast, the present experiments had the strength of precisely measuring $[Ca^{2+}]_i$ in cells and verifying the concentration multiple times on the same apparatus and at the equivalent conditions used during current and APs recordings (chapter 3).

On the other hand, Nagy et al., in a study from 2009 that has already been cited within this work, decided to investigate I_{SK} under normal (non-AF-remodelled) conditions, based on the hypothesis that I_{SK} might contribute, along with the main repolarizing currents, to the APD adaptation governed by changes in $[Ca^{2+}]_i$ and/or calcium handling proteins (203, 409). However, under the experimental conditions used in this paper (described in Chapter 5) administration of high – dose apamin (100 nM) showed no effect at high $[Ca^{2+}]_i$ (supposed 900 nM) (203). However, these experiments were executed on canine and rat left ventricle, which leaves unsolved the possible outcomes in atria. Therefore, the work outlined in this thesis tried to answer this, confirming the absence of effect of apamin on the current in sinus rhythm cells (human) and rabbit left atrial myocytes under physiological conditions, which contrasts with most of the literature (27-30, 200, 201, 410).

More recently, Fan et al. showed reduced expression of SK channel proteins in patients with chronic AF compared to sinus rhythm, but upregulation of SK current. This last result, contrary to the previous data reported by Skibsbye

et al., has been justified through the increased SK channels $[Ca^{2+}]_i$ -sensitivity mainly due to CAMKII phosphorylation and $[Ca^{2+}]_i$ rise in AF (29, 30). Although this could explain in part my findings, implying the presence of a small -and possibly not detectable- I_{SK} current under normal conditions, Fan et al. as well as Skibsbye et al., showed also an apamin-sensitive current in sinus rhythm at $[Ca^{2+}]_i$ of 500 nM and 300 nM, respectively, which contrasts with the data showed in this thesis. If, on one hand, Fan et al. measured $[Ca^{2+}]_i$ in cells with fluorescent dyes, the use of a slow calcium buffer as EGTA does not ensure precise clamping of $[Ca^{2+}]_i$ compared to the much faster BAPTA, used in my solutions. On the other hand, Skibsbye et al. under unphysiological experimental conditions with high extracellular $[K^+]$ (20 mM, instead of ~5 mM), which might have increased I_{SK} amplitude, and $[Ca^{2+}]_i$ of 300 nM (calculated), showed a small yet significant effect of the SK blocker ICA (1 µM) compared to TMCs in atrial myocytes from sinus rhythm tissue (29). On the contrary, at any of the $[Ca^{2+}]_i$ used in the study presented in this thesis (Chapter 5) ICA showed no effect on the current at -115 mV (Fig. 5.8 and 5.9) in myocytes from both sinus rhythm patients and rabbit left atria.

It is worth to mention that an apamin-sensitive current might have been activated at 300 nM $[Ca^{2+}]_i$ at -115 mV in 6% of the cells studied. However, the effect was not reversable and of little amplitude, which led to the appropriately cautious conclusion that I_{SK} might be either non-existent or rare under physiological conditions in rabbit or human atrial cardiomyocytes, at $[Ca^{2+}]_i$ typical of global diastolic-to-systolic values.

8.4 I_{SK} does not contribute to atrial repolarization under physiological conditions

Apamin is considered the prototypical SK channel blocker, however, it has been shown to have negligible-if any- effect on action potential duration in both human and mouse atria (203, 365, 366). Furthermore, nanomolar concentrations of apamin have been shown to be effective in blocking Kv1.3 channels, which demonstrated lack of specificity of this peptide for SK channels, implying a possible overestimation of previously reported I_{SK} roles (359). On the other hand, a different SK channel inhibitor, ICAGEN, has been previously studied both in vivo and ex vivo, showing an antiarrhythmic effect by terminating and preventing

AF, induced either by acetylcholine (ACh) combined with burst pacing (196, 374) or electrical stimulation alone (197), and provoked APD prolongation in single cells from sinus rhythm patients (29). For this reason, the small molecule compound ICA was chosen for the studies presented in chapter 6. This molecule has been previously introduced, which acts equally on all SK channels subtypes and provides a selective inhibition although less powerfully compared to apamin.

In accordance with previous studies, SK channel inhibition by the direct block, can exert an anti-arrhythmic effect resulting from increased APD_{90} and a prolonged effective refractory period (ERP), which leads to increased wavelength and consequently protection against reentry (29, 197). Conversely, studies in rabbit failing ventricles have shown that inhibition of the apamin-sensitive current (I_{KAS}) induces EADs from areas of secondary $[Ca^{2+}]_i$ rise, implying that I_{SK} is important in maintaining the repolarization reserve (324). Therefore, in the present study APD_{90} was analysed as relevant to ERP and thus reentry (see page 212), in addition to APD_{70}, relevant to the AP plateau and thus EADs. Given the importance of EADs in the generation of ectopic foci and promotion of arrhythmias, monitoring APD_{70} was considered most appropriate to better investigate the role of I_{SK} in atrial APs. Nevertheless, ICA at an assumed selective concentration (1 µM) failed to alter action potential morphology in the atrial myocytes from humans and rabbits at pacing frequency of 1 Hz. Furthermore, ICA was tested at higher pacing frequency (2-3 Hz) intended to raise $[Ca^{2+}]_i$, but even under these conditions no effect was observed at any percentage level of repolarization in either human or rabbit. These results were rather unexpected and interesting, and potentially very important, thus warranting critique. The enzymatic dissociation process could have possibly caused an impairment of potassium channels, which might have generated action potential instability or attenuation of effect of the SK channel blocker. Nevertheless, the ex vivo experiments presented by Skibsbye et al. described similar isolation procedures, which involved the use of the "chunk method" and the same type of enzymes were used (collagenase and protease). It is worth to mention that they supplemented the storage solutions with 2,3 - butanedione monoxime (BDM) (29, 411), contrary to the solutions used here. However, BDM (used during rabbit cell isolation process) was tested in a small number of cells (n=5 cells, n=2 rabbits Fig. 5.16) in voltage clamp experiments (chapter 5) as a possible condition for

apamin effect, but no significant difference was observed. Another possible reason for the difference between the studies could reside in the presence of an unphysiological [K^+] in the solution, used by Skibsbye et al., which could have augmented I_{SK} and made it detectable in atrial myocytes from sinus rhythm tissue (29). Skibsbye et al. also showed an indirect inhibition of Na^+ channels due to the depolarization of resting membrane potential (RMP) exerted by ICA (29). This was not observed in the present experiments as well as absence of effect on V_{max} (surrogate of I_{Na}), and so is unlikely to be having its anti-arrhythmic effect by inhibiting spiral wave reentry (see page 16, chapter 1), contrary to what was described by Skibsbye et al., in a later study (197).

In the present experiments, ICA at a higher concentration (10 μM) provoked a significant prolongation of both APD_{70} and APD_{90}. These results are in accordance with previous findings (29) which also report the inability to reverse the drug effect by wash. Nevertheless, since a minor inhibitory effect has been reported on I_{TO} (IC_{50} = 21 μM) a possible non-selective effect of ICA cannot be ruled out. In addition, the selectivity profile of ICA did not include a study of $I_{Na/Ca}$. In the last set of experiments (described in chapter 7) I used $I_{Na/Ca}$ as a means to increase [Ca^{2+}]$_i$ to high levels, and this also provided an opportunity to study effects of ICA on $I_{Na/Ca}$.

8.5 I_{SK} is non-existent in rabbit ventricle

During the replication of the protocol (chapter 7) that was originally utilised by Weber et al. to study the allosteric regulation of the Na^+/Ca^{2+} - exchanger (NCX) (382), the current was monitored simultaneously to the [Ca^{2+}]$_i$, which reached values up to 2.8 μM in the present study, through the repetitive stimulation of reverse-mode $I_{Na/Ca}$. The supra-physiological global levels of peak [Ca^{2+}]$_i$ obtained with very low buffering power (0.01 mM EGTA) were aimed to elicit I_{SK}, since previous clamped or rate-dependently increased [Ca^{2+}]$_i$ have been demonstrated unsuccessful. The replication of the protocol was done firstly in ventricular cells, the cell type used in the original study, for optimization. Throughout this set of experiments, due to the controlled conditions, many currents were either blocked or not present consequent to the absence of potassium in the solutions. During these studies 10 μM ICA was tested on $I_{Na/Ca}$ (virtually the only flowing current) and compared to the selective $I_{Na/Ca}$ blocker,

NiCl$_2$ (10mM). I found that ICA significantly reduced both outward and inward current at +100 and -100 mV, respectively, in these ventricular cells. The reduction of peak [Ca^{2+}]$_i$ (significant only at -100 mV) along with the current, leave space for speculation of a possible effect of ICA, administrated at this high concentration, on I$_{Na/Ca}$. The block provided by ICA was similar to that of NiCl$_2$ (10mM, selective for NCX), supporting the hypothesis that ICA may affect I$_{Na/Ca}$, thus potentially relevant to APD modulation. It was verified that a portion of current, insensitive to ICA but NiCl$_2$-sensitive, was present and the difference was significant. Thus, albeit partial, it has been speculated that there is a possible inhibitory activity on I$_{Na/Ca}$ by ICA (10 μM) which however cannot account for the APD prolongation at physiological [Na$^+$]$_i$ as observed in rabbit atrial myocytes. In fact, I$_{Na/Ca}$ is considered to generate an inward, depolarising, current for most of the AP, accompanied by calcium efflux (forward-mode), thus, the block of this current is expected to produce an APD shortening rather than prolongation (396, 412), indicating that the APD$_{90}$-prolongation by 10 μM ICA in the atrial cells must have been by affecting another current. The IC$_{50}$ values of ICA for different currents presented by Skibsbye et al., demonstrated the specificity of this compound for I$_{SK}$, albeit it could provoke the inhibition of some currents at higher concentrations (i.e. 10 μM). In the paper, it has been described a minor inhibitory effect on I$_{TO}$ (IC$_{50}$= 21 μM) and I$_{K1}$ (IC$_{50}$> 100 μM), but no effect on other tested currents (29). Thus, given the results presented in this thesis, ICA 10 μM could exert an inhibitory effect on other currents other than I$_{SK}$, as previously described (see page 215), which opens the possibility that its effect on action potential morphology could have been misinterpreted in some previous studies.

In addition, and in part mentioned earlier, I$_{SK}$ could, in theory, exert a protective action against AF by negating the generation of afterdepolarizations resulting from spontaneous calcium release, since this repolarizing current is triggered by calcium and can oppose the focal activity. In a recent study by Peñaranda et al., performed through several mathematical models, the results were not clear whether I$_{SK}$ counteracts these abnormal depolarizations by opposing the activity of I$_{Na/Ca}$ or reducing the membrane potential elevation (413). The first hypothesis implies a negative-feedback mechanism played by I$_{SK}$ to oppose the forward-mode I$_{Na/Ca}$, which intruding Ca^{2+} could augment I$_{SK}$ that

might abolish extra depolarization. This mechanism is in accordance with previous findings, which show a pro-arrhythmic effect of I_{SK} inhibition by apamin in rabbit ventricles (324). Interestingly, Armoundas et al. demonstrated that $I_{Na/Ca}$ possesses a significant repolarizing force starting from $[Na^+]_i$ of 10 mM, through reverse-mode $I_{Na/Ca}$. This contribution to repolarization could increase in failing ventricles characterized by high $[Na^+]_i$ (395). On the other hand, I_{SK} has been shown to be increased in failing human ventricles, contrary to all other known K^+ currents, along with its Ca^{2+}-sensitivity and protein expression (305, 343). Therefore, it seems plausible that blocking either $I_{Na/Ca}$ or I_{SK}, under certain conditions in ventricles, could produce APD prolongation. However, considering the reduction of $I_{Na/Ca}$ obtained by acute superfusion with 10 μM ICA (i.e. 20x IC_{50} for I_{SK}), it become difficult to understand the reason behind APD prolongation in APs experiments previously presented. In order to answer this question, firstly ICA was tested at selective concentration (i.e. 1 μM; 2x IC_{50} for I_{SK}) in rabbit ventricles, where physiological $[K^+]$ were used and compared to $NiCl_2$. If on one hand $NiCl_2$ still blocked significantly both outward and inward currents along with peak $[Ca^{2+}]_i$, under these new conditions (i.e. K^+ currents restored) along with the presence of supra-physiological peak $[Ca^{2+}]_i$ ICA (1 μM; should be selective for I_{SK}) failed to alter either currents or $[Ca^{2+}]_i$ in ventricle. Thus, confirming the absence of effect of this SK blocker on $I_{Na/Ca}$ (at 1 μM) and the already established minor role played by I_{SK} in ventricle under physiological conditions (27-29, 203). In fact, the presence of this current has been shown only in failing ventricle due to remodelling, channel overexpression and increased $[Ca^{2+}]_i$-sensitivity. The fact that I_{SK} was confirmed to be absent in ventricle under physiological conditions, also during extremely elevated $[Ca^{2+}]_i$, indicates that in order to obtain a possible contribution of this current to repolarization, with all the consequent protective effects hypothesized by some studies in failing rabbit ventricles (i.e. prevent the occurrence of EADs, premature ventricle beats and torsade de pointes) (306, 324, 414), the elevation of $[Ca^{2+}]_i$ is not sufficient. More likely, for I_{SK} to play a role in failing ventricle it requires upregulation of I_{SK} along with increased I_{SK} sensitivity to $[Ca^{2+}]_i$ caused by remodelling during heart failure (HF).

In conclusion, it seems plausible that the slight, yet significant, APD prolongation observed with 10 μM ICA, in the experiments outlined in chapter 6,

could be due to partial block of a different K^+ current rather than I_{SK} inhibition. Finally, ICA at higher, putatively non-selective concentration appears to provide a significant block of $I_{Na/Ca}$ which, albeit limited by low sample size, can be considered a novel finding and will require further investigation.

8.6 Clinical implication

The results reported in this thesis concerning the absence of I_{SK} at any $[Ca^{2+}]_i$ and condition tested could be considered as rather discouraging from an atrial and AF targeting therapy perspective, but is, nevertheless, extremely important to know. All the experiments were conducted under physiological conditions, as well as with elevated $[Ca^{2+}]_i$, which suggests that the activation of this current may require phenotype remodelling due to pathological conditions, such as chronic AF. On the other hand, calcium handling during early-onset AF could be especially relevant to this work, since only acute remodelling with AP abbreviation has occurred and the increase in atrial rate along with the substantial influx of Ca^{2+} through I_{Ca} at each action potential (84), could increase SK current flow during APs. However, given the findings herein reported (with stimulation rates of up to 180 bpm for up to 2 mins), it appears that a pharmacological treatment involving the targeting of these channels under elevated $[Ca^{2+}]_i$ is not feasible to obtain an APD prolongation and, therefore, possible termination of acute, low rate, AF. Moreover, as already mentioned, the pro-or antiarrhythmic role of SK channels is not clear. For example, a study reported APD prolongation in atrial myocytes in vitro and inducible atrial fibrillation in vivo using a SK knock-out mouse model (200). Similar results, including APD heterogeneity, were observed in canine left atrium (325). These studies suggest a protective role against AF played by I_{SK}, showing an increased occurrence of EADs, electrical alternans and wave breaks, as well as increased APD heterogeneity, following I_{SK} blockade. In agreement with these hypotheses, it has been reported a reduction in SK current and channel expression in human atrial tissue from patients with chronic AF (29, 211). On the contrary, some studies have described increased SK current in patients with persistent AF, although reduced SK channel expression (30, 213). Moreover, many publications demonstrate reduced AF-inducibility in either remodelled atria (after 7-day atrial tachypacing) (202) or in an acute pacing-induced model of AF by aERP prolongation and termination of AF with common selective SK blockers (including

ICA) or negative modulators (196, 209, 210). Apparently, SK channels seem to participate differently to short-or long term AF, but the mechanisms remain obscure. In fact, as previously hypothesised, an initial up-regulation of these channels could represent the trigger for an arrhythmic event and participate in maintenance of reentries (201). While during long term AF these channels could undergo extensive structural and electrical remodelling losing their possible protective effect and promoting the perpetuation of the arrhythmias. Moreover, the documented reduced SK channel expression could prevent the possibility to use these channels as a therapeutic target. On the other hand, if SK channels were to participate in atrial repolarisation during recent onset AF (i.e. non-remodelled atria), their inhibition could provoke APD prolongation, but at the same time promote afterdepolarizations, which make a therapy targeting these channels also not suitable under these pathological condition.

Finally, it is well-known that forms of persistent AF become increasingly difficult to treat using currently available pharmacological alternatives. Most of the approved antiarrhythmic drugs, as already mentioned, showed low success rate in converting AF (415, 416), besides known side effects, especially in patients suffering from heart failure, which limits their use as a therapeutic option. Therefore, the demand for antiarrhythmic drugs with a higher efficacy and safer profile is high. Although I_{SK} could appear as a promising new atrial-selective target for treatment of AF, avoiding fatal ventricular proarrhythmic effects, again the controversy in the literature about its role and the results herein presented, leave doubts concerning its potential utility.

It can be concluded that, given the extensive discrepancies between the existing publications, in addition to the present results, which show absence of I_{SK} under elevated $[Ca^{2+}]_i$ typical of short term AF condition, in contrast with most of the literature, I_{SK} block as a pharmacological treatment might not be as promising as expected.

8.7 Limitations

The experiments described within this work represents a further step into the investigation of I_{SK} in single cells from rabbit and human tissue. However, there are inherent and theoretical limitations in performing studies using such cells.

The availability and quality of human atrial tissue is a fundamental variable that cannot easily be controlled. The cardiac tissue can be obtained only at the time of cardiac surgery, where a small tip of the right atrial appendage is suitable to be excised and the consent from the patient has been previously acquired. Furthermore, the sample of tissue is of small dimensions (weight: 0.25 ± 0.02 g), which usually allows the isolation of relatively few (compared to rabbit) atrial cells, per tissue. Also, the patients are frequently affected by confounding comorbidities and pharmacological therapies, in addition to the effects of age and gender which can potentially complicate the applicability of some experimental results.

As aforementioned, the chunk method of enzymatic dissociation process could possibly result in action potential instability or drug effect attenuation, in addition to recognised delivery of cells which are depolarised. However, the rabbit atrial cells were not isolated by the chunk method, showing similar results, thus suggesting that the different cell dissociation methods might not be implicated in the absence of I_{SK}. Furthermore, during ruptured patch clamp technique, which is more straightforward technically than perforated patch, the lifetime of cells is limited, and prolonged recording protocols are difficult to be maintained, and intracellular signalling more likely to be disrupted. This is true especially under the experimental conditions used during the majority of these experiments, characterized by constant or transient presence of high $[Ca^{2+}]_i$. Moreover, myocytes from AF patients were not studied, given the difficulty of reaching an acceptable sample size due to the rarity of operation involving patients with such condition. Tissues from AF patients would have been extremely useful to investigate the possible effect of remodelling on I_{SK} in atria, which however was not the purpose of this work. In addition, controversy exists between electrophysiological studies on myocytes from cAF tissue, which suggests that patch clamp technique may not be the best tool to address this matter. Furthermore, hypothesis were made regarding the necessity to apply supra-physiological stimulation rates higher than 180 bpm achieved in the present experiments (AF can have rates of 300-600 bpm). Also, the duration of these bursts was no longer than 2 mins which may not be sufficient to activate I_{SK} (201) and cannot be increased much during whole-cell patch clamp, due to the limited lifetime of cells after rupture. Finally, cells might require more time

of perfusion with ICA for the I_{SK} block to be detectable. However, the effect observed following application of a higher concentration of ICA (10 μM) was in the order of seconds (from ~30 to 60s), which strengthen the results obtained throughout this work. Notably, as deeply described in section 8.2, possibilities remain regarding the detection of I_{SK} exclusively under controlled conditions, i.e. artificially adjusted solutions or questionable $[Ca^{2+}]_i$, which do not accurately resemble physiological conditions and were, therefore, not considered for the present project.

Importantly, in this study the wash out of the drugs could not be attained. However, specifically, for ICAGEN TMCs were used to prove the stability and strength of the recordings. In addition, inconsistency in SK channel expression among different tissues have been reported. For example, it has been shown that intermittent burst pacing in rabbit pulmonary vein region, results in locally APD shortening due to the trafficking of SK2 channel to the membrane (201). Moreover, in a relatively recent publication, SK2 subunit expression and SK current have been shown to be greater in canine PV versus LA. Therefore, since the present study involved experimentation on myocytes from human right atrial and rabbit left atrial tissue regional differences cannot be ruled out.

8.8 Future work

Despite more than a decade of research, the role of SK channels in cardiac electrophysiology remains incompletely understood. As discussed, many studies performed in normal atrium in both animal and human tissue, have been conflicting regarding the effective functional contribution of SK channels to atrial repolarization under physiological conditions, which continue to be central to the debate.

The present experiments were primarily focused on ensuring elevation of $[Ca^{2+}]_i$, considered necessary and sufficient for I_{SK} activation. However, in view of the results from $[Ca^{2+}]_i$ measurements, this statement appears to be not true during physiological conditions. By this means, the data obtained strongly supports the possibility that particular pathological conditions may be required, such as electrical remodelling, changes in SK channel expression or increased SK

channel Ca^{2+}-sensitivity resulted in different and contrasting outcomes (29, 30, 211, 212, 305).

The uncertainties regarding SK channels are numerous, including whether their expression is up- or down-regulated in patients diagnosed with cAF and whether these channels are more relevant to early stage (onset) or chronic AF is still unknown. Therefore, the question about the possibility of targeting these channels as a novel treatment for AF, with little or no effect on ventricle, remains open.

It is true that the last described protocol (in which $[Ca^{2+}]_i$ was increased by stimulating reverse mode $I_{Na/Ca}$; though limited to ventricular cells by time constraints) could represent a promising future method to further investigate I_{SK} activation at extremely high $[Ca^{2+}]_i$ in atrial myocytes with the whole-cell patch clamp technique. Nevertheless, with the substantial data obtained here, from the large number of well validated experiments described, using physiological recording conditions, different drug types and concentrations, and atrial cells from two different species including, importantly, human, it can be concluded that I_{SK} is either rare or non-existent at $[Ca^{2+}]_i$ of global systolic or supra-physiological values in myocytes from either human or rabbit atrial tissue.

8.9 References

1.   Wakili R, Voigt N, Kääb S, Dobrev D, Nattel S. Recent advances in the molecular pathophysiology of atrial fibrillation. J Clin Invest. 2011;121(8):2955-68.
2.   Bers DM. Cardiac excitation-contraction coupling. Nature. 2002;415(6868):198-205.
3.   Ackerman MJ, Clapham DE. Ion Channels — Basic Science and Clinical Disease. New England Journal of Medicine. 1997;336(22):1575-86.
4.   Kachel HS, Buckingham SD, Sattelle DB. Insect toxins - selective pharmacological tools and drug/chemical leads. Curr Opin Insect Sci. 2018;30:93-8.
5.   Bartos DC, Grandi E, Ripplinger CM. Ion Channels in the Heart. Compr Physiol. 2015;5(3):1423-64.
6.   Workman AJ, Kane KA, Rankin AC. Cellular bases for human atrial fibrillation. Heart Rhythm. 2008;5(6 Suppl):S1-6.
7.   Grynkiewicz G, Poenie M, Tsien RY. A new generation of Ca2+ indicators with greatly improved fluorescence properties. J Biol Chem. 1985;260(6):3440-50.
8.   Nattel S, Burstein B, Dobrev D. Atrial remodelling and atrial fibrillation: mechanisms and implications. Circ Arrhythm Electrophysiol. 2008;1(1):62-73.
9.   Tsien RY, Harootunian AT. Practical design criteria for a dynamic ratio imaging system. Cell Calcium. 1990;11(2-3):93-109.
10.   Schmitt N, Grunnet M, Olesen SP. Cardiac potassium channel subtypes: new roles in repolarization and arrhythmia. Physiol Rev. 2014;94(2):609-53.
11.   Comtois P, Kneller J, Nattel S. Of circles and spirals: bridging the gap between the leading circle and spiral wave concepts of cardiac reentry. Europace. 2005;7 Suppl 2:10-20.
12.   Quinn FR, Currie S, Duncan AM, Miller S, Sayeed R, Cobbe SM, et al. Myocardial infarction causes increased expression but decreased activity of the myocardial Na+-Ca2+ exchanger in the rabbit. J Physiol. 2003;553(Pt 1):229-42.
13.   Hucker WJ, Sharma V, Nikolski VP, Efimov IR. Atrioventricular conduction with and without AV nodal delay: two pathways to the bundle of His in the rabbit heart. Am J Physiol Heart Circ Physiol. 2007;293(2):H1122-30.
14.   Nattel S. New ideas about atrial fibrillation 50 years on. Nature. 2002;415(6868):219-26.
15.   Xu H, Guo W, Nerbonne JM. Four kinetically distinct depolarization-activated K+ currents in adult mouse ventricular myocytes. J Gen Physiol. 1999;113(5):661-78.
16.   Li GR, Feng J, Yue L, Carrier M, Nattel S. Evidence for two components of delayed rectifier K+ current in human ventricular myocytes. Circ Res. 1996;78(4):689-96.
17.   Shibata EF, Drury T, Refsum H, Aldrete V, Giles W. Contributions of a transient outward current to repolarization in human atrium. Am J Physiol. 1989;257(6 Pt 2):H1773-81.
18.   Perez-Reyes E. Molecular physiology of low-voltage-activated t-type calcium channels. Physiol Rev. 2003;83(1):117-61.
19.   Lee KS, Marban E, Tsien RW. Inactivation of calcium channels in mammalian heart cells: joint dependence on membrane potential and intracellular calcium. J Physiol. 1985;364:395-411.
20.   Sanguinetti MC, Jurkiewicz NK. Two components of cardiac delayed rectifier K+ current. Differential sensitivity to block by class III antiarrhythmic agents. J Gen Physiol. 1990;96(1):195-215.

21. Sanguinetti MC, Jurkiewicz NK. Delayed rectifier outward K+ current is composed of two currents in guinea pig atrial cells. Am J Physiol. 1991;260(2 Pt 2):H393-9.

22. Roden DM. Taking the "idio" out of "idiosyncratic": predicting torsades de pointes. Pacing Clin Electrophysiol. 1998;21(5):1029-34.

23. Ibarra J, Morley GE, Delmar M. Dynamics of the inward rectifier K+ current during the action potential of guinea pig ventricular myocytes. Biophys J. 1991;60(6):1534-9.

24. Hashimoto N, Yamashita T, Tsuruzoe N. Tertiapin, a selective IKACh blocker, terminates atrial fibrillation with selective atrial effective refractory period prolongation. Pharmacol Res. 2006;54(2):136-41.

25. Dobrev D, Friedrich A, Voigt N, Jost N, Wettwer E, Christ T, et al. The G protein-gated potassium current I(K,ACh) is constitutively active in patients with chronic atrial fibrillation. Circulation. 2005;112(24):3697-706.

26. Olson TM, Alekseev AE, Liu XK, Park S, Zingman LV, Bienengraeber M, et al. Kv1.5 channelopathy due to KCNA5 loss-of-function mutation causes human atrial fibrillation. Hum Mol Genet. 2006;15(14):2185-91.

27. Xu Y, Tuteja D, Zhang Z, Xu D, Zhang Y, Rodriguez J, et al. Molecular identification and functional roles of a Ca(2+)-activated K+ channel in human and mouse hearts. J Biol Chem. 2003;278(49):49085-94.

28. Tuteja D, Xu D, Timofeyev V, Lu L, Sharma D, Zhang Z, et al. Differential expression of small-conductance Ca2+-activated K+ channels SK1, SK2, and SK3 in mouse atrial and ventricular myocytes. Am J Physiol Heart Circ Physiol. 2005;289(6):H2714-23.

29. Skibsbye L, Poulet C, Diness JG, Bentzen BH, Yuan L, Kappert U, et al. Small-conductance calcium-activated potassium (SK) channels contribute to action potential repolarization in human atria. Cardiovasc Res. 2014;103(1):156-67.

30. Fan X, Yu Y, Lan H, Ou X, Yang L, Li T, et al. Ca2+/Calmodulin-Dependent Protein Kinase II (CaMKII) Increases Small-Conductance Ca2+-Activated K+ Current in Patients with Chronic Atrial Fibrillation. Med Sci Monit. 2018;24:3011-23.

31. Bers DM. Excitation–Contraction Coupling and Cardiac Contractile Force. 2nd ed. Kluwer Academic, Dordrecht, Netherlands2001.

32. Peterson BZ, DeMaria CD, Adelman JP, Yue DT. Calmodulin is the Ca2+ sensor for Ca2+ -dependent inactivation of L-type calcium channels. Neuron. 1999;22(3):549-58.

33. Einthoven W. Le telecardiogramme. [French]. A*rch. Int. Physiol.* 1906. p. 132–64

34. Lewis T. REPORT CXIX. AURICULAR FIBRILLATION: A COMMON CLINICAL CONDITION. Br Med J. 1909;2(2552):1528.

35. Rich MW. Epidemiology of atrial fibrillation. J Interv Card Electrophysiol. 2009;25(1):3-8.

36. Miyasaka Y, Barnes ME, Bailey KR, Cha SS, Gersh BJ, Seward JB, et al. Mortality trends in patients diagnosed with first atrial fibrillation: a 21-year community-based study. J Am Coll Cardiol. 2007;49(9):986-92.

37. Nattel S. Basic electrophysiology of the pulmonary veins and their role in atrial fibrillation: precipitators, perpetuators, and perplexers. J Cardiovasc Electrophysiol. 2003;14(12):1372-5.

38. Haïssaguerre M, Jaïs P, Shah DC, Takahashi A, Hocini M, Quiniou G, et al. Spontaneous initiation of atrial fibrillation by ectopic beats originating in the pulmonary veins. N Engl J Med. 1998;339(10):659-66.

39. Pedersen OD, Abildstrøm SZ, Ottesen MM, Rask-Madsen C, Bagger H, Køber L, et al. Increased risk of sudden and non-sudden cardiovascular death in patients

with atrial fibrillation/flutter following acute myocardial infarction. Eur Heart J. 2006;27(3):290-5.

40.   Benjamin EJ, Wolf PA, D'Agostino RB, Silbershatz H, Kannel WB, Levy D. Impact of atrial fibrillation on the risk of death: the Framingham Heart Study. Circulation. 1998;98(10):946-52.

41.   Hart RG, Pearce LA, Rothbart RM, McAnulty JH, Asinger RW, Halperin JL. Stroke with intermittent atrial fibrillation: incidence and predictors during aspirin therapy. Journal of the American College of Cardiology. 2000;35(1):183.

42.   Hart Robert G, Halperin Jonathan L. Atrial Fibrillation and Stroke. Stroke. 2001;32(3):803-8.

43.   Sandercock P, Bamford J, Dennis M, Burn J, Slattery J, Jones L, et al. Atrial fibrillation and stroke: prevalence in different types of stroke and influence on early and long term prognosis (Oxfordshire community stroke project). British Medical Journal. 1992;305(6867):1460.

44.   Gustafsson C, Britton M. Pathogenetic mechanism of stroke in non-valvular atrial fibrillation: follow-up of stroke patients with and without atrial fibrillation. Journal of Internal Medicine. 1991;230(1):11-6.

45.   Broderick JP, Phillips SJ, O'Fallon WM, Frye RL, Whisnant JP. Relationship of cardiac disease to stroke occurrence, recurrence, and mortality. Stroke. 1992;23(9):1250-6.

46.   Candelise L, Pinardi G, Morabito A. Mortality in acute stroke with atrial fibrillation. The Italian Acute Stroke Study Group. Stroke. 1991;22(2):169-74.

47.   Wolf PA, Kannel WB, McGee DL, Meeks SL, Bharucha NE, McNamara PM. Duration of atrial fibrillation and imminence of stroke: the Framingham study. Stroke. 1983;14(5):664-7.

48.   Friedman PJ. Atrial fibrillation after stroke in the elderly. Stroke. 1991;22(2):209-14.

49.   Censori B, Camerlingo M, Casto L, Ferraro B, Gazzaniga GC, Cesana B, et al. Prognostic factors in first-ever stroke in the carotid artery territory seen within 6 hours after onset. Stroke. 1993;24(4):532-5.

50.   Gallagher JJ. Tachycardia and cardiomyopathy: the chicken-egg dilemma revisited. J Am Coll Cardiol. 1985;6(5):1172-3.

51.   Fenelon G, Wijns W, Andries E, Brugada P. Tachycardiomyopathy: mechanisms and clinical implications. Pacing Clin Electrophysiol. 1996;19(1):95-106.

52.   Shinbane JS, Wood MA, Jensen DN, Ellenbogen KA, Fitzpatrick AP, Scheinman MM. Tachycardia-induced cardiomyopathy: a review of animal models and clinical studies. J Am Coll Cardiol. 1997;29(4):709-15.

53.   Nattel S. Atrial electrophysiology and mechanisms of atrial fibrillation. J Cardiovasc Pharmacol Ther. 2003;8 Suppl 1:S5-11.

54.   Lévy S, Sbragia P. [Remodelling in atrial fibrillation]. Arch Mal Coeur Vaiss. 2005;98(4):308-12.

55.   Lévy S. Factors predisposing to the development of atrial fibrillation. Pacing Clin Electrophysiol. 1997;20(10 Pt 2):2670-4.

56.   Nattel S, Shiroshita-Takeshita A, Brundel BJ, Rivard L. Mechanisms of atrial fibrillation: lessons from animal models. Prog Cardiovasc Dis. 2005;48(1):9-28.

57.   Wit AL, Boyden PA. Triggered activity and atrial fibrillation. Heart Rhythm. 2007;4(3 Suppl):S17-23.

58.   Workman AJ, Marshall GE, Rankin AC, Smith GL, Dempster J. Transient outward K+ current reduction prolongs action potentials and promotes afterdepolarisations: a dynamic-clamp study in human and rabbit cardiac atrial myocytes. J Physiol. 2012;590(17):4289-305.

59.   Levin MD, Lu MM, Petrenko NB, Hawkins BJ, Gupta TH, Lang D, et al. Melanocyte-like cells in the heart and pulmonary veins contribute to atrial arrhythmia triggers. J Clin Invest. 2009;119(11):3420-36.

60.   Ehrlich JR, Cha TJ, Zhang L, Chartier D, Melnyk P, Hohnloser SH, et al. Cellular electrophysiology of canine pulmonary vein cardiomyocytes: action potential and ionic current properties. J Physiol. 2003;551(Pt 3):801-13.

61.   Volders PG, Vos MA, Szabo B, Sipido KR, de Groot SH, Gorgels AP, et al. Progress in the understanding of cardiac early afterdepolarizations and torsades de pointes: time to revise current concepts. Cardiovasc Res. 2000;46(3):376-92.

62.   Antzelevitch C, Sicouri S. Clinical relevance of cardiac arrhythmias generated by afterdepolarizations. Role of M cells in the generation of U waves, triggered activity and torsade de pointes. J Am Coll Cardiol. 1994;23(1):259-77.

63.   el-Sherif N, Zeiler RH, Craelius W, Gough WB, Henkin R. QTU prolongation and polymorphic ventricular tachyarrhythmias due to bradycardia-dependent early afterdepolarizations. Afterdepolarizations and ventricular arrhythmias. Circ Res. 1988;63(2):286-305.

64.   Burashnikov A, Antzelevitch C. Reinduction of atrial fibrillation immediately after termination of the arrhythmia is mediated by late phase 3 early afterdepolarization-induced triggered activity. Circulation. 2003;107(18):2355-60.

65.   Kettlewell S, Saxena P, Dempster J, Colman MA, Myles RC, Smith GL, et al. Dynamic clamping human and rabbit atrial calcium current: narrowing ICaL window abolishes early afterdepolarizations. The Journal of Physiology. 2019;597(14):3619-38.

66.   Choi BR, Burton F, Salama G. Cytosolic Ca2+ triggers early afterdepolarizations and Torsade de Pointes in rabbit hearts with type 2 long QT syndrome. J Physiol. 2002;543(Pt 2):615-31.

67.   Zygmunt AC, Goodrow RJ, Weigel CM. INaCa and ICl(Ca) contribute to isoproterenol-induced delayed after depolarizations in midmyocardial cells. Am J Physiol. 1998;275(6):H1979-92.

68.   Guinamard R, Chatelier A, Demion M, Potreau D, Patri S, Rahmati M, et al. Functional characterization of a Ca(2+)-activated non-selective cation channel in human atrial cardiomyocytes. J Physiol. 2004;558(Pt 1):75-83.

69.   Burashnikov A, Antzelevitch C. Late-phase 3 EAD. A unique mechanism contributing to initiation of atrial fibrillation. Pacing Clin Electrophysiol. 2006;29(3):290-5.

70.   Weiss JN, Garfinkel A, Karagueuzian HS, Chen PS, Qu Z. Early afterdepolarizations and cardiac arrhythmias. Heart Rhythm. 2010;7(12):1891-9.

71.   Allessie MA, Bonke FI, Schopman FJ. Circus movement in rabbit atrial muscle as a mechanism of tachycardia. III. The "leading circle" concept: a new model of circus movement in cardiac tissue without the involvement of an anatomical obstacle. Circ Res. 1977;41(1):9-18.

72.   Allessie MA, Bonke FI, Schopman FJ. Circus movement in rabbit atrial muscle as a mechanism of trachycardia. Circ Res. 1973;33(1):54-62.

73.   Kléber AG, Rudy Y. Basic mechanisms of cardiac impulse propagation and associated arrhythmias. Physiol Rev. 2004;84(2):431-88.

74.   Wijffels MC, Dorland R, Mast F, Allessie MA. Widening of the excitable gap during pharmacological cardioversion of atrial fibrillation in the goat: effects of cibenzoline, hydroquinidine, flecainide, and d-sotalol. Circulation. 2000;102(2):260-7.

75.   Kneller J, Kalifa J, Zou R, Zaitsev AV, Warren M, Berenfeld O, et al. Mechanisms of atrial fibrillation termination by pure sodium channel blockade in an ionically-realistic mathematical model. Circ Res. 2005;96(5):e35-47.

76.   Bjerkelund C, Orning OM. An evaluation of DC shock treatment of atrial arrhythmias. Acta Med Scand. 1968;184(6):481-91.

77.   Wijffels MC, Kirchhof CJ, Dorland R, Allessie MA. Atrial fibrillation begets atrial fibrillation. A study in awake chronically instrumented goats. Circulation. 1995;92(7):1954-68.

78.   Attuel P, Childers R, Cauchemez B, Poveda J, Mugica J, Coumel P. Failure in the rate adaptation of the atrial refractory period: its relationship to vulnerability. Int J Cardiol. 1982;2(2):179-97.

79.   Workman AJ, Kane KA, Rankin AC. The contribution of ionic currents to changes in refractoriness of human atrial myocytes associated with chronic atrial fibrillation. Cardiovasc Res. 2001;52(2):226-35 **.

80.   Yue L, Feng J, Gaspo R, Li GR, Wang Z, Nattel S. Ionic remodelling underlying action potential changes in a canine model of atrial fibrillation. Circ Res. 1997;81(4):512-25.

81.   Van Wagoner DR, Pond AL, Lamorgese M, Rossie SS, McCarthy PM, Nerbonne JM. Atrial L-type Ca2+ currents and human atrial fibrillation. Circ Res. 1999;85(5):428-36.

82.   Konings KT, Smeets JL, Penn OC, Wellens HJ, Allessie MA. Configuration of unipolar atrial electrograms during electrically induced atrial fibrillation in humans. Circulation. 1997;95(5):1231-41.

83.   Jalife J. Déjà vu in the theories of atrial fibrillation dynamics. Cardiovasc Res. 2011;89(4):766-75.

84.   Sun H, Chartier D, Leblanc N, Nattel S. Intracellular calcium changes and tachycardia-induced contractile dysfunction in canine atrial myocytes. Cardiovasc Res. 2001;49(4):751-61.

85.   Courtemanche M, Ramirez RJ, Nattel S. Ionic mechanisms underlying human atrial action potential properties: insights from a mathematical model. Am J Physiol. 1998;275(1):H301-21.

86.   Lai LP, Su MJ, Lin JL, Lin FY, Tsai CH, Chen YS, et al. Down-regulation of L-type calcium channel and sarcoplasmic reticular Ca(2+)-ATPase mRNA in human atrial fibrillation without significant change in the mRNA of ryanodine receptor, calsequestrin and phospholamban: an insight into the mechanism of atrial electrical remodelling. J Am Coll Cardiol. 1999;33(5):1231-7.

87.   Morillo CA, Klein GJ, Jones DL, Guiraudon CM. Chronic rapid atrial pacing. Structural, functional, and electrophysiological characteristics of a new model of sustained atrial fibrillation. Circulation. 1995;91(5):1588-95.

88.   Ausma J, Wijffels M, Thoné F, Wouters L, Allessie M, Borgers M. Structural changes of atrial myocardium due to sustained atrial fibrillation in the goat. Circulation. 1997;96(9):3157-63.

89.   Goette A, Honeycutt C, Langberg JJ. Electrical remodelling in atrial fibrillation. Time course and mechanisms. Circulation. 1996;94(11):2968-74.

90.   Schotten U, Duytschaever M, Ausma J, Eijsbouts S, Neuberger HR, Allessie M. Electrical and contractile remodelling during the first days of atrial fibrillation go hand in hand. Circulation. 2003;107(10):1433-9.

91.   Shapiro EP, Effron MB, Lima S, Ouyang P, Siu CO, Bush D. Transient atrial dysfunction after conversion of chronic atrial fibrillation to sinus rhythm. Am J Cardiol. 1988;62(17):1202-7.

92.   Daoud EG, Marcovitz P, Knight BP, Goyal R, Man KC, Strickberger SA, et al. Short-term effect of atrial fibrillation on atrial contractile function in humans. Circulation. 1999;99(23):3024-7.

93.   Manning WJ, Silverman DI, Katz SE, Riley MF, Come PC, Doherty RM, et al. Impaired left atrial mechanical function after cardioversion: relation to the duration of atrial fibrillation. J Am Coll Cardiol. 1994;23(7):1535-40.

94.   Everett TH, Li H, Mangrum JM, McRury ID, Mitchell MA, Redick JA, et al. Electrical, morphological, and ultrastructural remodelling and reverse remodelling in a canine model of chronic atrial fibrillation. Circulation. 2000;102(12):1454-60.

95.   Sparks PB, Jayaprakash S, Vohra JK, Kalman JM. Electrical remodelling of the atria associated with paroxysmal and chronic atrial flutter. Circulation. 2000;102(15):1807-13.

96.   Yu WC, Lee SH, Tai CT, Tsai CF, Hsieh MH, Chen CC, et al. Reversal of atrial electrical remodelling following cardioversion of long-standing atrial fibrillation in man. Cardiovasc Res. 1999;42(2):470-6.

97.   Elvan A, Wylie K, Zipes DP. Pacing-induced chronic atrial fibrillation impairs sinus node function in dogs. Electrophysiological remodelling. Circulation. 1996;94(11):2953-60.

98.   Manios EG, Kanoupakis EM, Chlouverakis GI, Kaleboubas MD, Mavrakis HE, Vardas PE. Changes in atrial electrical properties following cardioversion of chronic atrial fibrillation: relation with recurrence. Cardiovasc Res. 2000;47(2):244-53.

99.   Daoud EG, Knight BP, Weiss R, Bahu M, Paladino W, Goyal R, et al. Effect of verapamil and procainamide on atrial fibrillation-induced electrical remodelling in humans. Circulation. 1997;96(5):1542-50.

100. Leistad E, Aksnes G, Verburg E, Christensen G. Atrial contractile dysfunction after short-term atrial fibrillation is reduced by verapamil but increased by BAY K8644. Circulation. 1996;93(9):1747-54.

101. Lee SH, Yu WC, Cheng JJ, Hung CR, Ding YA, Chang MS, et al. Effect of verapamil on long-term tachycardia-induced atrial electrical remodelling. Circulation. 2000;101(2):200-6.

102. Page RL, Wilkinson WE, Clair WK, McCarthy EA, Pritchett EL. Asymptomatic arrhythmias in patients with symptomatic paroxysmal atrial fibrillation and paroxysmal supraventricular tachycardia. Circulation. 1994;89(1):224-7.

103. Calkins H, Kuck KH, Cappato R, Brugada J, Camm AJ, Chen S-A, et al. 2012 HRS/EHRA/ECAS Expert Consensus Statement on Catheter and Surgical Ablation of Atrial Fibrillation: Recommendations for Patient Selection, Procedural Techniques, Patient Management and Follow-up, Definitions, Endpoints, and Research Trial Design: A report of the Heart Rhythm Society (HRS) Task Force on Catheter and Surgical Ablation of Atrial Fibrillation. Developed in partnership with the European Heart Rhythm Association (EHRA), a registered branch of the European Society of Cardiology (ESC) and the European Cardiac Arrhythmia Society (ECAS); and in collaboration with the American College of Cardiology (ACC), American Heart Association (AHA), the Asia Pacific Heart Rhythm Society (APHRS), and the Society of Thoracic Surgeons (STS). Endorsed by the governing bodies of the American College of Cardiology Foundation, the American Heart Association, the European Cardiac Arrhythmia Society, the European Heart Rhythm Association, the Society of Thoracic Surgeons, the Asia Pacific Heart Rhythm Society, and the Heart Rhythm Society. EP Europace. 2012;14(4):528-606.

104. Krahn AD, Manfreda J, Tate RB, Mathewson FA, Cuddy TE. The natural history of atrial fibrillation: incidence, risk factors, and prognosis in the Manitoba Follow-Up Study. Am J Med. 1995;98(5):476-84.

105. Wyse DG, Love JC, Yao Q, Carlson MD, Cassidy P, Greene LH, et al. Atrial fibrillation: a risk factor for increased mortality--an AVID registry analysis. J Interv Card Electrophysiol. 2001;5(3):267-73.

106. Stewart S, MacIntyre K, Chalmers JW, Boyd J, Finlayson A, Redpath A, et al. Trends in case-fatality in 22968 patients admitted for the first time with atrial fibrillation in Scotland, 1986-1995. Int J Cardiol. 2002;82(3):229-36.

107. Hart RG, Pearce LA, Aguilar MI. Meta-analysis: antithrombotic therapy to prevent stroke in patients who have nonvalvular atrial fibrillation. Ann Intern Med. 2007;146(12):857-67.

108. Gage BF, Boechler M, Doggette AL, Fortune G, Flaker GC, Rich MW, et al. Adverse outcomes and predictors of underuse of antithrombotic therapy in medicare beneficiaries with chronic atrial fibrillation. Stroke. 2000;31(4):822-7.

109. Kirchhof P, Benussi S, Kotecha D, Ahlsson A, Atar D, Casadei B, et al. 2016 ESC Guidelines for the Management of Atrial Fibrillation Developed in Collaboration With EACTS. Rev Esp Cardiol (Engl Ed). 2017;70(1):50.

110. Fuster V, Rydén LE, Cannom DS, Crijns HJ, Curtis AB, Ellenbogen KA, et al. ACC/AHA/ESC 2006 guidelines for the management of patients with atrial fibrillation: full text: a report of the American College of Cardiology/American Heart Association Task Force on practice guidelines and the European Society of Cardiology Committee for Practice Guidelines (Writing Committee to Revise the 2001 guidelines for the management of patients with atrial fibrillation) developed in collaboration with the European Heart Rhythm Association and the Heart Rhythm Society. Europace. 2006;8(9):651-745.

111. Pappone C, Vicedomini G, Augello G, Manguso F, Saviano M, Baldi M, et al. Radiofrequency catheter ablation and antiarrhythmic drug therapy: a prospective, randomized, 4-year follow-up trial: the APAF study. Circ Arrhythm Electrophysiol. 2011;4(6):808-14.

112. Mont L, Bisbal F, Hernández-Madrid A, Pérez-Castellano N, Viñolas X, Arenal A, et al. Catheter ablation vs. antiarrhythmic drug treatment of persistent atrial fibrillation: a multicentre, randomized, controlled trial (SARA study). Eur Heart J. 2014;35(8):501-7.

113. Walfridsson H, Walfridsson U, Nielsen JC, Johannessen A, Raatikainen P, Janzon M, et al. Radiofrequency ablation as initial therapy in paroxysmal atrial fibrillation: results on health-related quality of life and symptom burden. The MANTRA-PAF trial. Europace. 2015;17(2):215-21.

114. Kelly JP, DeVore AD, Wu J, Hammill BG, Sharma A, Cooper LB, et al. Rhythm Control Versus Rate Control in Patients With Atrial Fibrillation and Heart Failure With Preserved Ejection Fraction: Insights From Get With The Guidelines-Heart Failure. J Am Heart Assoc. 2019;8(24):e011560.

115. Gillinov AM, Bagiella E, Moskowitz AJ, Raiten JM, Groh MA, Bowdish ME, et al. Rate Control versus Rhythm Control for Atrial Fibrillation after Cardiac Surgery. N Engl J Med. 2016;374(20):1911-21.

116. Wyse DG, Waldo AL, DiMarco JP, Domanski MJ, Rosenberg Y, Schron EB, et al. A comparison of rate control and rhythm control in patients with atrial fibrillation. N Engl J Med. 2002;347(23):1825-33.

117. Wyse DG. Rate control vs rhythm control strategies in atrial fibrillation. Prog Cardiovasc Dis. 2005;48(2):125-38.

118. Carlsson J, Miketic S, Windeler J, Cuneo A, Haun S, Micus S, et al. Randomized trial of rate-control versus rhythm-control in persistent atrial fibrillation: the Strategies of Treatment of Atrial Fibrillation (STAF) study. J Am Coll Cardiol. 2003;41(10):1690-6.

119. Hohnloser SH, Crijns HJ, van Eickels M, Gaudin C, Page RL, Torp-Pedersen C, et al. Effect of dronedarone on cardiovascular events in atrial fibrillation. N Engl J Med. 2009;360(7):668-78.

120. Shantha G, Alyesh D, Ghanbari H, Yokokawa M, Saeed M, Cunnane R, et al. Antiarrhythmic drug therapy and all-cause mortality after catheter ablation of atrial fibrillation: A propensity-matched analysis. Heart Rhythm. 2019;16(9):1368-73.

121.   Waldo AL, Camm AJ, deRuyter H, Friedman PL, MacNeil DJ, Pauls JF, et al. Effect of d-sotalol on mortality in patients with left ventricular dysfunction after recent and remote myocardial infarction. The SWORD Investigators. Survival With Oral d-Sotalol. Lancet. 1996;348(9019):7-12.

122.   Flaker GC, Blackshear JL, McBride R, Kronmal RA, Halperin JL, Hart RG. Antiarrhythmic drug therapy and cardiac mortality in atrial fibrillation. The Stroke Prevention in Atrial Fibrillation Investigators. J Am Coll Cardiol. 1992;20(3):527-32.

123.   Vaughan Williams EM. Classification of antidysrhythmic drugs. Pharmacol Ther B. 1975;1(1):115-38.

124.   Campbell TJ, Vaughan Williams EM. Voltage- and time-dependent depression of maximum rate of depolarisation of guinea-pig ventricular action potentials by two new antiarrhythmic drugs, flecainide and lorcainide. Cardiovasc Res. 1983;17(5):251-8.

125.   Dukes ID, Vaughan Williams EM. Effects of selective alpha 1-, alpha 2-, beta 1-and beta 2-adrenoceptor stimulation on potentials and contractions in the rabbit heart. J Physiol. 1984;355:523-46.

126.   Echt DS, Liebson PR, Mitchell LB, Peters RW, Obias-Manno D, Barker AH, et al. Mortality and morbidity in patients receiving encainide, flecainide, or placebo. The Cardiac Arrhythmia Suppression Trial. N Engl J Med. 1991;324(12):781-8.

127.   Danzi S, Klein I. Amiodarone-induced thyroid dysfunction. J Intensive Care Med. 2015;30(4):179-85.

128.   Lei M, Wu L, Terrar DA, Huang CL. Modernized Classification of Cardiac Antiarrhythmic Drugs. Circulation. 2018;138(17):1879-96.

129.   Carmeliet E. Voltage- and time-dependent block of the delayed K+ current in cardiac myocytes by dofetilide. J Pharmacol Exp Ther. 1992;262(2):809-17.

130.   Lee KS. Ibutilide, a new compound with potent class III antiarrhythmic activity, activates a slow inward Na+ current in guinea pig ventricular cells. J Pharmacol Exp Ther. 1992;262(1):99-108.

131.   Piccini JP, Hasselblad V, Peterson ED, Washam JB, Califf RM, Kong DF. Comparative efficacy of dronedarone and amiodarone for the maintenance of sinus rhythm in patients with atrial fibrillation. J Am Coll Cardiol. 2009;54(12):1089-95.

132.   WEGENER FT, EHRLICH JR, HOHNLOSER SH. Dronedarone: An Emerging Agent with Rhythm- and Rate-Controlling Effects. Journal of Cardiovascular Electrophysiology. 2006;17(s2):S17-S20.

133.   Mitcheson JS. hERG potassium channels and the structural basis of drug-induced arrhythmias. Chem Res Toxicol. 2008;21(5):1005-10.

134.   Mitcheson JS, Chen J, Lin M, Culberson C, Sanguinetti MC. A structural basis for drug-induced long QT syndrome. Proc Natl Acad Sci U S A. 2000;97(22):12329-33.

135.   Islam MA. Pharmacological modulations of cardiac ultra-rapid and slowly activating delayed rectifier currents: potential antiarrhythmic approaches. Recent Pat Cardiovasc Drug Discov. 2010;5(1):33-46.

136.   Machida T, Hashimoto N, Kuwahara I, Ogino Y, Matsuura J, Yamamoto W, et al. Effects of a highly selective acetylcholine-activated K+ channel blocker on experimental atrial fibrillation. Circ Arrhythm Electrophysiol. 2011;4(1):94-102.

137.   Burashnikov A, Antzelevitch C. Atrial-selective sodium channel block for the treatment of atrial fibrillation. Expert Opin Emerg Drugs. 2009;14(2):233-49.

138.   Burashnikov A, Di Diego JM, Zygmunt AC, Belardinelli L, Antzelevitch C. Atrium-selective sodium channel block as a strategy for suppression of atrial fibrillation: differences in sodium channel inactivation between atria and ventricles and the role of ranolazine. Circulation. 2007;116(13):1449-57.

139. Antzelevitch C, Burashnikov A. Atrial-selective sodium channel block as a novel strategy for the management of atrial fibrillation. J Electrocardiol. 2009;42(6):543-8.

140. Tamkun MM, Knoth KM, Walbridge JA, Kroemer H, Roden DM, Glover DM. Molecular cloning and characterization of two voltage-gated K+ channel cDNAs from human ventricle. FASEB J. 1991;5(3):331-7.

141. Ford JW, Milnes JT. New drugs targeting the cardiac ultra-rapid delayed-rectifier current (I Kur): rationale, pharmacology and evidence for potential therapeutic value. J Cardiovasc Pharmacol. 2008;52(2):105-20.

142. Christ T, Wettwer E, Voigt N, Hála O, Radicke S, Matschke K, et al. Pathology-specific effects of the IKur/Ito/IK,ACh blocker AVE0118 on ion channels in human chronic atrial fibrillation. Br J Pharmacol. 2008;154(8):1619-30.

143. Fedida D. Vernakalant (RSD1235): a novel, atrial-selective antifibrillatory agent. Expert Opinion on Investigational Drugs. 2007;16(4):519-32.

144. Van Wagoner DR, Pond AL, McCarthy PM, Trimmer JS, Nerbonne JM. Outward K+ current densities and Kv1.5 expression are reduced in chronic human atrial fibrillation. Circ Res. 1997;80(6):772-81.

145. Grammer JB, Bosch RF, Kühlkamp V, Seipel L. Molecular remodelling of Kv4.3 potassium channels in human atrial fibrillation. J Cardiovasc Electrophysiol. 2000;11(6):626-33.

146. Loose S, Mueller J, Wettwer E, Knaut M, Ford J, Milnes J, et al. Effects of IKur blocker MK-0448 on human right atrial action potentials from patients in sinus rhythm and in permanent atrial fibrillation. Front Pharmacol. 2014;5:26.

147. Ford J, Milnes J, Wettwer E, Christ T, Rogers M, Sutton K, et al. Human electrophysiological and pharmacological properties of XEN-D0101: a novel atrial-selective Kv1.5/IKur inhibitor. J Cardiovasc Pharmacol. 2013;61(5):408-15.

148. Yamada M, Inanobe A, Kurachi Y. G protein regulation of potassium ion channels. Pharmacol Rev. 1998;50(4):723-60.

149. Bettahi I, Marker CL, Roman MI, Wickman K. Contribution of the Kir3.1 subunit to the muscarinic-gated atrial potassium channel IKACh. J Biol Chem. 2002;277(50):48282-8.

150. Anumonwo JM, Lopatin AN. Cardiac strong inward rectifier potassium channels. J Mol Cell Cardiol. 2010;48(1):45-54.

151. Hibino H, Inanobe A, Furutani K, Murakami S, Findlay I, Kurachi Y. Inwardly rectifying potassium channels: their structure, function, and physiological roles. Physiol Rev. 2010;90(1):291-366.

152. Kovoor P, Wickman K, Maguire CT, Pu W, Gehrmann J, Berul CI, et al. Evaluation of the role of I(KACh) in atrial fibrillation using a mouse knockout model. J Am Coll Cardiol. 2001;37(8):2136-43.

153. Dobrev D, Graf E, Wettwer E, Himmel HM, Hála O, Doerfel C, et al. Molecular basis of downregulation of G-protein-coupled inward rectifying K(+) current (I(K,ACh) in chronic human atrial fibrillation: decrease in GIRK4 mRNA correlates with reduced I(K,ACh) and muscarinic receptor-mediated shortening of action potentials. Circulation. 2001;104(21):2551-7.

154. Juhász V, Hornyik T, Benák A, Nagy N, Husti Z, Pap R, et al. Comparison of the effects of IK,ACh, IKr, and INa block in conscious dogs with atrial fibrillation and on action potentials in remodeled atrial trabeculae. Canadian Journal of Physiology and Pharmacology. 2017;96(1):18-25.

155. GARDOS G. The function of calcium in the potassium permeability of human erythrocytes. Biochim Biophys Acta. 1958;30(3):653-4.

156. Vergara C, Latorre R, Marrion NV, Adelman JP. Calcium-activated potassium channels. Curr Opin Neurobiol. 1998;8(3):321-9.

157.   Krnjević K, Lisiewicz A. Injections of calcium ions into spinal motoneurones. J Physiol. 1972;225(2):363-90.

158.   Chen MX, Gorman SA, Benson B, Singh K, Hieble JP, Michel MC, et al. Small and intermediate conductance Ca(2+)-activated K+ channels confer distinctive patterns of distribution in human tissues and differential cellular localisation in the colon and corpus cavernosum. Naunyn Schmiedebergs Arch Pharmacol. 2004;369(6):602-15.

159.   Berkefeld H, Fakler B, Schulte U. Ca2+-activated K+ channels: from protein complexes to function. Physiol Rev. 2010;90(4):1437-59.

160.   Kuiper EF, Nelemans A, Luiten P, Nijholt I, Dolga A, Eisel U. K(Ca)2 and k(ca)3 channels in learning and memory processes, and neurodegeneration. Front Pharmacol. 2012;3:107.

161.   Stocker M. Ca2+-activated K+ channels: molecular determinants and function of the SK family. Nature Reviews Neuroscience. 2004;5(10):758-70.

162.   Zhang Q, Timofeyev V, Lu L, Li N, Singapuri A, Long MK, et al. Functional roles of a Ca2+-activated K+ channel in atrioventricular nodes. Circ Res. 2008;102(4):465-71.

163.   Tuteja D, Rafizadeh S, Timofeyev V, Wang S, Zhang Z, Li N, et al. Cardiac small conductance Ca2+-activated K+ channel subunits form heteromultimers via the coiled-coil domains in the C termini of the channels. Circ Res. 2010;107(7):851-9.

164.   Church TW, Weatherall KL, Corrêa SA, Prole DL, Brown JT, Marrion NV. Preferential assembly of heteromeric small conductance calcium-activated potassium channels. Eur J Neurosci. 2015;41(3):305-15.

165.   Xia XM, Fakler B, Rivard A, Wayman G, Johnson-Pais T, Keen JE, et al. Mechanism of calcium gating in small-conductance calcium-activated potassium channels. Nature. 1998;395(6701):503-7.

166.   Lester RA, Clements JD, Westbrook GL, Jahr CE. Channel kinetics determine the time course of NMDA receptor-mediated synaptic currents. Nature. 1990;346(6284):565-7.

167.   Maconochie DJ, Zempel JM, Steinbach JH. How quickly can GABAA receptors open? Neuron. 1994;12(1):61-71.

168.   Ishii TM, Silvia C, Hirschberg B, Bond CT, Adelman JP, Maylie J. A human intermediate conductance calcium-activated potassium channel. Proc Natl Acad Sci U S A. 1997;94(21):11651-6.

169.   Strøbaek D, Jørgensen TD, Christophersen P, Ahring PK, Olesen SP. Pharmacological characterization of small-conductance Ca(2+)-activated K(+) channels stably expressed in HEK 293 cells. Br J Pharmacol. 2000;129(5):991-9.

170.   Grunnet M, Jespersen T, Angelo K, Frøkjaer-Jensen C, Klaerke DA, Olesen SP, et al. Pharmacological modulation of SK3 channels. Neuropharmacology. 2001;40(7):879-87.

171.   Weatherall KL, Goodchild SJ, Jane DE, Marrion NV. Small conductance calcium-activated potassium channels: from structure to function. Prog Neurobiol. 2010;91(3):242-55.

172.   Marrion NV, Tavalin SJ. Selective activation of Ca2+-activated K+ channels by co-localized Ca2+ channels in hippocampal neurons. Nature. 1998;395(6705):900-5.

173.   Pedarzani P, Mosbacher J, Rivard A, Cingolani LA, Oliver D, Stocker M, et al. Control of electrical activity in central neurons by modulating the gating of small conductance Ca2+-activated K+ channels. J Biol Chem. 2001;276(13):9762-9.

174.   Lu L, Zhang Q, Timofeyev V, Zhang Z, Young JN, Shin HS, et al. Molecular coupling of a Ca2+-activated K+ channel to L-type Ca2+ channels via alpha-actinin2. Circ Res. 2007;100(1):112-20.

175.   Blatz AL, Magleby KL. Single apamin-blocked Ca-activated K+ channels of small conductance in cultured rat skeletal muscle. Nature. 1986;323(6090):718-20.

176.   Castle NA, Haylett DG, Jenkinson DH. Toxins in the characterization of potassium channels. Trends in Neurosciences. 1989;12(2):59-65.

177.   Burgess GM, Claret M, Jenkinson DH. Effects of quinine and apamin on the calcium-dependent potassium permeability of mammalian hepatocytes and red cells. J Physiol. 1981;317:67-90.

178.   Ishii TM, Maylie J, Adelman JP. Determinants of apamin and d-tubocurarine block in SK potassium channels. J Biol Chem. 1997;272(37):23195-200.

179.   Grunnet M, Jensen BS, Olesen SP, Klaerke DA. Apamin interacts with all subtypes of cloned small-conductance Ca2+-activated K+ channels. Pflugers Arch. 2001;441(4):544-50.

180.   Shakkottai VG, Regaya I, Wulff H, Fajloun Z, Tomita H, Fathallah M, et al. Design and characterization of a highly selective peptide inhibitor of the small conductance calcium-activated K+ channel, SkCa2. J Biol Chem. 2001;276(46):43145-51.

181.   Castle NA, Haylett DG, Morgan JM, Jenkinson DH. Dequalinium: a potent inhibitor of apamin-sensitive K+ channels in hepatocytes and of nicotinic responses in skeletal muscle. Eur J Pharmacol. 1993;236(2):201-7.

182.   Rosa JC, Galanakis D, Ganellin CR, Dunn PM, Jenkinson DH. Bis-quinolinium cyclophanes: 6,10-diaza-3(1,3),8(1,4)-dibenzena-1,5(1,4)-diquinolinacyclodecaphane (UCL 1684), the first nanomolar, non-peptidic blocker of the apamin-sensitive Ca(2+)-activated K+ channel. J Med Chem. 1998;41(1):2-5.

183.   Gentles RG, Grant-Young K, Hu S, Huang Y, Poss MA, Andres C, et al. Initial SAR studies on apamin-displacing 2-aminothiazole blockers of calcium-activated small conductance potassium channels. Bioorg Med Chem Lett. 2008;18(19):5316-9.

184.   Strøbæk D, Hougaard C, Johansen TH, Sørensen US, Nielsen EØ, Nielsen KS, et al. Inhibitory Gating Modulation of Small Conductance Ca^{2+}-Activated K^{+} Channels by the Synthetic Compound (*R*)*-N*-(Benzimidazol-2-yl)-1,2,3,4-tetrahydro-1-naphtylamine (NS8593) Reduces Afterhyperpolarizing Current in Hippocampal CA1 Neurons. Molecular Pharmacology. 2006;70(5):1771.

185.   Graulich A, Mercier F, Scuvée-Moreau J, Seutin V, Liégeois JF. Synthesis and biological evaluation of N-methyl-laudanosine iodide analogues as potential SK channel blockers. Bioorg Med Chem. 2005;13(4):1201-9.

186.   Strøbaek D, Hougaard C, Johansen TH, Sørensen US, Nielsen E, Nielsen KS, et al. Inhibitory gating modulation of small conductance Ca2+-activated K+ channels by the synthetic compound (R)-N-(benzimidazol-2-yl)-1,2,3,4-tetrahydro-1-naphtylamine (NS8593) reduces afterhyperpolarizing current in hippocampal CA1 neurons. Mol Pharmacol. 2006;70(5):1771-82.

187.   Sørensen US, Strøbaek D, Christophersen P, Hougaard C, Jensen ML, Nielsen E, et al. Synthesis and structure-activity relationship studies of 2-(N-substituted)-aminobenzimidazoles as potent negative gating modulators ofsmall conductance Ca2+-activated K+ channels. J Med Chem. 2008;51(23):7625-34.

188.   Lamy C, Goodchild SJ, Weatherall KL, Jane DE, Liégeois JF, Seutin V, et al. Allosteric block of KCa2 channels by apamin. J Biol Chem. 2010;285(35):27067-77.

189. Strøbæk D, Jørgensen TD, Christophersen P, Ahring PK, Olesen S-P. Pharmacological characterization of small-conductance Ca2+-activated K+ channels stably expressed in HEK 293 cells. British Journal of Pharmacology. 2000;129(5):991-9.

190. Nolting A, Ferraro T, D'hoedt D, Stocker M. An amino acid outside the pore region influences apamin sensitivity in small conductance Ca2+-activated K+ channels. J Biol Chem. 2007;282(6):3478-86.

191. Pedarzani P, Stocker M. Molecular and cellular basis of small--and intermediate-conductance, calcium-activated potassium channel function in the brain. Cell Mol Life Sci. 2008;65(20):3196-217.

192. Messier C, Mourre C, Bontempi B, Sif J, Lazdunski M, Destrade C. Effect of apamin, a toxin that inhibits Ca2+-dependent K+ channels, on learning and memory processes. Brain Research. 1991;551(1):322-6.

193. Moreno M, Giralt E. Three valuable peptides from bee and wasp venoms for therapeutic and biotechnological use: melittin, apamin and mastoparan. Toxins (Basel). 2015;7(4):1126-50.

194. Cosand WL, Merrifield RB. Concept of internal structural controls for evaluation of inactive synthetic peptide analogs: synthesis of [Orn13,14]apamin and its guanidination to an apamin derivative with full neurotoxic activity. Proc Natl Acad Sci U S A. 1977;74(7):2771-5.

195. Lallement G, Fosbraey P, Baille-Le-Crom V, Tattersall JE, Blanchet G, Wetherell JR, et al. Compared toxicity of the potassium channel blockers, apamin and dendrotoxin. Toxicology. 1995;104(1-3):47-52.

196. Diness JG, Sørensen US, Nissen JD, Al-Shahib B, Jespersen T, Grunnet M, et al. Inhibition of small-conductance Ca2+-activated K+ channels terminates and protects against atrial fibrillation. Circ Arrhythm Electrophysiol. 2010;3(4):380-90.

197. Skibsbye L, Wang X, Axelsen LN, Bomholtz SH, Nielsen MS, Grunnet M, et al. Antiarrhythmic Mechanisms of SK Channel Inhibition in the Rat Atrium. J Cardiovasc Pharmacol. 2015;66(2):165-76.

198. Eisner DA, Vaughan-Jones RD. Do calcium-activated potassium channels exist in the heart? Cell Calcium. 1983;4(5-6):371-86.

199. Giles WR, Imaizumi Y. Comparison of potassium currents in rabbit atrial and ventricular cells. J Physiol. 1988;405:123-45.

200. Li N, Timofeyev V, Tuteja D, Xu D, Lu L, Zhang Q, et al. Ablation of a Ca2+-activated K+ channel (SK2 channel) results in action potential prolongation in atrial myocytes and atrial fibrillation. J Physiol. 2009;587(Pt 5):1087-100.

201. Ozgen N, Dun W, Sosunov EA, Anyukhovsky EP, Hirose M, Duffy HS, et al. Early electrical remodelling in rabbit pulmonary vein results from trafficking of intracellular SK2 channels to membrane sites. Cardiovasc Res. 2007;75(4):758-69.

202. Qi XY, Diness JG, Brundel BJ, Zhou XB, Naud P, Wu CT, et al. Role of small-conductance calcium-activated potassium channels in atrial electrophysiology and fibrillation in the dog. Circulation. 2014;129(4):430-40.

203. Nagy N, Szuts V, Horváth Z, Seprényi G, Farkas AS, Acsai K, et al. Does small-conductance calcium-activated potassium channel contribute to cardiac repolarization? J Mol Cell Cardiol. 2009;47(5):656-63.

204. Heijman J, Voigt N, Nattel S, Dobrev D. Cellular and molecular electrophysiology of atrial fibrillation initiation, maintenance, and progression. Circ Res. 2014;114(9):1483-99.

205. Kopecky SL, Gersh BJ, McGoon MD, Whisnant JP, Holmes DR, Ilstrup DM, et al. The natural history of lone atrial fibrillation. A population-based study over three decades. N Engl J Med. 1987;317(11):669-74.

206. Ellinor PT, Lunetta KL, Glazer NL, Pfeufer A, Alonso A, Chung MK, et al. Common variants in KCNN3 are associated with lone atrial fibrillation. Nat Genet. 2010;42(3):240-4.

207. Luo Z, Yan C, Zhang W, Shen X, Zheng W, Chen F, et al. Association between SNP rs13376333 and rs1131820 in the KCNN3 gene and atrial fibrillation in the Chinese Han population. Clin Chem Lab Med. 2014;52(12):1867-73.

208. Olesen MS, Jabbari J, Holst AG, Nielsen JB, Steinbrüchel DA, Jespersen T, et al. Screening of KCNN3 in patients with early-onset lone atrial fibrillation. Europace. 2011;13(7):963-7.

209. Skibsbye L, Diness JG, Sørensen US, Hansen RS, Grunnet M. The duration of pacing-induced atrial fibrillation is reduced in vivo by inhibition of small conductance Ca(2+)-activated K(+) channels. J Cardiovasc Pharmacol. 2011;57(6):672-81.

210. Diness JG, Skibsbye L, Jespersen T, Bartels ED, Sørensen US, Hansen RS, et al. Effects on atrial fibrillation in aged hypertensive rats by Ca(2+)-activated K(+) channel inhibition. Hypertension. 2011;57(6):1129-35.

211. Yu T, Deng C, Wu R, Guo H, Zheng S, Yu X, et al. Decreased expression of small-conductance Ca2+-activated K+ channels SK1 and SK2 in human chronic atrial fibrillation. Life Sci. 2012;90(5-6):219-27.

212. Ling TY, Wang XL, Chai Q, Lau TW, Koestler CM, Park SJ, et al. Regulation of the SK3 channel by microRNA-499--potential role in atrial fibrillation. Heart Rhythm. 2013;10(7):1001-9.

213. Li ML, Li T, Lei M, Tan XQ, Yang Y, Liu TP, et al. [Increased small conductance calcium-activated potassium channel (SK2 channel) current in atrial myocytes of patients with persistent atrial fibrillation]. Zhonghua Xin Xue Guan Bing Za Zhi. 2011;39(2):147-51.

214. Kirchhefer U, Schmitz W, Scholz H, Neumann J. Activity of cAMP-dependent protein kinase and Ca2+/calmodulin-dependent protein kinase in failing and nonfailing human hearts. Cardiovascular Research. 1999;42(1):254-61.

215. Anderson ME. Calmodulin kinase signaling in heart: an intriguing candidate target for therapy of myocardial dysfunction and arrhythmias. Pharmacology & Therapeutics. 2005;106(1):39-55.

216. Bosch RF, Zeng X, Grammer JB, Popovic K, Mewis C, Kühlkamp V. Ionic mechanisms of electrical remodelling in human atrial fibrillation. Cardiovasc Res. 1999;44(1):121-31.

217. Leistad E, Christensen G, Ilebekk A. Atrial contractile performance after cessation of atrial fibrillation. Am J Physiol. 1993;264(1 Pt 2):H104-9.

218. Daoud Emile G, Bogun F, Goyal R, Harvey M, Man KC, Strickberger SA, et al. Effect of Atrial Fibrillation on Atrial Refractoriness in Humans. Circulation. 1996;94(7):1600-6.

219. Yu W-C, Chen S-A, Lee S-H, Tai C-T, Feng A-N, Kuo Benjamin I-T, et al. Tachycardia-Induced Change of Atrial Refractory Period in Humans. Circulation. 1998;97(23):2331-7.

220. Lopatin AN, Nichols CG. Inward rectifiers in the heart: an update on I(K1). J Mol Cell Cardiol. 2001;33(4):625-38.

221. Dhamoon AS, Jalife J. The inward rectifier current (IK1) controls cardiac excitability and is involved in arrhythmogenesis. Heart Rhythm. 2005;2(3):316-24.

222. Marshall GE, Russell JA, Tellez JO, Jhund PS, Currie S, Dempster J, et al. Remodelling of human atrial K+ currents but not ion channel expression by chronic ß-blockade. Pflugers Arch. 2012;463(4):537-48.

223. Ferreira G, Yi J, Ríos E, Shirokov R. Ion-dependent inactivation of barium current through L-type calcium channels. J Gen Physiol. 1997;109(4):449-61.

224. Lesage F, Guillemare E, Fink M, Duprat F, Heurteaux C, Fosset M, et al. Molecular properties of neuronal G-protein-activated inwardly rectifying K+ channels. J Biol Chem. 1995;270(48):28660-7.

225. DiFrancesco D, Ferroni A, Visentin S. Barium-induced blockade of the inward rectifier in calf Purkinje fibres. Pflugers Arch. 1984;402(4):446-53.

226. Kubo Y, Baldwin TJ, Jan YN, Jan LY. Primary structure and functional expression of a mouse inward rectifier potassium channel. Nature. 1993;362(6416):127-33.

227. Koumi S, Backer CL, Arentzen CE. Characterization of inwardly rectifying K+ channel in human cardiac myocytes. Alterations in channel behavior in myocytes isolated from patients with idiopathic dilated cardiomyopathy. Circulation. 1995;92(2):164-74.

228. Wang Z, Yue L, White M, Pelletier G, Nattel S. Differential distribution of inward rectifier potassium channel transcripts in human atrium versus ventricle. Circulation. 1998;98(22):2422-8.

229. Melnyk P, Zhang L, Shrier A, Nattel S. Differential distribution of Kir2.1 and Kir2.3 subunits in canine atrium and ventricle. Am J Physiol Heart Circ Physiol. 2002;283(3):H1123-33.

230. Xia M, Jin Q, Bendahhou S, He Y, Larroque MM, Chen Y, et al. A Kir2.1 gain-of-function mutation underlies familial atrial fibrillation. Biochem Biophys Res Commun. 2005;332(4):1012-9.

231. Schimpf R, Wolpert C, Gaita F, Giustetto C, Borggrefe M. Short QT syndrome. Cardiovasc Res. 2005;67(3):357-66.

232. Kabaeva Z, Zhao M, Michele DE. Blebbistatin extends culture life of adult mouse cardiac myocytes and allows efficient and stable transgene expression. American Journal of Physiology-Heart and Circulatory Physiology. 2008;294(4):H1667-H74.

233. Matsushita O, Koide T, Kobayashi R, Nagata K, Okabe A. Substrate recognition by the collagen-binding domain of Clostridium histolyticum class I collagenase. J Biol Chem. 2001;276(12):8761-70.

234. Wilensky RL, Tranum-Jensen J, Coronel R, Wilde AA, Fiolet JW, Janse MJ. The subendocardial border zone during acute ischemia of the rabbit heart: an electrophysiologic, metabolic, and morphologic correlative study. Circulation. 1986;74(5):1137-46.

235. World Medical Association Declaration of Helsinki. Recommendations guiding physicians in biomedical research involving human subjects. Cardiovasc Res. 1997;35(1):2-3.

236. Escande D, Coulombe A, Faivre JF, Deroubaix E, Coraboeuf E. Two types of transient outward currents in adult human atrial cells. Am J Physiol. 1987;252(1 Pt 2):H142-8.

237. Harding SE, Jones SM, O'Gara P, Vescovo G, Poole-Wilson PA. Reduced beta-agonist sensitivity in single atrial cells from failing human hearts. Am J Physiol. 1990;259(4 Pt 2):H1009-14.

238. Neher E. Correction for liquid junction potentials in patch clamp experiments. Methods Enzymol. 1992;207:123-31.

239. Yang WQ, Peng L. Image reconstruction algorithms for electrical capacitance tomography. Measurement Science and Technology. 2002;14(1):R1-R13.

240. Sakmann B, Neher E. Patch clamp techniques for studying ionic channels in excitable membranes. Annu Rev Physiol. 1984;46:455-72.

241. Schram G, Pourrier M, Melnyk P, Nattel S. Differential distribution of cardiac ion channel expression as a basis for regional specialization in electrical function. Circ Res. 2002;90(9):939-50.

242. Matsuda H, Saigusa A, Irisawa H. Ohmic conductance through the inwardly rectifying K channel and blocking by internal Mg2+. Nature. 1987;325(7000):156-9.

243. Albeck JG, Burke JM, Aldridge BB, Zhang M, Lauffenburger DA, Sorger PK. Quantitative analysis of pathways controlling extrinsic apoptosis in single cells. Mol Cell. 2008;30(1):11-25.

244. Spencer SL, Gaudet S, Albeck JG, Burke JM, Sorger PK. Non-genetic origins of cell-to-cell variability in TRAIL-induced apoptosis. Nature. 2009;459(7245):428-32.

245. Warren M, Guha PK, Berenfeld O, Zaitsev A, Anumonwo JM, Dhamoon AS, et al. Blockade of the inward rectifying potassium current terminates ventricular fibrillation in the guinea pig heart. J Cardiovasc Electrophysiol. 2003;14(6):621-31.

246. Coleman HA, Tare M, Parkington HC. Nonlinear effects of potassium channel blockers on endothelium-dependent hyperpolarization. Acta Physiol (Oxf). 2017;219(1):324-34.

247. Bhoelan BS, Stevering CH, van der Boog ATJ, van der Heyden MAG. Barium toxicity and the role of the potassium inward rectifier current. Clinical Toxicology. 2014;52(6):584-93.

248. Hoshino S, Omatsu-Kanbe M, Nakagawa M, Matsuura H. Postnatal developmental decline in IK1 in mouse ventricular myocytes isolated by the Langendorff perfusion method: comparison with the chunk method. Pflugers Arch. 2012;463(5):649-68.

249. Wang H, Li T, Zhang L, Yang Y, Zeng XR. [Effects of intracellular calcium alteration on SK currents in atrial cardiomyocytes from patients with atrial fibrillation]. Zhongguo Ying Yong Sheng Li Xue Za Zhi. 2014;30(4):296-300, 5.

250. Föhr KJ, Warchol W, Gratzl M. Calculation and control of free divalent cations in solutions used for membrane fusion studies. Methods Enzymol. 1993;221:149-57.

251. Simó-Vicens R, Sauter DRP, Grunnet M, Diness JG, Bentzen BH. Effect of antiarrhythmic drugs on small conductance calcium - activated potassium channels. Eur J Pharmacol. 2017;803:118-23.

252. McGuigan JA, Kay JW, Elder HY, Lüthi D. Comparison between measured and calculated ionised concentrations in Mg2+ /ATP, Mg2+ /EDTA and Ca2+ /EGTA buffers; influence of changes in temperature, pH and pipetting errors on the ionised concentrations. Magnes Res. 2007;20(1):72-81.

253. McGuigan JA, Lüthi D, Buri A. Calcium buffer solutions and how to make them: a do it yourself guide. Can J Physiol Pharmacol. 1991;69(11):1733-49.

254. Terentyev D, Rochira JA, Terentyeva R, Roder K, Koren G, Li W. Sarcoplasmic reticulum Ca^{2+} release is both necessary and sufficient for SK channel activation in ventricular myocytes. American journal of physiology Heart and circulatory physiology. 2014;306(5):H738-H46.

255. Meech RW. The sensitivity of Helix aspersa neurones to injected calcium ions. J Physiol. 1974;237(2):259-77.

256. McGuigan JA, Stumpff F. Calculated and measured [Ca(2+)] in buffers used to calibrate Ca(2+) macroelectrodes. Anal Biochem. 2013;436(1):29-35.

257. Ni Y, Wang T, Zhuo X, Song B, Zhang J, Wei F, et al. Bisoprolol reversed small conductance calcium-activated potassium channel (SK) remodelling in a volume-overload rat model. Mol Cell Biochem. 2013;384(1-2):95-103.

258. Lüthi D, Spichiger U, Forster I, McGuigan JA. Calibration of Mg(2+)-selective macroelectrodes down to 1 mumol l-1 in intracellular and Ca(2+)-containing extracellular solutions. Exp Physiol. 1997;82(3):453-67.

259. McGuigan JA, Kay JW, Elder HY. Critical review of the methods used to measure the apparent dissociation constant and ligand purity in Ca2+ and Mg2+ buffer solutions. Prog Biophys Mol Biol. 2006;92(3):333-70.

260. Berridge MJ. Inositol trisphosphate and calcium signalling. Nature. 1993;361(6410):315-25.

261. Takahashi A, Camacho P, Lechleiter JD, Herman B. Measurement of intracellular calcium. Physiol Rev. 1999;79(4):1089-125.

262. Hirschberg B, Maylie J, Adelman JP, Marrion NV. Gating properties of single SK channels in hippocampal CA1 pyramidal neurons. Biophys J. 1999;77(4):1905-13.

263. Naraghi M. T-jump study of calcium binding kinetics of calcium chelators. Cell Calcium. 1997;22(4):255-68.

264. Markram H, Roth A, Helmchen F. Competitive calcium binding: implications for dendritic calcium signaling. J Comput Neurosci. 1998;5(3):331-48.

265. Burrone J, Neves G, Gomis A, Cooke A, Lagnado L. Endogenous calcium buffers regulate fast exocytosis in the synaptic terminal of retinal bipolar cells. Neuron. 2002;33(1):101-12.

266. Uto A, Arai H, Ogawa Y. Reassessment of Fura-2 and the ratio method for determination of intracellular Ca2+ concentrations. Cell Calcium. 1991;12(1):29-37.

267. Lakowicz JR. Principles of Fluorescence Spectroscopy: Kluwer Academic / Plenum Publishers; 1999.

268. Hayashi H, Miyata H. Fluorescence imaging of intracellular Ca2+. J Pharmacol Toxicol Methods. 1994;31(1):1-10.

269. Becker PL, Fay FS. Photobleaching of fura-2 and its effect on determination of calcium concentrations. Am J Physiol. 1987;253(4 Pt 1):C613-8.

270. Gee KR, Archer EA, Lapham LA, Leonard ME, Zhou ZL, Bingham J, et al. New ratiometric fluorescent calcium indicators with moderately attenuated binding affinities. Bioorg Med Chem Lett. 2000;10(14):1515-8.

271. Paredes RM, Etzler JC, Watts LT, Zheng W, Lechleiter JD. Chemical calcium indicators. Methods. 2008;46(3):143-51.

272. Tsien RY, Pozzan T, Rink TJ. Calcium homeostasis in intact lymphocytes: cytoplasmic free calcium monitored with a new, intracellularly trapped fluorescent indicator. J Cell Biol. 1982;94(2):325-34.

273. Nemeth EF, Scarpa A. Cytosolic Ca2+ and the regulation of secretion in parathyroid cells. FEBS Lett. 1986;203(1):15-9.

274. Williams DA, Fay FS. Intracellular calibration of the fluorescent calcium indicator Fura-2. Cell Calcium. 1990;11(2-3):75-83.

275. Kao JP. Practical aspects of measuring [Ca2+] with fluorescent indicators. Methods Cell Biol. 1994;40:155-81.

276. Groden DL, Guan Z, Stokes BT. Determination of Fura-2 dissociation constants following adjustment of the apparent Ca-EGTA association constant for temperature and ionic strength. Cell Calcium. 1991;12(4):279-87.

277. Poenie M, Alderton J, Steinhardt R, Tsien R. Calcium rises abruptly and briefly throughout the cell at the onset of anaphase. Science. 1986;233(4766):886-9.

278. Lattanzio FA. The effects of pH and temperature on fluorescent calcium indicators as determined with Chelex-100 and EDTA buffer systems. Biochem Biophys Res Commun. 1990;171(1):102-8.

279. YEAGER M, FEIGENSON G. Direct determination of the dissociation-constant for calcium sensitive indicators. Biophysical Journal, BIOPHYSICAL SOCIETY, 9650 ROCKVILLE PIKE, BETHESDA, MD 20814-3998. 1988;53 (2):A332-A part:2

280.   Connor JA, Tseng HY, Hockberger PE. Depolarization- and transmitter-induced changes in intracellular Ca2+ of rat cerebellar granule cells in explant cultures. J Neurosci. 1987;7(5):1384-400.

281.   Bruschi G, Bruschi ME, Regolisti G, Borghetti A. Myoplasmic Ca2+-force relationship studied with fura-2 during stimulation of rat aortic smooth muscle. Am J Physiol. 1988;254(5 Pt 2):H840-54.

282.   Jacobs WR, Mandel LJ. Fluorescent measurements of intracellular free calcium in isolated toad urinary bladder epithelial cells. J Membr Biol. 1987;97(1):53-62.

283.   Wier WG, Cannell MB, Berlin JR, Marban E, Lederer WJ. Cellular and subcellular heterogeneity of [Ca2+]i in single heart cells revealed by fura-2. Science. 1987;235(4786):325-8.

284.   Schöfl C, Sandow J, Knepel W. GRF elevates cytosolic free calcium concentration in rat anterior pituitary cells. Am J Physiol. 1987;253(5 Pt 1):E591-4.

285.   Yang Z, Steele DS. Effects of cytosolic ATP on spontaneous and triggered Ca2+-induced Ca2+ release in permeabilised rat ventricular myocytes. J Physiol. 2000;523 Pt 1:29-44.

286.   Duncan L BF, Smith GL. REACT: calculation of free metal and ligand concentrations using a Windows-based computer program (Abstract). J. Physiol (Lond) 5*17* 1999 P2P1999.

287.   Smith GL, Miller DJ. Potentiometric measurements of stoichiometric and apparent affinity constants of EGTA for protons and divalent ions including calcium. Biochim Biophys Acta. 1985;839(3):287-99.

288.   Malgaroli A, Meldolesi J. [Ca2+]i oscillations from internal stores sustain exocytic secretion from the chromaffin cells of the rat. FEBS Lett. 1991;283(2):169-72.

289.   Petr MJ, Wurster RD. Determination of in situ dissociation constant for Fura-2 and quantitation of background fluorescence in astrocyte cell line U373-MG. Cell Calcium. 1997;21(3):233-40.

290.   Kettlewell S, Burton FL, Smith GL, Workman AJ. Chronic myocardial infarction promotes atrial action potential alternans, afterdepolarizations, and fibrillation. Cardiovasc Res. 2013;99(1):215-24.

291.   Mackenzie L, Roderick HL, Berridge MJ, Conway SJ, Bootman MD. The spatial pattern of atrial cardiomyocyte calcium signalling modulates contraction. J Cell Sci. 2004;117(Pt 26):6327-37.

292.   Williams DA, Fogarty KE, Tsien RY, Fay FS. Calcium gradients in single smooth muscle cells revealed by the digital imaging microscope using Fura-2. Nature. 1985;318(6046):558-61.

293.   Tsien RY, Rink TJ, Poenie M. Measurement of cytosolic free Ca2+ in individual small cells using fluorescence microscopy with dual excitation wavelengths. Cell Calcium. 1985;6(1-2):145-57.

294.   Cheng H, Lederer WJ, Cannell MB. Calcium sparks: elementary events underlying excitation-contraction coupling in heart muscle. Science. 1993;262(5134):740-4.

295.   Blatter LA, Kockskämper J, Sheehan KA, Zima AV, Hüser J, Lipsius SL. Local calcium gradients during excitation-contraction coupling and alternans in atrial myocytes. J Physiol. 2003;546(Pt 1):19-31.

296.   Pethig R, Kuhn M, Payne R, Adler E, Chen TH, Jaffe LF. On the dissociation constants of BAPTA-type calcium buffers. Cell Calcium. 1989;10(7):491-8.

297.   Allbritton NL, Meyer T, Stryer L. Range of messenger action of calcium ion and inositol 1,4,5-trisphosphate. Science. 1992;258(5089):1812-5.

298. Simó-Vicens R, Kirchhoff JE, Dolce B, Abildgaard L, Speerschneider T, Sørensen US, et al. A new negative allosteric modulator, AP14145, for the study of small conductance calcium-activated potassium (K. Br J Pharmacol. 2017;174(23):4396-408.

299. Maier LS, Bers DM. Calcium, calmodulin, and calcium-calmodulin kinase II: heartbeat to heartbeat and beyond. J Mol Cell Cardiol. 2002;34(8):919-39.

300. Tocchetti CG, Wang W, Froehlich JP, Huke S, Aon MA, Wilson GM, et al. Nitroxyl improves cellular heart function by directly enhancing cardiac sarcoplasmic reticulum Ca2+ cycling. Circ Res. 2007;100(1):96-104.

301. Clapham DE. Calcium signaling. Cell. 1995;80(2):259-68.

302. Wulff H, Kolski-Andreaco A, Sankaranarayanan A, Sabatier JM, Shakkottai V. Modulators of small- and intermediate-conductance calcium-activated potassium channels and their therapeutic indications. Curr Med Chem. 2007;14(13):1437-57.

303. Ellinor PT, Lunetta KL, Albert CM, Glazer NL, Ritchie MD, Smith AV, et al. Meta-analysis identifies six new susceptibility loci for atrial fibrillation. Nat Genet. 2012;44(6):670-5.

304. Chang PC, Chen PS. SK channels and ventricular arrhythmias in heart failure. Trends Cardiovasc Med. 2015;25(6):508-14.

305. Chang PC, Turker I, Lopshire JC, Masroor S, Nguyen BL, Tao W, et al. Heterogeneous upregulation of apamin-sensitive potassium currents in failing human ventricles. J Am Heart Assoc. 2013;2(1):e004713.

306. Chua SK, Chang PC, Maruyama M, Turker I, Shinohara T, Shen MJ, et al. Small-conductance calcium-activated potassium channel and recurrent ventricular fibrillation in failing rabbit ventricles. Circ Res. 2011;108(8):971-9.

307. Fanger CM, Ghanshani S, Logsdon NJ, Rauer H, Kalman K, Zhou J, et al. Calmodulin mediates calcium-dependent activation of the intermediate conductance KCa channel, IKCa1. J Biol Chem. 1999;274(9):5746-54.

308. Keen JE, Khawaled R, Farrens DL, Neelands T, Rivard A, Bond CT, et al. Domains responsible for constitutive and Ca(2+)-dependent interactions between calmodulin and small conductance Ca(2+)-activated potassium channels. J Neurosci. 1999;19(20):8830-8.

309. Schumacher MA, Crum M, Miller MC. Crystal structures of apocalmodulin and an apocalmodulin/SK potassium channel gating domain complex. Structure. 2004;12(5):849-60.

310. Jenkins DP, Strøbæk D, Hougaard C, Jensen ML, Hummel R, Sørensen US, et al. Negative gating modulation by (R)-N-(benzimidazol-2-yl)-1,2,3,4-tetrahydro-1-naphthylamine (NS8593) depends on residues in the inner pore vestibule: pharmacological evidence of deep-pore gating of K(Ca)2 channels. Mol Pharmacol. 2011;79(6):899-909.

311. Lee CH, MacKinnon R. Activation mechanism of a human SK-calmodulin channel complex elucidated by cryo-EM structures. Science. 2018;360(6388):508-13.

312. Park YB. Ion selectivity and gating of small conductance Ca(2+)-activated K+ channels in cultured rat adrenal chromaffin cells. J Physiol. 1994;481 (Pt 3):555-70.

313. Hirschberg B, Maylie J, Adelman JP, Marrion NV. Gating of recombinant small-conductance Ca-activated K+ channels by calcium. J Gen Physiol. 1998;111(4):565-81.

314. Soh H, Park CS. Inwardly rectifying current-voltage relationship of small-conductance Ca2+-activated K+ channels rendered by intracellular divalent cation blockade. Biophys J. 2001;80(5):2207-15.

315.   Bruening-Wright A, Schumacher MA, Adelman JP, Maylie J. Localization of the activation gate for small conductance Ca2+-activated K+ channels. J Neurosci. 2002;22(15):6499-506.
316.   Ilse VH, Bo BH, Vincent S, Hemenegild A, Mary MM, Neil VM, et al. Model development of SK channel gating incorporating calcium sensitivity and drug interaction. Poster session2018.
317.   Strøbaek D, Teuber L, Jørgensen TD, Ahring PK, Kjaer K, Hansen RS, et al. Activation of human IK and SK Ca2+ -activated K+ channels by NS309 (6,7-dichloro-1H-indole-2,3-dione 3-oxime). Biochim Biophys Acta. 2004;1665(1-2):1-5.
318.   Köhler M, Hirschberg B, Bond CT, Kinzie JM, Marrion NV, Maylie J, et al. Small-conductance, calcium-activated potassium channels from mammalian brain. Science. 1996;273(5282):1709-14.
319.   Isenberg G. Is potassium conductance of cardiac Purkinje fibres controlled by [Ca2+]i? Nature. 1975;253(5489):273-4.
320.   Wang W, Watanabe M, Nakamura T, Kudo Y, Ochi R. Properties and expression of Ca2+-activated K+ channels in H9c2 cells derived from rat ventricle. Am J Physiol. 1999;276(5):H1559-66.
321.   Khan MA, Ahmed F, Neyses L, Mamas MA. Atrial fibrillation in heart failure: The sword of Damocles revisited. World J Cardiol. 2013;5(7):215-27.
322.   Maisel WH, Stevenson LW. Atrial fibrillation in heart failure: epidemiology, pathophysiology, and rationale for therapy. The American Journal of Cardiology. 2003;91(6, Supplement 1):2-8.
323.   Kamada R, Yokoshiki H, Mitsuyama H, Watanabe M, Mizukami K, Tenma T, et al. Arrhythmogenic ß-adrenergic signaling in cardiac hypertrophy: The role of small-conductance calcium-activated potassium channels via activation of CaMKII. Eur J Pharmacol. 2019;844:110-7.
324.   Chang PC, Hsieh YC, Hsueh CH, Weiss JN, Lin SF, Chen PS. Apamin induces early afterdepolarizations and torsades de pointes ventricular arrhythmia from failing rabbit ventricles exhibiting secondary rises in intracellular calcium. Heart Rhythm. 2013;10(10):1516-24.
325.   Hsueh CH, Chang PC, Hsieh YC, Reher T, Chen PS, Lin SF. Proarrhythmic effect of blocking the small conductance calcium activated potassium channel in isolated canine left atrium. Heart Rhythm. 2013;10(6):891-8.
326.   Joiner WJ, Wang LY, Tang MD, Kaczmarek LK. hSK4, a member of a novel subfamily of calcium-activated potassium channels. Proc Natl Acad Sci U S A. 1997;94(20):11013-8.
327.   Logsdon NJ, Kang J, Togo JA, Christian EP, Aiyar J. A novel gene, hKCa4, encodes the calcium-activated potassium channel in human T lymphocytes. J Biol Chem. 1997;272(52):32723-6.
328.   Nattel S, Maguy A, Le Bouter S, Yeh YH. Arrhythmogenic ion-channel remodelling in the heart: heart failure, myocardial infarction, and atrial fibrillation. Physiol Rev. 2007;87(2):425-56.
329.   Nattel S, Harada M. Atrial remodelling and atrial fibrillation: recent advances and translational perspectives. J Am Coll Cardiol. 2014;63(22):2335-45.
330.   Dreixler JC, Bian J, Cao Y, Roberts MT, Roizen JD, Houamed KM. Block of rat brain recombinant SK channels by tricyclic antidepressants and related compounds. Eur J Pharmacol. 2000;401(1):1-7.
331.   Gentles RG, Hu S, Huang Y, Grant-Young K, Poss MA, Andres C, et al. Preliminary SAR studies on non-apamin-displacing 4-(aminomethylaryl)pyrrazolopyrimidine K(Ca) channel blockers. Bioorg Med Chem Lett. 2008;18(20):5694-7.
332.   Turker I, Yu CC, Chang PC, Chen Z, Sohma Y, Lin SF, et al. Amiodarone inhibits apamin-sensitive potassium currents. PLoS One. 2013;8(7):e70450.

333. Adelman JP, Maylie J, Sah P. Small-conductance Ca2+-activated K+ channels: form and function. Annu Rev Physiol. 2012;74:245-69.

334. Bond CT, Maylie J, Adelman JP. Small-conductance calcium-activated potassium channels. Ann N Y Acad Sci. 1999;868:370-8.

335. Pribnow D, Johnson-Pais T, Bond CT, Keen J, Johnson RA, Janowsky A, et al. Skeletal muscle and small-conductance calcium-activated potassium channels. Muscle Nerve. 1999;22(6):742-50.

336. Jäger H, Adelman JP, Grissmer S. SK2 encodes the apamin-sensitive Ca(2+)-activated K(+) channels in the human leukemic T cell line, Jurkat. FEBS Lett. 2000;469(2-3):196-202.

337. Barfod ET, Moore AL, Lidofsky SD. Cloning and functional expression of a liver isoform of the small conductance Ca2+-activated K+ channel SK3. Am J Physiol Cell Physiol. 2001;280(4):C836-42.

338. Habermann E. Apamin. Pharmacol Ther. 1984;25(2):255-70.

339. Shah M, Haylett DG. The pharmacology of hSK1 Ca2+-activated K+ channels expressed in mammalian cell lines. Br J Pharmacol. 2000;129(4):627-30.

340. Dale TJ, Cryan JE, Chen MX, Trezise DJ. Partial apamin sensitivity of human small conductance Ca2+-activated K+ channels stably expressed in Chinese hamster ovary cells. Naunyn Schmiedebergs Arch Pharmacol. 2002;366(5):470-7.

341. Terstappen GC, Pula G, Carignani C, Chen MX, Roncarati R. Pharmacological characterisation of the human small conductance calcium-activated potassium channel hSK3 reveals sensitivity to tricyclic antidepressants and antipsychotic phenothiazines. Neuropharmacology. 2001;40(6):772-83.

342. Ravens U, Odening KE. Atrial fibrillation: Therapeutic potential of atrial K. Pharmacol Ther. 2017;176:13-21.

343. Lee YS, Chang PC, Hsueh CH, Maruyama M, Park HW, Rhee KS, et al. Apamin-sensitive calcium-activated potassium currents in rabbit ventricles with chronic myocardial infarction. J Cardiovasc Electrophysiol. 2013;24(10):1144-53.

344. Modzelewska B, Kostrzewska A, Sipowicz M, Kleszczewski T, Batra S. Apamin inhibits NO-induced relaxation of the spontaneous contractile activity of the myometrium from non-pregnant women. Reprod Biol Endocrinol. 2003;1:8.

345. Slagsvold KH, Johnsen AB, Rognmo O, Høydal M, Wisløff U, Wahba A. Comparison of left versus right atrial myocardium in patients with sinus rhythm or atrial fibrillation - an assessment of mitochondrial function and microRNA expression. Physiological reports. 2014;2(8):e12124.

346. Mandapati R, Skanes A, Chen J, Berenfeld O, Jalife J. Stable microreentrant sources as a mechanism of atrial fibrillation in the isolated sheep heart. Circulation. 2000;101(2):194-9.

347. Mansour M, Mandapati R, Berenfeld O, Chen J, Samie FH, Jalife J. Left-to-right gradient of atrial frequencies during acute atrial fibrillation in the isolated sheep heart. Circulation. 2001;103(21):2631-6.

348. Li D, Zhang L, Kneller J, Nattel S. Potential ionic mechanism for repolarization differences between canine right and left atrium. Circ Res. 2001;88(11):1168-75.

349. Bers DM. Calcium fluxes involved in control of cardiac myocyte contraction. Circ Res. 2000;87(4):275-81.

350. Hove-Madsen L, Bers DM. Passive Ca buffering and SR Ca uptake in permeabilized rabbit ventricular myocytes. Am J Physiol. 1993;264(3 Pt 1):C677-86.

351. Taylor BL, Gerrodette T. The Uses of Statistical Power in Conservation Biology: The Vaquita and Northern Spotted Owl. Conservation Biology. 1993;7(3):489-500.

352.   Nagy N, Acsai K, Kormos A, Sebők Z, Farkas AS, Jost N, et al. [Ca^{2+}] i-induced augmentation of the inward rectifier potassium current (IK1) in canine and human ventricular myocardium. Pflugers Arch. 2013;465(11):1621-35.

353.   Grunnet M, Bentzen BH, Sørensen US, Diness JG. Cardiac ion channels and mechanisms for protection against atrial fibrillation. Rev Physiol Biochem Pharmacol. 2012;162:1-58.

354.   Wittekindt OH, Visan V, Tomita H, Imtiaz F, Gargus JJ, Lehmann-Horn F, et al. An apamin- and scyllatoxin-insensitive isoform of the human SK3 channel. Mol Pharmacol. 2004;65(3):788-801.

355.   Blanchard EM, Smith GL, Allen DG, Alpert NR. The effects of 2,3-butanedione monoxime on initial heat, tension, and aequorin light output of ferret papillary muscles. Pflugers Arch. 1990;416(1-2):219-21.

356.   Horiuti K, Higuchi H, Umazume Y, Konishi M, Okazaki O, Kurihara S. Mechanism of action of 2, 3-butanedione 2-monoxime on contraction of frog skeletal muscle fibres. J Muscle Res Cell Motil. 1988;9(2):156-64.

357.   Li T, Sperelakis N, Teneick RE, Solaro RJ. Effects of diacetyl monoxime on cardiac excitation-contraction coupling. J Pharmacol Exp Ther. 1985;232(3):688-95.

358.   Daly MJ, Elz JS, Nayler WG. Contracture and the calcium paradox in the rat heart. Circ Res. 1987;61(4):560-9.

359.   Voos P, Yazar M, Lautenschläger R, Rauh O, Moroni A, Thiel G. The small neurotoxin apamin blocks not only small conductance Ca2+ activated K+ channels (SK type) but also the voltage dependent Kv1.3 channel. European Biophysics Journal. 2017;46(6):517-23.

360.   Dobi S, Smith GL. The Effect of the SK Channel Inhibitor ICAGEN in Intact Atria and Atrial Cardiomyocytes. Biophysical Journal. 2019;116(3):31a.

361.   Gussak I, Chaitman BR, Kopecky SL, Nerbonne JM. Rapid ventricular repolarization in rodents: electrocardiographic manifestations, molecular mechanisms, and clinical insights. J Electrocardiol. 2000;33(2):159-70.

362.   Lippiat JD. Whole-Cell Recording Using the Perforated Patch Clamp Technique. In: Lippiat JD, editor. Potassium Channels: Methods and Protocols. Totowa, NJ: Humana Press; 2009. p. 141-9.

363.   Faber ES, Delaney AJ, Sah P. SK channels regulate excitatory synaptic transmission and plasticity in the lateral amygdala. Nat Neurosci. 2005;8(5):635-41.

364.   Yue L, Feng J, Li GR, Nattel S. Transient outward and delayed rectifier currents in canine atrium: properties and role of isolation methods. Am J Physiol. 1996;270(6 Pt 2):H2157-68.

365.   Shamsaldeen YA, Culliford L, Clout M, James AF, Ascione R, Hancox JC, et al. Role of SK channel activation in determining the action potential configuration in freshly isolated human atrial myocytes from the SKArF study. Biochem Biophys Res Commun. 2019;512(4):684-90.

366.   Hancock JM, Weatherall KL, Choisy SC, James AF, Hancox JC, Marrion NV. Selective activation of heteromeric SK channels contributes to action potential repolarization in mouse atrial myocytes. Heart Rhythm. 2015;12(5):1003-15.

367.   Allessie MA. Atrial electrophysiologic remodelling: another vicious circle? J Cardiovasc Electrophysiol. 1998;9(12):1378-93.

368.   Zhang XD, Coulibaly ZA, Chen WC, Ledford HA, Lee JH, Sirish P, et al. Coupling of SK channels, L-type Ca. Sci Rep. 2018;8(1):4670.

369.   Gao Y, Chotoo CK, Balut CM, Sun F, Bailey MA, Devor DC. Role of S3 and S4 transmembrane domain charged amino acids in channel biogenesis and gating of KCa2.3 and KCa3.1. J Biol Chem. 2008;283(14):9049-59.

370.   Klöckner U, Isenberg G. Calcium currents of cesium loaded isolated smooth muscle cells (urinary bladder of the guinea pig). Pflugers Arch. 1985;405(4):340-8.

371.   Boyle WA, Nerbonne JM. Two functionally distinct 4-aminopyridine-sensitive outward K+ currents in rat atrial myocytes. J Gen Physiol. 1992;100(6):1041-67.

372.   Lei M, Honjo H, Kodama I, Boyett MR. Characterisation of the transient outward K+ current in rabbit sinoatrial node cells. Cardiovasc Res. 2000;46(3):433-41.

373.   Fermini B, Wang Z, Duan D, Nattel S. Differences in rate dependence of transient outward current in rabbit and human atrium. Am J Physiol. 1992;263(6 Pt 2):H1747-54.

374.   Kirchhoff JE, Diness JG, Sheykhzade M, Grunnet M, Jespersen T. Synergistic antiarrhythmic effect of combining inhibition of Ca^{2+}-activated K^+ (SK) channels and voltage-gated Na^+ channels in an isolated heart model of atrial fibrillation. Heart Rhythm. 2015;12(2):409-18.

375.   Obreztchikova MN, Patberg KW, Plotnikov AN, Ozgen N, Shlapakova IN, Rybin AV, et al. IKr contributes to the altered ventricular repolarization that determines long-term cardiac memory. Cardiovascular Research. 2006;71(1):88-96.

376.   Sosunov EA, Anyukhovsky EP, Hefer D, Rosen TS, Danilo P, Janse MJ, et al. Region-specific, pacing-induced changes in repolarization in rabbit atrium: an example of sensitivity to the rare. Cardiovasc Res. 2005;67(2):274-82.

377.   Nattel S. Calcium-activated potassium current: a novel ion channel candidate in atrial fibrillation. The Journal of physiology. 2009;587(Pt 7):1385-6.

378.   Fakler B, Adelman JP. Control of K(Ca) channels by calcium nano/microdomains. Neuron. 2008;59(6):873-81.

379.   Kirsh JA, Sahakian AV, Baerman JM, Swiryn S. Ventricular response to atrial fibrillation: Role of atrioventricular conduction pathways. Journal of the American College of Cardiology. 1988;12(5):1265.

380.   Workman AJ, Pau D, Redpath CJ, Marshall GE, Russell JA, Kane KA, et al. Post-operative atrial fibrillation is influenced by beta-blocker therapy but not by pre-operative atrial cellular electrophysiology. J Cardiovasc Electrophysiol. 2006;17(11):1230-8.

381.   Workman AJ, Pau D, Redpath CJ, Marshall GE, Russell JA, Norrie J, et al. Atrial cellular electrophysiological changes in patients with ventricular dysfunction may predispose to AF. Heart Rhythm. 2009;6(4):445-51.

382.   Weber CR, Ginsburg KS, Philipson KD, Shannon TR, Bers DM. Allosteric regulation of Na/Ca exchange current by cytosolic Ca in intact cardiac myocytes. J Gen Physiol. 2001;117(2):119-31.

383.   Kimura J, Miyamae S, Noma A. Identification of sodium-calcium exchange current in single ventricular cells of guinea-pig. J Physiol. 1987;384:199-222.

384.   Reeves JP, Hale CC. The stoichiometry of the cardiac sodium-calcium exchange system. J Biol Chem. 1984;259(12):7733-9.

385.   Bers DM, Bridge JH. Relaxation of rabbit ventricular muscle by Na-Ca exchange and sarcoplasmic reticulum calcium pump. Ryanodine and voltage sensitivity. Circ Res. 1989;65(2):334-42.

386.   Crespo LM, Grantham CJ, Cannell MB. Kinetics, stoichiometry and role of the Na-Ca exchange mechanism in isolated cardiac myocytes. Nature. 1990;345(6276):618-21.

387.   Mullins LJ. The generation of electric currents in cardiac fibers by Na/Ca exchange. Am J Physiol. 1979;236(3):C103-10.

388. Hilgemann DW. Regulation and deregulation of cardiac Na(+)-Ca2+ exchange in giant excised sarcolemmal membrane patches. Nature. 1990;344(6263):242-5.
389. Boyman L, Hagen BM, Giladi M, Hiller R, Lederer WJ, Khananshvili D. Proton-sensing Ca2+ binding domains regulate the cardiac Na+/Ca2+ exchanger. J Biol Chem. 2011;286(33):28811-20.
390. Hilgemann DW, Collins A, Matsuoka S. Steady-state and dynamic properties of cardiac sodium-calcium exchange. Secondary modulation by cytoplasmic calcium and ATP. J Gen Physiol. 1992;100(6):933-61.
391. Torrente AG, Zhang R, Wang H, Zaini A, Kim B, Yue X, et al. Contribution of small conductance K+ channels to sinoatrial node pacemaker activity: insights from atrial-specific Na+/Ca2+ exchange knockout mice. The Journal of Physiology. 2017;595(12):3847-65.
392. Qi XY, Yeh YH, Xiao L, Burstein B, Maguy A, Chartier D, et al. Cellular signaling underlying atrial tachycardia remodelling of L-type calcium current. Circ Res. 2008;103(8):845-54.
393. Tanaka H, Nishimaru K, Aikawa T, Hirayama W, Tanaka Y, Shigenobu K. Effect of SEA0400, a novel inhibitor of sodium-calcium exchanger, on myocardial ionic currents. Br J Pharmacol. 2002;135(5):1096-100.
394. Armoundas AA, Hobai IA, Tomaselli GF, Winslow RL, O'Rourke B. Role of sodium-calcium exchanger in modulating the action potential of ventricular myocytes from normal and failing hearts. Circ Res. 2003;93(1):46-53.
395. Despa S, Islam MA, Weber CR, Pogwizd SM, Bers DM. Intracellular Na(+) concentration is elevated in heart failure but Na/K pump function is unchanged. Circulation. 2002;105(21):2543-8.
396. Bénardeau A, Hatem SN, Rücker-Martin C, Le Grand B, Macé L, Dervanian P, et al. Contribution of Na+/Ca2+ exchange to action potential of human atrial myocytes. Am J Physiol. 1996;271(3 Pt 2):H1151-61.
397. Coraboeuf E, Nargeot J. Electrophysiology of human cardiac cells. Cardiovasc Res. 1993;27(10):1713-25.
398. Eisner DA, Caldwell JL, Trafford AW, Hutchings DC. The Control of Diastolic Calcium in the Heart: Basic Mechanisms and Functional Implications. Circ Res. 2020;126(3):395-412.
399. Eisner DA, Caldwell JL, Kistamás K, Trafford AW. Calcium and Excitation-Contraction Coupling in the Heart. Circ Res. 2017;121(2):181-95.
400. Rusticus SA, Lovato CY. Impact of Sample Size and Variability on the Power and
Type I Error Rates of Equivalence Tests: A Simulation Study. Practical Assessment, Research, and
Evaluation; 2014.
401. Xu H, Li H, Nerbonne JM. Elimination of the transient outward current and action potential prolongation in mouse atrial myocytes expressing a dominant negative Kv4 alpha subunit. J Physiol. 1999;519 Pt 1:11-21.
402. Maltsev VA, Silverman N, Sabbah HN, Undrovinas AI. Chronic heart failure slows late sodium current in human and canine ventricular myocytes: implications for repolarization variability. Eur J Heart Fail. 2007;9(3):219-27.
403. Bassani RA. Transient outward potassium current and Ca2+ homeostasis in the heart: beyond the action potential. Braz J Med Biol Res. 2006;39(3):393-403.
404. Calaghan SC, Le Guennec JY, White E. Modulation of Ca(2+) signaling by microtubule disruption in rat ventricular myocytes and its dependence on the ruptured patch-clamp configuration. Circ Res. 2001;88(4):E32-7.
405. Pelzer D, Pelzer S, McDonald TF. Properties and regulation of calcium channels in muscle cells. Rev Physiol Biochem Pharmacol. 1990;114:107-207.

406. Blanchard EM, Smith GL, Allen DG, Alpert NR. The effects of 2,3-butanedione monoxime on initial heat, tension, and aequorin light output of ferret papillary muscles. Pflügers Archiv. 1990;416(1):219-21.

407. Horiuti K, Higuchi H, Umazume Y, Konishi M, Okazaki O, Kurihara S. Mechanism of action of 2, 3-butanedione 2-monoxime on contraction of frog skeletal muscle fibres. Journal of Muscle Research & Cell Motility. 1988;9(2):156-64.

408. Li T, Sperelakis N, Teneick RE, Solaro RJ. Effects of diacetyl monoxime on cardiac excitation-contraction coupling. Journal of Pharmacology and Experimental Therapeutics. 1985;232(3):688.

409. Xu Y, Zhang Z, Timofeyev V, Sharma D, Xu D, Tuteja D, et al. The effects of intracellular Ca2+ on cardiac K+ channel expression and activity: novel insights from genetically altered mice. J Physiol. 2005;562(Pt 3):745-58.

410. Zhang X-D, Timofeyev V, Li N, Myers RE, Zhang D-M, Singapuri A, et al. Critical roles of a small conductance Ca2+-activated K+ channel (SK3) in the repolarization process of atrial myocytes. Cardiovascular Research. 2013;101(2):317-25.

411. Dobrev D, Wettwer E, Himmel HM, Kortner A, Kuhlisch E, Schüler S, et al. G-Protein β3-Subunit 825T Allele Is Associated With Enhanced Human Atrial Inward Rectifier Potassium Currents. Circulation. 2000;102(6):692-7.

412. Janvier NC, Boyett MR. The role of Na-Ca exchange current in the cardiac action potential. Cardiovascular Research. 1996;32(1):69-84.

413. Peñaranda A, Cantalapiedra IR, Alvarez-Lacalle E, Echebarria B. Electrophysiological Effects of Small Conductance Ca^{2+}-Activated K^+ Channels in Atrial Myocytes. In: Carballido-Landeira J, Escribano B, editors. Biological Systems: Nonlinear Dynamics Approach. Cham: Springer International Publishing; 2019. p. 19-37.

414. Hsieh YC, Chang PC, Hsueh CH, Lee YS, Shen C, Weiss JN, et al. Apamin-sensitive potassium current modulates action potential duration restitution and arrhythmogenesis of failing rabbit ventricles. Circ Arrhythm Electrophysiol. 2013;6(2):410-8.

415. Roy D, Pratt CM, Torp-Pedersen C, Wyse DG, Toft E, Juul-Moller S, et al. Vernakalant hydrochloride for rapid conversion of atrial fibrillation: a phase 3, randomized, placebo-controlled trial. Circulation. 2008;117(12):1518-25.

416. Pratt CM, Roy D, Torp-Pedersen C, Wyse DG, Toft E, Juul-Moller S, et al. Usefulness of vernakalant hydrochloride injection for rapid conversion of atrial fibrillation. Am J Cardiol. 2010;106(9):1277-83.